# Thermoresponsive Hydrogels from ABC Triblock Terpolymers

A DISSERTATION
SUBMITTED TO THE FACULTY OF THE GRADUATE SCHOOL
OF THE UNIVERSITY OF MINNESOTA
BY

Can Zhou

IN PARTIAL FULFILLMENT OF THE REQUIREMENTS
FOR THE DEGREE OF
DOCTOR OF PHILOSOPHY

Advisers: Marc A. Hillmyer and Timothy P. Lodge

March 2014

# Acknowledgements

A Ph.D. is truly a milestone in my life, and it cannot be achieved without the help and support from many people. First and foremost, I would like to thank my advisors, Prof. Tim Lodge and Prof. Marc Hillmyer, for their guidance, patience and encouragement through the course of my graduate education. They are really outstanding scientists and dedicated teachers, from whom I have learned a lot about how to think critically, thoroughly and creatively, and how to work quickly, accurately, and efficiently in order to conduct good scientific research. I want to thank my written, oral, and final defense committee members, Prof. Frank Bates, Prof. Theresa Reineke, Prof. Tom Hoye, and Prof. Phil Buhlmann for their guidance and suggestion.

I must thank Isha Konnar for collaboration on a very interesting and exciting project in this Ph.D. thesis. She has always been dedicated, helpful and productive. I thank Prof. Ronald A. Siegel for his input and guidance in this collaborative research. I also want to thank Dr. Gilman E. Toombes, Dr. Matthew Wasbrough, Dr. Paul Butler for their collaboration on the SANS project in my thesis. I thank two summer undergraduates, Scott Danielsen and Cecilia Hall, for their contribution to this thesis.

I have enjoyed working with many past and present members of the Lodge, Hillmyer groups and Polymer group, and I would like to thank them for their friendship, insightful comments and helpful discussions: Dr. Ligeng Yin, Dr. Chun Liu, Dr. Rajiv Tarabagil, Dr. Yuanyan Gu, Dr. Zhifeng Bai, Dr. Sipei Zhang, Dr. Luciana Meli, Dr. Yang Qin, Dr. Jihua Zhang, Dr. Marc Rodwogin, Dr. Louis Pitet, Dr. Joshua Speros, Dr. Mark Amendt, Dr. Shingo Kobayashi, Dr. Mark Martello, Dr. Grayce Theryo, Dr. Jihoon

Shin, Dr. Gina Fiore, Dr. Soo-Hyung Choi, Dr. Hau-Nan Lee, Dr. Brad Jones, Dr. Adam Moughton, Dr. Joe Lott, Dr. Yuewen Xu, Dr. Yu Lei, Dr. Sara Arvidson, Dr. Jie Song, Morgan Schulze, Zhen Ren, Dr. Justin Kennemur, John McAllister, Lucas McIntosh, Soonyong So, Matt Irwin, Jie Lu, Dr. Donglin Tang, Dr. Sangwoo Lee and Tim Gillard. I also thank Chris Frethem, Bob Hafner and David Giles for their help with cryogenic electron microscopy and rheological experiments.

Last but not least, I want to express my deepest gratitude to my parents, my sister and my wife, Ye, for their endless love, care and support. Without their support, I would have never achieved this far in my life. To them I dedicate this work.

*To my parents, sister and Ye*

# Abstract

Two-compartment hydrogels, which are three-dimensional networks with two distinguishable hydrophobic domains, have been prepared from aqueous self-assembly of poly(ethylene-*alt*-propylene)-*b*-poly(ethylene oxide)-*b*-poly(*N*-isopropylacrylamide) (PEP-*b*-PEO-*b*-PNIPAm, PON) triblock terpolymers. The PON terpolymers were synthesized using a combination of anionic and reversible addition-fragmentation chain transfer (RAFT) polymerization. They self-assembled into well-defined micelles with hydrophobic PEP cores surrounded by hydrophilic PEO-PNIPAm coronae at low temperatures and these micelles associated to form larger aggregated structures upon heating above the lower critical solution temperature (LCST) of PNIPAm in dilute aqueous solutions (0.5 and 0.05 wt%). At higher polymer concentrations (1–5 wt%), micellar aggregation manifests itself as gelation on heating due to the non-covalent association of PNIPAm blocks. The separation of micellization and gelation leads to the formation of a two-compartment network with a very high fraction of bridging conformations for the PEO midblocks. Therefore, gelation can be achieved at a much lower concentration, with a much higher modulus at a given polymer concentration and a much sharper sol-gel transition, as compared to poly(*N*-isopropylacrylamide)-*b*-poly(ethylene oxide)-*b*-poly(*N*-isopropylacrylamide) (NON) copolymer hydrogels, in which both looping and bridging conformations are possible.

The formation of a micellar network with two discrete PEP and PNIPAm hydrophobic domains in PON hydrogels is verified by cryogenic scanning electron microscopy (cryo-SEM) and cryogenic transmission electron microscopy (cryo-TEM)

experiments and is further confirmed by small-angle neutron scattering (SANS) measurements of two PON triblocks with a normal PNIPAm and a deuterated PNIPAm block. This study confirms the assumption that the formation of two-compartment networks in PON terpolymer hydrogels results in better gelation properties compared with NON copolymer hydrogels.

In addition to temperature, it is desirable to have other stimuli such as pH to control the polymer self-assembly. Therefore, poly(ethylene-*alt*-propylene)-*b*-poly(ethylene oxide)-*b*-poly(*N*-isopropylacrylamide-*co*-acrylic acid) (PO(N/A)) triblock terpolymers in which the PNIPAm block contains a small fraction of AA monomers were prepared to achieve the dual pH- and temperature-sensitive micellar aggregation and gelation in aqueous solutions.

Finally, the self-assembly of PON triblock terpolymers in the ionic liquid 1-ethyl-3-methyl-imidazolium bis(trifluoromethylsulfonyl)amide ([EMI][TFSA]) shows well-defined sol-gel transitions upon cooling with a lower gelation concentration and a higher modulus when compared with NON copolymers, which further confirms that ABC triblock terpolymers can be beneficial for gel formation in comparison to ABA triblock copolymers.

Overall, we demonstrated that the rational design of two immiscible, hydrophobic endblocks in ABC triblocks is crucial for the preparation of compartmentized hydrogels with improved gelation properties. These studies will help guide the design and development of new systems with enhanced performance.

# Table of Contents

# List of Figures

# List of Tables

# List of Schemes

# Chapter 1

# Background

This chapter reviews the experimental and theoretical developments in the field of multicompartment colloidal assemblies available from block copolymers in selective solvents, with an emphasis on ABC triblock terpolymers. Section 1.1 introduces various intricate multicompartment micellar structures in dilute aqueous solutions of linear and miktoarm star ABC triblock terpolymers and reviews the limited set of multicompartment gels discovered in concentrated solutions, and points out the need for the design and preparation of multicompartment well characterized networks from novel ABC terpolymers. Section 1.2 compares the hydrogel formation from ABA triblock copolymers and ABC triblock terpolymers and reveals that the distinct compartments in the ABC terpolymer network could be beneficial for this purpose. This further warrants a systematic and detailed investigation of multicompartment networks. Section 1.3 discusses the solution behavior of thermoresponsive copolymers, as a thermoresponsive block will be incorporated into the ABC terpolymer to prepare multicompartment hydrogels. Section 1.4 summarizes the research motivation and thesis outline.

## 1.1 Multicompartment Micelles and Gels from ABC Triblock Terpolymers

Multicompartment micelles or gels from multiblock copolymers are nanoscopic aggregates with subdivided solvophobic cores, or three-dimensional networks with

distinguishable compartments, respectively. The concept of multicompartment micelles or gels draw inspiration from biological systems such as eukaryotic cells, which possess distinct subunits that enable them to perform multiple functions simultaneously.[1] Since then, they have attracted considerable interest in the area of self-assembled soft materials due to their potential applications in biomedicine, pharmacy and biotechnology.[2, 3] The discrete subdomains of these colloidal assemblies can facilitate the concurrent storage and delivery of two or more incompatible active agents such as drug molecules, gene therapy agents, or pesticides in a prescribed manner, supporting their technological interest and potential importance in biomedical applications.[4]

While AB diblock copolymers are incapable of forming such complex assemblies as they are limited to the partition of space into "inside" and "outside" areas, ABC triblock terpolymers with one solvophilic block and two incompatible solvophobic blocks can serve as model systems to create distinct compartments within the micelle core or network.[5-7] In this section, I will provide a brief introduction on AB diblock copolymer micelles to illustrate the general principles governing the self-assembly of block copolymers and then focus on the development of multicompartment micelles and gels from ABC triblock terpolymers.

### 1.1.1 Micelles from AB Diblock Copolymers

When an AB diblock copolymer is dispersed in a solvent selective for one block, say B, the polymer will spontaneously self-assemble into micelles with the A block forming the solvophobic core surrounded by the solvophilic corona composed of solvated B

chains. The free energy of the micelles from AB diblock copolymers is expressed as the sum of the A-B interfacial tension (enthalpy) and the chain stretching energies of both core and corona (entropy), and can be adjusted by modulating solvent selectivity and copolymer composition. Therefore, the micellar morphologies can vary from spheres to cylinders to vesicles by manipulating solvent selectivity and copolymer composition.[8-10] The micelle assembly undergoes a transition from sphere to cylinder with increasing solvent selectivity, in an attempt to reduce the interfacial area per chain without incurring the entropic penalty of chain stretching. Solvent selectivity can be modulated by using mixture of different solvents or by changing temperature or pH.[11-13] For example, Bang and Lodge discovered that poly(styrene)-*b*-poly(isoprene) (PS-*b*-PI) micelles formed in a mixture of diallyl phthalates can transform from vesicles to cylinder to spheres by decreasing solvent selectivity via changing the solvent composition of the phthalate mixtures.[11] The same transition can be induced by increasing solvent temperature.[12] Similar morphological transitions can also be accessed by changing block copolymer composition. Higher solvophilic block volume fraction favors a shape with higher curvatures, like a sphere.[14-16] Won and Bates investigated dilute aqueous solutions of poly(1,2-butadiene)-*b*-poly(ethylene oxide) (PB-*b*-PEO) in water with varying copolymer compositions and found that the micellar morphology changed from vesicles to cylinders to spheres with increasing the hydrophilic block (PEO) volume fraction.[14]

### 1.1.2 Multicompartment Micelles from ABC Triblock Terpolymers

As discussed earlier, ABC triblock terpolymers with three mutually immiscible

components can serve as model systems to prepare multicompartment micelles. The simplest recipe is to prepare a dilute aqueous solution of a linear or miktoarm star (three blocks converge at one common junction point) triblock terpolymer, consisting of a hydrophilic polymer and two mutually incompatible hydrophobic blocks.[17] Hydrocarbon and fluorocarbon based polymers, which are highly mutually immiscible, are commonly chosen as the two hydrophobic blocks in both architectures. In the case of the linear architecture, Laschewsky and coworkers reported the formation of raspberry-like multicompartment micelles from both poly(4-methyl-4-(4-vinylbenzyl)morpholin-4-ium chloride)-*b*-polystyrene-*b*-poly(pentafluorophenyl 4-vinylbenzyl ether) (PVBM-*b*-PS-*b*-PVBFP) with PVBM as the hydrophilic endblock and poly(2-ethylhexyl acrylate)-*b*-poly(oligoethyleneglycol monomethylether acrylate)-*b*-poly(1*H*,1*H*,2*H*,2*H*-perfluorodecyl acrylate) (PEHA-*b*-POEGA-*b*-PFDA) with POEGA as the hydrophilic midblock.[18, 19] Multicompartment micellar morphologies have also been reported in water/organic solvent mixtures or organic solvents. Segmented worm-like micelles were observed in a dilute $H_2O$/THF (15 wt% $H_2O$) solution of poly(ethylene oxide)-*b*-poly(2-vinylpyridine)-*b*-polystyrene (PEO-*b*-P2VP-*b*-PS).[20] Undulated multi-compartment cylinder were reported in an ethanol solution of poly(4-*tert*-butoxstyrene)-*b*-poly(butadiene)-*b*-poly(*tert*-butyl methacrylate) (PtBS-*b*-PB-*b*-PtBMA) in which PB was modified with a fluorinated side group.[21] In the case of the miktoarm star architecture, Li, Hillmyer and Lodge prepared a variety of multicompartment micellar structures from aqueous solutions of a series of miktoarm star terpolymers $\mu$-EOF consisting of hydrophobic poly(ethyl ethylene) (PEE/E), hydrophilic poly(ethylene oxide)

(PEO/O), and lipophobic/hydrophobic poly(perfluoropropylene oxide) (PFPO/F) (Figure 1.1).[7, 22-24] In all these $\mu$-EOF polymers, the three blocks are strongly segregated from one another including the hydrophobic E/F pair, thus the micellar cores all involve separate subdomains of E and F. The micellar morphology transition with varying terpolymer composition is consistent with the results in AB diblock copolymer system. As the volume ratio of solvophilic block (O) to solvophobic (E+F) decrease, $\mu$-EOF multicompartment micelles change from hamburger-like micelles to segmented or multicompartment worms and finally to laterally nanostructured vesicle or polygonal bilayers. Similar miktoarm star terpolymers with the less hydrophobic poly($\gamma$-methyl-$\varepsilon$-caprolactone) (PMCL) substituted for PFPO can also form different multicompartment structures including hamburger, segmented wormlike and raspberry micelles by varying the PMCL block length.[25]

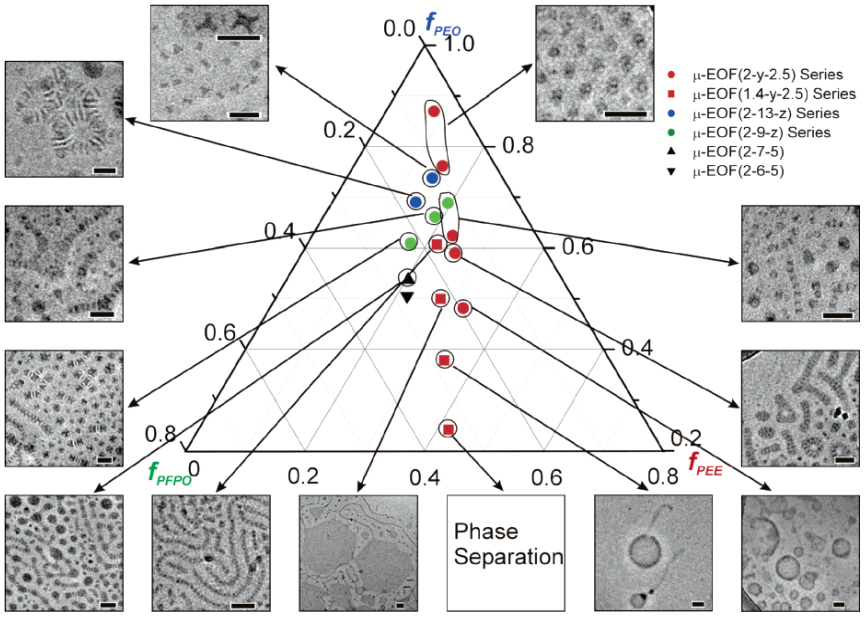


**Figure 1.1** Multicompartment micelle morphology diagram for μ-EOF in dilute aqueous solution as a function of composition. $f_{PEE}$, $f_{PEO}$, and $f_{PFPO}$ are the volume fractions of the PEE, PEO, and PFPO blocks, respectively. The scale bar indicates 50 nm. The numbers in the parenthesis represent the molecular weights of each block in units of kg/mol. Reprinted with permission from Li, Z.; Hillmyer, M. A.; Lodge, T. P. *Langmuir* **2006**, *22*, 9409-9417.

### 1.1.3 Multicompartment Gels from ABC Triblock Terpolymers

This rich polymorphism in dilute solution (multicompartment micelles) of ABC triblock terpolymers discussed in the previous section can be translated to diverse structural possibilities in concentrated dispersions (multicompartment gels). However, there have only been a few reports on multicompartment gels. For example, Weberskirch, *et al.* studied the self-association behavior of poly(*N*-acylethyleneimine) polymers

end-capped with a fluorocarbon group and a hydrocarbon group, and showed the segregation of the end groups using NMR spectroscopy at relatively high polymer concentration (31 wt%).[26] Similarly, Komenda *et al.* prepared a multicompartment micellar hydrogel from poly(2-*n*-nonyl-2-oxazoline)-*b*-poly(2-methyl-2-oxazoline)-*b*-poly(2-(1'H,1'H,2'H,2'H-perfluorohexyl)-2-oxazoline) (PNOx-*b*-PMOx-*b*-PFOx) and inferred the presence of a micellar network with spherical PNOx cores and ellipsoidal PFOx cores using small angle neutron scattering (SANS) experiments.[27] Yamaguchi *et al.* reported the structure of thermoplastic elastomer gels composed of polystyrene-*b*-polybutadiene-*b*-poly(methyl methacrylate) (PS-*b*-PB-*b*-PMMA) in an aliphatic oil. They observed that the PS and PMMA endblocks are mixed into spherical microdomains at low polymer concentration, and segregated in distinct cylindrical or lamellar microdomains at sufficiently large polymer concentration, using transmission electron microscopy (TEM) and small angle x-ray scattering (SAXS) experiments.[28] Recently, Taribagil, Hillmyer and Lodge investigated the morphology of a compartmentalized hydrogel from a telechelic poly(ethylene oxide) (PEO) end-capped with mutually incompatible hydrophobic blocks (poly(1,2-butadiene) (PB) and poly(perfluoropropylene oxide) (PFPO) and revealed a bicontinuous structure composed of PFPO disks distributed within a hydrophobic PB sheet covered by hydrophilic PEO brush by cryogenic scanning electron microscopy (cryo-SEM) and SANS (Figure 1.2).[29, 30]

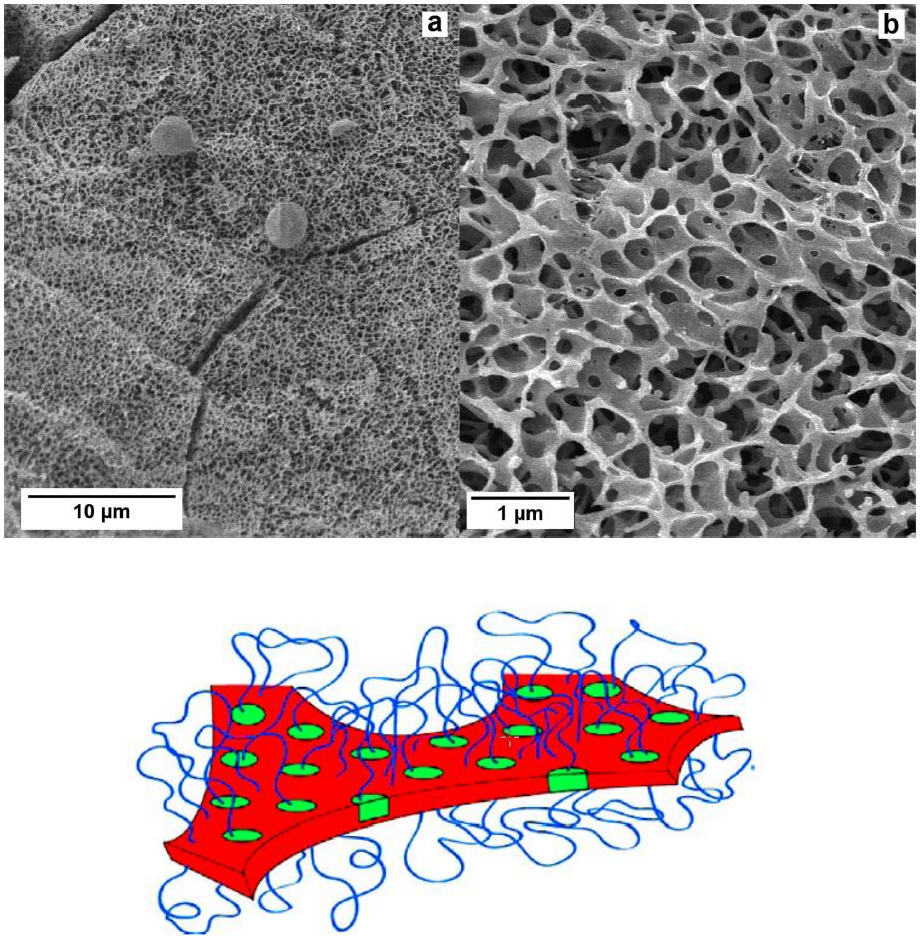


**Figure 1.2** Upper: Cryo-SEM micrograph for 10 wt % PB-*b*-PEO-*b*-PFPO(1.9-26-2.3) in water at two different magnifications. The numbers in the parenthesis represent the molecular weights of each block in units of kg/mol. Bottom: Schematic illustration of the compartmentalized network from PB-*b*-PEO-*b*-PFPO. PB sheet, PFPO disks, and PEO chains are represented in red, green, and blue, respectively. Reprinted with permission from Taribagil, R. R.; Hillmyer, M. A.; Lodge, T. P. *Macromoelcues* **2009**, *42*, 1796-1800.

As discussed above, there has been substantial progress in this field of multicompartment colloidal assemblies over the past decade, with an emphasis on the

preparation of multicompartment micelles from dilute solutions of ABC terpolymers, but only limited studies on developing multicompartment gels from their concentrated solutions. It is therefore of interest to explore the formation of multicompartment gels more systematically.[31] It is also of great importance to characterize the morphological properties of these compartmentized networks in detail as they are generally poorly characterized so far. Overall, understanding the underlying principles governing the self-assembly of ABC triblock terpolymers in these systems is of fundamental importance to the control and application of these hierarchical structures.

### 1.2 Hydrogels from ABA and ABC Triblock Polymers

Hydrogels are water-swollen polymeric networks with broadly tunable characteristics that enable wide utility in, *e.g.*, coating, cosmetic, drug delivery, tissue engineering, and sensing applications.[32-39] Both chemical hydrogels, formed by covalent crosslinking of hydrophilic polymers, and physical hydrogels comprising block copolymers or other self-associating polymers held together by hydrophobic, hydrogen bonding or ionic interactions, are of interest. Reversible physical hydrogels from block polymers are particularly appealing, as they can exhibit a sol-gel transition in response to external stimuli, and have great potential for site-specific drug-delivery applications.[38-40] In addition, mechanical properties and mesh size can be readily tuned by changing copolymer concentration, composition and molar mass.

### 1.2.1 ABA Triblock Copolymer Hydrogels

The ABA triblock copolymers used for hydrogel formation typically have long hydrophilic midblocks with short hydrophobic endblocks.[41-48] Above a critical micelle concentration (CMC), the hydrophobic endblocks associate to form micellar cores. The hydrophilic midblocks loop to form the corona around the core, resulting in the formation of flow-like micelles.[49] As the concentration is increased, these flower-like micelles come closer and the midblock can overcome the entropic penalty of looping by bridging to another micellar core.[50] Above another critical concentration called the critical gelation concentration (CGC), more bridges form, the viscosity of the solution starts to rise steeply, solid-like behavior emerges, and a gel is formed.[51, 52] For small hydrophobic endblocks, the hydrophobic junctions (hydrophobic micellar cores) can be reversibly broken and reformed; the resulting hydrogels are classified as transient networks and their rheological behavior can be described by transient network theory. The first systematic study on transient network theory was presented by Green and Tobolsky, in which stress relaxation was treated by a kinetic theory of rubber elasticity where junctions are allowed to break or reform during the network deformation.[53] By providing a clear molecular picture for the breakage and annihilation of junctions in the network structure, Tanaka and Edwards further developed this theory to describe unentangled networks where the molecular weight between junctions was smaller than the entanglement molecular weight.[54] The theory predicted Maxwell-type viscoelastic behavior with a high frequency storage modulus $G$ (= $\nu k_B T$, where $\nu$ is the number density of elastically effective chains) and a single relaxation time $\tau$ (the reciprocal of the

chain end disengagement rate). Tanaka and Edwards characterized the chain end disengagement as an Arrhenius-type activation process with an activation energy $E_m$, relaxation time $\tau \sim \exp(E_m/k_BT)$. Annable *et al.* experimentally confirmed that aqueous solutions of associative polymers, consisting of poly(ethylene glycol) (PEG) endcapped by long-chain alkanols, exhibit single relaxation time Maxwell-type viscoelasticity with a relaxation time that varies exponentially with the hydrophobe length.[41] Recently, Inomata *et al.* reported that viscoelastic master curves of the transient network formed from poly(methyl methacrylate)-*b*-poly(*tert*-butyl acrylate)-*b*-poly(methyl methacrylate) (PMMA-*b*-PtBA-*b*- PMMA) in 1-butanol resembled the Maxwell-type modulus curve with a narrow relaxation time distribution.[55] Shull and coworkers investigated gelation behavior of poly(methyl methacrylate)-*b*-poly(*n*-butyl acrylate)-*b*-poly(methyl methacrylate) (PMMA-*b*-PnBA-*b*-PMMA) in 2-ethylhexanol. Master curves could be fitted with the Maxwell model with a narrow range of relaxation times.[56] Relaxation times were found to depend on temperature and endblock length. Increasing endblock length and decreasing temperature led to an increase of the relaxation time.

The transition from solid-like behavior to liquid-like behavior near a sol-gel transition temperature is characterized by critical gelation temperature ($T_{gel}$). The linear viscoelastic behavior in the vicinity of the sol-gel transition point has been extensively studied for both chemical gels and physical gels. Winter and Chambon showed that the storage and loss moduli, $G'(\omega)$ and $G''(\omega)$, follow a simple power law on the angular frequency $\omega$ at the critical gelation point: $G'(\omega) \approx G''(\omega) \sim \omega^n$.[57, 58]

### 1.2.2 ABC Triblock Terpolymer Hydrogels

Hydrogel formation by ABA triblock copolymers containing hydrophilic midblocks and hydrophobic endblocks has been extensively studied. However, in general the gelation of such systems is inefficient, in the sense that minimum gelation concentrations often exceed 10 wt% polymer. This is because there are three possible conformations for the midblocks in ABA hydrogels: (i) loops, when both end blocks belong to the same microdomain; (ii) bridges, when the end blocks connect two different microdomains; (iii) dangling ends, when one end block is unassociated with any microdomain. Both looped chains and dangling ends are network defects, whereas only bridges contribute to the network elasticity; it is difficult to achieve a majority of bridges in ABA systems.[28] It is therefore of interest to consider ABC triblock terpolymers, in which A and C are both hydrophobic, but mutually immiscible (Figure 1.3). In principle, the A and C endblocks can associate to form distinct micellar cores, resulting in the formation of a two compartment micellar network with exclusive B bridges.[59] This situation would lead to both improved gelation efficiency (*i.e.*, lower critical gelation concentration) and mechanical properties (*e.g.*, high ermodulus).

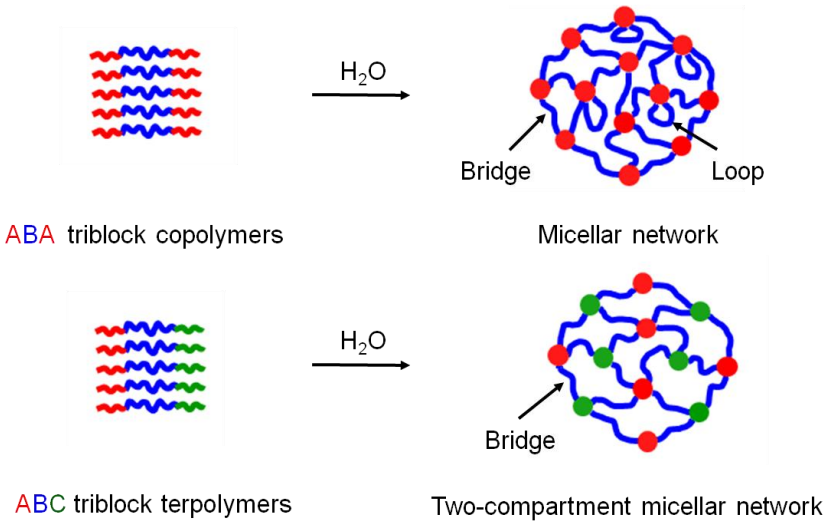


**Figure 1.3** Schematic illustration of gelation of ABA and ABC triblock polymers.

In prior work on ABC triblock terpolymers, Tsitsilianis and coworkers attempted to identify the differences between polystyrene-*b*-poly(sodium acrylate)-*b*-poly(*n*-butyl methacrylate) (PS-*b*-PANa-*b*-PnBMA) and PS-PANa-PS gels, but no clear conclusion was obtained.[60] Tew *et al.* reported that poly(methyl methacrylate)-*b*-poly [oligo(ethylene glycol)methyl methacrylate]-*b*-poly(3,3,4,4,5,5,6,6,7,7,8,8,9,9,10,10,10-heptadecafluorodecyl methacrylate) (PMMA-*b*- POEGMA-*b*-PFM) formed a hydrogel at a concentration above 29 wt%, whereas PMMA-b-POEGMA-*b*-PMMA did not gel at concentrations as high as 45 wt% polymer.[61] Reinicke and coworkers prepared pH and thermoresponsive hydrogels from poly(2-vinylpyridine)-*b*-poly(ethylene oxide)-*b*-poly (glycidyl methyl ether-*co*-ethyl glycidyl ether) (P2VP-*b*-PEO-*b*-P(GME-*co*-EGE)) triblock terpolymers at high polymer concentration (18 wt%), but gelation of the corresponding ABA copolymers was not studied.[62, 63] Armes *et al.* reported the mechanical response of thermoresponsive hydrogels from poly(propylene

oxide)-*b*-poly(2-methacryloyloxyethyl phosphorylcholine)-*b*-poly(*N*-isopropylacrylamide) (PPO-*b*-PMPC-*b*-PNIPAm) and PNIPAm-*b*-PMPC-*b*-PNIPAm, but remarkably they found that the gelation efficiency and mechanical properties of PNIPAm-*b*-PMPC-*b*-PNIPAm hydrogels were superior to PPO-*b*-PMPC-*b*-PNIPAm hydrogels, in conflict with our working hypothesis.[64] One possible explanation is the availability of rapid exchange of PPO chains between micelles.[65, 66] Conversely, Shen *et al.* demonstrated that looping was suppressed in hydrogels formed from a triblock protein with dissimilar end domains, leading to slightly better mechanical properties.[67] Thus, whether ABC triblock terpolymers are beneficial for hydrogel formation in comparison to ABA triblock copolymers remains an open question.

Towards this question, a thermoresponsive polymer with a lower critical solution temperature (LCST) could be introduced into the system to prepare the two-compartment micellar network (Figure 1.4). In this design, the triblock terpolymer has a long hydrophilic midblock B with a short hydrophobic endblock A and a thermoresponsive endblock C. When dispersed in water, the terpolymers form well-defined micelles with hydrophobic A cores surrounded by hydrophilic B-C coronae at low temperatures. These micelles associate to form a hydrogel upon heating above the LCST of the C block. The separation of micellization and gelation leads to the formation of a two-compartment network with exclusively bridging conformations for the midblocks. Therefore, gelation might be achieved at a much lower concentration, with improved mechanical properties, as compared to ABA copolymer hydrogels. As a thermoresponsive polymer will be incorporated into ABC triblock terpolymers to prepare the two-compartment network, I

will give the following introduction to the solution behavior of thermoresponsive copolymers.

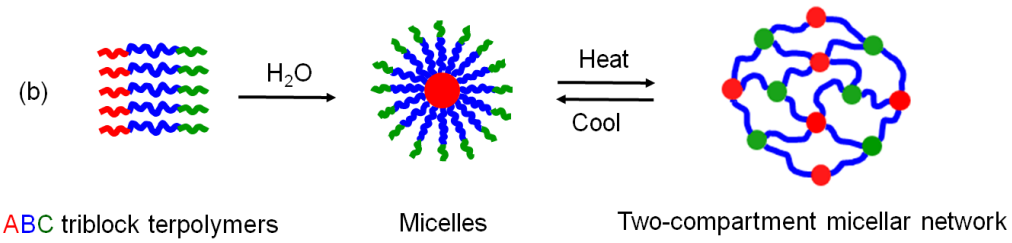


**Figure 1.4** Schematic illustration of gelation of thermoresponsive ABC terpolymers.

### 1.3 Thermoresponsive Copolymers

Block copolymers in which at least one block is a thermoresponsive polymer have attracted considerable interest in the area of self-assembled soft materials. They can show interesting properties such as thermoreversible aggregation and gelation, and have found use as biomaterials for drug delivery and tissue engineering applications.[68-71]

Poly(*N*-isopropylacrylamide) (PNIPAm), exhibiting a lower critical solution temperature (LCST) in water at *ca.* 32 ℃, has been extensively employed as a thermoresponsive block since its LCST is both close to body temperature and tunable by copolymerization with other monomers, and the transition is particularly sharp and nearly independent of polymer concentration.[72-77] In very dilute solutions, PNIPAm collapses into globules upon heating, while at higher concentrations a rather sharp precipitation occurs, as observed by a rapid onset of turbidity. These phenomena stem from segregation of PNIPAm from water as temperature increases, an entropically driven

process manifesting liberation of hydrophobically structured water and association of PNIPAm side chains.[78-82] The LCST of PNIPAm is affected by internal factors such as substituents,[75, 76] molar mass,[83, 84] end groups,[85] and external factors such as salts[83] and surfactants.[86] These factors can be explained by a balance between the hydrogen bonding between the amide groups and water, and hydrophobic interaction between isopropyl groups. Those factors that increase hydrophobic interactions decrease the LCST while those that increase hydrogen bonding increase the LCST. For example, poly(*N*-*tert*-butylacrylamide) (PtBAm) is insoluble at room temperature due to stronger hydrophobic interactions between *tert*-butyl groups, while poly(*N*,*N*-dimethylacrylamide) (PDMA) is soluble in the experimental temperature range due to the weaker hydrophobic interactions between methyl groups.[75, 76] Stover *et al.* studied the molar mass dependence of the LCST for PNIPAm prepared by atom transfer radical polymerization (ATRP). They reported a strong decrease of the phase transition temperature with increasing molecular weight (when the molecular weight increased from 2.8 to 26.5 kg/mol, the cloud point dropped from 43.0 ℃ to 33.3 ℃).[84] In addition, the LCST of PNIPAm increases if it is copolymerized with monomers that are more hydrophilic while it decreases if more hydrophobic monomers are copolymerized. For example, Pelton *et al.* prepared poly(*N*-isopropylacrylamide-*co*-acrylamide) (P(NIPAm-*co*-AAm)) copolymers by free radical polymerization and showed that the LCST increases with decreasing the mole fraction of NIPAm.[87] Another example is poly(*N*-isopropylacrylamide-*co*-vinyl laurate) (P(NIPAm-*co*-VL)) in which the incorporation of hydrophobic vinyl laurate leads to a lower LCST.[88]

There are typically two classes of PNIPAm-containing AB diblock copolymers reported in the literature. First, double hydrophilic block copolymers, in which PNIPAm is coupled to a hydrophilic block, can be dissolved in aqueous solution at low temperatures and form micelles with PNIPAm cores above the LCST of PNIPAm.[89-99] For example, using poly(ethylene oxide)-*b*- poly(*N*-isopropylacrylamide) (PEO-*b*-PNIPAm) AB diblock copolymers Zhang *et al.* reported the formation of spherical micelles at high PEO volume fractions,[95] and Qin *et al.* demonstrated that vesicles can be prepared using block copolymers with high PNIPAm volume fractions.[96] The other class is amphiphilic block copolymers in which PNIPAm is coupled to a hydrophobic block such as polystyrene (PS), poly(*n*-butylmethacrylate) (PBMA), poly(*D,L*-lactide) (PLA) or poly($\varepsilon$-caprolactone) (PCL).[100-108] These block copolymers can form micelles with hydrophobic cores and hydrophilic PNIPAm coronas below the LCST of PNIPAm. At higher temperatures the PNIPAm coronas collapse around the hydrophobic cores and this can induce micellar aggregation.

There have been a few reports on the incorporation of PNIPAm into ABC triblock terpolymers.[109-122] In these studies, PNIPAm has been used as the core, shell or corona block for micelle formation, and the possible thermo-induced structure changes are summarized in Figure 1.5. As shown in Figure 1.5a, triblock terpolymers with PNIPAm as the core block form micelles above the LCST of PNIPAm. For example, McCormick *et al.* showed that poly(ethylene oxide)-*b*-poly[(*N*,*N*-dimethylacrylamide)-*stat*-(*N*-acryloxysuccinimide)]-*b*-poly(*N*-isopropylacrylamide) (PEO-*b*-P(DMA-*stat*-NAS)-*b*-PNIPAm) formed micelles with PNIPAm cores above 37 ℃. In this particular case, the

shell of the micelle could be reversibly cross-linked to control subsequent drug delivery.[110] When PNIPAm is used as the shell block, the micelles can change into a different morphology such as cylindrical micelles or vesicles at higher temperatures when the hydrophobic core is very short, allowing for structural rearrangement (Figure 1.5b). Grubbs and coworkers reported that poly(ethylene oxide)-*b*-poly(*N*-isopropylacrylamide) -*b*-polyisoprene (PEO-*b*-PNIPAm-*b*-PI) formed spherical micelles with hydrophobic PI cores, PNIPAm shells and PEO coronas, and they transformed into large vesicles above the LCST due to the change in the hydrophobic/hydrophilic volume ratio.[116] It is also possible that the PNIPAm shell will collapse around the hydrophobic core above the LCST (Figure 1.5b). Shi *et al.* prepared core-shell-corona micelles with PNIPAm shells from poly(ethylene oxide)-*b*-poly(*N*-isopropylacrylamide)-*b*-polystyrene (PEO-*b*-PNIPAm-*b*-PS) and observed the collapse of PNIPAm chains above the LCST.[118] When PNIPAm is used as the corona block with PEO (or other hydrophilic) midblocks, the PNIPAm blocks might collapse around the hydrophobic core above the LCST to form "flower-like micelles" with the PEO on the exterior, or they could collapse around the hydrophilic shell to form a thin layer or sticky patches, resulting in a decrease of micelle size in very dilute solution (Figure 1.5c). For example, micelles with thermoresponsive PNIPAm coronas have been prepared from poly(2-(diethylamino)ethyl methacrylate)-*b*-poly(2-(dimethylamino) ethyl methacrylate)-*b*-poly(*N*-isopropylacrylamide) and poly(ε-caprolactone)-*b*-PEO-*b*-PNIPAm (PCL-*b*-PEO-*b*-PNIPAm).[120, 121] The collapse of PNIPAm coronas at temperatures above the LCST resulted in a decrease in micelle size. At higher concentrations, micelles with a thin layer or sticky patches of PNIPAm on the

exterior can associate to form larger aggregated structures. In addition, such micellar aggregation can lead to hydrogel formation in more concentrated solutions, and these ABC hydrogels are multicompartment networks with two types of domains capable of performing different functions, as discussed earlier.[29, 30] Therefore, it is interesting to investigate the solution behavior of triblock terpolymers with PNIPAm coronas.

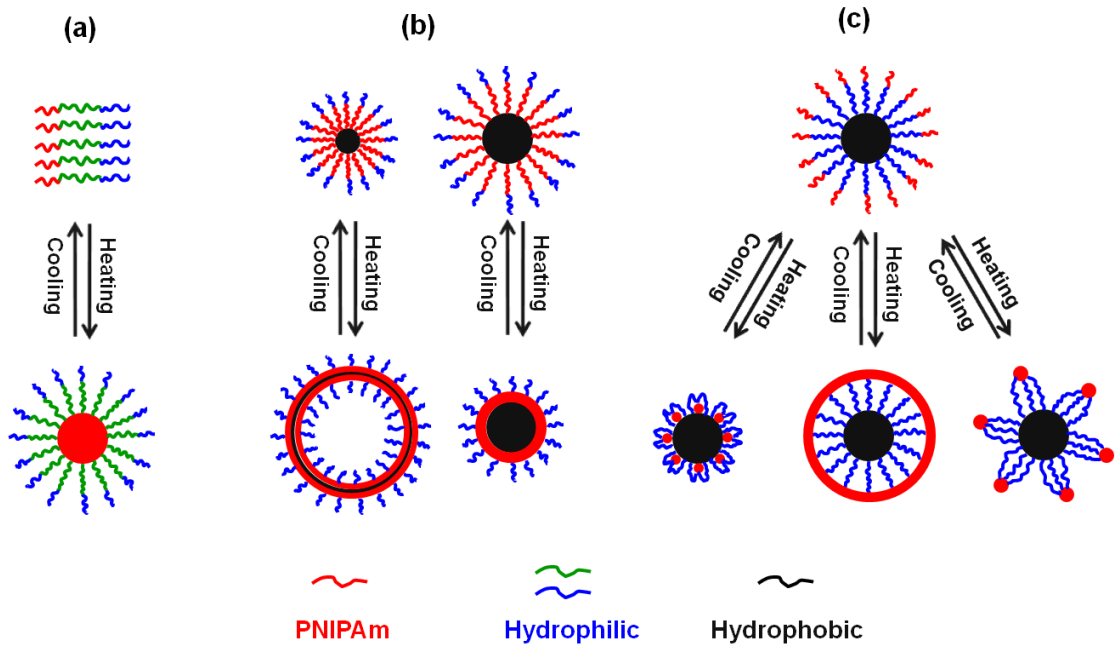


**Figure 1.5** Schematic illustration of the possible thermo-induced structure changes of PNIPAm-containing triblock terpolymer micelles with (a) PNIPAm as the core, (b) PNIPAm as the shell, (c) PNIPAm as the corona.

### 1.4 Research Motivation and Thesis Overview.

As discussed earlier, the incorporation of a thermoresponsive polymer into ABC triblock terpolymer with a long hydrophilic midblock B and a short hydrophobic

endblock A encourages a stepwise gelation involving micellization at room temperature and gelation at elevated temperatures. The separation of micellization and gelation leads to the formation of a two-compartment network. Based on this design, a poly(ethylene-*alt*-propylene)-*b*-poly(ethylene oxide)-*b*-poly(*N*-isopropylacrylamide) (PEP-*b*-PEO-*b*-PNIPAm, PON) triblock terpolymer was chosen as the model ABC triblock terpolymer (Scheme 1.1). The poly(ethylene-*alt*-propylene) (PEP/P) block, with a glass transition well below room temperature, high hydrophobicity, and a low molecular weight, was chosen as the hydrophobic core to mitigate kinetic complications of the micellization behavior associated with a glassy core.[123-127] Poly(ethylene oxide) (PEO/O) was chosen as the hydrophilic midblock due to its good water solubility at the temperatures of interest. Poly(*N*-isopropylacrylamide) (PNIPAm/N) was chosen as the thermoresponsive endblock due to the well-studied LCST phase behavior and sharp phase transition. Overall, my project focuses on the development and characterization of two-compartment networks from PON terpolymers in aqueous solutions.

**Scheme 1.1** Chemical structure of PON and NON triblock polymers.

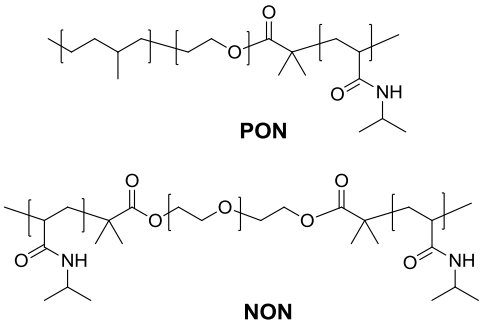

The thesis is organized as follows: Chapter 2 described the synthesis and aqueous self-assembly behavior of three PON triblock terpolymers with different block lengths of PNIPAm. These PON terpolymers were prepared using a combination of anionic and reversible addition-fragmentation chain transfer (RAFT) polymerizations, and their micellization and micellar aggregation behavior in dilute aqueous solutions were examined by DLS and cryo-TEM.

In Chapter 3. the hydrogel formation of PON terpolymers in more concentrated solutions was studied using rheology, differential scanning calorimetry, and variable-temperature $^{1}$H NMR spectroscopy. The comparison between PON hydrogels and the corresponding ABA hydrogels, poly(*N*-isopropylacrylamide)-*b*-poly(ethylene oxide)-*b*-poly(*N*-isopropylacrylamide) (PNIPAm- *b*-PEO-*b*-PNIPAm, NON) hydrogels (Figure 1.6), and the effect of polymer composition and concentration on gelation properties were investigated by oscillatory shear measurements.

The morphology of the aqueous solutions of PON triblock terpolymers was then characterized using a combination of cryogenic microscopy (cryo-SEM and cryo-TEM) and scattering (SANS) experiments. The detailed results were given in Chapter 4.

As for biomedical applications, it is desirable to have another stimulus such as pH to control the polymer self-assembly. In Chapter 5, two poly(ethylene-*alt*-propylene)-*b*-poly(ethylene oxide)-*b*-poly(*N*-isopropylacrylamide-*co*-acrylic acid) (PEP-*b*-PEO-*b*-P(NIPAm-*co*-AA), PO(N/A)) triblock terpolymers in which the PNIPAm block contains a small fraction of AA monomers were synthesized by a combination of anionic and RAFT polymerizations, followed by acid hydrolysis. The dual pH- and

temperature-sensitive self-assembly behavior in both dilute and concentrated aqueous solutions was systematically studied by DLS and rheology.

Finally, it would be interesting to explore the gelation properties of PON triblocks in other solvents besides water. Chapter 6 presented the study on viscoelastic properties of a PON terpolymer in two ionic liquids (1-ethyl-3-methylimidazolium bis(trifluoromethyl-sulfonyl)amide ([EMI][TFSA]) and 1-butyl-3-methylimidazolium tetrafluoroborate ([BMI][$BF_4$])), and the comparison between the PON and NON ion gels.

Chapter 7 is a summary of my thesis project along with the outlook on further work of thermoresponsive ABC hydrogels.

## 1.5 References


1. Ringsdorf, H.; Lehmann, P.; Weberskirch, R. *Book of Abstracts*, 217th National Meeting of the American Chemical Society, Anaheim, CA, March 221-225, 1999.
2. Laschewsky, A. *Curr. Opin. Colloid Interface Sci.* **2003**, *8*, 274-281.
3. Lutz, J. F.; Laschewsky, A. *Macromol. Chem. Phys* **2005**, *206*, 813-817.
4. Lodge, T. P.; Rasdal, A.; Li, Z.; Hillmyer, M. A. *J. Am. Chem. Soc.* **2005**, *127*, 17608-17609.
5. Zhou, Z.; Li, Z.; Ren, Y.; Hillmyer, M. A.; Lodge, T. P. *J. Am. Chem. Soc.* **2003**, *125*, 10182-10183.
6. Lodge, T. P.; Hillmyer, M. A.; Zhou, Z.; Talmon, Y. *Macromolecules* **2004**, *37*, 6680-6682.

7. Li, Z.; Kesselman, E.; Talmon, Y.; Hillmyer, M. A.; Lodge, T. P. *Science* **2004**, *306*, 98-101.
8. Lodge, T. P.; Bang, J. A.; Li, Z.; Hillmyer, M. A.; Talmon, Y. *Faraday Discuss.* **2005**, *128*, 1-12.
9. Gohy, J. F. *Adv. Polym. Sci.* **2005**, *190*, 65-136.
10. Rodriguez-Hernandez, J.; Checot, F.; Gnanou, Y.; Lecommandoux, S. *Prog. Polym. Sci.* **2005**, *30*, 691-724.
11. Bang, J.; Jain, S. M.; Li, Z.; Lodge, T. P.; Pedersen, J. S.; Kesselman, E.; Talmon, Y. *Macromolecules* **2006**, *39*, 1199-1208.
12. Abbas, S.; Li, Z.; Hassan, H.; Lodge, T. P. *Macromolecules* **2007**, *40*, 4048-4052.
13. Shen, H.; Zhang, L.; Eisenberg, A. *J. Am. Chem. Soc.* **1999**, *121*, 2728-2740.
14. Won, Y. Y.; Brannan, A. K.; Davis, H. T.; Bates, F. S. *J. Phys. Chem. B* **2002**, *106*, 3354-3364.
15. Jain, S.; Bates, F. S. *Science* **2003**, *300*, 460-464.
16. He, Y.; Li, Z.; Simone, P.; Lodge, T. P. *J. Am. Chem. Soc.* **2006**, *128*, 2745-2750.
17. Moughton, A. O.; Hillmyer, M. A.; Lodge, T. P. *Macromolecules* **2012**, *45*, 2-19.
18. Kubowicz, S.; Baussard, J. F.; Lutz, J. F.; Thunemann, A. F.; von Berlepsch, H.; Laschewsky, A. *Angew. Chem., Int. Ed.* **2005**, *44*, 5262-5265.
19. Von Berlepsch, H.; Bottcher, C.; Skrabania, K.; Laschewsky, A. *Chem. Commun.* **2009**, 2290-2292.
20. Zhu, J.; Jiang, W. *Macromolecules* **2005**, *38*, 9315-9323.
21. Fang, B.; Walther, A.; Wolf, A.; Xu, Y.; Yuan, J.; Muller, A. H. E. *Angew. Chem., Int.*

*Ed.* **2009**, *48*, 2877-2880.

22. Li, Z.; Hillmyer, M. A.; Lodge, T. P. *Macromolecules* **2004**, *37*, 8933-8940.
23. Li, Z.; Hillmyer, M. A.; Lodge, T. P. *Nano Lett.* **2006**, *6*, 1245-1249.
24. Li, Z.; Hillmyer, M. A.; Lodge, T. P. *Langmuir* **2006**, *22*, 9409-9417.
25. Saito, N.; Liu, C.; Lodge, T. P.; Hillmyer, M. A. *Macromolecules* **2008**, *41*, 8815-8822.
26. Weberskirch, R.; Preuschen, J.; Spiess, H. W.; Nuyken, O. *Macromol. Chem. Phys* **2000**, *201*, 995-1007.
27. Komenda, T.; Luedtke, K.; Jordan, R.; Ivanova, R.; Bonne, T. B.; Papadakis, C. M. *Polym. Prepr. (Am. Chem. Soc., Div. Polym. Chem.)* **2006**, *47*, 763-764.
28. Yamaguchi, D.; Cloitre, M.; Panine, P.; Leibler, L. *Macromolecules* **2005**, *38*, 7798-7806.
29. Taribagil, R. R.; Hillmyer, M. A.; Lodge, T. P. *Macromolecules* **2009**, *42*, 1796-1800.
30. Taribagil, R. R.; Hillmyer, M. A.; Lodge, T. P. *Macromolecules* **2010**, *43*, 5396-5404.
31. Patrickios, C. S.; Georgiou, T. K. *Curr. Opin. Colloid Interface Sci.* **2003**, *8*, 76-85.
32. Hoffman, A. S. *Adv. Drug Deliv. Rev.* **2002**, *54*, 3-12.
33. Peppas, N. A.; Hilt, J. Z.; Khademhosseini, A.; Langer, R. *Adv. Mater.* **2006**, *18*, 1345-1360.
34. Lin, C.; Metters, A. T. *Adv. Drug Deliv. Rev.* **2006**, *58*, 1379-1408.
35. Kopecek, J. *Biomaterials* **2007**, *28*, 5185-5192.
36. Hendrickson, G. R.; Lyon, L. A. *Soft Matter* **2009**, *5*, 29-35.
37. Calvert, P. *Adv. Mater.* **2009**, *21*, 743-756.

38. Jeong, B.; Kim, S. W.; Bae, Y. H. *Adv. Drug Deliv. Rev.* **2002**, *54*, 37-51.

39. Yu, L.; Ding, J. *Chem. Soc. Rev.* **2008**, *37*, 1473-1481.

40. He, C.; Kim, S. W.; Lee, D. S. *J. Controlled Release* **2008**, *127*, 189-207.

41. Annable, T.; Buscall, R.; Ettelaie, R.; Whittlestone, D. *J. Rheol.* **1993**, *37*, 695-726.

42. Tae, G.; Kornfield, J. A.; Hubbell, J. A.; Johannsmann, D.; Hogen-Esch, T. E. *Macromolecules* **2001**, *34*, 6409-6419.

43. Ricardo, N. M. P. S.; Honorato, S. B.; Yang, Z.; Castelletto, V.; Hamley, I. W.; Yuan, X. F.; Attwood, D.; Booth, C. *Langmuir* **2004**, *20*, 4272-4278.

44. Zhang, H.; Yu, L.; Ding, J. *Macromolecules* **2008**, *41*, 6493-6499.

45. Li, C.; Tang, Y.; Armes, S. P.; Morris, C. J.; Rose, S. F.; Lloyd, A. W.; Lewis, A. L. *Biomacromolecules* **2005**, *6*, 994-999.

46. Kirkland, S. E.; Hensarling, R. M.; McConaughy, S. D.; Guo, Y.; Jarrett, W. L.; McCormick, C. L. *Biomacromolecules* **2008**, *9*, 481-486.

47. Ge, Z.; Zhou, Y.; Tong, Z.; Liu, S. *Langmuir* **2011**, *27*, 1143-1151.

48. O'Lenick, T. G.; Jin, N.; Woodcock, J. W.; Zhao, B. *J. Phys. Chem. B* **2011**, *115*, 2870-2881.

49. Balsara, N. P.; Tirrell, M.; Lodge, T. P. *Macromolecules* **1991**, *24*, 1975-1986.

50. Xu, B.; Li, L.; Yekta, A.; Masoumi, Z.; Kanagalingam, S.; Winnik, M. A.; Zhang, K.; Macdonald, P. M. *Langmuir* **1997**, *13*, 2447-2456.

51. Kelarakis, A.; Yuan, X.; Mai, S.; Yang, Y.; Booth, C. *Phys. Chem. Chem. Phys.* **2003**, *5*, 2628-2634.

52. Kelarakis, A.; Havredaki, V.; Yuan, X.; Chaibundit, C.; Booth, C. *Macromol. Chem.*

*Phys* **2006**, *207*, 903-909.

53. Green, M. S.; Tobolsky, A. V. *J. Chem. Phys.* **1946**, *14*, 80-92.
54. Tanaka, F.; Edwards, S. F. *Macromolecules* **1992**, *25*, 1516-1523.
55. Inomata, K.; Nakanishi, D.; Banno, A.; Nakanishi, E.; Abe, Y.; Kurihara, R.; Fujimoto, K.; Nose, T. *Polymer* **2003**, *44*, 5303-5310.
56. Seitz, M. E.; Burghardt, W. R.; Faber, K. T.; Shull, K. R. *Macromolecules* **2007**, *40*, 1218-1226.
57. Chambon, F.; Petrovic, Z. S.; Macknight, W. J.; Winter, H. H. *Macromolecules* **1986**, *19*, 2146-2149.
58. Winter, H. H.; Chambon, F. *J. Rheol.* **1986**, *30*, 367-382.
59. Hillmyer, M. A.; Lodge, T. P. *J. Polym. Sci., Part A: Polym. Chem.* **2002**, *40*, 1-8.
60. Tsitsilianis, C.; Katsampas, I.; Sfika, V. *Macromolecules* **2000**, *33*, 9054-9059.
61. Shunmugam, R.; Smith, C. E.; Tew, G. N. *J. Polym. Sci., Part A: Polym. Chem.* **2007**, *45*, 2601-2608.
62. Reinicke, S.; Schmelz, J.; Lapp, A.; Karg, M.; Hellweg, T.; Schmalz, H. *Soft Matter* **2009**, *5*, 2648-2657.
63. Reinicke, S.; Schmalz, H. *Colloid Polym. Sci.* **2011**, *289*, 497-512.
64. Li, C.; Buurma, N. J.; Haq, I.; Turner, C.; Armes, S. P.; Castelletto, V.; Hamley, I. W.; Lewis, A. L. *Langmuir* **2005**, *21*, 11026-11033.
65. Zana, R.; Marques, C.; Johner, A. *adv. Colloid Interface Sci.* **2006**, *123*, 345-351.
66. Kadam, V.; Nicolai, T.; Nicol, E.; Benyahia, L. *Macromolecules* **2011**, *44*, 8225-8232.

67. Shen, W.; Zhang, K.; Kornfield, J. A.; Tirrell, D. A. *Nat. Mater.* **2006**, *5*, 153-158.

68. McCormick, C. L.; Sumerlin, B. S.; Lokitz, B. S.; Stempka, J. E. *Soft Matter* **2008**, *4*, 1760-1773.

69. York, A. W.; Kirkland, S. E.; McCormick, C. L. *Adv. Drug Deliv. Rev.* **2008**, *60*, 1018-1036.

70. Xu, J.; Liu, S. *Soft Matter* **2008**, *4*, 1745-1749.

71. Liu, R.; Fraylich, M.; Saunders, B. R. *Colloid Polym. Sci.* **2009**, *287*, 627-643.

72. Heskins, M.; Guillet, J. E. *J. Macromol. Sci. Chem.* **1968**, *A2*, 1441-1455.

73. Schild, H. G. *Prog. Polym. Sci.* **1992**, *17*, 163-249.

74. Wu, C.; Wang, X. *Phys. Rev. Lett.* **1998**, *80*, 4092-4094.

75. Liu, H.; Zhu, X. *Polymer* **1999**, *40*, 6985-6990.

76. Cao, Y.; Zhu, X.; Luo, J.; Liu, H. *Macromolecules* **2007**, *40*, 6481-6488.

77. Fujishige, S.; Kubota, K.; Ando, I. *J. Phys. Chem.* **1989**, *93*, 3311-3313.

78. Winnik, F. M. *Macromolecules* **1990**, *23*, 233-242.

79. Shibayama, M.; Morimoto, M.; Nomura, S. *Macromolecules* **1994**, *27*, 5060-5066.

80. Maeda, Y.; Higuchi, T.; Ikeda, I. *Langmuir* **2000**, *16*, 7503-7509.

81. Kogure, H.; Nanami, S.; Masuda, Y.; Toyama, Y.; Kubota, K. *Colloid Polym. Sci.* **2005**, *283*, 1163-1171.

82. Ono, Y.; Shikata, T. *J. Am. Chem. Soc.* **2006**, *128*, 10030-10031.

83. Schild, H. G.; Tirrell, D. A. *J. Phys. Chem.* **1990**, *94*, 4352-4356.

84. Xia, Y.; Yin, X.; Burke, N. A. D.; Stover, H. D. H. *Macromolecules* **2005**, *38*, 5937-5943.

85. Xia, Y.; Burke, N. A. D.; Stover, H. D. H. *Macromolecules* **2006**, *39*, 2275-2283.

86. Cho, C. S.; Jung, J. H.; Sung, Y. K.; Lee, Y. M. *Macromol. Rapid Commun.* **1994**, *15*, 727-732.

87. Zhang, J.; Pelton, R. *J. Polym. Sci., Part A: Polym. Chem.* **1999**, *37*, 2137-2143.

88. Cao, Z.; Liu, W.; Gao, P.; Yao, K.; Li, H.; Wang, G. *Polymer* **2005**, *46*, 5268-5277.

89. Topp, M. D. C.; Dijkstra, P. J.; Talsma, H.; Feijen, J. *Macromolecules* **1997**, *30*, 8518-8520.

90. Zhu, P.; Napper, D. H. *Macromolecules* **1999**, *32*, 2068-2070.

91. Zhu, P.; Napper, D. H. *Langmuir* **2000**, *16*, 8543-8545.

92. Hong, C.; You, Y.; Pan, C. *J. Polym. Sci., Part A: Polym. Chem.* **2004**, *42*, 4873-4881.

93. Virtanen, J.; Holappa, S.; Lemmetyinen, H.; Tenhu, H. *Macromolecules* **2002**, *35*, 4763-4769.

94. Motokawa, R.; Morishita, K.; Koizumi, S.; Nakahira, T.; Annaka, M. *Macromolecules* **2005**, *38*, 5748-5760.

95. Zhang, W.; Shi, L.; Wu, K.; An, Y. *Macromolecules* **2005**, *38*, 5743-5747.

96. Qin, S.; Geng, Y.; Discher, D. E.; Yang, S. *Adv. Mater.* **2006**, *18*, 2905-2909.

97. Yan, J.; Ji, W.; Chen, E.; Li, Z.; Liang, D. *Macromolecules* **2008**, *41*, 4908-4913.

98. Mei, A.; Guo, X.; Ding, Y.; Zhang, X.; Xu, J.; Fan, Z.; Du, B. *Macromolecules* **2010**, *43*, 7312-7320.

99. Convertine, A. J.; Lokitz, B. S.; Vasileva, Y.; Myrick, L. J.; Scales, C. W.; Lowe, A. B.; McCormick, C. L. *Macromolecules* **2006**, *39*, 1724-1730.

100. Cammas, S.; Suzuki, K.; Sone, C.; Sakurai, Y.; Kataoka, K.; Okano, T. *J. Controlled Release* **1997**, *48*, 157-164.

101. Chung, J. E.; Yokoyama, M.; Aoyagi, T.; Sakurai, Y.; Okano, T. *J. Controlled Release* **1998**, *53*, 119-130.

102. Chung, J. E.; Yokoyama, M.; Yamato, M.; Aoyagi, T.; Sakurai, Y.; Okano, T. *J. Controlled Release* **1999**, *62*, 115-127.

103. Chung, J. E.; Yokoyama, M.; Okano, T. *J. Controlled Release* **2000**, *65*, 93-103.

104. Kohori, F.; Sakai, K.; Aoyagi, T.; Yokoyama, M.; Sakurai, Y.; Okano, T. *J. Controlled Release* **1998**, *55*, 87-98.

105. Nakayama, M.; Okano, T.; Miyazaki, T.; Kohori, F.; Sakai, K.; Yokoyama, M. *J. Controlled Release* **2006**, *115*, 46-56.

106. Nakayama, M.; Okano, T. *Macromolecules* **2008**, *41*, 504-507.

107. Nuopponen, M.; Ojala, J.; Tenhu, H. *Polymer* **2004**, *45*, 3643-3650.

108. Wei, H.; Zhang, X.; Zhou, Y.; Cheng, S.; Zhuo, R. *Biomaterials* **2006**, *27*, 2028-2034.

109. Patrickios, C. S.; Forder, C.; Armes, S. P.; Billingham, N. C. *J. Polym. Sci., Part A: Polym. Chem.* **1997**, *35*, 1181-1195.

110. Li, Y.; Lokitz, B. S.; Armes, S. P.; McCormick, C. L. *Macromolecules* **2006**, *39*, 2726-2728.

111. Li, Y.; Lokitz, B. S.; McCormick, C. L. *Macromolecules* **2006**, *39*, 81-89.

112. Lokitz, B. S.; Convertine, A. J.; Ezell, R. G.; Heidenreich, A.; Li, Y.; McCormick, C. L. *Macromolecules* **2006**, *39*, 8594-8602.

113. Zhang, W. Q.; Shi, L. Q.; Ma, R. J.; An, Y. L.; Xu, Y. L.; Wu, K. *Macromolecules* **2005**, *38*, 8850-8852.

114. Xu, X.; Liu, C.; Huang, J. *J. Appl. Polym. Sci.* **2008**, *108*, 2180-2188.

115. Xu, H.; Meng, F.; Zhong, Z. *J. Mater. Chem.* **2009**, *19*, 4183-4190.

116. Sundararaman, A.; Stephan, T.; Grubbs, R. B. *J. Am. Chem. Soc.* **2008**, *130*, 12264-+.

117. Lin, S.; Fuchise, K.; Chen, Y.; Sakai, R.; Satoh, T.; Kakuchi, T.; Chen, W. *Soft Matter* **2009**, *5*, 3761-3770.

118. Zhang, W.; Jiang, X.; He, Z.; Xiong, D.; Zheng, P.; An, Y.; Shi, L. *Polymer* **2006**, *47*, 8203-8209.

119. Cheng, C.; Wei, H.; Zhu, J.; Chang, C.; Cheng, H.; Li, C.; Cheng, S.; Zhang, X.; Zhuo, R. *Bioconjugate Chem.* **2008**, *19*, 1194-1201.

120. Jiang, X.; Ge, Z.; Xu, J.; Liu, H.; Liu, S. *Biomacromolecules* **2007**, *8*, 3184-3192.

121. Sun, P.; Zhang, Y.; Shi, L.; Gan, Z. *Macromol. Biosci.* **2010**, *10*, 621-631.

122. Qu, T.; Wang, A.; Yuan, J.; Gao, Q. *J. Colloid Interface Sci.* **2009**, *336*, 865-871.

123. Song, J.; Bringuier, A.; Kobayashi, S.; Baker, A. M.; Macosko, C. W. *Polym. J.* **2012**, *44*, 939-945.

124. Kobayashi, S.; Song, J.; Silvis, H. C.; Macosko, C. W.; Hillmyer, M. A. *Ind. Eng. Chem. Res.* **2011**, *50*, 3274-3279.

125. Song, J.; Ewoldt, R. H.; Hu, W.; Silvis, H. C.; Macosko, C. W. *AlChE J.* **2011**, *57*, 3496-3506.

126. Song, J.; Baker, A. M.; Macosko, C. W.; Ewoldt, R. H. *AlChE J.* **2013**, *59*, 3391-3402.

127. Song, J.; Thurber, C. M.; Kobayashi, S.; Baker, A. M.; Macosko, C. W.; Silvis, H. C. *Polymer* **2012**, *53*, 3636-3641.

# Chapter 2

# Micellization and Micellar Aggregation of PON Triblock Terpolymers in Water*

## 2.1 Introduction

The development of multicompartment gels from thermoresponsive ABC triblock terpolymers draws inspiration from mimicking the structural intricacy of biological entities such as eukaryotic cells.[1-3] We also aim to design novel ABC gels with much better gelation efficiency and mechanical properties in comparison to ABA gels.[4] For this purpose, a poly(ethylene-*alt*-propylene)-*b*-poly(ethylene oxide)-*b*-poly(*N*-isopropyl-acrylamide) (PEP-*b*-PEO-*b*-PNIPAm, PON) triblock terpolymer with a long hydrophilic midblock B (PEO), a short hydrophobic endblock A (PEP) and a short thermoresponsive endblock C (PNIPAm) was chosen as a model system to construct multicompartment micellar networks. To better understand the gelation properties of PON triblock terpolymers in concentrated solutions, it is necessary to study their micellization properties in dilute solution to illustrate the general principles governing self-assembly of PON triblock terpolymers in water.

In this chapter, we report the micellization and micellar aggregation behavior of

---

* This chapter is reproduced in part with permission from Zhou, C.; Hillmyer, M. A.; Lodge, T. P. *Macromolecules* **2011**, *44*, 1635-1641.

PON triblock terpolymers in dilute aqueous solutions. We will describe the synthesis and aqueous self-assembly of PON triblock terpolymers with different block lengths of PNIPAm, and focus on the effect of a PNIPAm endblock on the micellization and micellar aggregation properties.[5]

## 2.2 Experimental Section

### 2.2.1 Materials

All reagents were used as received unless otherwise noted. Isoprene was purchased from Aldrich and purified with *n*-butyllithium twice. Ethylene oxide was obtained from Aldrich and purified with n-butylmagnesium chloride twice. *sec*-Butyllithium (1.4 M in cyclohexane) was used as received. $Pd/CaCO_3$ catalyst (5 wt% Pd, Aldrich) was used as received. Cyclohexane and toluene were passed through two columns of activated alumina and a supported copper catalyst. Tetrahydrofuran (THF) was purified by passing through a column packed with molecular sieves. Dichloromethane ($CH_2Cl_2$) was purified on a MBraun solvent purification system. 2,2'-Azobisisobutyronitrile (AIBN) and *N*-isopropylacrylamide (NIPAm) were purchased from Aldrich and purified by recrystallization from methanol and benzene/*n*-hexane (65/35 v/v), respectively. The chain transfer agent (CTA), *S*-1-docecyl-*S'*-($\alpha,\alpha'$-dimethyl-$\alpha''$-acetic acid) trithiocarbonate, was synthesized following a reported procedure.[6] Methyl acrylate was obtained from Aldrich and passed through a basic alumina column prior to use.

### 2.2.2 Synthesis of PON Triblock Terpolymers

The PON triblock terpolymers were prepared using a combination of anionic and

reversible addition-fragmentation chain transfer (RAFT) polymerizations (Scheme 2.1).

**Scheme 2.1** Synthesis of PON triblock terpolymers

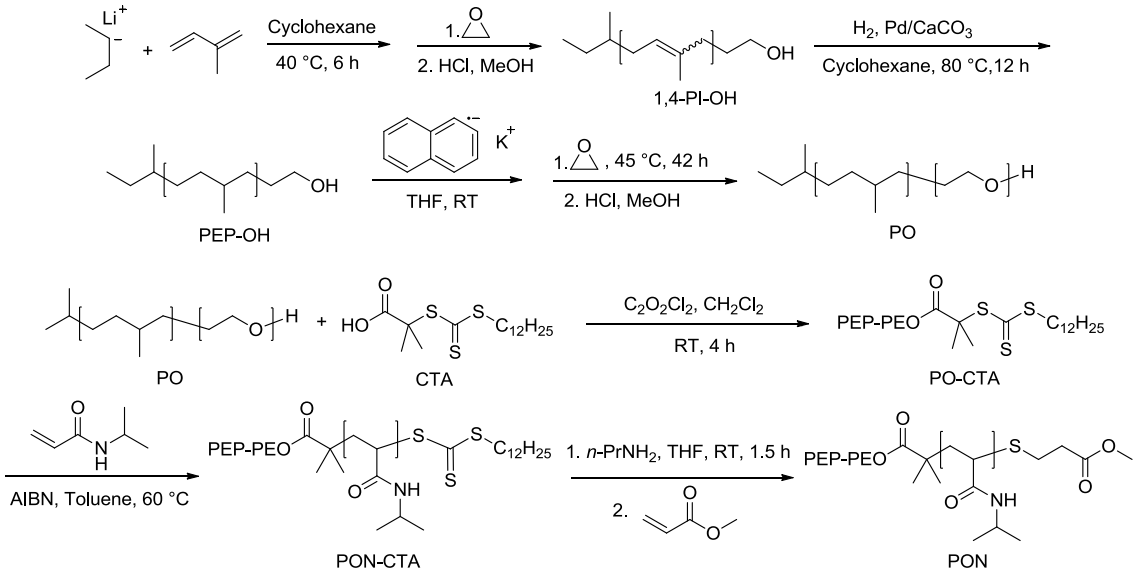


A poly(ethylene-*alt*-propylene)-*b*-poly(ethylene oxide) (PO) diblock copolymer was synthesized by a two-step anionic polymerization following a reported procedure.[7, 8] The first step involve the preparation of hydroxyl-terminated 1,4-polyisoprene (1,4-PI-OH). The polymerization was performed in a 2 L round-bottom glass reactor equipped with 5 ACE-THREADS connectors and a glass-coated magnetic stir bar. The reactor was flame-dried under vacuum to remove residual moisture, followed by 5 vacuum-Ar refill cycles to remove air. After that, the Ar pressure in the reactor was kept constant at a pressure 5 psi higher than atmosphere pressure to maintain the oxygen/water-free environment. Cyclohexane (1 L) and *sec*-butyllithium (9.10 mL, 11.8 mmol) were sequentially added to the reactor, followed by the addition of isoprene (35.36 g, 0.519 mol) at room temperature. The reaction mixture was heated to 45 ℃ and stirred for 6 h,

after which ethylene oxide (24 g, 0.545 mol) was added at 0 ℃. The solution was stirred at room temperature overnight before being quenched with 5 mL of degassed acidic methanol (2 mL HCl in 25 mL methanol). The crude product solution was washed with 100 mL distilled water six times, and cyclohexane was removed by rotary distillation. The resulting viscous liquid was dried under vacuum at 40 ℃ for two days to afford the final product. 1,4-PI-OH was hydrogenated to give the corresponding hydroxyl-terminated poly(ethylene-*alt*-propylene) (PEP-OH). Hydrogenation was performed in a 250 mL high-pressure stainless-steel reactor equipped with a mechanical stir bar and heating band. The $Pd/BaCO_3$ catalyst (5.57 g) was added to the reactor, and activated at 100 ℃ under 120 psi of hydrogen for at least 1 hour. The degassed polymer solution (11 g 1,4-PI-OH in 175 mL cyclohexane, 3.5 mmol) and $H_2$ (500 psi) were then introduced, and the reaction mixture was stirred at 80 ℃ for 12 hours. The catalyst and cyclohexane were removed by filtration and rotary distillation, respectively. The resulting polymer was dried under vacuum at 60 ℃ for 2 days. Next, PEP-OH served as a macroinitiator to prepare a hydroxyl-terminated poly(ethylene-*alt*-propylene)-*b*-poly(ethylene oxide) (PO) diblock copolymer. The polymerization was carried out in a 2L glass reactor under inert atmosphere. PEP-OH (7.0 g, 2.2 mmol, dissolved in THF) and THF (1 L) were added to the reactor and titrated with potassium naphthalenide solution (1.21 g potassium and 3.97 g naphthalene in 90 mL THF) until a light green solution persisted for at least 30 min at room temperature. Ethylene oxide (58.3 g, 1.33 mol) was then introduced at 0 ℃, and the solution was heated to 45 ℃ and stirred for 2 days. The reaction was terminated with degassed acidic methanol and the product was precipitated in acetone three times at –78 ℃ and dried under vacuum at 60 ℃ for 2 days.

The PON triblock terpolymers (PON-CTAs) were synthesized by RAFT polymerization from the PO diblock copolymer.[9] The first step was the preparation of the PO-CTA macroinitiator. CTA (1.3 g, 3.6 mmol) was mixed with excess oxalyl chloride (3.2 mL, 37 mmol) in dry $CH_2Cl_2$ (20 mL) under nitrogen atmosphere and stirred at room temperature for 4 h, after which $CH_2Cl_2$ and excess oxalyl chloride were removed under vacuum. PO (10.1 g in 80 mL $CH_2Cl_2$, 0.36 mmol) was then introduced and the reaction mixture was stirred at room temperature for 24 hours. The polymer was precipitated in acetone at –78 ℃ once and in pentane twice, and dried in a vacuum oven at 50 ℃ overnight. In a representative synthesis towards PON-CTA, PO-CTA macroinitiator (3.0 g, 0.11 mmol), NIPAm (3.2 g, 0.028 mol) and AIBN (2 mg, 0.011 mmol) were dissolved in toluene (30 mL), degassed by three freeze-pump-thaw cycles and reacted at 60 ℃ for 4 h. After that the reaction was quenched by cooling to 0 ℃. The solution was diluted with $CH_2Cl_2$ and precipitated in pentane three times. The resulting polymer was dried under vacuum oven at 50 ℃ overnight. Products with different PNIPAm block lengths were achieved by controlling the reaction time and the amount of NIPAm added.

The trithiocarbonate end groups of PON-CTAs were removed by aminolysis and Michael addition.[10] A typical procedure is briefly described as follows. PON-CTA (1.5 g, 0.04 mmol), *n*-propylamine (0.1 g, 2 mmol) and tris(2-carboxyethyl) phosphine hydrochloride (11 mg, 0.04 mmol) was dissolved in THF (15 mL). The reaction mixture was stirred at room temperature for 1.5 h under a nitrogen atmosphere. Methyl acrylate (0.6 mL, 7 mmol) was added to the reaction solution and stirred for 36 h. Most of the THF was removed under vacuum. The residual mixture was diluted with $CH_2Cl_2$ (15 mL) and precipitated three times in pentane. The resulting product was dried under vacuum

oven at 50 ℃ overnight.

### 2.2.3 Characterization

$^{1}$H NMR spectra were recorded on a Varian Inova 500 MHz spectrometer at room temperature with $CDCl_3$ as the solvent. SEC was performed on a Waters 150C ALC/GPC equipped with three Phenogel (Phenomenex) columns with pore sizes of $10^3$, $10^4$, and $10^5$ Å, a Wyatt DAWN multiangle light-scattering detector and a Wyatt OPTILAB rEX refractive index detector. THF containing 1 % tetramethylethylenediamine by volume was used as the eluent at a flow rate of 1.0 mL/min.

### 2.2.4 Solution Preparation

The 0.5 wt% PO and PON micelle solutions were prepared by two different protocols: thin-film hydration (TF) and dialysis (DI). In the thin-film hydration protocol, appropriate amounts of bulk polymer were dissolved in $CH_2Cl_2$, followed by evaporation of the solvent to yield a thin film on the walls of the vial. The thin film was then hydrated, and the resulting mixture was stirred at room temperature for at least 2 weeks before further characterization. In the dialysis procedure, the bulk polymer was dissolved in THF, and then dialyzed against water. Water was changed twice a day for 5 days. After dialysis, the micelle solution was stirred at room temperature for at least 1 week prior to further analysis. The concentration of PON micelle solutions was varied from 0.005 to 0.5 wt %. The lower concentration samples were made by dilution of a 0.5 wt % solution with water prepared through the above-mentioned TF or DI procedure.

### 2.2.5 Cloud Point Measurements

Cloud points were determined by optical transmittance measurements at 632.8 nm at a heating rate of roughly 1 ℃/min. The temperature dependence of transmittance was monitored using a laser power detector while the solution was stirred in a temperature-controlled oil bath.

### 2.2.6 Dynamic Light Scattering (DLS)

The micellization and micellar aggregation of the PO diblock and PON triblock terpolymers were investigated by DLS. The solutions were passed through 0.45 $\mu$m filters into glass tubes with a diameter of 0.25 inch. DLS measurements were carried out using a home-built photometer equipped with an electrically heated silicon oil bath, a Lexel 75 Ar+ laser operating at 488 nm, a Brookhaven BI-DS photomultiplier, and a Brookhaven BI-9000 correlator. Experiments were performed at various temperatures from 25 to 60 ℃, and the intensity correlation functions $g_2(t)$ were recorded at three scattering angles between 60 ° and 120 °. The squared electric field correlation functions $g_1^2(t)$ were calculated from $g_2(t)$ according to Siegert relation $g_2(\mathrm{t}) = 1 + \beta g_1^2(t)$. The cumulant method was used to fit $g_1^2(t)$ to extract the average decay rate $\Gamma$.

$$g_1^2(t) = A\exp(-2\Gamma \cdot t)(1+\frac{\mu_2}{2!}t^2 - \frac{\mu_3}{3!}t^3 + \cdots)^2 \qquad (2\text{-}1)$$

The mutual diffusion coefficient $D_\mathrm{m}$ was determined by linear regression of $\Gamma$ vs $q^2$ according to the relation $D_\mathrm{m} = \Gamma/q^2$, where $q$ is the scattering vector ($q = 4\pi n/\lambda \sin(\theta/2)$, $n$ is the refractive index of the solution, $\lambda$ is the laser wavelength, and $\theta$ is the scattering angle). Then, the hydrodynamic radius ($R_\mathrm{h}$) was determined by using the Stoke-Einstein

equation:

$$R_h = \frac{k_B T}{6\pi\eta_s D_m} \tag{2-2}$$

The estimated uncertainty of $R_h$ is ±5 %. The size distribution could be estimated by the reduced second cumulant ($\mu_2/\Gamma^2$), which is a measure of the width of the decay rate distribution (assuming it is monomodal). The hydrodynamic radius distribution could also be extracted from the decay rate distribution generated through the inverse Laplace transform program REPES.[11]

### 2.2.7 Cryogenic Transmission Electron Microscopy (Cryo-TEM)

Cryo-TEM samples were prepared in a controlled environment vitrification system (CEVS) at room temperature.[12] A micropipet was used to load a drop of micelle solution (ca. 5 $\mu$L) onto a lacey Formvar carbon-supported TEM grid. The excess solution was blotted with a piece of filter paper, resulting in the formation of thin films with thicknesses of ca. 100–300 nm in the mesh holes. After at least 20 s was allowed for relaxation of any stresses induced during the blotting, the samples were quickly plunged into a reservoir of liquid ethane cooled by liquid nitrogen. The vitrified samples were then stored in liquid nitrogen until they were transferred to a cryogenic sample holder (Gatan 626) and examined with a JEOL 1210 TEM instrument operated at an acceleration voltage of 120 kV at about –178 ℃. The phase contrast was enhanced by acquiring images at a nominal underfocus of 6–15 $\mu$m. Images were recorded on a Gatan 724 multiscan CCD camera and processed with DigitalMicrograph, version 3.3.1. More than 50 micelles were measured to obtain the average diameter. The mean aggregation number

was calculated using the following equation:

$$p = \frac{\rho_{\text{PEP}} \times \frac{4}{3}\pi(d/2)^3 \times N_A}{M_{\text{PEP}}} \quad (2\text{-}3)$$

where $\rho$ is the polymer density, $d$ is the diameter of the micelle core, $N_A$ is Avogadro's number, and $M$ is the polymer molecular weight.

## 2.3 Results and Discussion

### 2.3.1 Synthesis of PON Triblock Terpolymers

The PON triblock terpolymers were prepared using a combination of anionic and reversible addition-fragmentation chain transfer (RAFT) polymerizations. Briefly, hydroxyl-terminated 1,4-PI-OH was prepared by anionic polymerization of isoprene followed by end-capping with ethylene oxide. Only one unit of ethylene oxide was added to the polyisoprene chain end as a result of using a lithium counterion.[13] The polymer was analyzed by $^1$H NMR spectroscopy (Figure 2.1) and found to contain 91% 1,4-units and 9% 3,4-units by comparing the signal intensities of olefinic protons associated with the 1,4-structure at 5.1 ppm ($H_a$) and the 3,4-structure at 4.7 ppm ($H_b$). The molecular weight was 3.1 kg/mol, calculated from signal intensity ratio between olefinic protons ($H_a + H_b$) and methylene protons next to the hydroxyl end group ($H_c$). 1,4-PI-OH was hydrogenated to give the corresponding hydroxyl-terminated PEP-OH. The disappearance of the olefin resonances at 5.1 ppm and 4.7 ppm in the $^1$H NMR spectrum indicated the complete saturation of the double bonds. Next, the potassium alkoxide version of PEP-OH was used to initiate the anionic polymerization of ethylene oxide to afford hydroxyl-terminated PEP-PEO (PO) diblock copolymer. The appearance of a broad

–$OCH_2CH_2O$- resonance at 3.64 ppm confirmed the successful incorporation of PEO into PEP-OH. The molecular weight of PEO was 25 kg/mol, as determined by $^1$H NMR analysis. The hydroxyl end-goups of PO were coupled to the chain transfer agent (CTA), *S*-1-dodecyl-*S'*-(*α,α'*-dimethyl-*α''*-acetic acid) trithiocarbonate (CTA), *via* an acid chloride intermediate. The signal ratio between the methylene protons ($H_a$) of PEO next to the ester group (δ = 4.26 ppm) and methylene protons ($H_b$) of CTA next to the trithiocarbonate unit (δ = 3.26 ppm) was almost 1:1, indicating efficient end group conversion (Figure 2.2). CTA-end capped PO (PO-CTA) was subsequently used to grow PNIPAm blocks by RAFT polymerization. The appearance of new resonances associated with PNIPAm ($H_a$, $H_b$, $H_c$, and $H_d$ in Figure 2.2) confirmed the successful incorporation of PNIPAm into the PON-CTA triblock terpolymer. The trithiocarbonate end group of the resulting PON-CTA was removed by aminolysis and Michael addition to afford PON triblock terpolymers free of the hydrophobic dodecyl chains associated with the CTA. The absence of methylene protons next to the trithiocarbonate unit (δ = 3.3 ppm) and the presence of methylene protons of the added acrylate (δ = 2.6, 2.8 ppm) (Figure 2.3), along with the disappearance of the absorption band of the trithiocarbonate group centered at *ca.* 310 nm (Figure 2.4), indicated the complete removal of the dodecyl end groups. We recognized the importance of removal of the dodecyl end groups stemming from the RAFT agent as this hydrophobic moiety impeded the micellization behavior of the PON triblock terpolymers. For example, PON-CTA samples are not fully dispersible in water using the TF technique even after several months. PON samples, on the other hand, can be dispersed in less than one hour. Using DI, PON-CTAs can be dispersed in water, but the hydrophobic end group was still a concern since it has been shown that

alkyl-terminated PNIPAm could form micelles with alkyl end groups as the hydrophobic cores when the alkyl end groups contain 12 carbons or more.[14] The product of each reaction step was characterized by size exclusion chromatography (SEC) (Figure 2.5). Samples investigated in this work are listed in Table 2.1 along with the molecular characteristics.

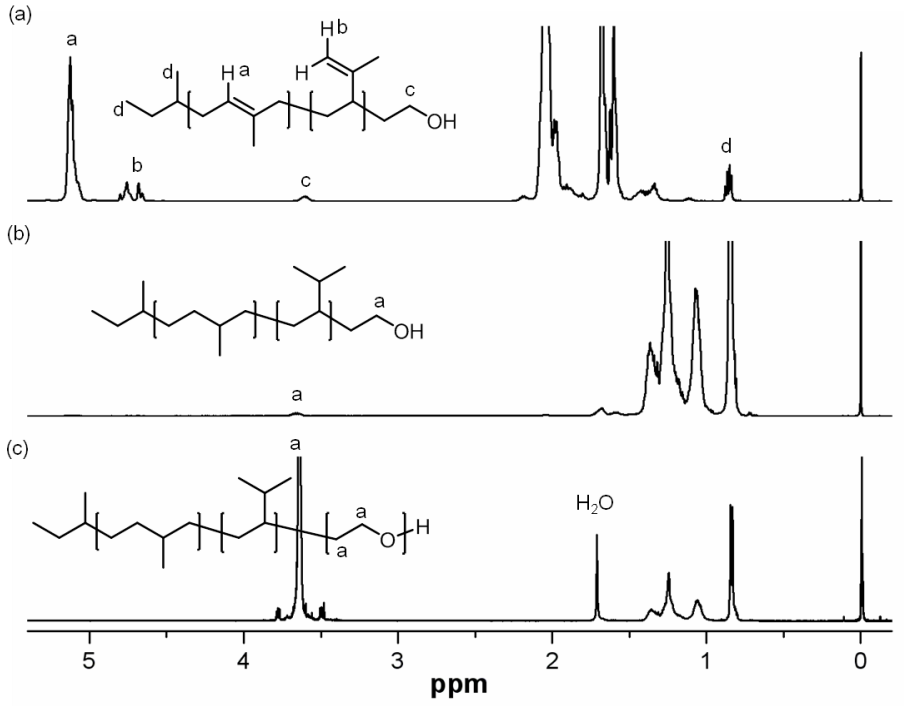


**Figure 2.1** $^{1}$H NMR spectra of (a) 1,4-PI-OH, (b) PEP-OH, and (c) PO(3-25) in $CDCl_3$.

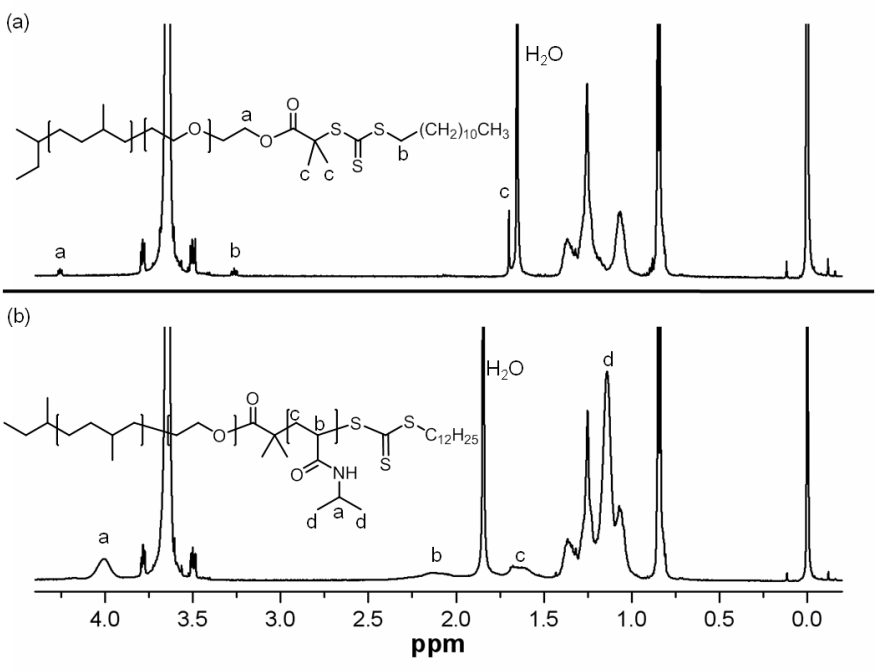


**Figure 2.2** $^{1}$H NMR spectra of (a) PO-CTA and (b) PON-CTA in $CDCl_3$.

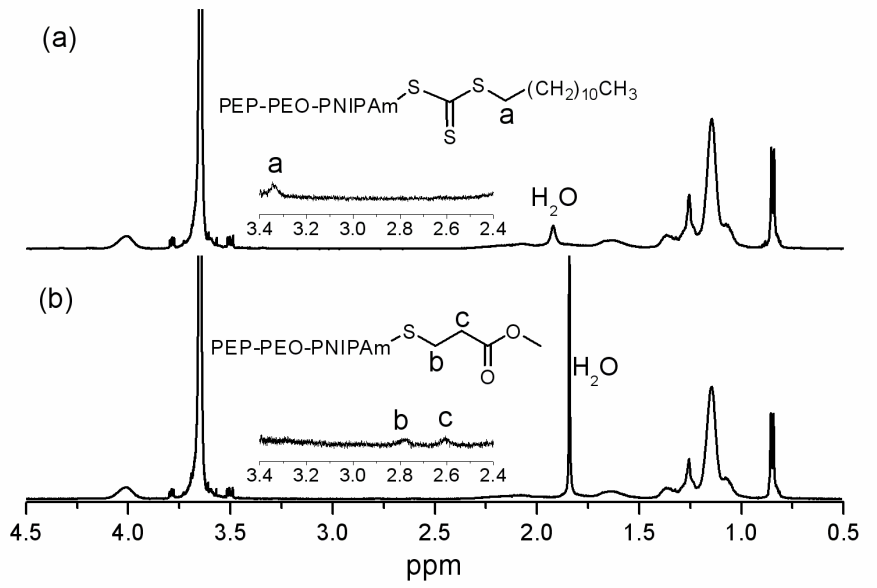


**Figure 2.3** $^{1}$H NMR spectra of (a) PON-CTA(3-25-10) and (b) PON(3-25-10) in $CDCl_3$. The area from 3.4 to 2.4 ppm is enlarged in each spectrum to monitor end group conversion.

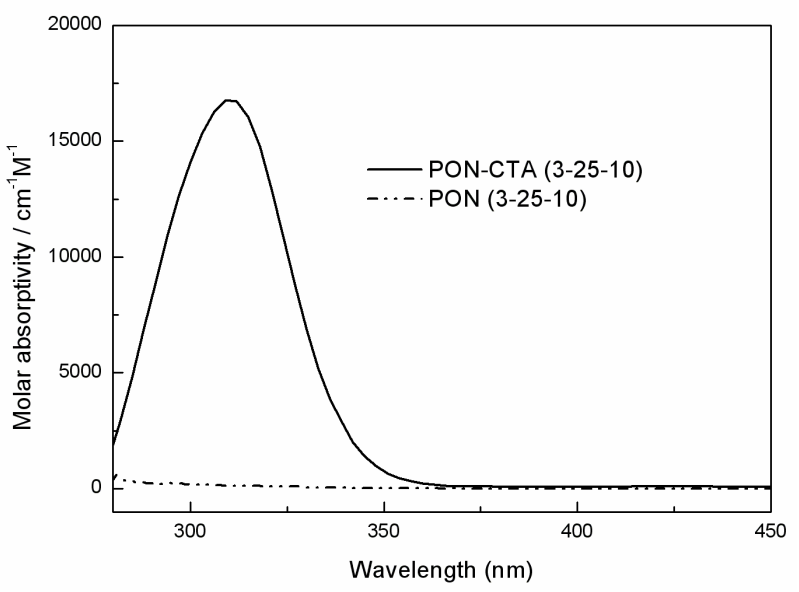


**Figure 2.4** UV-Vis spectra of PON-CTA(3-25-10) and PON(3-25-10) in $CHCl_3$.

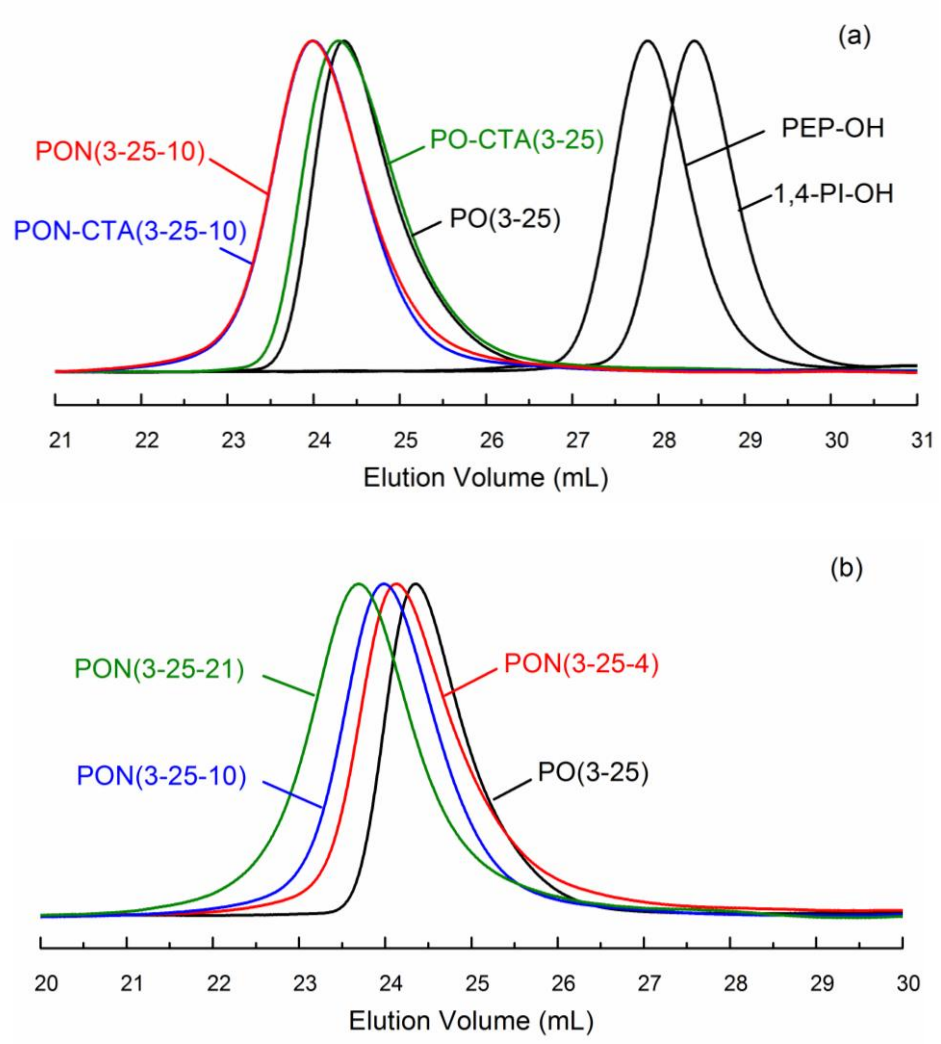


**Figure 2.5** (a) SEC trace of 1,4-PI-OH, PEP-OH, PO(3-25), PO-CTA(3-25), PON-CTA(3-25-10), and PON(3-25-10). (b) SEC trace of PO(3-25), PON(3-25-4), PON(3-25-10) and PON(3-25-21). THF/*N*,*N*,*N*',*N*'-tetramethylethylenediamine was used as the eluting solvent at a flow rate of 1.0 mL/min.

**Table 2.1** Molecular parameters of PO and PON block polymers

| Sample[a] | $N_{PEP}$[b] | $N_{PEO}$[b] | $N_{PNIPAm}$[b] | $f_{PEP}$[c] | $f_{PEO}$[c] | $f_{PNIPAm}$[c] | $Đ$[d] |
|---|---|---|---|---|---|---|---|
| PO(3-25) | 45 | 565 | – | 0.14 | 0.86 | – | 1.02 |
| PON(3-25-4) | 45 | 565 | 33 | 0.13 | 0.76 | 0.12 | 1.05 |
| PON(3-25-10) | 45 | 565 | 89 | 0.11 | 0.63 | 0.26 | 1.05 |
| PON(3-25-21) | 45 | 565 | 187 | 0.08 | 0.49 | 0.43 | 1.05 |

[a] The numbers in the parentheses correspond to the molecular weights of PEP, PEO, and PNIPAm, respectively, in kg/mol as determined by $^1$H NMR spectroscopy. [b] Number average degree of polymerization as determined by $^1$H NMR spectroscopy end group analysis. [c] The volume fraction was calculated using the molecular weight and the RT densities: ρ(PEP) = 0.856 g/cm$^3$,[15] ρ(PEO) = 1.12 g/cm$^3$,[16] and ρ(PNIPAm) = 1.07 g/cm$^3$.[17] [d] The dispersity was measured by SEC with THF/ *N*,*N*,*N*',*N*'-tetramethylethylenediamine as the eluting solvent.

### 2.3.2 Micellization of PON Triblock Terpolymers

The PON(3-25-10) solutions were characterized by DLS. The measured correlation functions were analyzed by the cumulant method. This analysis yielded the average hydrodynamic radius $R_h$ and the width of the size distribution (the reduced second cumulant $\mu_2/\Gamma^2$). Figure 2.6 shows a representative example of the squared electric field correlation functions $g_1^2(t)$, cumulant fits and linear regression of Γ vs $q^2$. The linear fit of Γ vs $q^2$ with zero intercept indicates that the relaxation in these samples is diffusive.

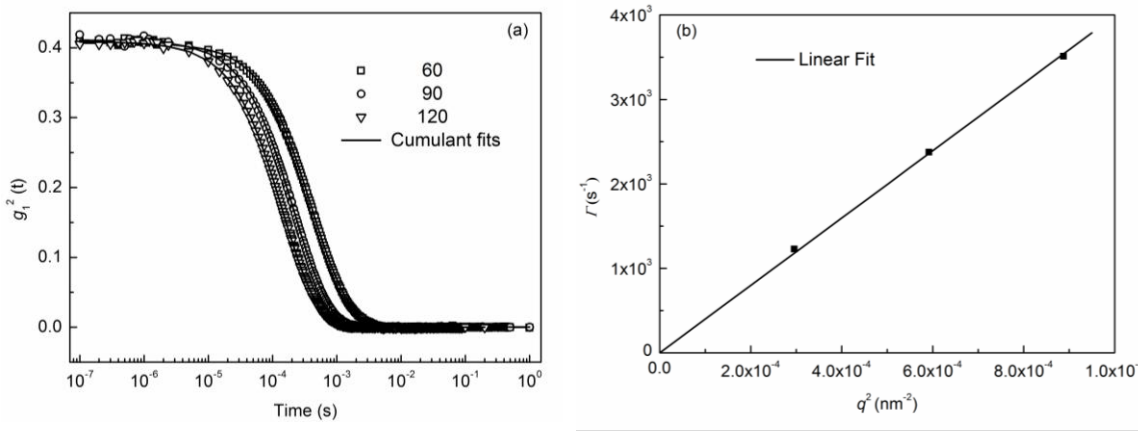


**Figure 2.6** (a) The squared electric field correlation functions $g_1^2(t)$ of the PON(3.2-25-10) micelles prepared by thin-film hydration with a concentration of 0.5 wt% at three different angles (60 °, 90 °, 120 °) and room temperature (25 ℃). The solid lines are cumulant fits. (b) The linear fit of decay rate Γ vs $q^2$.

Micelles prepared by the DI method gave a mean $R_h$ value of ca. 30 nm and those prepared by the TF method gave $R_h$ = 51–62 nm (Table 2.2). A comparison of the hydrodynamic radius distribution between the two preparation procedures, obtained by the application of inverse Laplace transformation (REPES) directly to the correlation functions,[11] are shown in Figures 2.7. This difference is consistent with the recent reports from Meli and Lodge, who studied how the size of the PB-PEO micelles in ionic liquids depends on the preparation procedure.[18, 19] At room temperature we expect that PON triblock copolymers form micelles with an insoluble PEP core and a solvated PEO-PNIPAm corona. Using the DI technique we anticipate that as the THF is exchanged with water the interfacial tension between the PEP block and the solvent increases gradually, and micelles were formed at a relatively low interfacial energy between the PEP and the THF/$H_2O$ solvent mixture. This results in a lower aggregation

number and thus smaller micelles. On the other hand, the high incompatibility between the PEP and pure water in the TF technique leads to structures with larger hydrodynamic radii due to the high interfacial tension. This is also true for PO(3-25) diblock copolymer micelles with the size of DI-prepared micelles being much smaller than the TF-prepared micelles (Table 2.2 and Figure 2.8).

**Table 2.2** Hydrodynamic radii ($R_h$) and size distributions ($\mu_2/\Gamma^2$) of PON(3-25-10) and PO(3-25) micelles at room temperature

| Sample | Preparation[a] | Concentration | $R_h$ (nm) [b] | $\mu_2/\Gamma^2$ ($\theta = 90^o$) |
|---|---|---|---|---|
| PON(3-25-10) | TF | 0.5 wt% | 62 | 0.49 |
| PON(3-25-10) | TF | 0.05 wt% | 51 | 0.22 |
| PON(3-25-10) | TF | 0.005 wt% | 54 | 0.20 |
| PON(3-25-10) | DI | 0.5 wt% | 29 | 0.20 |
| PON(3-25-10) | DI | 0.05 wt% | 30 | 0.16 |
| PO(3-25) | TF | 0.5 wt% | 51 | 0.16 |
| PO(3-25) | TF | 0.05 wt% | 49 | 0.07 |
| PO(3-25) | DI | 0.4 wt% | 28 | 0.19 |

[a] TF: thin-film hydration, DI: dialysis. [b] calculated from three different angles (60 °, 90 °, 120 °) by the cumulant method.

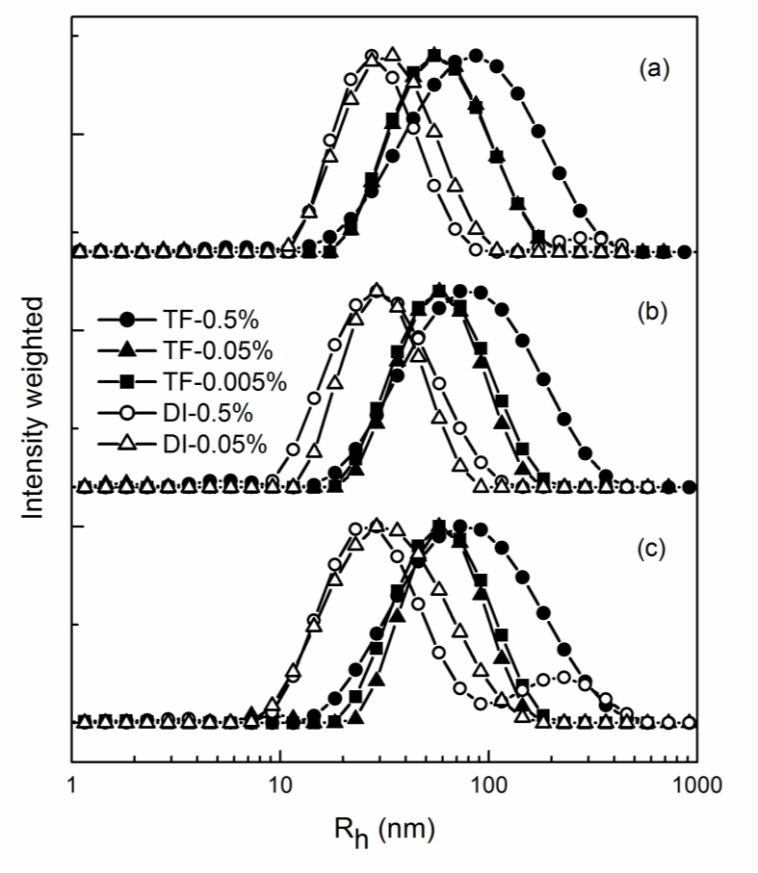


**Figure 2.7** Hydrodynamic radius distributions for PON(3-25-10) micelles at 25 ℃ and scattering angles of (a) 120 °, (b) 90 °, and (c) 60 °. TF-0.5%, TF-0.05% and TF-0.005% denote the samples prepared by thin-film hydration with the concentration of 0.5 wt%, 0.05 wt% and 0.005 wt%, respectively. DI-0.5% and DI-0.05% denote the samples prepared by dialysis with the concentration of 0.5 wt% and 0.05 wt%, respectively.

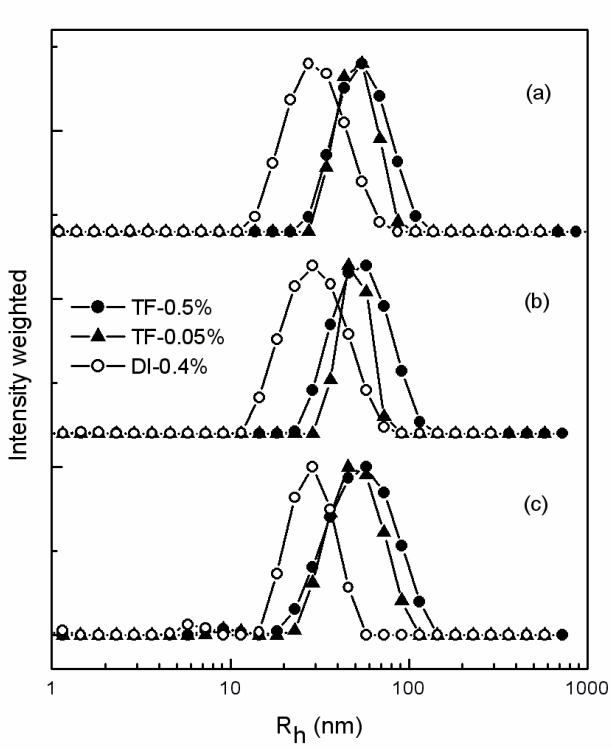


**Figure 2.8** Hydrodynamic radius distributions for PO(3-25) micelles at 25 ℃ and scattering angles of (a) 120 °, (b) 90 °, and (c) 60 °. TF-0.5% and TF-0.05% denote the samples prepared by thin-film hydration with the concentration of 0.5 wt% and 0.05 wt%, respectively. DI-0.4% is the sample prepared by dialysis with a concentration of 0.4 wt%.

The size of the TF-prepared PON(3-25-10) micelles exhibits a strong concentration dependence. At a concentration of 0.5 wt%, large micelles ($R_h$ = 62 nm) with a very broad size distribution ($\mu_2/\Gamma^2$ = 0.49) were formed. As shown in Figure 2.7, decreasing the concentration to 0.05 wt% and 0.005 wt% resulted in the formation of micelles with smaller hydrodynamic radii ($R_h \approx$ 50 nm) and much narrower size distributions ($\mu_2/\Gamma^2 \approx$ 0.2). The decrease in $R_h$ and size polydispersity upon dilution can be achieved by an increase in the number of micelles through either fission of the large aggregates or

nucleation and growth of new micelles. However, theoretical studies suggest that fusion and fission mechanisms are inefficient kinetic pathways to micelle equilibration,[20] and nucleation and growth of new micelles require expulsion of unimers from a given aggregate, which should be very slow due to the extremely low critical micellar concentration (cmc) of block copolymer solutions.[21, 22] Therefore, both processes are highly unlikely in this case. Cryo-TEM observations of these TF-prepared micelles at 0.5 wt% and 0.05 wt% are shown in Figure 2.9. At both concentrations, the micelles showed the same spherical morphology with similar core radii ($R_c \approx 8 \pm 2$ nm) and thus similar mean aggregation number ($p \approx 350$). In contrast, we observed no significant concentration dependence of TF-prepared PO(3-25) diblock copolymer micelles (Figure 2.8).

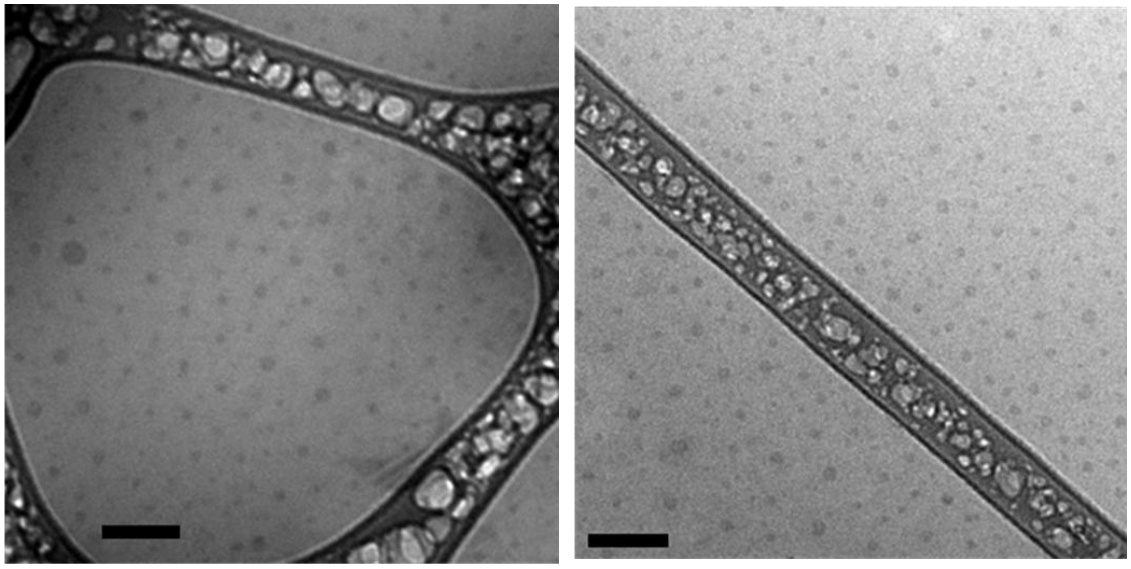

**Figure 2.9** Cryo-TEM images of PON(3-25-10) micelles prepared by thin-film hydration at room temperature. Left: 0.5 wt%, Right: 0.05 wt%. Scale bars: 100 nm.

This concentration dependence seen in the PON samples at room temperature could be explained by the formation of a small number of micelle aggregates. Several groups have reported that PNIPAm-containing block copolymers can form "abnormal aggregates" at low temperature where all the blocks are ostensibly soluble in water. Topp *et al.* first reported that PEO-*b*-PNIPAm showed aggregation in water below the LCST of PNIPAm,[23] and Annaka *et al.* reported the formation of disordered micelles from PEO-*b*-PNIPAm at about 17 ℃ and attributed it to the asymmetric swelling of PEO and PNIPAm chains: PNIPAm chains are less well-dissolved than are the PEO chains.[24] Recently, Liang and Du studied the chain conformations of PEO-*b*-PNIPAm and PNIPAm-*b*-PEO-*b*-PPO-*b*-PEO-*b*-PNIPAm in water, respectively, and found that loose associates were also formed at low temperature.[25, 26] They suggested the incompatibility between PEO and PNIPAm was the driving force for the associate structures containing PEO-rich domains and PNIPAm-rich domains. It is likely that these aggregated structures were also formed in PON micelles at a concentration of 0.5 wt% resulting from the formation of PNIPAm-rich domains. However, the PNIPAm chains are still hydrophilic, so the aggregation should be weak, and only a slight increase in $R_h$ was observed upon increasing concentration. The PNIPAm chains are solvated by a large amount of water and should adopt a loose or extended conformation, and we suggest micelle aggregates with a broad size distribution were formed.

In contrast to the TF prepared micelles, the DI-prepared PON(3-25-10) micelles do not exhibit such dependence of size on concentration (Tables 2.2). However, the hydrodynamic radius distribution gave a small peak centered at around 200 nm for DI-prepared micelles at 0.5 wt% and scattering angle of 60 °that was not apparent at 0.05

wt% (Figure 2.7). These larger micelles can also be attributed to micelle aggregates as discussed above.

### 2.3.3 Micellar Aggregation of PON Triblock Terpolymers

DLS experiments were also performed above room temperature on PO and PON micelle solutions. Figure 2.10 compares the temperature dependent hydrodynamic radii and relative scattering intensity of TF-prepared PO(3-25) and PON micelles. Both $R_h$ and scattering intensity for PO(3-25) and PON(3-25-4) micelles were nearly constant up to 60 ℃. On the other hand, $R_h$ and scattering intensity for PON(3-25-10) and PON(3-25-21) micelles both increased around 42 ℃ and 36 ℃, respectively. This was also confirmed by a comparison of the hydrodynamic radius distribution of these micelles at different temperatures (Figure 2.11) and cloud point measurements (Figure 2.12). In addition, we observed a hysteresis loop where the critical aggregation temperature is lower by 3–4 ℃ during cooling than upon heating (Figure 2.13). This is also consistent with the transmittance measurement (Figure 2.12). The increase of $R_h$ and scattering intensity upon heating can be explained in terms of micellar aggregation. On increasing the temperature above the LCST, the PNIPAm chains can minimize their contact with water by forming larger multi-micellar aggregates. Based on the micelle aggregation number and hydrodynamic radius, the effective volume fraction of micelles can be calculated; the effective micelle volume fraction of 0.5 wt% PON(3.2-25-10) micelle is 22%. Such a high micelle volume fraction clearly indicates that some micelle aggregation will occur above the LCST of PNIPAm.

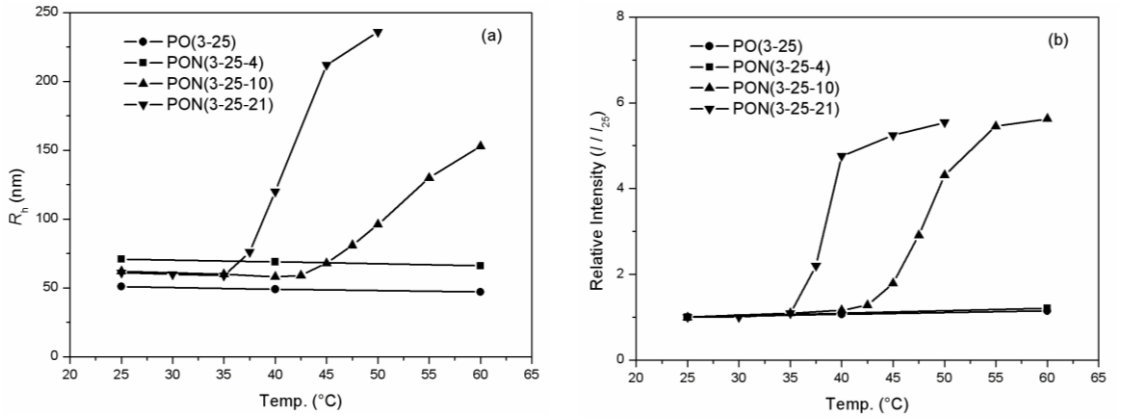


**Figure 2.10** Temperature dependence of hydrodynamic radius (a) and intensity (b) for PO and PON micelles prepared by thin-film hydration with a concentration of 0.5 wt%. $R_h$ was calculated from three different angles (60°, 90°, 120°) by the cumulant method. Intensity is measured at a 90°scattering angle, and the vertical axis is the relative intensity ($I/I_{25}$) where $I_{25}$ is the intensity recorded at 25 ℃.

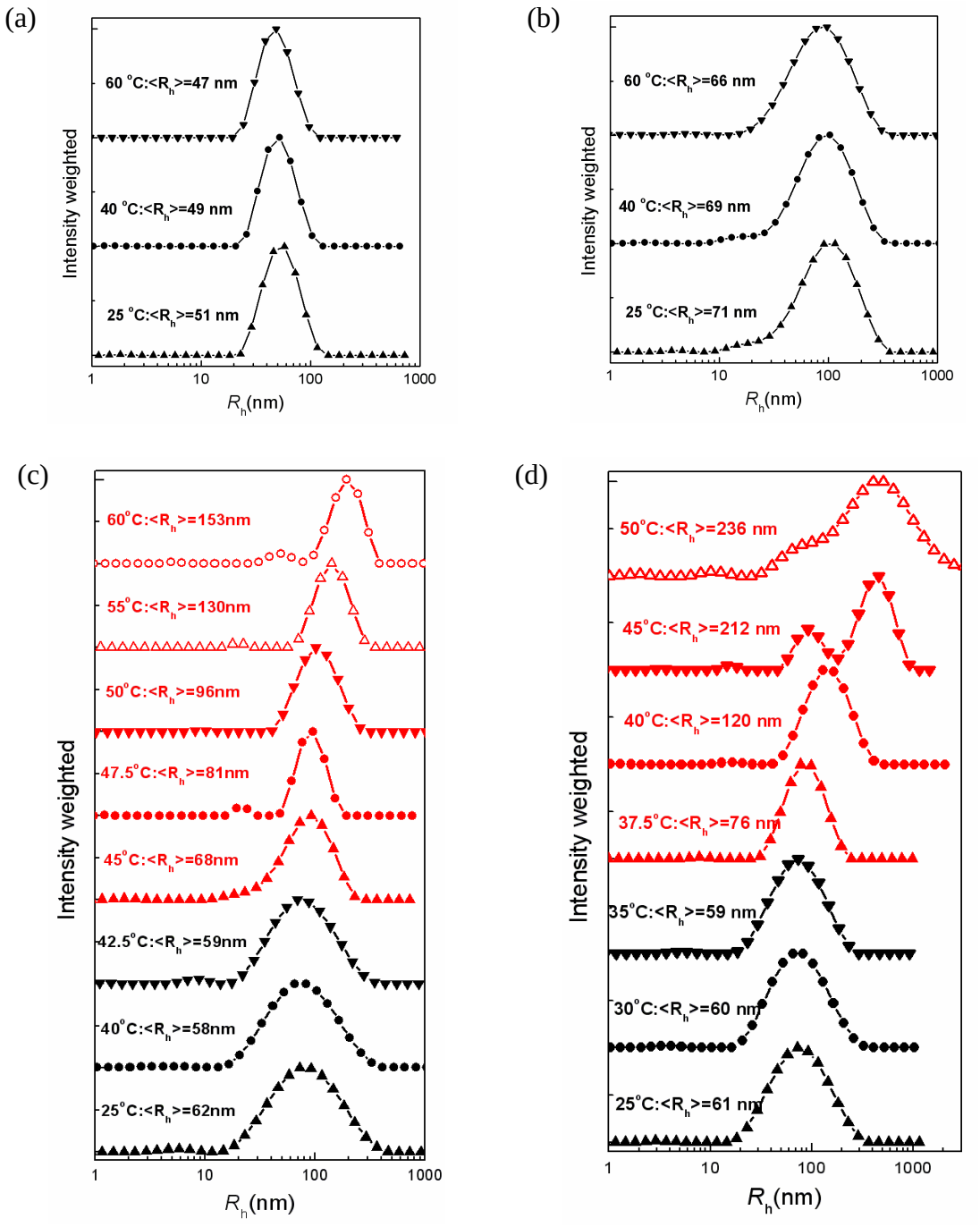


**Figure 2.11** Evolution of the hydrodynamic radius distribution as a function of temperature at a 90 ° scattering angle for PO and PON micelles prepared by thin-film hydration with a concentration of 0.5 wt%. (a): PO(3-25). (b): PON(3-25-4). (c): PON(3-25-10). (d): PON(3-25-21).

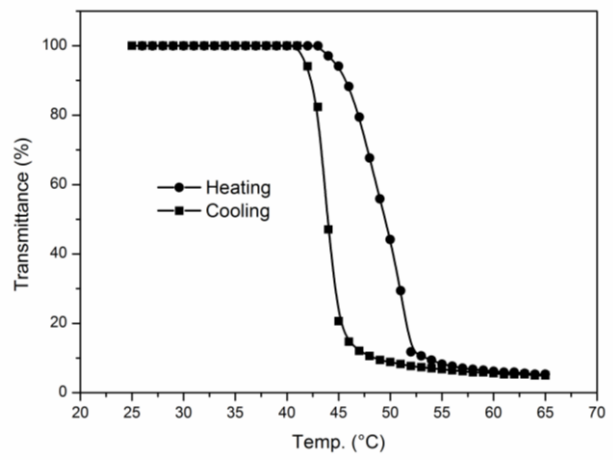


**Figure 2.12** Temperature dependence of transmittance at 632.8 nm for PON(3-25-10) micelles prepared by thin-film hydration with a concentration of 0.5 wt% measured at a heating or cooling rate of ~1 ℃/min.

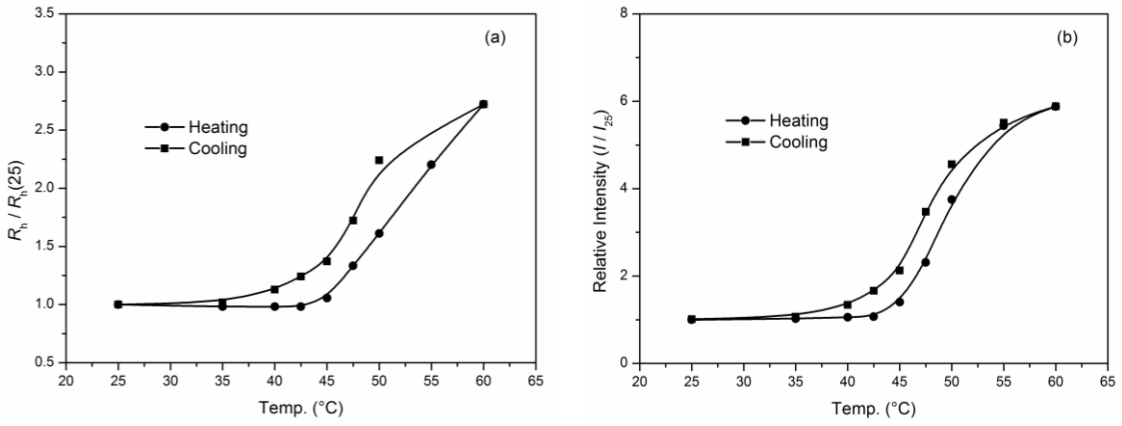


**Figure 2.13** Temperature dependence of hydrodynamic radius (a) and intensity (b) for PON(3-25-10) micelles prepared by thin-film hydration with a concentration of 0.5 wt%. $R_h$ was calculated from three different angles (60 °, 90 °, 120 °) by the cumulant method. $R_h(25)$ is the hydrodynamic radius at 25 ℃. Intensity is measured at a 90 ° scattering angle, and the vertical axis is the relative intensity ($I/I_{25}$) where $I_{25}$ is the intensity recorded at 25 ℃.

We observed a strong molecular weight dependence of the critical micellar aggregation temperature in the PON triblock terpolymers. The critical micellar aggregation temperatures for PON(3-25-21) and PON(3-25-10) were determined from Figure 2.10 to be 36 ℃ and 42 ℃, respectively. For PON(3-25-4) no such micellar aggregation was observed up to 60 ℃. The commonly reported value of the LCST of PNIPAm is 32 ℃.[27, 28] The relatively high critical micellar aggregation temperatures for the PON micelles is attributable to two factors. First, the low molecular weight of PNIPAm leads to a higher LCST. Stover *et al.* studied the molecular weight dependence of the LCST for PNIPAm prepared by atom transfer radical polymerization (ATRP). They reported a strong decrease of the phase transition temperature with increasing molecular weights (when the molecular weight increased from 2.8 to 26.5 kg/mol, the cloud point dropped from 43.0 ℃ to 33.3 ℃).[29] Second, it has been shown that the incorporation of hydrophilic groups into PNIPAm raises the LCST of PNIPAm.[30] Tenhu *et al.* observed a very slight increase of the LCST (from 32 ℃ to 34 ℃) with increasing PEO content in PEO-*b*-PNIPAm samples,[31] and Yang *et al.* reported a very strong LCST dependence on PEO content in similar PEO-*b*-PNIPAm systems. They found that the LCST of PNIPAm in these diblock copolymers were around 37 ℃ with 7.6 wt% PEO and a 24 kg/mol PNIPAm, while it was higher than 90 ℃ with 27 wt% PEO and a 5 kg/mol PNIPAm.[32] Both the relatively low molar mass of the PNIPAm blocks and the presence of PEO in the PON samples should lead to critical micelle aggregation temperatures that are higher than the LCST of higher molar mass PNIPAm, consistent with our results.

The critical micellar aggregation temperature of PON triblock terpolymers was also

dependent on concentration. We found that the critical micellar aggregation temperature of TF-prepared PON(3-25-10) micelles increased from 42 ℃ to 47 ℃ as the polymer concentration decreased from 0.5 wt% to 0.05 wt% (Figure 2.14). This was also true for the DI-prepared PON(3-25-10) micelles, where 0.5 wt% and 0.05 wt% PON solutions had a critical micellar aggregation temperature of 45 ℃ and 47 ℃, respectively (Figure 2.15). The higher critical micellar aggregation temperature of PON micelles at lower polymer concentration is consistent with the concentration dependence of the LCST of PNIPAm in homopolymer and PEO-*b*-PNIPAm below 1 wt%.[27, 33-35]

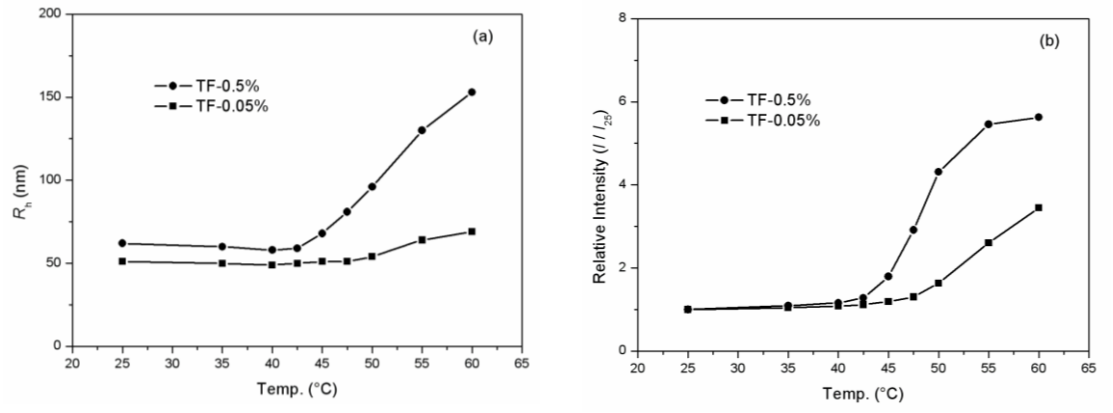


**Figure 2.14** Temperature dependence of hydrodynamic radius (a) and intensity (b) for PON(3-25-10) micelles prepared by thin-film hydration with a concentration of 0.5 wt% and 0.05 wt%, respectively. $R_h$ was calculated from three different angles (60 °, 90 °, 120 °) by the cumulant method. Intensity is measured at a 90 ° scattering angle, and the vertical axis is the relative intensity ($I/I_{25}$) where $I_{25}$ is the intensity recorded at 25 ℃.

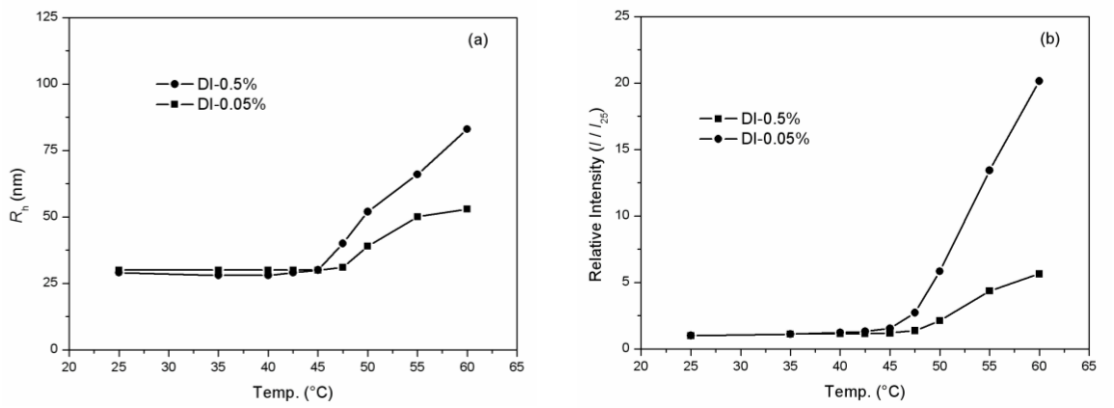


**Figure 2.15** Temperature dependence of hydrodynamic radius (a) and intensity (b) for PON(3-25-10) micelles prepared by dialysis with a concentration of 0.5 wt% and 0.05 wt%, respectively. $R_h$ was calculated from three different angles (60°, 90°, 120°) by the cumulant method. Intensity is measured at a 90° scattering angle, and the vertical axis is the relative intensity ($I/I_{25}$) where $I_{25}$ is the intensity recorded at 25 ℃.

As discussed in Chapter 1, there are three possible thermo-induced structured changes of triblock terpolymer micelles with PNIPAm coronas: (i) PNIPAm collapse around the hydrophobic core to form flower-like micelles, or collapse around the hydrophilic shell to form (ii) thin layers or (iii) sticky patches above the LCST of PNIPAm (see Figure 1.5). These changes could lead to a decrease in micelle size in very dilute solution. However, we are not able to resolve any micelle shrinkage even at a concentration of 0.005 wt% (Figure 2.16). Instead, only the aggregation of micelles was observed in the investigated concentration range (0.5–0.005 wt%). It is possible that micelle shrinkage is overshadowed by micelle aggregation. The observed micelle aggregation suggests that the formation of flower-like micelles above the LCST of PNIPAm is unlikely because the collapsed PNIPAM is surrounded by the hydrophilic

shell and thus cannot aggregate around the PEP core at higher temperatures. Although we do not know the detailed structure of micelle aggregates above the LCST of PNIPAm, we speculate that PNIPAm is likely to collapse into sticky patches instead of a thin layer. This would be entropically favored for the PEO midblocks and is consistent with the formation of micelle aggregates

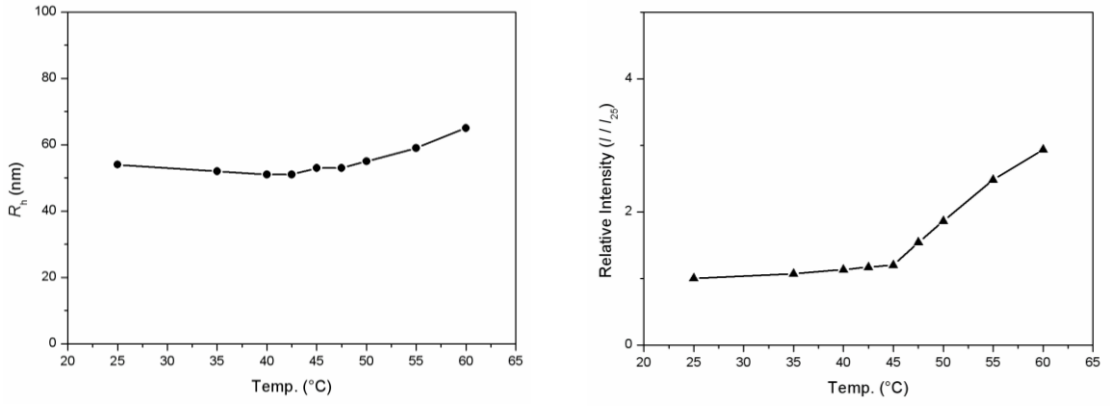


**Figure 2.16** Temperature dependence of hydrodynamic radius (a) and intensity (b) for PON(3-25-10) micelles prepared by thin-film hydration with a concentration of 0.005 wt%. $R_h$ was calculated from three different angles (60°, 90°, 120°) by the cumulant method. Intensity is measured at a 90° scattering angle, and the vertical axis is the relative intensity ($I/I_{25}$) where $I_{25}$ is the intensity recorded at 25 ℃.

## 2.4 Summary

We have synthesized well-defined PON triblock terpolymers using a combination of anionic and RAFT polymerization and studied the micellization and micellar aggregation of these polymers in dilute aqueous solution by DLS and cryo-TEM. At room temperature, micelles with hydrophobic PEP cores, hydrophilic PEO shells and PNIPAm

coronas were formed. We found that the DI-prepared PON micelles were much smaller than the TF-prepared PON micelles due to the lower interfacial energy between the hydrophobic PEP block and the solvent in the course of micelle formation. In addition, the PON micelles formed some aggregated species at a concentration of 0.5 wt% even below the LCST. At temperatures higher than the LCST of PNIPAm, micellar aggregation occurred, resulting in an increase in $R_h$ and scattering intensity. The critical micellar aggregation temperature depended on both the molecular weight of PNIPAm and polymer concentration. The longer PNIPAm block length and higher polymer concentration resulted in a lower critical micellar aggregation temperature.

## 2.5 References


1. Ringsdorf, H.; Lehmann, P.; Weberskirch, R. *Book of Abstracts*, 217th National Meeting of the American Chemical Society, Anaheim, CA, March 221-225, 1999.
2. Laschewsky, A. *Curr. Opin. Colloid Interface Sci.* **2003**, *8*, 274-281.
3. Lutz, J. F.; Laschewsky, A. *Macromol. Chem. Phys* **2005**, *206*, 813-817.
4. Hillmyer, M. A.; Lodge, T. P. *J. Polym. Sci., Part A: Polym. Chem.* **2002**, *40*, 1-8.
5. Zhou, C.; Hillmyer, M. A.; Lodge, T. P. *Macromolecules* **2011**, *44*, 1635-1641.
6. Lai, J. T.; Filla, D.; Shea, R. *Macromolecules* **2002**, *35*, 6754-6756.
7. Hillmyer, M. A.; Bates, F. S. *Macromolecules* **1996**, *29*, 6994-7002.
8. Allgaier, J.; Poppe, A.; Willner, L.; Richter, D. *Macromolecules* **1997**, *30*, 1582-1586.
9. Rzayev, J.; Hillmyer, M. A. *J. Am. Chem. Soc.* **2005**, *127*, 13373-13379.

10. Qiu, X.; Winnik, F. M. *Macromol. Rapid Commun.* **2006**, *27*, 1648-1653.
11. Jakes, J. *Collect. Czech. Chem. Commun.* **1995**, *60*, 1781-1797.
12. Bellare, J. R.; Davis, H. T.; Scriven, L. E.; Talmon, Y. *J. Electron Microsc.* **1988**, *10*, 87-111.
13. Quirk, R. P.; Ma, J. *J. Polym. Sci., Part A: Polym. Chem.* **1988**, *26*, 2031-2037.
14. Chung, J. E.; Yokoyama, M.; Suzuki, K.; Aoyagi, T.; Sakurai, Y.; Okano, T. *Colloids Surf., B* **1997**, *9*, 37-48.
15. Fetters, L. J.; Lohse, D. J.; Richter, D.; Witten, T. A.; Zirkel, A. *Macromolecules* **1994**, *27*, 4639-4647.
16. Smith, G. D.; Yoon, D. Y.; Jaffe, R. L.; Colby, R. H.; Krishnamoorti, R.; Fetters, L. J. *Macromolecules* **1996**, *29*, 3462-3469.
17. Shields, D. J.; Coover, H. W. *J. Polym. Sci.* **1959**, *39*, 532-533.
18. Meli, L.; Santiago, J. M.; Lodge, T. P. *Macromolecules* **2010**, *43*, 2018-2027.
19. Meli, L.; Lodge, T. P. *Macromolecules* **2009**, *42*, 580-583.
20. Nyrkova, I. A.; Semenov, A. N. *Macromol. Theory Simul.* **2005**, *14*, 569-585.
21. Won, Y. Y.; Davis, H. T.; Bates, F. S. *Macromolecules* **2003**, *36*, 953-955.
22. Jain, S.; Bates, F. S. *Macromolecules* **2004**, *37*, 1511-1523.
23. Topp, M. D. C.; Dijkstra, P. J.; Talsma, H.; Feijen, J. *Macromolecules* **1997**, *30*, 8518-8520.
24. Motokawa, R.; Morishita, K.; Koizumi, S.; Nakahira, T.; Annaka, M. *Macromolecules* **2005**, *38*, 5748-5760.
25. Yan, J.; Ji, W.; Chen, E.; Li, Z.; Liang, D. *Macromolecules* **2008**, *41*, 4908-4913.
26. Mei, A.; Guo, X.; Ding, Y.; Zhang, X.; Xu, J.; Fan, Z.; Du, B. *Macromolecules* **2010**,

*43*, 7312-7320.

27. Heskins, M.; Guillet, J. E. *J. Macromol. Sci. Chem.* **1968**, *A2*, 1441-1455.
28. Wu, C.; Wang, X. *Phys. Rev. Lett.* **1998**, *80*, 4092-4094.
29. Xia, Y.; Yin, X.; Burke, N. A. D.; Stover, H. D. H. *Macromolecules* **2005**, *38*, 5937-5943.
30. Chung, J. E.; Yokoyama, M.; Aoyagi, T.; Sakurai, Y.; Okano, T. *J. Controlled Release* **1998**, *53*, 119-130.
31. Virtanen, J.; Holappa, S.; Lemmetyinen, H.; Tenhu, H. *Macromolecules* **2002**, *35*, 4763-4769.
32. Qin, S.; Geng, Y.; Discher, D. E.; Yang, S. *Adv. Mater.* **2006**, *18*, 2905-2909.
33. Zhang, W.; Shi, L.; Wu, K.; An, Y. *Macromolecules* **2005**, *38*, 5743-5747.
34. Zhu, P.; Napper, D. H. *Macromolecules* **1999**, *32*, 2068-2070.
35. Zhu, P.; Napper, D. H. *Langmuir* **2000**, *16*, 8543-8545.

# Chapter 3

# Gelation of PON Triblock Terpolymers in Water*

## 3.1 Introduction

The self-assembly of associating triblock copolymers into complex and responsive nanostructures is an active and exciting area of research, due to potential applications of these fascinating materials in surface coatings, cosmetics, oil recovery, drug delivery and tissue engineering.[1-4] Their technological importance is due to their ability to form networks via self-assembly, with midblocks bridging endblock domains. There are three possible conformations of the midblocks in ABA triblock copolymer gels: (i) loops, when both end blocks belong to the same microdomain; (ii) bridges, when the end blocks connect two different microdomains; (iii) dangling ends, when one end block does not associate with any microdomain.[5, 6] Both looped chains and dangling ends are network defects, whereas only bridges can transmit stress between connected microdomains and contribute to the network elasticity. Due in part to the presence of looping conformations, the gelation concentration of ABA hydrogels is usually 10–20 wt%,[7-17] but lower

* This chapter is reproduced in part with permission from Zhou, C.; Hillmyer, M. A.; Lodge, T. P. *J. Am. Chem. Soc.* **2012**, *134*, 10365-10368.

concentrations are often desirable for biomedical applications. It is therefore of interest to consider ABC triblock terpolymers with mutually immiscible hydrophobic A and C endblocks. In principle, this architecture could give two-compartment networks which should completely suppress looping conformations.[18] In our design, we chose a C block that undergoes reversible association to produce the two-compartment gels in a stepwise manner, by first forming micelles with an A core, then gels by subsequent C block association (Figure 3.1). This should result in better gelation efficiencies and improved mechanical properties in ABC gels.

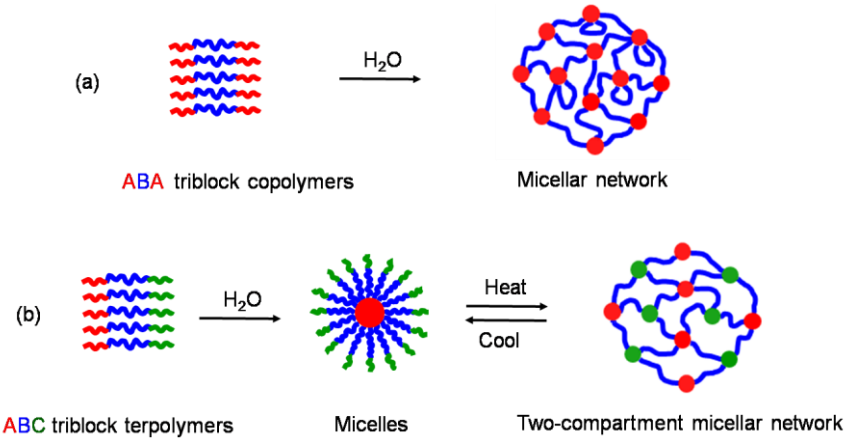


**Figure 3.1** Schematic illustration of gelation of (a) ABA and (b) thermoresponsive ABC polymers.

In Chapter 2, we reported the micellization and micellar aggregation behavior of poly(ethylene-*alt*-propylene)-*b*-poly(ethylene oxide)-*b*-poly(*N*-isopropylacrylamide) (PON) triblock terpolymers in water at the low concentrations of 0.5 wt% and 0.05 wt%.[19] The terpolymers formed well-defined micelles with hydrophobic PEP cores surrounded by hydrophilic PEO-PNIPAm coronae at low temperatures, and these

micelles associated to form larger aggregated structures upon heating above the lower critical solution temperature (LCST) of PNIPAm. In this chapter, we explore more concentrated solutions to prepare thermoresponsive ABC hydrogels. We will describe the gelation behavior of PON terpolymers, compare the hydrogel formation between a PON terpolymer and a poly(*N*-isopropylacrylamide)-*b*-poly(ethylene oxide)-*b*-poly(*N*-isopropylacrylamide) (NON) copolymer,[20] and investigate the effect of PNIPAm and PEO block length and polymer concentration on gelation properties of PON terpolymers.

## 3.2 Experimental Section

### 3.2.1 Materials

We prepared four PON triblock terpolymers and one NON triblock copolymer (Scheme 3.1). Three PON triblock terpolymer was prepared using a combination of anionic and reversible addition-fragmentation chain transfer (RAFT) polymerizations (see Chapter 2).[19] A new PON triblock terpolymer with a different PEO block length was synthesized from 1,4-PI-OH[19] following the same protocol[19] by varying the amount of ethylene oxide added during the growth of PEO block. The product of each reaction step was confirmed by $^1$H NMR spectroscopy and characterized by size exclusion chromatography (SEC) (Figures 3.2).

The NON triblock copolymer was synthesized by RAFT polymerization from a *α*,*ω*-dihydroxy-PEO precursor ($M_n$ = 20 kDa) following a reported procedure (Scheme 3.2).[21] Briefly, the hydroxyl end-groups of PEO were coupled to the chain transfer agent (CTA) *S*-1-dodecyl-*S'*-(*α,α'*-dimethyl-*α"*-acetic acid) trithiocarbonate, to give the macroinitiator CTA-PEO-CTA. The degree of CTA attachment is ~100% as determined

from the relative intensity of the PEO and CTA resonance peaks in NMR spectra with the molecular weight of the starting PEO ($M_n$ = 20 kDa) as a reference. The macroinitiator CTA-PEO-CTA was then used to grow PNIPAm blocks by RAFT polymerization. The resulting CTA-NON-CTA triblock copolymer had the trithiocarbonate end groups on both ends and they were removed by aminolysis and Michael addition to afford the final NON triblock copolymers.[22] The product of each reaction step was confirmed by $^1$H NMR spectroscopy and characterized by SEC (Figures 3.3). In the elugram, a small broad peak at elution volume of 27–31 mL is observed for both CTA-NON-CTA and NON triblocks. This is likely due to the presence of a small amount of PNIPAm homopolymer. The molecular characteristics of the polymers investigated in this work are summarized in Table 3.1.

**Scheme 3.1** Chemical structure of PON and NON triblock polymers

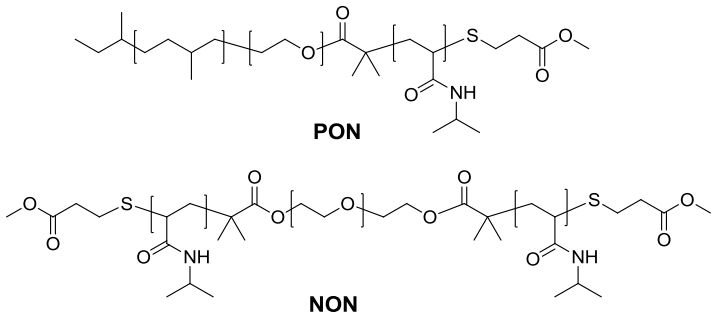

**Scheme 3.2** Synthesis of NON triblock copolymer

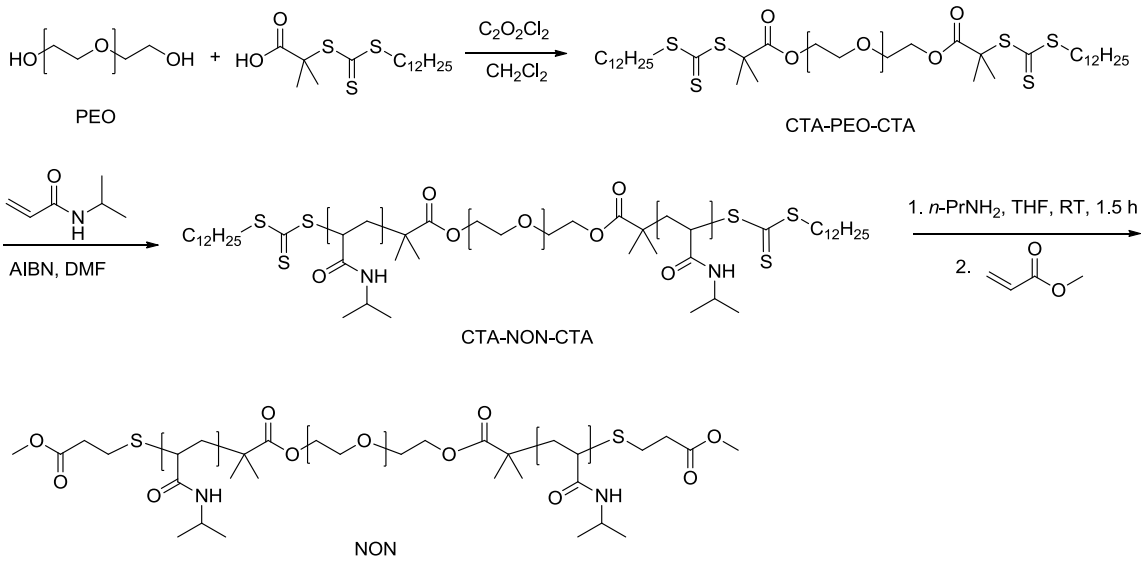


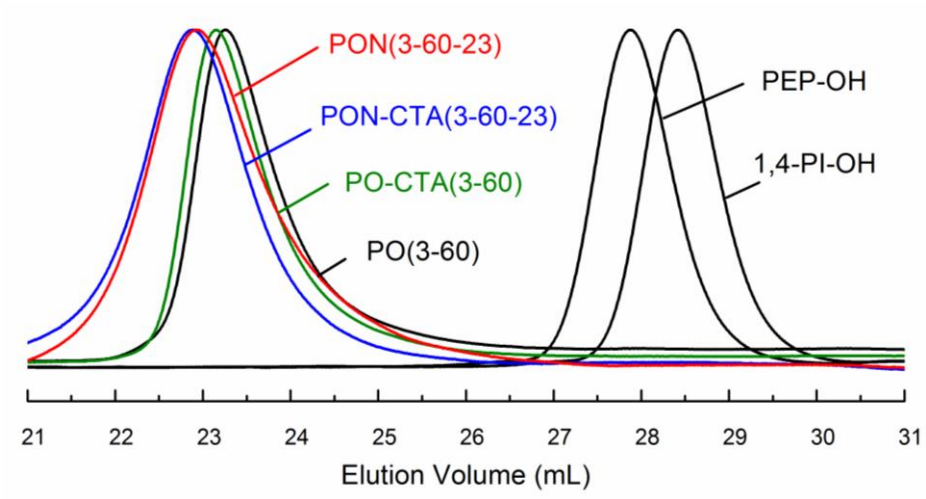


**Figure 3.2** SEC trace of 1,4-PI-OH, PEP-OH, PO(3-60), PO-CTA(3-60), PON-CTA(3-60-23), and PON(3-60-23). THF/*N*,*N*,*N*',*N*'-tetramethylethylenediamine was used as the eluting solvent at a flow rate of 1.0 mL/min.

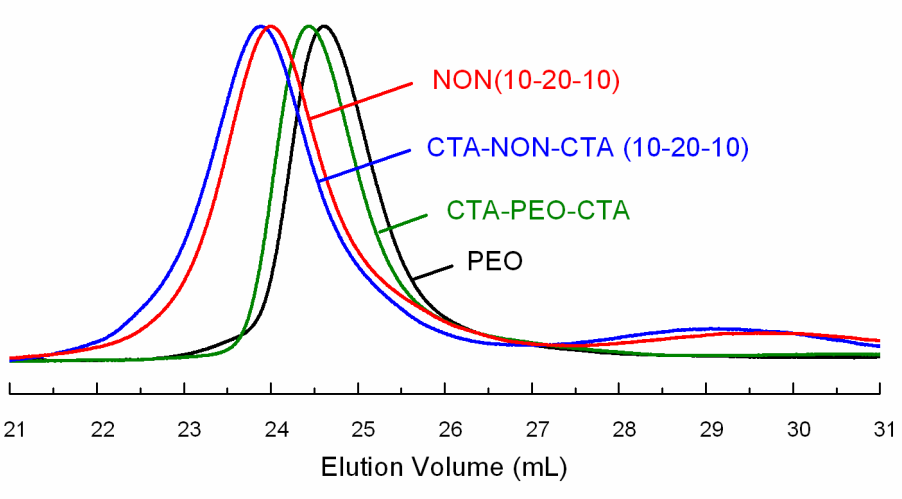


**Figure 3.3** SEC traces of PEO, CTA-PEO-CTA, CTA-NON-CTA(10-20-10), NON(10-20-10). THF/*N*,*N*,*N*',*N*'-tetramethylethylenediamine was used as the eluting solvent at a flow rate of 1.0 mL/min.

**Table 3.1** Molecular parameters of PON and NON triblock polymers

| Sample[a] | $N_{PEP}$[b] | $N_{PEO}$[b] | $N_{PNIPAm}$[b] | $f_{PEP}$[c] | $f_{PEO}$[c] | $f_{PNIPAm}$[c] | $Đ$[d] |
|---|---|---|---|---|---|---|---|
| PON(3-25-4) | 45 | 565 | 33 | 0.13 | 0.76 | 0.12 | 1.05 |
| PON(3-25-10) | 45 | 565 | 89 | 0.11 | 0.63 | 0.26 | 1.05 |
| PON(3-25-21) | 45 | 565 | 187 | 0.08 | 0.49 | 0.43 | 1.05 |
| PON(3-60-23) | 45 | 1358 | 203 | 0.05 | 0.68 | 0.27 | 1.09 |
| NON(10-20-10) | – | 454 | 91 | – | 0.49 | 0.51 | 1.06 |

[a] The numbers in the parentheses correspond to the molar masses of PEP, PEO, and PNIPAm, respectively, in kg mol$^{-1}$ as determined by $^1$H NMR spectroscopy. [b] Number average degree of polymerization as determined by $^1$H NMR spectroscopy. [c] The volume fraction was calculated using the molecular weight and the RT densities:

$\rho$(PEP) = 0.856 g/cm$^3$,[23] $\rho$(PEO) = 1.12 g/cm$^3$,[24] and $\rho$(PNIPAm) = 1.07 g/cm$^3$.[25 d] The dispersity was measured by SEC with THF/ *N*,*N*,*N*',*N*'-tetramethylethylenediamine as the eluting solvent.

### 3.2.2 Solution Preparation

All the polymer solutions were prepared by the thin-film hydration method. Appropriate amounts of bulk polymer were dissolved in $CH_2Cl_2$, followed by evaporation of the solvent to yield a thin film on the walls of the vial. The thin film was then hydrated with a defined amount of water, and the resulting mixture was stirred at room temperature for at least 1 month before further characterization.

### 3.2.3 Rheology

Rheological measurements were performed using an AR-G2 rheometer with a Couette geometry that contains the sample in a 1 mm concentric cylindrical gap between a cup with a diameter of 30 mm and a bob with a diameter of 28 mm. About 15 mL of the sample was first loaded on the cup at room temperature (25 ℃). This amount filled the gap as the bob was lowered. The temperature was controlled using a Peltier temperature controller. To avoid any water evaporation from the sample, the whole fixture assembly was shielded by a metal cover with a wet sponge. Dynamic strain sweep experiments were performed at three different angular frequencies (1, 10, 100 rad/s). Dynamic frequency sweeps were examined in the linear viscoelastic regime, as determined by dynamic strain sweep experiments. The temperature dependences of $G'$ and $G''$ were measured with a frequency of 10 rad/s, and a heating rate of 1 ℃/min.

### 3.2.4 Differential Scanning Calorimetry (DSC)

The thermal transitions associated with the gelation of aqueous triblock terpolymer solutions were studied using a TA Discovery DSC. The aqueous polymer solution and the reference solution (pure water) were loaded in a Tzero hermetic pan at room temperature (25 ℃). Each solution was alternately heated and cooled between 20 and 55 ℃ at a scan rate of 2 ℃/min. All scans were performed twice and found to be reproducible. The second heating and cooling scans are reported. Samples were reweighed after measurement and no mass changes were observed.

### 3.2.5 Variable-temperature $^{1}$H NMR Spectroscopy

$^{1}$H NMR spectra were recorded on a Varian INOVA 500 spectrometer. Deuterated water (Aldrich) was used as the solvent and a pulse delay of 10 s was employed to ensure complete relaxation. Experiments were performed at various temperatures from 25 to 55 ℃, and 10 min was allowed for equilibration at each temperature prior to the measurement.

## 3.3 Results and Discussion

### 3.3.1 Gelation of PON Triblock Terpolymer

Aqueous solutions of PON(3-25-10) triblock are free-flowing transparent liquids at room temperature, and become free-standing hydrogels at high polymer concentrations (10 wt% and 5 wt%) or soft hydrogels at lower concentrations (2 wt% and 1 wt%) when heated to 50 ℃ (Figure 3.4).[7] Repeated heating and cooling experiments indicate that the sol-gel transition is thermoreversible.

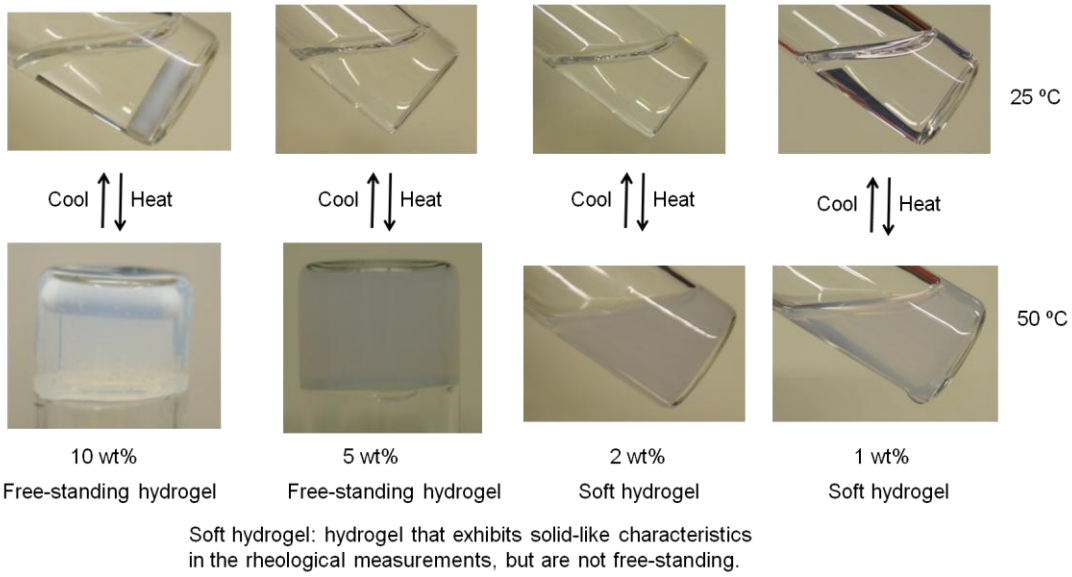


**Figure 3.4** Photographs of PON(3-25-10) solutions at varying polymer concentrations and the indicated temperatures.

Dynamic shear measurements were performed on 5 wt% PON(3-25-10) sample over the temperature range of 25–55 ℃ to study gelation properties. Dynamic strain sweep experiments were first carried out to determine the linear viscoelastic regime. The linear viscoelastic regime is defined as the region below the critical stain ($\gamma_c$ is defined as the critical value below which the storage modulus ($G'$) remains invariant with respect to strain). For the 5 wt% sample of PON(3-25-10), the liquid solution at 25 ℃ has a large $\gamma_c$ value (> 100%) and the hydrogel at 45 ℃ has a smaller $\gamma_c$ value (10-20%) (Figure 3.5). A strain amplitude of 2% was then used to ensure that the dynamic frequency sweep measurements were taken in the linear viscoelastic regime. Representative data at 25, 42, and 45 ℃ are shown in Figure 3.6. At 25 ℃, $G'$ is smaller than the loss modulus ($G''$) and follows typical terminal rheological behavior for a viscoelastic fluid. At an intermediate temperature of 42 ℃, $G'$ is almost equal to $G''$ and both show similar power law

dependences on $\omega$: $G' \approx G'' \sim \omega^{0.5}$. This temperature is identified as the critical gelation temperature ($T_{gel}$), which is the signature of the transition between liquid-like and solid-like behavior.[26, 27] At 45 ℃, $G' > G''$ at all frequencies and is nearly frequency independent, indicating solid-like behavior.

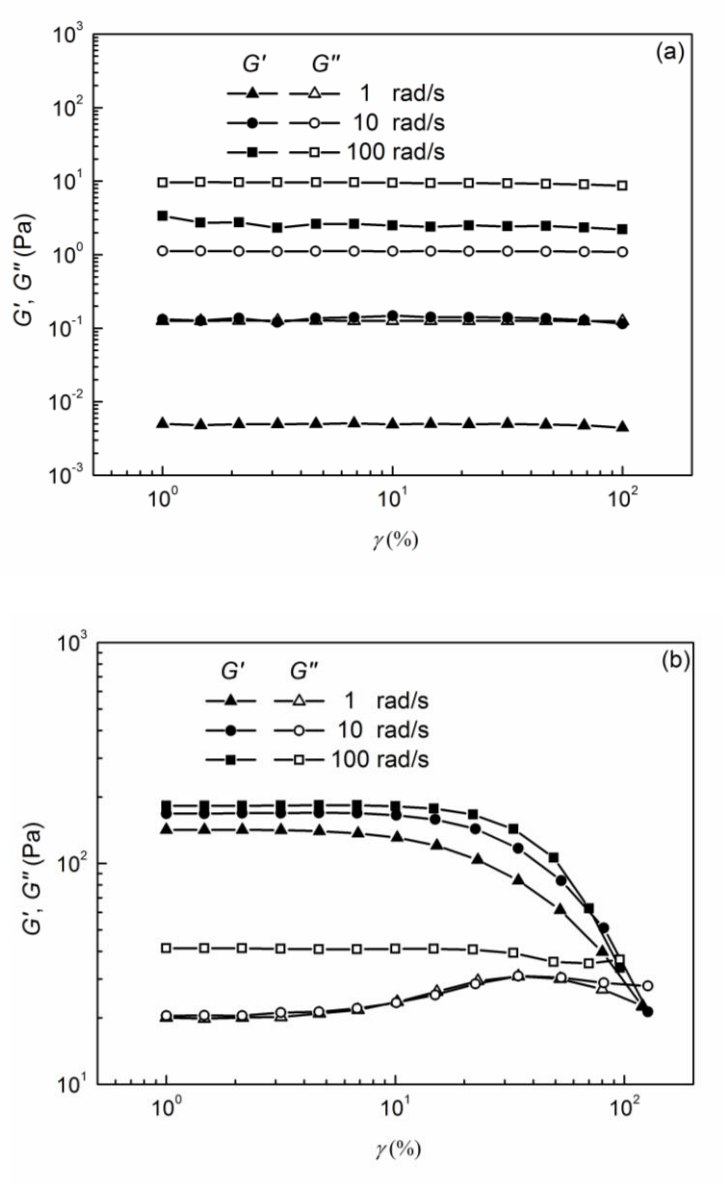


**Figure 3.5** Dynamic shear moduli ($G'$ and $G''$) as a function of strain for 5 wt%

PON(3-25-10) solution measured at three frequencies (1, 10, 100 rad/s) and at 25 ℃ (a) and 45 ℃ (b).

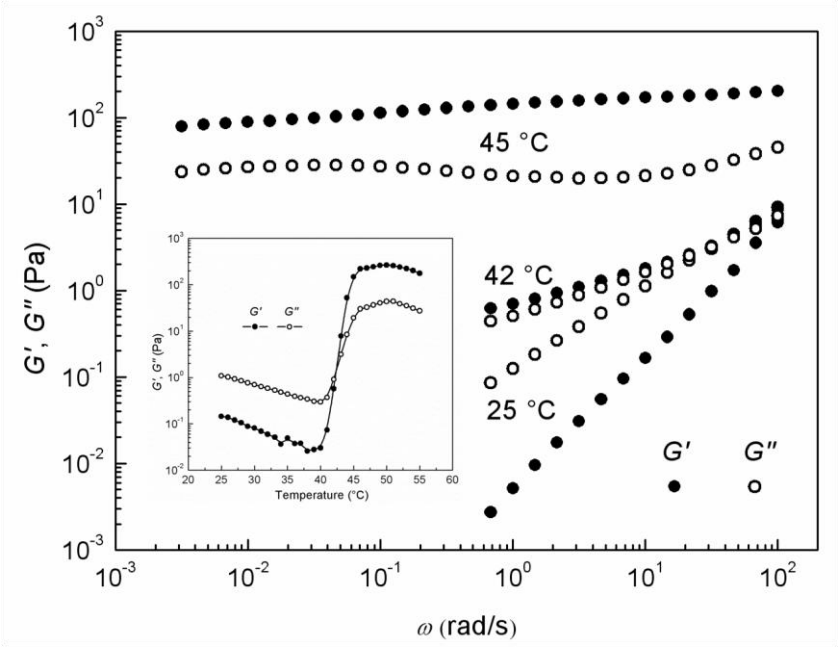


**Figure 3.6** Dynamic shear moduli ($G'$ and $G''$) as a function of frequency for 5 wt% PON(3-25-10) solution measured at a strain $\gamma$ = 2% and three indicated temperatures. The inset is temperature-dependent dynamic shear moduli ($G'$ and $G''$) for 5 wt% PON(3-25-10) solutions at a strain $\gamma$ = 2%, a frequency $\omega$ = 10 rad/s and heating rate of 1 ℃/min.

The thermoreversible nature of this sol-gel transition was verified using dynamic temperature sweep measurements (inset in Figure 3.6), in which $G'$ and $G''$ were measured as a function of temperature during a ramp from 25 to 55 ℃ at a heating rate of 1 ℃/min. At low temperature, the values of both $G'$ and $G''$ are low, and $G' < G''$, indicating a free-flowing sol state. On increasing temperature, the magnitude of both $G'$

and $G''$ increase abruptly and then $G'$ reaches a plateau. As the increase in $G'$ is more significant than $G''$, $G'$ becomes larger than $G''$ at higher temperatures indicating the solid-like behavior. The crossover of $G'$ and $G''$, identified as $T_{gel}$, is 42 ℃, consistent with the results in the dynamic frequency sweep measurements. The remarkably sharp gelation transition is unprecedented for flexible coil block polymers at such low concentrations.

The gelation behavior was also examined using differential scanning calorimetry (DSC) and variable temperature $^1$H NMR spectroscopy. DSC traces obtained for 5 wt% PON(3-25-10) solution are presented in Figure 3.7. It shows an endothermic transition starting at 41 ℃ in the heating process and an exothermic transition ending at 40 ℃ during the cooling. The endothermic peak associated with the gelation is consistent with the coil-to-globule transition of PNIPAm, indicating that hydrogel formation is due to the aggregation of PNIPAm blocks.[28] It is also worth noting that the transition temperature agrees very well with the value of $T_{gel}$ determined from rheological measurements.

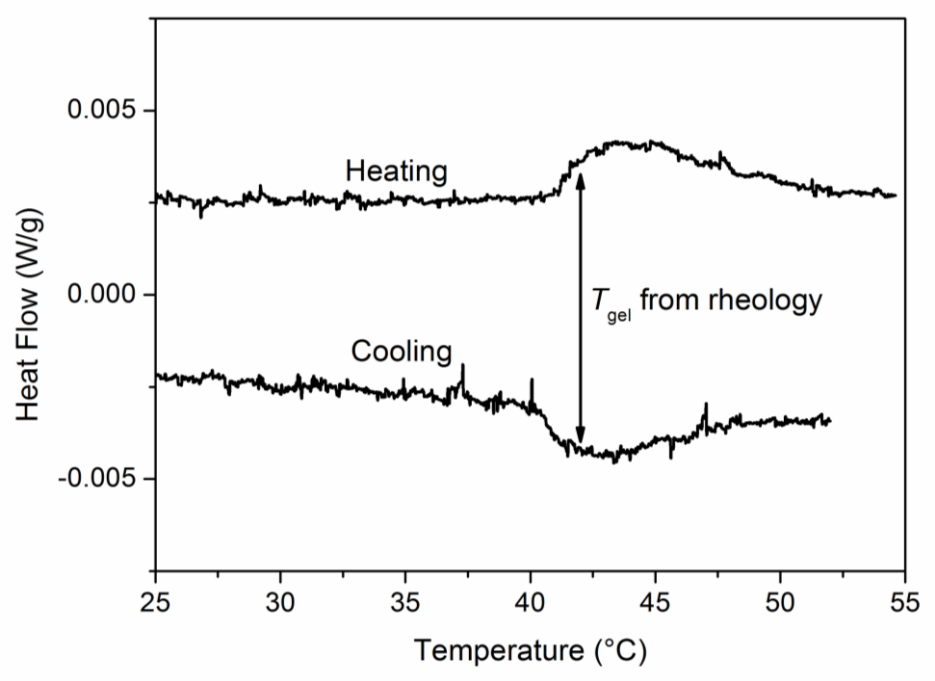


**Figure 3.7** Temperature dependence of heat flow for the 5 wt% PON(3-25-10) solution measured at heating and cooling rates of ±2 ℃/min. $T_{gel}$ is obtained from Figure 3.6 on heating.

$^1$H NMR spectra at various temperatures from 25 to 55 ℃ are presented in Figure 3.8. The $^1$H NMR signals for the PEO and PNIPAM blocks are apparent at 25 ℃, while the resonances for the PEP blocks are not, indicating the formation of micelles with PEP cores and PEO-PNIPAm coronas at this temperature.[11] On increasing the solution temperature to 45 ℃, the $^1$H NMR signals corresponding to the PNIPAM blocks become diminished in intensity and are no longer observed at 55 ℃, indicating the aggregation of PNIPAM chains at higher temperatures. This result also confirms that the formation of the micellar network is based on hydrophobic associations between PNIPAM chains. It should be noted that the dehydration of the PNIPAm block occurred not only at around

$T_{gel}$ (42 ℃), but also well above the $T_{gel}$ (50 ℃).

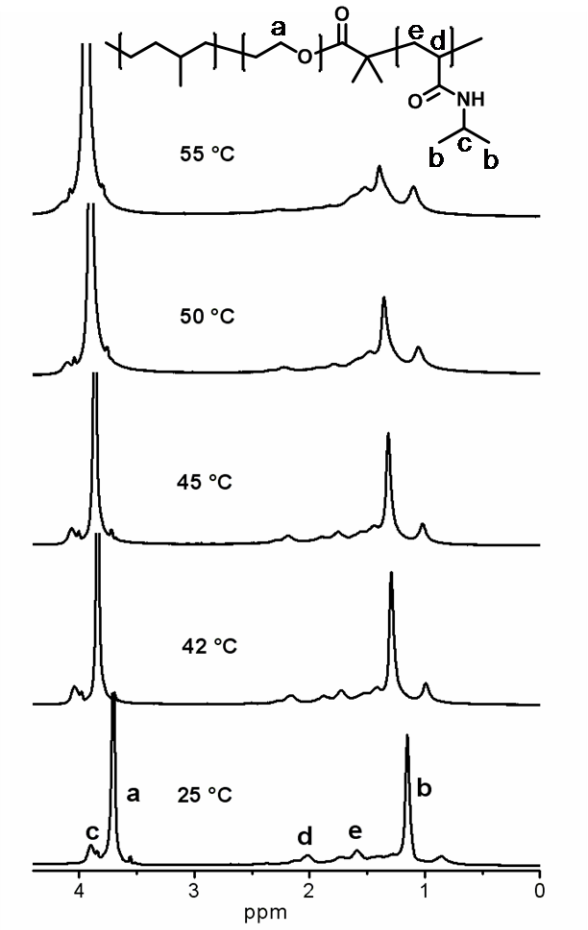


**Figure 3.8** Variable-temperature $^1$H NMR spectra for 5 wt% PON(3-25-10) in $D_2O$.

PON terpolymers form well-defined micelles with hydrophobic PEP cores surrounded by PEO-PNIPAm coronae at room temperature. These micelles do not pack into an ordered lattice at room temperature, as the concentration (5 wt%) is not high enough. Therefore, it is a viscoelastic liquid. As the solution is heated above the LCST of PNIPAm, the PNIPAm chains on adjacent micelles can associate to form PNIPAm hydrophobic microdomains bridged to the PEP microdomains by the PEO midblocks,

resulting in the formation of an elastic network. It is worth noting that the critical micellar aggregation temperature for the 0.5 wt% polymer solution is also 42 ℃, consistent with $T_{gel}$ shown here.[19]

### 3.3.2 Comparsion between PON and NON Hydrogels

We compared the gelation properties between PON(3-25-10) and NON(10-20-10) with comparable PEO and PNIPAm block lengths by examining the temperature dependence of *G′* and *G″* at 5 wt% and 2 wt% polymer (Figure 3.9). PON gelation is very sharp, within 5 ℃, at both concentrations whereas the NON copolymer shows a very gradual and broad transition at the concentration of 5 wt% and no gelation at a concentration of 2 wt%. Such a broad sol-gel transition has been observed in other thermoresponsive ABA hydrogels. For example, PNIPAm-containing ABA triblock hydrogels have been prepared with different hydrophilic midblocks, such as poly(*N*,*N*-dimethylacrylamide) (PDMA)[15] and poly(2-methacryloyloxyethyl phosphorylcholine) (PMPC),[11] and the sol-gel transitions were very broad (>20 ℃). Other thermosensitive polymers including poly(methoxydi(ethylene glycol) methacrylate-*co*- methacrylic acid) (PDEGMMA),[17] poly(ethoxydi(ethylene glycol) acrylate-*co*-acrylic acid) (PDEGEA),[29] and poly(2-hydroxypropyl methacrylate) (PHPMA)[12] were used as hydrophobic endblocks for hydrogel formation and gelation typically occurred over a temperature range of 10 ℃ or larger. It is also worth noting that gelation of PON terpolymers is also much sharper than that of other thermoresponsive ABC terpolymers reported in the literature, such as poly(propylene oxide)-*b*-poly(2-methacryloyloxyethylphosphorylcholine)-*b*-poly(*N*-isopropyl-

acrylamide) (PPO-*b*-PMPC-*b*-PNIPAm),[28] poly(2-vinylpyridine)-*b*-poly(ethylene oxide)-*b*-poly- (glycidyl methyl ether-*co*-ethyl glycidyl ether) (P2VP-*b*-PEO-*b*-P(GME-*co*-EGE)),[30, 31] and poly(2-vinylpyridine)-*b*-poly(ethylene oxide)-*b*-poly(oligo(ethylene glycol) methacrylate) (P2VP-*b*-PEO-*b*-POEGMA),[32] all of which have sol-gel transitions of 10 ℃ or larger.

The plateau value of the storage modulus ($G_N$) could be used to characterize the gel strength. As shown in Figure 3.9, $G_N$ of PON terpolymer was much higher than that of NON copolymer, indicating the improved gel strength of PON hydrogels in comparison to NON hydrogels.

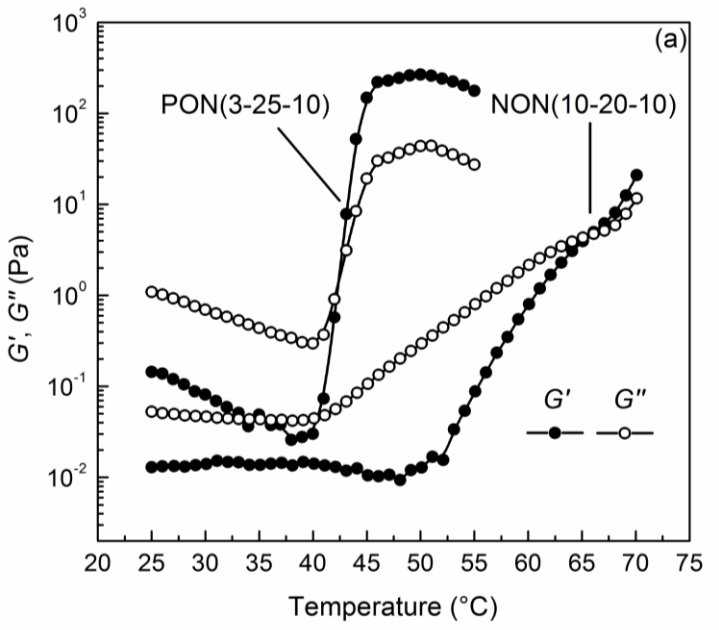

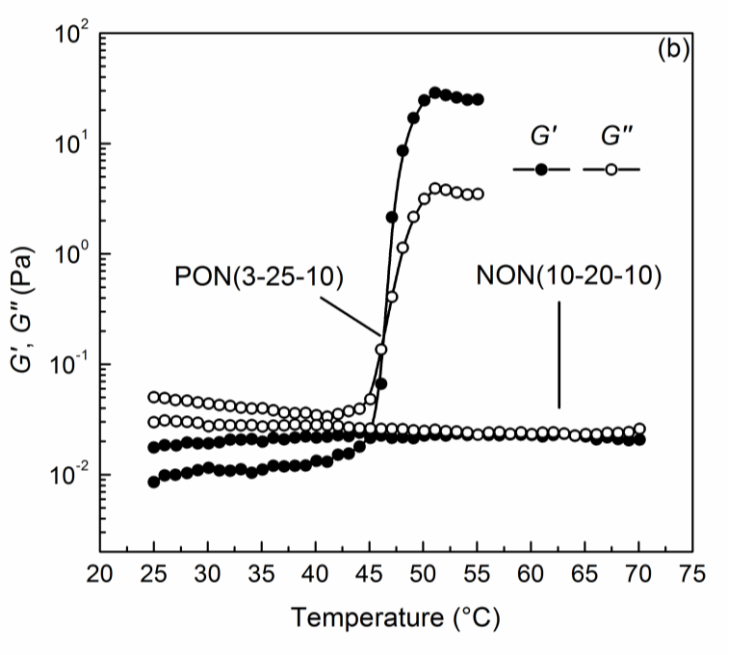


**Figure 3.9** Temperature-dependent dynamic shear moduli (*G′* and *G″*) for (a) 5 wt% PON(3-25-10) and NON(10-20-10) and (b) 2 wt% PON(3-25-10) and NON(10-20-10) solutions measured at a frequency $\omega$ = 10 rad/s and heating rate of 1 ℃/min.

The critical gelation concentration can be obtained from dynamic temperature sweep measurements at different concentrations. Figures 3.10 (a) and (b) show the temperature dependence of *G′* and *G″* obtained for aqueous solutions of PON(3-25-10) and NON(10-20-10) at varying polymer concentrations. The PON terpolymer shows temperature induced gelation behavior at 1, 2 and 5 wt%, while the NON copolymer does not form a well-defined hydrogel until a concentration of 10 wt%, suggesting that the critical gelation concentration of PON terpolymer is much smaller than that of NON copolymer. Such a low gelation concentration is surprising as the minimum gelation concentrations often exceed 10 wt % polymer for physically associated hydrogels.

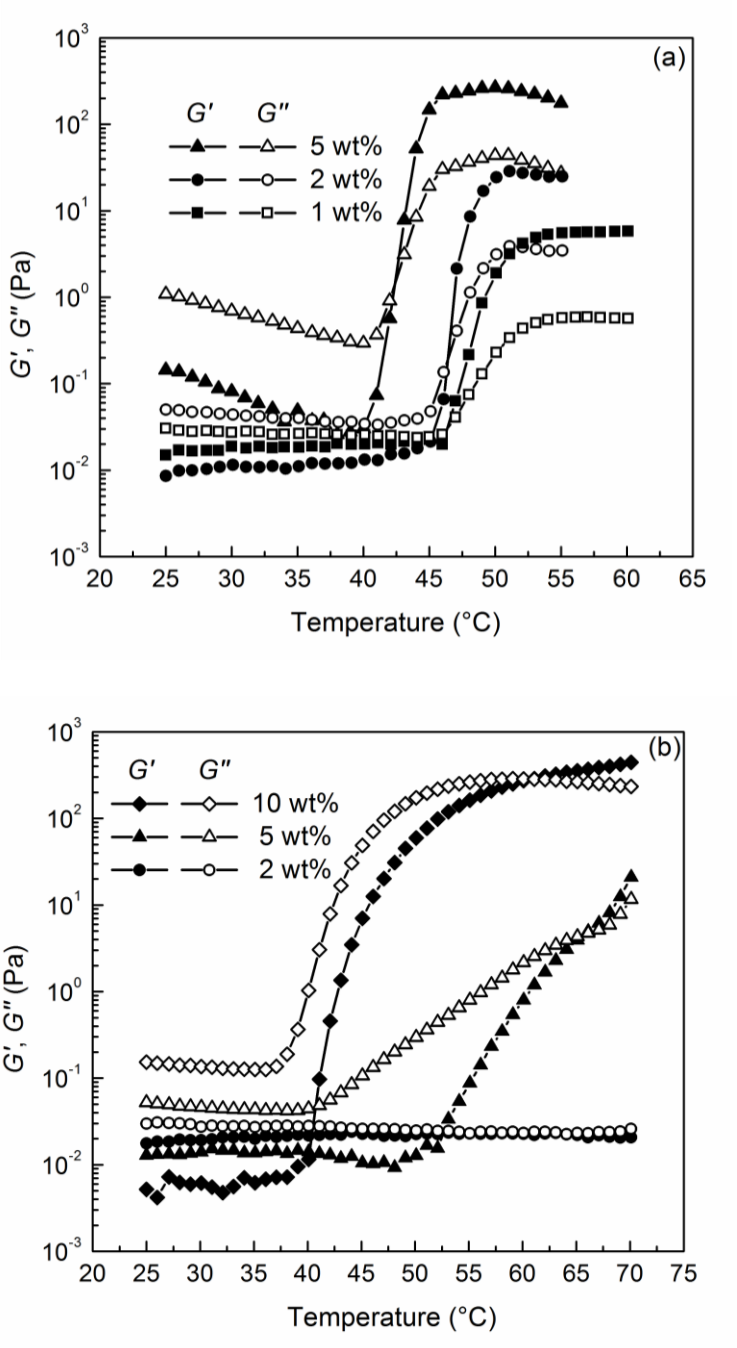


**Figure 3.10** Temperature-dependent dynamic shear moduli ($G'$ and $G''$) for (a) PON(3-25-10) and (b) NON(10-20-10) aqueous solutions with varying polymer concentrations at a frequency $\omega$ = 10 rad/s and heating rate of 1 ℃/min.

Based on these data, we posit that the PON terpolymer undergoes a two-step gelation mechanism, involving the initial formation of micelles with PEP cores at room temperature and gelation due to the PNIPAm block aggregation at elevated temperatures. The gelation of NON copolymers arises solely from the hydrophobic association of PNIPAm endblocks above the LCST; micellization and gelation occur simultaneously. We propose that the separation of micellization and gelation in the PON hydrogels leads to the formation of a two-compartment network with exclusively bridged conformations for the PEO midblocks, while both looping and bridging conformations are possible for the NON hydrogels. With more bridging chains in PON hydrogels, gelation can be achieved at a lower concentration with larger $G_N$. Furthermore, the presence of the PEP-core micelles serves to distribute the PNIPAm endblocks predominantly in the inter-micellar regions, thereby "pre-concentrating" the crosslinking moieties. In such a case, large-scale reorganization of the pre-formed micellar solution is no longer required, the sol-gel transition of PON terpolymers is very sharp.

### 3.3.3 Effect of PEO and PNIPAm Block Length on the Gelation Properties

We then compared the gelation properties of PON triblock terpolymers with different PNIPAm and PEO block lengths by examining the temperature dependence of $G'$ and $G''$ over the concentration range of 1–5 wt%. As shown in Figure 3.11, while no gelation was observed up to 60 ℃ for PON(3-25-4), sol-gel transitions were evident at 1, 2 and 5 wt% polymer for both PON(3-25-21) and PON(3-60-23), similar to PON(3-25-10) discussed earlier (Figure 3.10).

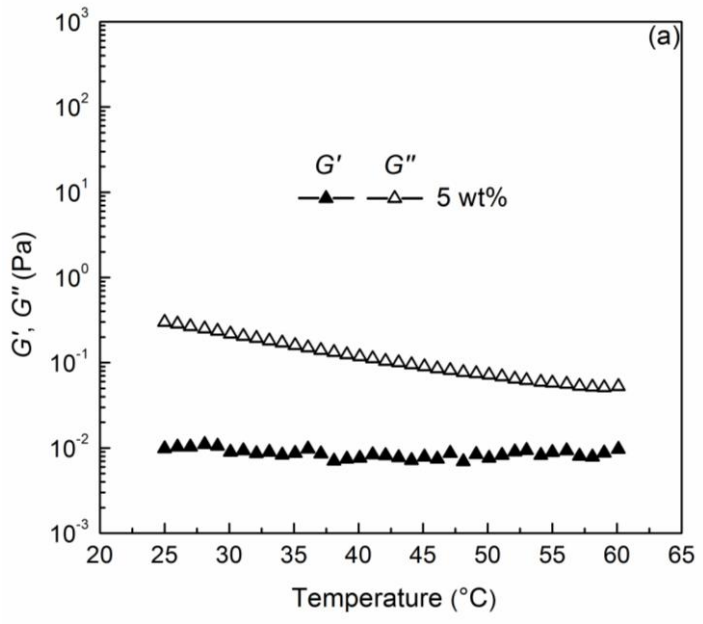
(a)
G′ G″
5 wt%
G′, G″ (Pa)
Temperature (°C)

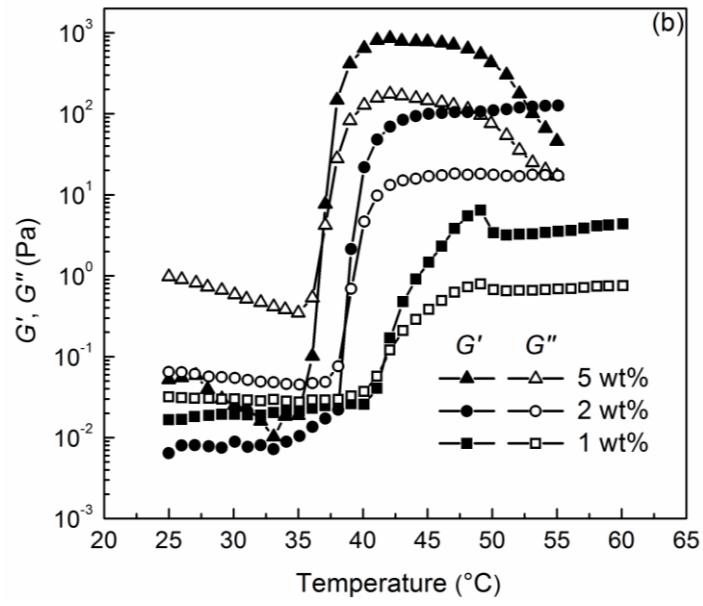
(b)
G′ G″
5 wt%
2 wt%
1 wt%
G′, G″ (Pa)
Temperature (°C)

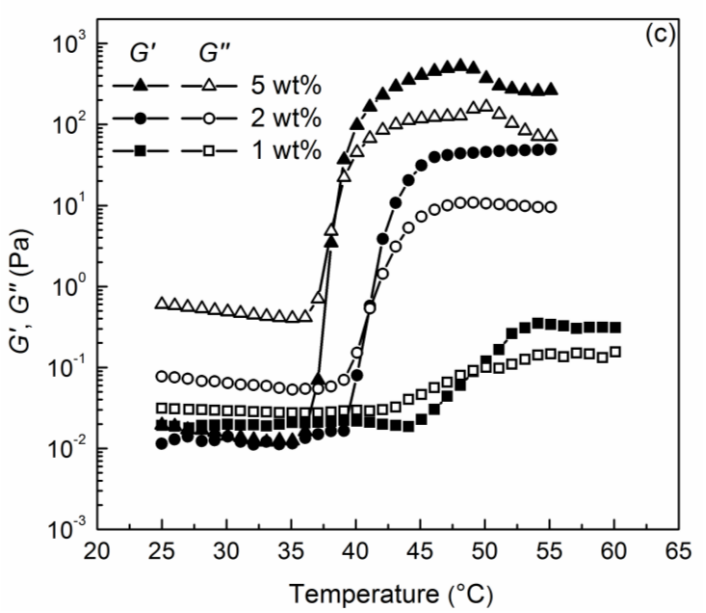


**Figure 3.11** Temperature-dependent dynamic shear moduli ($G'$ and $G''$) for (a) PON(3-25-4), (b) PON(3-25-21) and (c) PON(3-60-23) aqueous solutions with varying polymer concentrations at a frequency $\omega$ = 10 rad/s and heating rate of 1 ℃/min.

The critical gelation temperature ($T_{gel}$) and the plateau storage modulus ($G_N$) of PON triblock terpolymers, obtained from oscillatory shear measurements in Figures 3.10 and 3.11, are summarized in Table 3.2. $T_{gel}$ decreases with increasing PNIPAm molar mass and PON concentration and increases with increasing PEO block length, consistent with the molar mass and concentration dependence of the critical micellar aggregation temperature in dilute dispersions of PON terpolymers.[19] This is expected as both micellar aggregation in dilute solution and gelation in concentrated solution are due to the intermicellar association of the corona PNIPAm chains above the LCST of PNIPAm block. Conversely, larger PNIPAm block lengths, shorter PEO blocks and higher PON concentrations result in larger values of $G_N$.

**Table 3.2** Characteristics of PON hydrogels

| Sample | 5 wt% | | | 2 wt% | | | 1 wt% | | |
|---|---|---|---|---|---|---|---|---|---|
| | $T_{gel}$[a] (℃) | $G_N$[b] (Pa) | $f$[c] | $T_{gel}$[a] (℃) | $G_N$[b] (Pa) | $f$[c] | $T_{gel}$[a] (℃) | $G_N$[b] (Pa) | $f$[c] |
| PON (3-25-10) | 42 | 270 | 8% | 45 | 30 | 2% | 46 | 6 | 0.8% |
| PON (3-25-21) | 36 | 800 | 30% | 38 | 100 | 9% | 40 | 3 | 0.5% |
| PON (3-60-23) | 38 | 520 | 34% | 41 | 50 | 8% | 48 | 0.3 | 0.1% |

[a] Critical gelation temperature as determined from the crossover temperature at which $G' = G''$ in Figures 3.10 and 3.11.[b] Plateau storage modulus. [c] Fraction of elastically effective PEO chains.

For triblock copolymer gels with a midblock in the unentangled regime, the shear modulus can be predicted by classical rubber elasticity theory:

$$G = \nu\, kT = f\ nkT \tag{3-1}$$

where $\nu$ is the number density of elastically effective strands, $f$ is the fraction of bridging or elastically effective chains, $n$ is the chain number density, $k$ is the Boltzmann constant and $T$ is absolute temperature. An estimate of the number of entanglements per molecule, $n_e$, for a polymer in a good solvent is given by

$$n_e = N_e \varphi_p^{5/4} = \frac{M}{M_e} \varphi_p^{5/4} \tag{3-2}$$

where $N_e$ is the number of entanglements per molecule in the melt, $M$ is the polymer molecular weight, $M_e$ is the polymer entanglement molecular weight in the melt and $\varphi_p$ is the polymer volume fraction.[33, 34] For the 5 wt% sample of PON(3-60-23) with the highest PEO molar mass and highest concentration studied in this work, $M_{PEO}$ = 60

kg/mol, $M_{e,\ PEO}$ = 1.6 kg/mol, $\varphi_{PEO}$= 3%, $n_e$ is estimated to be ~0.5. Therefore, we conclude that PEO midblock entanglements are not present in these PON hydrogels, and we can apply equation 3-1 to estimate the fraction of bridging or elastically effective PEO chains:

$$f = \frac{G}{nkT} \tag{3-3}$$

where $G$ is measured plateau storage modulus, $nkT$ is the shear modulus of an ideal network in which 100% chains are elastically effective or f = 1. Table 3.2 shows the fraction of elastically effective PEO chains of PON terpolymers at varying polymer concentrations. The calculated fraction of bridging chains increases with increasing polymer concentration and PNIPAm endblock length, remains nearly constant as we raise the PEO midblock molar mass from 25 to 60 kg/mol. Based on the micelle aggregation number (p ≈ 350) and hydrodynamic radius ($R_h$ = 62 nm) of PON(3-25-10) micelles obtained at 0.5 wt%, the critical micelle overlap concentration of PON(3-25-10) micelles is estimated to be 2.3 wt%.[19] Therefore, upon decreasing the polymer concentration from 5 wt% to 1 wt%, a certain fraction of micelles may not be well integrated into the network structure leading to a decrease of the fraction of bridging chains and thus $G_N$. However, for PON(3-25-10), PON(3-25-21) and PON(3-60-23) at 5 wt%, which is about 2 times the critical micelle overlap concentration, the apparent fraction of bridging chains is still smaller than expected.

We attribute the lower than expected fraction of bridging chains in PON hydrogels to the following factors, all schematically depicted in Figure 3.12. First, the network structure is heterogeneous on large length scales. PON hydrogels are opaque over the

concentration range of 1–5 wt% (Figure 3.4), suggesting the presence of submicron to micron-sized voids in the micellar network. Second, it is possible that some PNIPAm hydrophobic microdomains only connect two PEP micellar cores, leading to the formation of linear constructs as opposed to true crosslinking domains. PEO chains in such structures would not be elastically effective although they adopt bridging conformations. Third, it is possible that some of the PNIPAm chains collapse on themselves within the hydrophilic PEO shells without crosslinking with other micelles to form what would be effectively dangling ends. This will lower the fraction of bridging chains. Similarly, PNIPAm chains might collapse around hydrophobic PEP cores thus forming PEO with looping conformations. However, looping conformations are highly unlikely as suggested by dilute solutions (0.5-0.005 wt%) in Chapter 2.[19] As we increase the molar mass of PNIPAm, the volume fraction of PNIPAm becomes higher at fixed polymer concentration. Therefore they have more chance to aggregate among different micelles instead of forming the aforementioned network defects. This leads to a higher fraction of elastically effective chains in PON terpolymers with longer PNIPAm blocks.

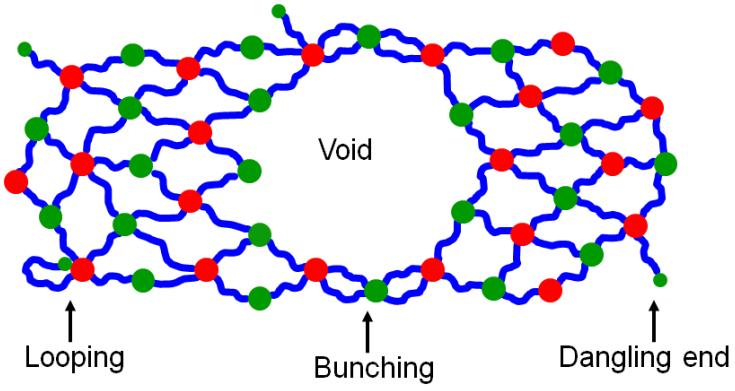


**Figure 3.12** Possible defects in PON hydrogel network.

In a physically associated hydrogel with stretched midblocks, increasing the midblock chain length leads to an increase in the fraction of elastically effective chains as the energy penalty for stretching the midblock to form bridges becomes less severe with a larger midblock, and thus the loop-to-bridge ratio decreases on increasing midblock length.[35] As noted earlier, PEO block length does not have a strong influence on the fraction of elastically effective chains, indicating that the PEO midblocks is not stretched, or at least not very stretched, which is consistent with small angle neutron scattering (SANS) analysis (see Chapter 4).[36] The plateau modulus is determined by two factors in equation 3-1: the chain number density and the elastically effective chain fraction. The lower chain number density in PON with a larger PEO midblock results in a lower value of $G_N$.

The fraction of elastically effective PEO chains for the NON(10-20-10) hydrogel at 10 wt% is ~6%, which smaller than that of PON(3-25-10) hydrogel (8%) at the concentration of 5 wt%. As the fraction of bridging chains in block copolymer hydrogels increases with polymer concentration, PON terpolymers would have a much higher $f$ value than NON copolymers at the same concentration. This further confirms that the formation of a two-compartment network structure in PON hydrogels leads to more bridging chains for PEO midblocks in comparison to NON hydrogels.

It should be noted that the fraction of elastically effective midblocks for other ABC hydrogels have been reported previously. For example, PPO-*b*-PMPC-*b*-PNIPAm hydrogel[28] at 20 wt% and ABC triblock protein hydrogel[37] at 7 w/v% have elastically effective midblock fraction of ~0.4% and 35%, respectively. While $f$ of the former is much smaller than that of all PON hydrogels, the latter has a comparable $f$ to PON

hydrogels with the larger PNIPAm block in this study.

We found that when the temperature increases above 50 ℃, $G'$ of PON(3-25-10) hydrogel decreases moderately and that of PON(3-25-21) and PON(3-60-23) hydrogels drops significantly at the concentration of 5 wt%, which is not observed at lower concentrations. We also note that a small amount of water on the surface of rheometer (couette fixture) is observed at the end of the heating process for the 5 wt% PON(3-25-10) sample. The decrease of $G'$ at higher temperatures is likely due to the syneresis of the PNIPAm blocks, which is more obvious for PON with longer PNIPAm block length at higher polymer concentration. This is consistent with a number of reports concerning the PNIPAm-containing block copolymer hydrogels.[38, 39]

### 3.4 Summary

In conclusion, we prepared thermoresponsive ABC hydrogels from PON triblock terpolymers. The terpolymers form micelles in water at low temperatures with hydrophobic PEP cores surrounded by hydrophilic PEO-PNIPAm coronae. These micelles associate to form a hydrogel upon heating above the LCST of PNIPAm. The separation of micellization and gelation leads to the formation of a two-compartment network with a very high fraction of bridging conformations for the PEO midblocks. Therefore, gelation can be achieved at a much lower concentration, with a much higher modulus and sharper sol-gel transition, as compared to NON copolymer hydrogels. The critical gelation aggregation temperature ($T_{gel}$) and the plateau storage modulus ($G_N$) of PON terpolymers are dependent on both the molar mass of PNIPAm and PEO and polymer concentration. The longer PNIPAm endblocks, shorter PEO midblocks and

higher polymer concentration resulted in a lower critical gelation temperature and a higher $G_N$.

### 3.5 References


1. Annable, T.; Buscall, R.; Ettelaie, R.; Whittlestone, D. *J. Rheol.* **1993**, *37*, 695-726.
2. Annable, T.; Buscall, R.; Ettelaie, R. *Colloids Surf., A* **1996**, *112*, 97-116.
3. Semenov, A. N.; Joanny, J. F.; Khokhlov, A. R. *Macromolecules* **1995**, *28*, 1066-1075.
4. Tam, K. C.; Jenkins, R. D.; Winnik, M. A.; Bassett, D. R. *Macromolecules* **1998**, *31*, 4149-4159.
5. Tsitsilianis, C.; Katsampas, I.; Sfika, V. *Macromolecules* **2000**, *33*, 9054-9059.
6. Yamaguchi, D.; Cloitre, M.; Panine, P.; Leibler, L. *Macromolecules* **2005**, *38*, 7798-7806.
7. Ricardo, N. M. P. S.; Honorato, S. B.; Yang, Z.; Castelletto, V.; Hamley, I. W.; Yuan, X. F.; Attwood, D.; Booth, C. *Langmuir* **2004**, *20*, 4272-4278.
8. Meng, X.; Russel, W. B. *J. Rheol.* **2006**, *50*, 189-205.
9. Tae, G.; Kornfield, J. A.; Hubbell, J. A.; Johannsmann, D.; Hogen-Esch, T. E. *Macromolecules* **2001**, *34*, 6409-6419.
10. Yu, L.; Zhang, H.; Ding, J. *Angew. Chem., Int. Ed.* **2006**, *45*, 2232-2235.
11. Li, C.; Tang, Y.; Armes, S. P.; Morris, C. J.; Rose, S. F.; Lloyd, A. W.; Lewis, A. L. *Biomacromolecules* **2005**, *6*, 994-999.
12. Madsen, J.; Armes, S. P.; Lewis, A. L. *Macromolecules* **2006**, *39*, 7455-7457.

13. Kirkland, S. E.; Hensarling, R. M.; McConaughy, S. D.; Guo, Y.; Jarrett, W. L.; McCormick, C. L. *Biomacromolecules* **2008**, *9*, 481-486.
14. Vogt, A. P.; Sumerlin, B. S. *Soft Matter* **2009**, *5*, 2347-2351.
15. Ge, Z.; Zhou, Y.; Tong, Z.; Liu, S. *Langmuir* **2011**, *27*, 1143-1151.
16. Vermonden, T.; Besseling, N. A. M.; van Steenbergen, M. J.; Hennink, W. E. *Langmuir* **2006**, *22*, 10180-10184.
17. O'Lenick, T. G.; Jiang, X.; Zhao, B. *Langmuir* **2010**, *26*, 8787-8796.
18. Hillmyer, M. A.; Lodge, T. P. *J. Polym. Sci., Part A: Polym. Chem.* **2002**, *40*, 1-8.
19. Zhou, C.; Hillmyer, M. A.; Lodge, T. P. *Macromolecules* **2011**, *44*, 1635-1641.
20. Zhou, C.; Hillmyer, M. A.; Lodge, T. P. *J. Am. Chem. Soc.* **2012**, *134*, 10365-10368.
21. He, Y.; Lodge, T. P. *Chem. Commun.* **2007**, 2732-2734.
22. Qiu, X.; Winnik, F. M. *Macromol. Rapid Commun.* **2006**, *27*, 1648-1653.
23. Fetters, L. J.; Lohse, D. J.; Richter, D.; Witten, T. A.; Zirkel, A. *Macromolecules* **1994**, *27*, 4639-4647.
24. Smith, G. D.; Yoon, D. Y.; Jaffe, R. L.; Colby, R. H.; Krishnamoorti, R.; Fetters, L. J. *Macromolecules* **1996**, *29*, 3462-3469.
25. Shields, D. J.; Coover, H. W. *J. Polym. Sci.* **1959**, *39*, 532-533.
26. Chambon, F.; Petrovic, Z. S.; Macknight, W. J.; Winter, H. H. *Macromolecules* **1986**, *19*, 2146-2149.
27. Winter, H. H.; Chambon, F. *J. Rheol.* **1986**, *30*, 367-382.
28. Li, C.; Buurma, N. J.; Haq, I.; Turner, C.; Armes, S. P.; Castelletto, V.; Hamley, I. W.; Lewis, A. L. *Langmuir* **2005**, *21*, 11026-11033.
29. O'Lenick, T. G.; Jin, N.; Woodcock, J. W.; Zhao, B. *J. Phys. Chem. B* **2011**, *115*,

2870-2881.

30. Reinicke, S.; Schmelz, J.; Lapp, A.; Karg, M.; Hellweg, T.; Schmalz, H. *Soft Matter* **2009**, *5*, 2648-2657.
31. Reinicke, S.; Karg, M.; Lapp, A.; Heymann, L.; Hellweg, T.; Schmalz, H. *Macromolecules* **2010**, *43*, 10045-10054.
32. Reinicke, S.; Schmalz, H. *Colloid Polym. Sci.* **2011**, *289*, 497-512.
33. Milner, S. T. *Macromolecules* **2005**, *38*, 4929-4939.
34. Seitz, M. E.; Burghardt, W. R.; Faber, K. T.; Shull, K. R. *Macromolecules* **2007**, *40*, 1218-1226.
35. Shen, W.; Kornfield, J. A.; Tirrell, D. A. *Soft Matter* **2007**, *3*, 99-107.
36. Two scattering peaks, observed for the 5 wt% PON(3-25-10) sample, corresponded to two different spatial correlation lengths of ~53 and 34 nm between micelles. The spatial correlation length represents micellar center-to-center distance. Subtracting the PEP and PNIPAm core radii from these distances gives the typical lengths of the PEO bridge between two micelles (~36nm and 17nm). The latter is roughly consistent with the Gaussian coil end-to-end distance (~14 nm) of the 25 kg/mol PEO midblock, suggesting that PEO midblock is not stretched. See Chapter 4 for details.
37. Shen, W.; Zhang, K.; Kornfield, J. A.; Tirrell, D. A. *Nat. Mater.* **2006**, *5*, 153-158.
38. Convertine, A. J.; Lokitz, B. S.; Vasileva, Y.; Myrick, L. J.; Scales, C. W.; Lowe, A. B.; McCormick, C. L. *Macromolecules* **2006**, *39*, 1724-1730.
39. Liu, J.; Chen, G.; Guo, M.; Jiang, M. *Macromolecules* **2010**, *43*, 8086-8093.

# Chapter 4

# Morphology of Two-compartment Hydrogels from PON Triblock Terpolymers

## 4.1 Introduction

The self-assembly of multiblock copolymers into multicompartment micelles or gels with distinguishable subdomains or compartments draw inspiration from biological systems such as eukaryotic cells, which possess distinct subunits that enable them to perform multiple functions simultaneously.[1-3] A variety of multicompartment micellar structures ("hamburger" micelles, segmented worms, nanostructured bilayers and vesicles, raspberry-like micelles and so on) have been successfully prepared in water or in water-organic solvent mixtures and well characterized by dynamic light scattering (DLS) and cryogenic transmission electron microscopy (cryo-TEM).[4-12] In contrast to the high numbers of studies on the self-assembly behavior of multicompartment micelles, there have been only a few reports on multicompartment gels. For example, Weberskirch, *et al.* studied the self-association behavior of poly(*N*-acylethyleneimine) polymers end-capped with a fluorocarbon group and a hydrocarbon group, and showed the segregation of the end groups using NMR spectroscopy at relatively high polymer concentration (31 wt%).[13] Similarly, Komenda *et al.* prepared a multicompartment micellar hydrogel from poly(2-*n*-nonyl-2-oxazoline)-*b*-poly(2-methyl-2-oxazoline)-*b*-poly(2-(1'H,1'H,2'H,2'H-

perfluorohexyl)-2-oxazoline) (PNOx-*b*-PMOx-*b*-PFOx) and inferred the presence of a micellar network with spherical PNOx cores and ellipsoidal PFOx cores using small angle neutron scattering (SANS) experiments.[14] Armes *et al.* studied the gelation behavior of thermoresponsive hydrogels from poly(propylene oxide)-*b*-poly (2-methacryloyloxyethylphosphorylcholine)-*b*-poly(*N*-isopropylacrylamide) (PPO-*b*-PMPC-*b*-PNIPAm) and proposed the formation of a micellar network with segregated PPO and PNIPAm cores. However, no morphological characterization was reported in this study.[15] Recently, Taribagil *et al.* investigated the morphology of a compartmentalized hydrogel from a telechelic poly(ethylene oxide) (PEO) end-capped with mutually incompatible hydrophobic blocks (poly(1,2-butadiene) (PB) and poly(perfluoropropylene oxide) (PFPO)), and revealed a bicontinuous structure composed of PFPO disks distributed within a hydrophobic PB sheet covered by hydrophilic PEO brushes, by cryogenic scanning electron microscopy (cryo-SEM) and SANS experiments.[16, 17]

In Chapter 3, we reported the gelation behavior of poly(ethylene-*alt*-propylene)-*b*-poly(ethylene oxide)-*b*-poly(*N*-isopropylacrylamide) (PON) triblock terpolymers.[18] The terpolymers form micelles in water at low temperatures with hydrophobic PEP cores surrounded by hydrophilic PEO-PNIPAm coronae. These micelles associate to form a hydrogel upon heating above the LCST of PNIPAm. The separation of micellization and gelation leads to the formation of a two-compartment network with a very high fraction of bridging conformations for the PEO midblocks. Therefore, gelation can be achieved at a much lower concentration, with a much sharper sol−gel transition, as compared to poly(*N*-isopropylacrylamide)-*b*-poly(ethylene

oxide)-*b*-poly(N-isopropylacrylamide) (NON) triblock copolymer hydrogels. The formation of two discrete PEP and PNIPAm hydrophobic domains in the hydrogel network is crucial for the preparation of compartmentized hydrogels with improved gelation properties. However, this interpretation is just a hypothesis, and not yet proved. In this chapter, we will present a detailed morphological characterization on the aqueous solutions of PON triblock terpolymers over the concentration range of 1−5 wt% at varying temperatures, and demonstrate that PON terpolymers form two-compartment hydrogels with discrete spherical PEP and PNIPAm micelles in water upon heating above the LCST of PNIPAm.

## 4.2 Experimental Section

### 4.2.1 Materials

We prepared two triblock terpolymers: PON with a normal PNIPAm block and $PON_{d7}$ with a deuterated PNIPAm block (Scheme 4.1). PON with a normal PNIPAm block was prepared using a combination of anionic and reversible addition-fragmentation chain transfer (RAFT) polymerizations (see Chapter 2).[19] $PON_{d7}$ with a deuterated PNIPAm block was synthesized following the same protocol using d7-*N*-isopropylacrylamide to grow the dPNIPAm block. The product of each reaction step was confirmed by $^1$H NMR spectroscopy and characterized by size exclusion chromatography (SEC) (Figure 4.1). In the elugram, some amount of tailing is observed for PON samples. The light scattering results confirmed that the tailing corresponded to the signals from PON triblocks instead of PO diblocks, suggesting that the apparent broadening is likely due to the interaction between PNIPAm and the column materials in

THF without amine additives. Samples investigated in this work are listed in Table 4.1 along with the molecular characteristics.

**Scheme 4.1** Chemical structure of PON and $PON_{d7}$ triblock terpolymers

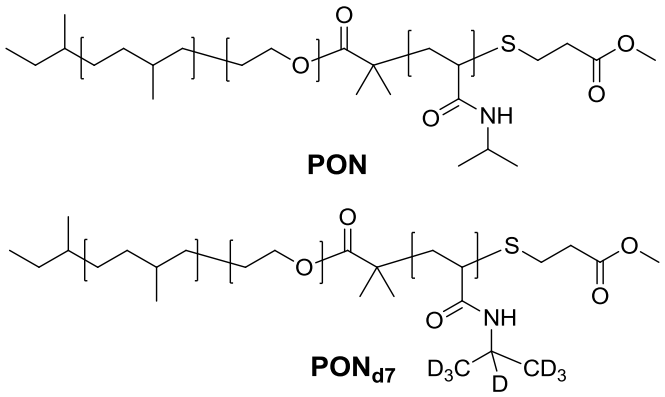


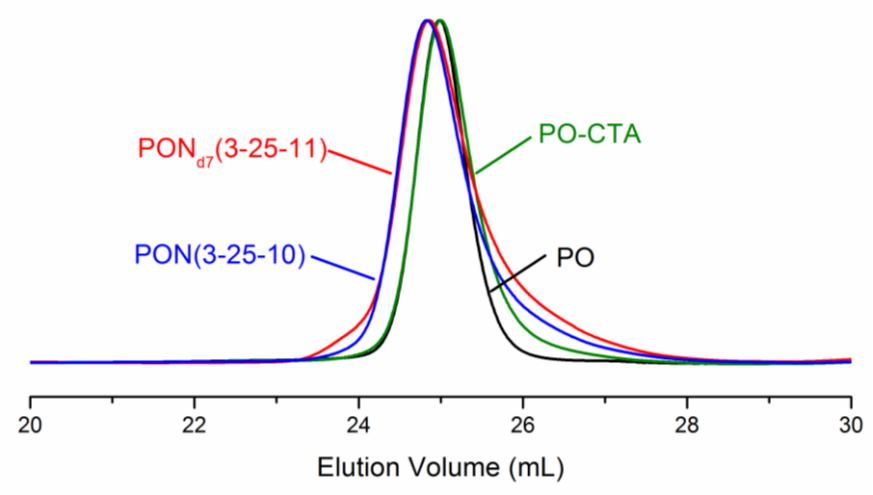


**Figure 4.1** SEC traces of PO, PO-CTA, PON(3-25-10), $PON_{d7}$(3-25-11). THF was used as the eluting solvent at a flow rate of 1.0 mL/min.

**Table 4.1** Molecular parameters of PON and $PON_{d7}$ triblock terpolymers

| Sample[a] | $N_{PEP}$[b] | $N_{PEO}$[b] | $N_{PNIPAm}$[b] | $f_{PEP}$[c] | $f_{PEO}$[c] | $f_{PNIPAm}$[c] | $Đ$[d] |
|---|---|---|---|---|---|---|---|
| PON(3-25-10) | 45 | 565 | 89 | 0.11 | 0.63 | 0.26 | 1.09 |
| $PON_{d7}$(3-25-11) | 45 | 565 | 95 | 0.10 | 0.62 | 0.28 | 1.11 |

[a] The numbers in the parentheses correspond to the molar masses of PEP, PEO, and PNIPAm(dPNIPAm), respectively, in kg $mol^{-1}$ as determined by $^1H$ NMR spectroscopy. [b] Number average degree of polymerization as determined by $^1H$ NMR spectroscopy. [c] The volume fraction was calculated using the molecular weight and the RT densities: ρ(PEP) = 0.856 $g/cm^3$,[20] ρ(PEO) = 1.12 $g/cm^3$, [21] and ρ(PNIPAm) = 1.07 $g/cm^3$.[22] [d] The dispersity was measured by SEC equipped with both light scattering and refractive index detectors with THF as the eluting solvent.

### 4.2.2 Solution Preparation

All the polymer solutions were prepared by the thin-film hydration method. Appropriate amounts of bulk polymer were dissolved in $CH_2Cl_2$, followed by evaporation of the solvent to yield a thin film on the walls of the vial. The thin film was then hydrated with a defined amount of water or heavy water, and the resulting mixture was stirred at room temperature for at least 1 month before further characterization. Water ($H_2O$, Chromasolv grade) was used as solvent for cryogenic scanning electron microscopy (cryo-SEM) and cryogenic transmission electron microscopy (cryo-TEM) experiments. For small-angle neutron scattering (SANS) experiments, heavy water ($D_2O$, 99.9% D, Cambridge Isotopes) or mixtures of water and heavy water with compositions varying

according to the desired contrast match, were used as solvents.

### 4.2.3 Cryogenic Scanning Electron Microscopy (cryo-SEM)

Cryo-SEM experiments were conducted on the 5 wt% PON sample following a reported protocol.[16, 23, 24] A small amount of sample was sandwiched between two "freezing hats" (each about 100 $\mu$m deep). The sandwiched sample was left at 25 ℃ or heated at 50 ℃ for 10 minutes in the chamber of a Bal-Tec HPM 010 high pressure freezing machine and rapidly frozen at the operating pressure of 2100 bar. The frozen sample was then transferred into a liquid nitrogen bath and pried open with a scalpel to fracture the sample, exposing its interior. Vitrified water near the surface and a few micrometers deep into the sample was then partially sublimed in a Balzers MED 010 freeze-drying and sputtering device at –105 ℃ and $\sim 2 \times 10^{-9}$ bar for about 5 min. The exposed surface was then coated with an 8 nm thick conducting layer of platinum at –130 ℃. The coated sample was transferred into a Hitachi S900 scanning electron microscope, maintained at about –175 ℃, and examined at a low acceleration voltage of 2 keV to avoid excessive charging and radiation damage of the areas imaged.

### 4.2.4 Cryogenic Transmission Electron Microscopy (cryo-TEM)

Cryo-TEM experiments were conducted on 1 wt% and 2 wt % PON aqueous solutions. Vitrified samples were prepared using an FEI Vitrobot Mark III automated vitrification device. The aqueous solutions were left at 25 ℃ or heated in an oil bath at 50 ℃ for 10 minutes and then rapidly applied to the lacey Formvar carbon-supported TEM grid within the climate chamber of the Vitrobot system, where the temperature was

kept at 25 ℃ or 50 ℃ and the relative humidity was kept at 100%. The excess solution was blotted with a piece of filter paper, resulting in the formation of thin films with thicknesses of *ca.* 100–300 nm in the mesh holes. The samples were quickly plunged into a reservoir of liquid ethane cooled by liquid nitrogen. The vitrified samples were then stored in liquid nitrogen until they were transferred to a cryogenic sample holder and examined with an FEI Technai Spirit BioTWIN transmission electron microscope with an Eagle CCD camera operated at an acceleration voltage of 120 kV at about –178 ℃. The phase contrast was enhanced by acquiring images at a nominal underfocus of 10–15 $\mu$m.

### 4.2.5 Small-Angle Neutron Scattering (SANS)

SANS experiments were conducted on aqueous samples of PON and $PON_{d7}$ over the concentration range of 1–5 wt%. Contrast matching was used to gain detailed information about individual components in multicomponent mixtures. Contrast matching involves choosing a solvent environment with scattering length density ($\rho$*) equal to that of the component to be contrast matched. This renders that particular component invisible to neutrons and enables getting better resolvable information about other components. For aqueous systems, this is done by mixing water ($\rho^* = -5.6\times10^9$ cm$^{-2}$) and heavy water ($\rho^* = 6.36\times10^{10}$ cm$^{-2}$). The scattering length density of the mixture is given by the sum of the scattering length densities of water and heavy water weighted by their volume fractions ($=\sum\phi_i\rho_i^*$). Solutions of PON were prepared in $D_2O$, as the scattering length densities of PEP ($\rho^* = -3.06\times10^9$ cm$^{-2}$), PEO ($\rho^* = 6.34\times10^9$ cm$^{-2}$) and PNIPAm ($\rho^* = 7.92\times10^9$ cm$^{-2}$) are not very different. The $PON_{d7}$ samples were prepared under two contrast matched conditions, namely PEP contrast matched (96% vol% $H_2O$) and zero mean contrast

(67.5% vol% $H_2O$). Figure 4.2 shows the dependence of the scattering intensity equation prefactor ($(\Delta b)^2 c M_w$) for the individual block in $PON_{d7}$(3-25-11) on composition of $H_2O/D_2O$ mixtures, where $c$ and $M_w$ are the concentration and molecular weight of the polymer, respectively, and $\Delta b$ is the difference between the scattering lengths of the polymer and the solvent.[16] The prefactor signifies the scattering intensity of the polymer without consideration of size, shape or structural correlations and provides a quick estimate of the scattering intensities for the polymer with changing solvent composition. The dip in the curve indicates a contrast matched condition where the coherent scattering capacity of the specific polymer is matched with that of the solvent. It can be seen that under PEP contrast matched condition (96% vol% $H_2O$), the deuterated PNIPAm block is the dominant scatterer. Zero mean contrast condition (67.5% vol% $H_2O$) indicates that the scattering length density of the solvent equals that of the triblock as a whole, instead of the individual blocks.

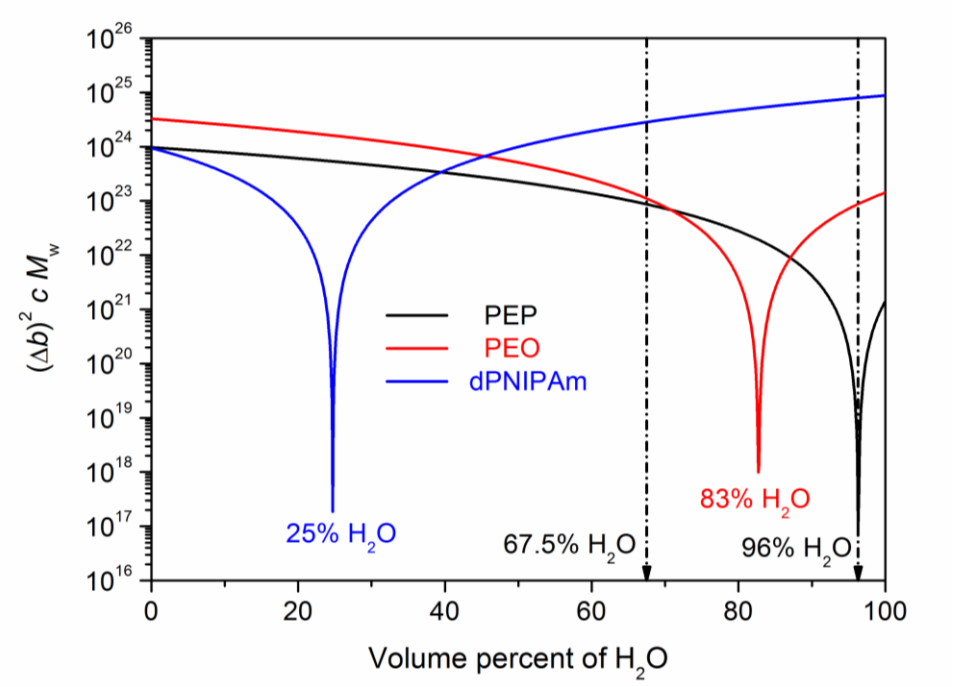


**Figure 4.2** Dependence of scattering intensity equation prefactor ($(\Delta b)^2 c M_w$) on composition of $H_2O/D_2O$ mixtures for PEP, PEO and dPNIPAm, the individual blocks of the 5 wt% aqueous solution of $PON_{d7}$(3-25-11). The two arrows indicate two contrast matched conditions: PEP contrast matched (96% vol% $H_2O$) and zero mean contrast (67.5% vol% $H_2O$).

The scattering experiments were performed at the National Institute of Standards and Technology (NIST) on the NG-7 30 m instrument of the Cold Neutron Research Facility.[25] A neutron wavelength of 7 Å or 8 Å was used in conjunction with detector distances of 1, 3, 13 and 15 m to cover scattering wave vectors from 0.001 to 0.3 $Å^{-1}$. The samples were loaded into NIST sample cells with a path length of 1 mm and heated at each desired discrete temperature for 5 minutes before taking the measurements. Using Igor Pro Macros, the resulting data were corrected for background, nonuniform detector

efficiency, empty cell scattering, and sample transmission. The scattering intensities were then scaled to absolute values on the basis of direct beam flux measurements.[26]

## 4.3 Results and Discussion

### 4.3.1 Structural Characterization by Cryo-SEM and Cryo-TEM

Cryo-SEM images of the 5 wt% PON(3-25-10) sample prepared at 25 ℃ and 50 ℃ are shown in Figure 4.3. The sample at 25 ℃ shows an array of spherical objects with radii in the range of 50–70 nm (Figure 4.3a). This is consistent with the formation of spherical micelles with PEP core and PEO-PNIPAm corona at room temperature. Quantitative determination of the size of PEP cores from this dimension is complicated by the presence of a *ca.* 8 nm platinum coat, and the difficulty in discriminating the core versus corona. Thus it is not considered further here. The cryo-SEM analysis at 50 ℃ reveals a network structure, with a significant number of voids (*i.e.*, water-filled chambers) (Figure 4.3b). The typical dimension of these voids is 200–300 nm. The higher magnification image shows clusters of spheres with diameters in the range of 20–30 nm (Figures 4.3c). This dimension includes the *ca.* 8 nm thick platinum coat and contributions primarily from the hydrophobic cores (PEP or PNIPAm). Therefore, the radius of the hydrophobic cores can be estimated to be between 5–10 nm. However, all the spheres in Figure 4.3c appeared to be very similar. Thus whether the micellar network contains two different hydrophobic domains (PEP and PNIPAm) or not cannot be verified. Overall, our cryo-SEM results suggest that the PON hydrogels formed at elevated temperatures are consisting of networks of spherical micelles, with the presence of large voids.

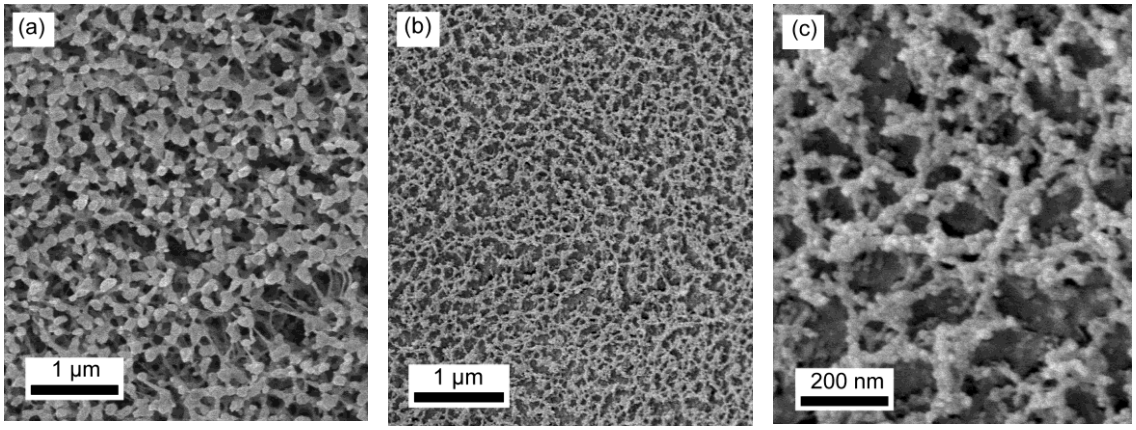


**Figure 4.3** Cryo-SEM images of the 5 wt% PON(3-25-10) sample prepared at (a) 25 ℃, (b) 50 ℃ and (c) 50 ℃.

Cryo-TEM images of the 1 wt% PON(3-25-10) sample prepared at 25 ℃ and 50 ℃ are shown in Figure 4.4. In Figure 4.4a, the sample was vitrified after annealing at 25 ℃, that is, below the gel temperature. The spherical PEP micellar cores with liquid-like arrangement are clearly visible ($R_c \approx 8 \pm 2$ nm). The same solution gave the image shown in Figure 4.4b after annealing at 50 ℃, in the gel state. A 3-4 fold increase in the number of micellar cores is clearly evident, thereby suggesting the formation of a different micellar core (PNIPAm), which leads to the two-compartment network structure. The average micellar core radii ($R_c \approx 9 \pm 2$ nm) have a comparable value with that at 25 ℃, in the micelle state, indicating that PNIPAm micelles have similar core radii to PEP micelles. Based on the assumption that PNIPAm and PEP micelles have comparable core radii, the ratio of PNIPAm to PEP volume fractions suggests that there should be 2-3 times more PNIPAm cores, roughly consistent with our cryo-TEM observation. It is worth noting that increasing the polymer concentration to 2 wt% gave almost identical results at both 25 ℃ and 50 ℃ (Figure 4.5).

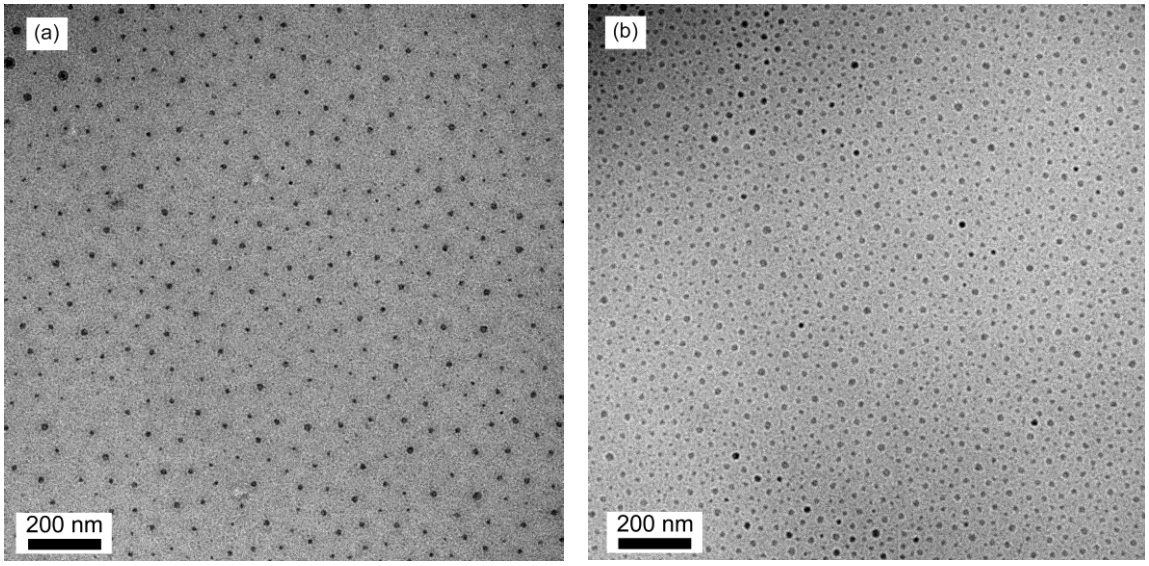


**Figure 4.4** Cryo-TEM images of the 1 wt% PON(3-25-10) sample prepared at (a) 25 ℃ and (b) 50 ℃.

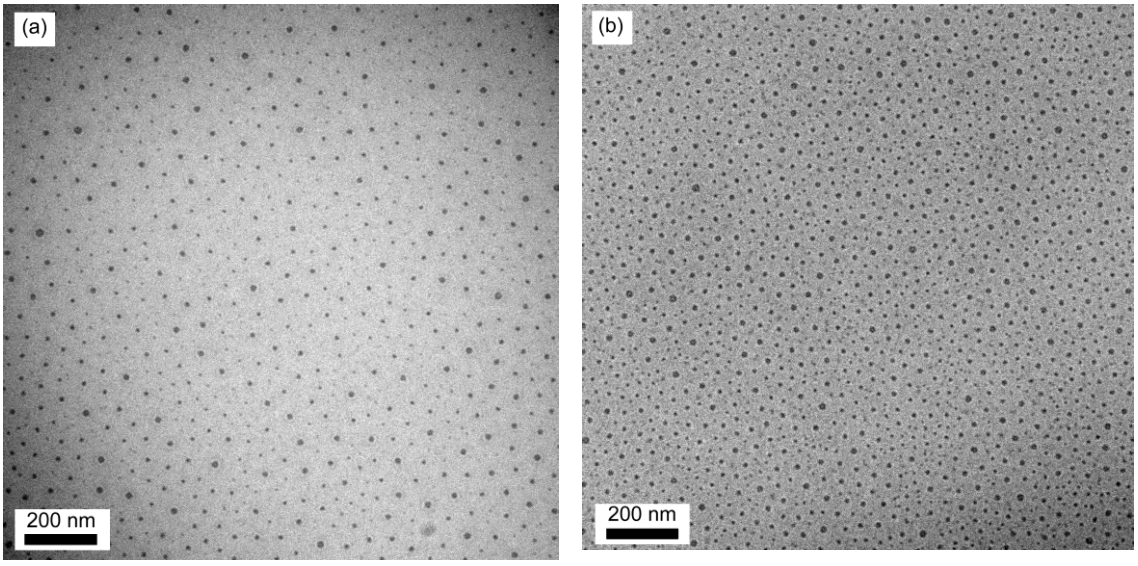


**Figure 4.5** Cryo-TEM images of the 2 wt% PON(3-25-10) sample prepared at (a) 25 ℃ and (b) 50 ℃.

On the basis of these observations, we proposed the morphology of the

two-compartment micellar network for PON hydrogels as illustrated in Figure 4.6, in which both PEP and PNIPAm form spherical micelles, bridged by PEO chains to give the two-compartment gel phase, with water-filled voids forming the other phase. The presence of voids is due to the low polymer concentration (1–5 wt%) used in this work, consistent with optical turbidity (see Figure 3.3 in Chapter 3). At such low polymer concentrations, there is insufficient material to permeate the entire sample volume at the preferred midblock extension, leading to large scale heterogeneity. The heterogeneities give rise to local pockets of water, which appear as voids upon sublimation of the water in the cryo-SEM experiments.

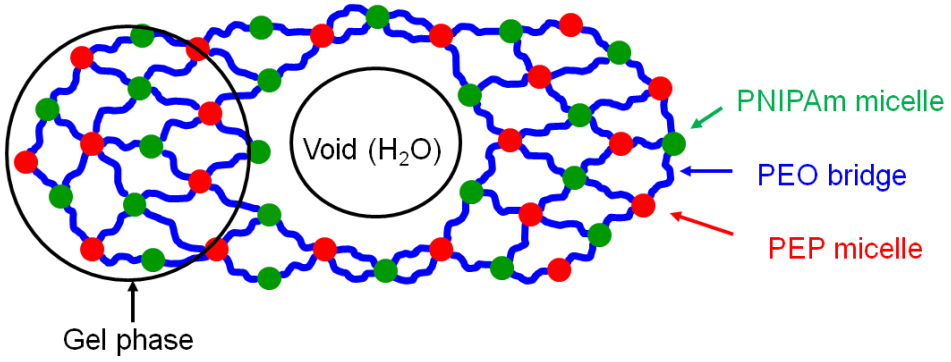


**Figure 4.6** Proposed morphology of the two-compartment network for PON hydrogels.

### 4.3.2 Structural Characterization by SANS

SANS measurements were performed to assess the viability of the two-compartment morphology depicted in Figure 4.6. The SANS intensity profiles of PON(3-25-10) samples in $D_2O$ with varying polymer concentrations from 1 wt% to 5 wt% at three different temperatures are shown in Figure 4.7. At 27 ℃, PON solutions show scattering curves that are typical for block copolymer micelles. The scattering peak of ~0.009 $Å^{-1}$,

evident at the concentration of 5 wt%, is not present at lower polymer concentrations of 2 wt% and 1 wt%. This is consistent with the presence of a spatial correlation between micelles at high concentrations. Upon heating above the gelation temperature, for example, at 46 ℃ and 55 ℃, in the gel state, a upturn in intensity at low $q$ with two scattering peaks at ~0.01 $Å^{-1}$ and ~0.02 $Å^{-1}$ was observed at all three concentrations. The low-$q$ upturn is consistent with the large voids (water-filled chambers) revealed in the cryo-SEM. The two scattering peaks, corresponding to two different spatial correlations between micelles, suggest the presence of two different micelles instead of one type of micelle.

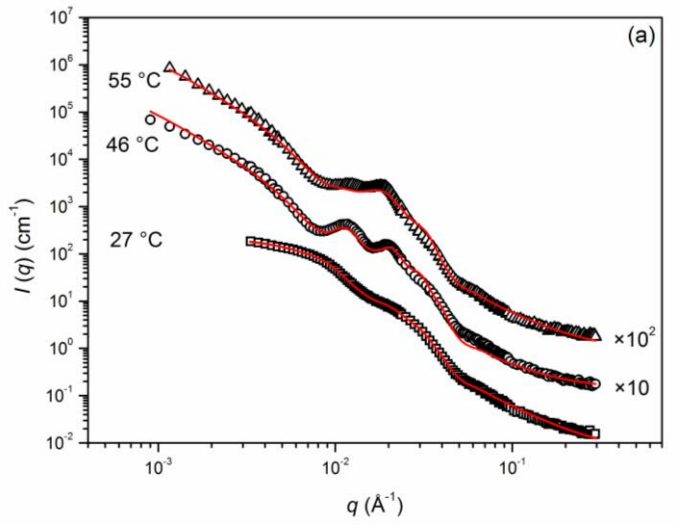
(a)
55 °C
46 °C
27 °C
×10²
×10
I (q) (cm⁻¹)
q (Å⁻¹)

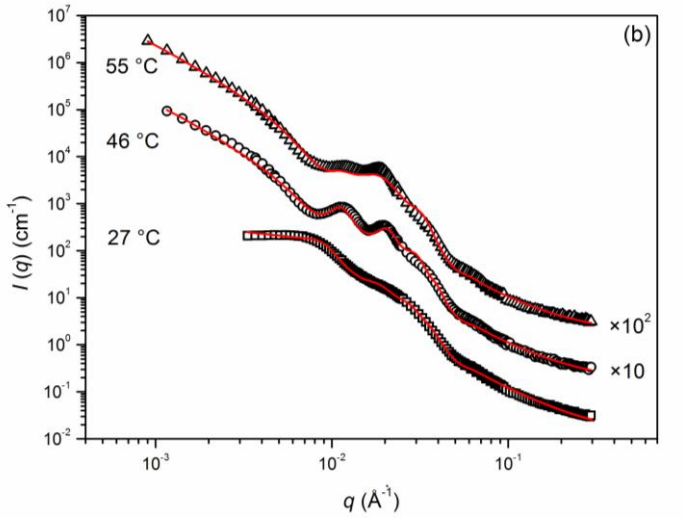
(b)
55 °C
46 °C
27 °C
×10²
×10
I (q) (cm⁻¹)
q (Å⁻¹)

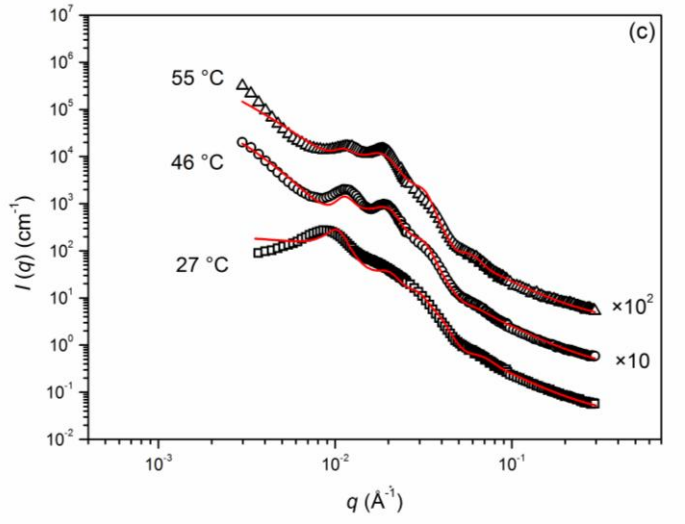
(c)
55 °C
46 °C
27 °C
×10²
×10
I (q) (cm⁻¹)
q (Å⁻¹)

**Figure 4.7** SANS intensity profiles obtained for (a) 1 wt%, (b) 2 wt% and (c) 5 wt% PON(3-25-10) samples in $D_2O$ measured at three different temperatures. For clarity, the intensity data for higher temperatures have been shifted vertically: 46 ℃ (×10), 55 ℃ (×$10^2$). The open black circles represent experimental data, while the red curves represent model fittings detailed in the text.

We used the block copolymer micelle model developed by Pedersen and co-workers to fit the intensity profiles of PON micelles at room temperature. The total coherent scattering intensity is expressed as a function of a micelle form factor and a monodisperse hard sphere structure factor.[27-31]

$$I(q) = \int D(R_c)(P_{\text{mic}}(q) + (A_{\text{mic}}(q))^2[S(q) - 1])dR_c \tag{4-1}$$

where $P_{\text{mic}}(q)$ is the scattering form factor for a micelle consisting of a spherical core and Gaussian corona chains attached to the core surface, $A_{\text{mic}}(q)$ is the form factor amplitude of the radial scattering length distribution of the micelle, $S(q)$ is the monodisperse hard sphere structure factor, and $D(R_c)$ is the Gaussian distribution for core radii.

Four terms are considered for $P_{\text{mic}}(q)$: the self-correlation of the core, the self-correlation of the corona chains, the cross term between the sphere and the corona chains, and the cross term between different corona chains.

$$\begin{aligned} P_{\text{mic}}(q) = {} & N_{\text{agg}}^2 \beta_{\text{core}}^2 A_{\text{core}}^2(q) + N_{\text{agg}} \beta_{\text{corona}}^2 P_{\text{chain}}(q) + \\ & 2N_{\text{agg}}^2 \beta_{\text{core}} \beta_{\text{corona}} A_{\text{core}}(q) A_{\text{corona}}(q) + N_{\text{agg}}(N_{\text{agg}} - 1)\beta_{\text{corona}}^2 A_{\text{corona}}^2(q) \end{aligned} \tag{4-2}$$

Here $q$ is the scattering vector, $N_{\text{agg}}$ is the aggregation number, and $\beta_{\text{core}}$ and $\beta_{\text{corona}}$ are total excess scattering lengths of core and corona blocks, respectively. They are defined as $\beta_{\text{core}} = \upsilon_{\text{core}}(\rho_{\text{core}} - \rho_{\text{solvent}})$ and $\beta_{\text{corona}} = \upsilon_{\text{corona}}(\rho_{\text{corona}} - \rho_{\text{solvent}})$, where $\upsilon_{\text{core}}$ and $\upsilon_{\text{corona}}$ are

the volumes of core and corona chains, respectively. Also, $\rho_{core}$, $\rho_{corona}$ and $\rho_{solvent}$ are the scattering length densities of core block, corona block and solvent, respectively.

The first term is the self-correlation of the spherical core with radius $R_c$ and a smoothly decaying scattering length density at the core-corona interface. $A_{core}^2(q)$ is given by

$$A_{core}^2(q) = \Phi^2(qR_C)\exp(-q^2\sigma_{int}^2) \tag{4-3}$$

where $\Phi(x) = 3[\sin(x) - x\cos(x)]/x^3$ is the hard sphere form factor and $\sigma_{int}$ takes into account the smoothly decaying density at the interface and represents the width of interface between core and corona.

The second term is the self-correlation of the corona chains, which is approximated by a Debye function where the chains are considered as Gaussian chains with radius of gyration $R_g$. $P_{chain}(q)$ is given by

$$P_{chain}(q) = \frac{2[\exp(-x)-1+x]}{x^2}; x = q^2R_g^2 \tag{4-4}$$

The last two terms are the cross term between core and corona and between corona chains, respectively. Both terms includes the form factor of the corona chains which is given as the normalized Fourier transform of the radial density distribution function of the corona chains ($\rho_{corona}(r)$)

$$A_{corona}(q) = \frac{4\pi\int \rho_{corona}(r)\frac{\sin(qr)}{qr}r^2dr}{4\pi\int \rho_{corona}(r)r^2dr}\exp(-q^2\sigma_{int}^2/2) \tag{4-5}$$

A linear combination of two partial cubic *b* spline functions was chosen for $\rho_{corona}(r)$, as explained elsewhere.[29, 32]

The form factor amplitude of the radial scattering length distribution of the micelle

($A_{mic}(q)$) is given by

$$A_{mic}(q) = N_{agg}(\beta_{core}A_{core}(q) + \beta_{corona}A_{corona}(q)) \tag{4-6}$$

The structure factor ($S(q)$) is described by a hard-sphere interaction model that considers short range repulsions between hard spheres of radius ($R_{hs}$). It is given by

$$S(q) = \frac{1}{1 + 24\eta G(2qR_{hs}, \eta)/2qR_{hs}} \tag{4-7}$$

where $G$ is a trigonometric function of $x = 2qR_{hs}$ and the hard sphere volume fraction ($\eta$)

$$\begin{aligned} G(x,\eta) = \alpha x^{-2}(\sin x - x\cos x) + \beta x^{-3}[2x\sin x + (2-x^2)\cos x - 2] + \\ \gamma x^{-5}[-x^4\cos x + 4[(2x^2-6)\cos x + (x^3-6x)\sin x + 6]] \end{aligned} \tag{4-8}$$

where $\alpha = (1+2\eta)^2/(1-\eta)^4$, $\beta = -6\eta(1+\eta/2)^2/(1-\eta)^4$, and $\gamma = 1/2\eta(1+2\eta)^2/(1-\eta)^4$.

The polydispersity in micelle size was accounted for by a Gaussian distribution for core radii:

$$D(R_C) = \frac{1}{\sqrt{2\pi}\sigma_R}\exp\left[\frac{-\left(R_C - \langle R_C \rangle\right)^2}{2\sigma_R^2}\right]; R_C > 0 \tag{4-9}$$

where $<R_C>$ is the average radius and $\sigma_R$ is the width of distribution truncated at $R_C = 0$.

In all, eight parameters could be adjusted in the fits: the core radius ($R_c$), the radius of gyration of the corona chains ($R_g$), the width of the core-corona interface ($\sigma_{int}$), the width of the distribution for the core radius ($\sigma_R$), two terms ($a_1$, $s$) in the cubic $b$ spline function for the corona term, the hard sphere radius ($R_{hs}$) and the hard sphere volume fraction ($\eta_{hs}$).

The model fitting was performed using IGOR Pro software. $R_c$ was fixed at 8 nm, as determined by cryo-TEM. As the scattering length densities of PEO ($\rho^* = 6.34\times10^9$ cm$^{-2}$) and PNIPAm ($\rho^* = 7.92\times10^9$ cm$^{-2}$) are very close, we used the average scattering length

density of $6.81\times10^{9}$ $cm^{-2}$ for PEO-PNIPAm coronae. As shown in Figure 4.7, the intensity profiles of PON micelles at 25 ℃ were successfully fitted using the above mentioned model, and all of the fitting parameters are summarized in Table 4.2. As stated in the model, the hard spheres radius ($R_{hs}$) should be strictly equal to half the minimum micellar center-to-center distance, which is the reciprocal of the scattering peak position $q^*$. The peak position for the 5 wt % solution (~0.009 $Å^{-1}$) corresponds to a micellar center-to-center distance of ~70 nm. This distance is approximately twice the hard sphere radius ($R_{hs}$ = 30–33 nm) derived from the model fittings, suggesting the validity of our fitting results. As the hard sphere radius remains nearly invariant with increasing polymer concentration, the hard sphere volume fraction should be approximately proportional to polymer weight fraction. However, the hard sphere volume fraction increases from 0.20 to 0.26, which is less than twice, when increasing polymer weight fraction from 1 wt% to 2 wt%. The same trend holds as the concentration is raised from 2 wt% to 5wt%. This is likely due to the limitation of hard sphere (excluded volume) interactions for describing the structure factor in the higher concentration samples, noting that the model fittings become progressively worse in the low-$q$ region on increasing polymer concentration.

**Table 4.2** Fitting parameters for PON(3-25-10) micelles in $D_2O$ at room temperature

| Conc. | $R_c$ (nm) | $\sigma_{int}$(nm) | $\sigma_R$ (nm) | $R_g$ (nm) | $a_1$ | $s$ (nm) | $R_{hs}$(nm) | $\eta_{hs}$ |
|---|---|---|---|---|---|---|---|---|
| 1 wt% | 8.0 | 2.5 | 0.1 | 9.5 | 0.27 | 41 | 30 | 0.20 |
| 2 wt% | 8.0 | 2.5 | 0.2 | 9.5 | 0.34 | 44 | 33 | 0.26 |
| 5 wt% | 8.0 | 1.7 | 0.2 | 9.1 | 0.29 | 39 | 31 | 0.37 |

Based on the hydrogel structure shown in Figure 4.6, there are three individual contributions to the scattering: the low-$q$ scattering resulting from spatial heterogeneities, form factors and structure factors for PEP and PNIPAm micellar cores, and high-$q$ scattering from PEO chains. The total scattering intensity of PON hydrogels is then given by

$$I(q) = n_1\overline{P_1(q)}S_{11}(q) + 2\sqrt{n_1 n_2}\,\overline{A_1(q)}\,\overline{A_2(q)}S_{12}(q) + n_2\overline{P_2(q)}S_{22}(q) + (\rho_{\mathrm{PEO}} - \rho_{\mathrm{solvent}})^2\frac{a}{q^2} + (\rho_{\mathrm{gel\,phase}} - \rho_{\mathrm{solvent}})^2 b\frac{\exp(-q^2 R_{\mathrm{int}}{}^2)}{q^2} + I_{\mathrm{incoherent}} \quad (4\text{-}10)$$

The first term in equation 4-10 represents the scattering intensity from the hydrophobic PEP and PNIPAm domains in the gel phase. This is treated as a binary mixture of smooth spheres. In this term, $n$ is the number density of spheres, $P(q)$ is the sphere form factor, and $A(q)$ is the form factor amplitude, given by:

$$P(q) = A(q)^2$$
$$A(q) = (\rho\frac{4}{3}\pi R_{\mathrm{c}}{}^3)\Phi(qR_{\mathrm{c}})\exp(\frac{-q^2\sigma_{\mathrm{int}}^2}{2}) \quad (4\text{-}11)$$

where $\Phi(x) = 3[\sin(x) - x\cos(x)]/x^3$ is the hard sphere form factor and $\sigma_{\mathrm{int}}$ takes into account the smoothly decaying density at the surface and represents the width of interface between core and corona. $S_{11}$(q), $S_{12}$(q) and $S_{22}$(q) are the inter-particle structure factors describing the correlation between 1-1, 1-2 and 2-2 spheres. As PEP spheres are presumably surrounded by PNIPAm spheres and vice versa, they are not packed randomly. Therefore, the structure factors for binary spheres interacting through hard sphere interactions cannot be used here.[33] To model the alternating feature of the two spheres, a sticky hard sphere structure factor (inter-particle structure factors for spheres with a narrow attractive well) was adopted.[34-36] In the sticky hard sphere model,

short-range repulsion between spheres is accounted for by the hard sphere radius ($R_{hs}$). Short-range attraction is accounted for by an adhesion energy between opposite sphere types. A-B contacts can be favored over A-A and B-B contacts, by adding an attractive adhesion between the spheres. The interaction potential is given by

$$u(r) = \begin{cases} \infty & 0 < r < \dfrac{D_i + D_j}{2} = D_{i,j} \\ -u_0 & D_{i,j} < r < D_{i,j} + \Delta_{i,j} \\ 0 & r < D_{i,j} + \Delta_{i,j} \end{cases} \qquad (4\text{-}12)$$

where $D_{i,j}$ is the hard sphere diameter, $\Delta_{i,j}$ is the width of the square well and $u_0$ is the depth of the well, in units of $kT$. The strength of the attractive well is described in terms of "stickiness", $\tau$, as defined below:

$$\tau = \frac{\exp(u_0 / kT)}{12\varepsilon}; \quad \varepsilon = \frac{\Delta}{D + \Delta} \qquad (4\text{-}13)$$

The stickiness can be varied to adjust the interaction strength, and therefore used as a fitting parameter. The binary sticky structure factors were calculated using the formulae described by Bergenholtz and coworkers.[35]

The second term corresponds to the high-$q$ scattering of PEO chains. This is fitted to $a/q^2 + I$, which is consistent with scattering from the polymer chains (tail of the Debye function) plus an incoherent background.

The third term stands for the low-$q$ scattering resulting from the spatial heterogeneities of the samples, and is fitted empirically as $b$*exp($-q^2$*$R_{int}^2$)/$q^2$, where $R_{int}$ is the length-scale below which the gel is uniform. Given the difficulty in accurately estimating and subtracting the incoherent background scattering, a small background term ($I_{incoherent}$) is included in equation 4-10.

In all, eleven parameters could be adjusted in the fits: the core radii of PEP and PNIPAm ($R_c$), width of the core-corona interface for PEP and PNIPAm micelles ($\sigma_{int}$), the hard sphere volume fraction of PEP and PNIPAm spheres ($\eta_{hs}$), interaction potential between PEP and PNIPAm spheres (stickiness, $\tau$), fraction of $H_2O$ in the gel phase, two prefactors for both the high-$q$ scattering and low-$q$ scattering ($a$, $b$), and $R_{int}$.

The model fitting was performed using Matlab software. $R_c$(PEP) and $\sigma_{int}$(PEP) were fixed at 8 nm and 2.4nm, respectively, as determined by cryo-TEM and SANS analysis of PON micelles. The range of $R_c$(PNIPAm) was set between 7.5–10 nm as the cryo-TEM observation suggests that PNIPAm micelles have similar or slightly larger core radii in comparison to PEP micelles. As shown in Figure 4.7, the intensity profiles of PON hydrogels at both 46 ℃ and 55 ℃ can be successfully fitted using the proposed scattering equation 4-10. The individual scattering contributions from each term of equation 4-10 for a representative PON sample are displayed in Figure 4.8. All of the fitting parameters are listed in Table 4.3. The two prefactors ($a$, $b$) have no physical meaning, and thus are not reported here. $R_{int}$ has a common value of ~20 nm for all the PON hydrogel samples and thus is not presented in Table 4.3.

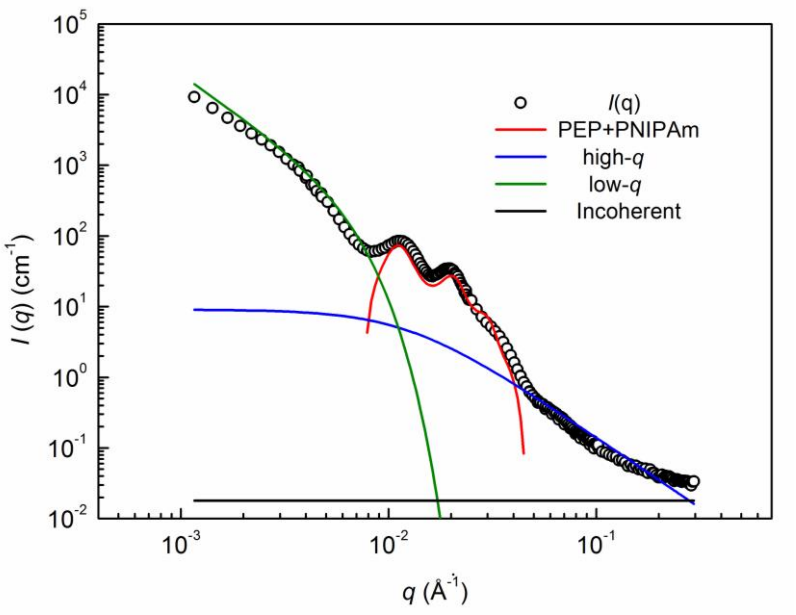


**Figure 4.8** SANS intensity profiles obtained for 2 wt% PON(3-25-10) in $D_2O$ measured at 46 ℃. The open circles are experimental data, and the solid curves are model fitting results represent the individual scattering contributions from the first term (PEP and PNIPAm micelles), second term (high-*q* scattering), third term (low-*q* scattering) and forth term (incoherent background) in equation 4-10.

**Table 4.3** Fitting parameters for PON(3-25-10) hydrogels in $D_2O$

| Concentration | 1 wt% | | 2 wt% | | 5 wt% | |
|---|---|---|---|---|---|---|
| Temperature (℃) | 46 | 55 | 46 | 55 | 46 | 55 |
| $R_c$(PNIPAm) (nm) | 8.6 | 9.6 | 8.5 | 9.5 | 8.9 | 9.6 |
| $\sigma_{int}$(PNIPAm) (nm) | 3.3 | 2.7 | 3.2 | 2.7 | 3.1 | 2.0 |
| Fraction of $H_2O$ in gel | 63% | 31% | 100% | 40% | 100% | 88% |
| $\eta_{hs}$(PEP) | 10% | 3% | 15% | 4% | 20% | 5% |
| $\eta_{hs}$(PNIPAm) | 26% | 17% | 30% | 28% | 43% | 33% |
| Micelle attraction ($\tau$) | 13 | 19 | 11 | 12 | 10 | 13 |
| $n$(PNIPAm)/$n$(PEP)[a] | 1.9 | 1.3 | 2.0 | 1.4 | 1.7 | 1.3 |

[a] Number of PNIPAm micelles relative to PEP micelles, as determined from $R_c$(PNIPAm).

We observed a slight increase in the core radius of PNIPAm along with a small decrease in core-corona interface thickness at all three concentrations when PON samples were heated from 46 ℃, which is just a few degree above the critical gelation temperature ($T_{gel}$, 42 ℃) to higher temperatures, for example, 55 ℃. PNIPAm becomes progressively more hydrophobic upon heating across and above the LCST, and the relatively higher hydrophobicity at 55 ℃ leads to the larger aggregation number (larger core radius) and less diffuse interface (smaller core-corona interface thickness) for PNIPAm micelles. This is consistent with our variable-temperature $^1H$ NMR results of the same PON triblock solution, in which continuous dehydration of the PNIPAm block

occurred on heating at and above the $T_{gel}$ (see Chapter 2). In addition, the fraction of water in the gel phase drops significantly upon heating from 46 ℃ to 55 ℃. This is likely due to the LCST phase behavior of PEO in water and the syneresis of PNIPAm above the LCST, consistent with a number of reports concerning PNIPAm-containing block copolymers.[37, 38] This trend is reversed on increasing the concentration at both 46 ℃ and 55 ℃, as expected from the factor that the heterogeneity decreases with increasing polymer concentration (see Chapter 2). It is also worth noting that no difference was observed for the size and interface thickness of PNIPAm spheres with varying concentration.

The number of PNIPAm micelles relative to PEP micelles, as determined from $R_c$(PNIPAm), is given by:

$$\frac{n(\text{PNIPAm})}{n(\text{PEP})} = \frac{f_{PEO}}{f_{\text{PNIPAm}}} \times \frac{R_c^3(\text{PNIPAm})}{R_c^3(\text{PEP})} \tag{4-14}$$

This ratio was estimated to be ~2 at 46 ℃, and decreased to ~1.5 at 55 ℃, which is slightly smaller than the suggested value (2-3) at 50 ℃ by cryo-TEM analysis. Given that nine parameters were included in the fitting procedure, such small disagreement should not affect the validity of our model equation.

Overall, the SANS analysis of PON(3-25-10) samples supports the two-compartment network structure proposed in Figure 4.6. However, the exact structural information for the individual blocks, especially PNIPAm, cannot be identified separately because the scattering length densities of PEP, PEO and PNIPAm are not very different and they contribute comparably to the total incoherent scattering. Therefore, we prepared a $PON_{d7}$ triblock with a deuterated PNIPAm block (dPNIPAm) and performed SANS

experiments under two different contrast matched conditions, namely PEP contrast matched (96% vol% $H_2O$) and zero mean contrast (67.5% vol% $H_2O$), to exact the size, shape and packing of the PNIPAm domains.

When the PEP is contrast matched, the scattering is dominated by the deuterated PNIPAm block (Figure 4.2), and therefore the structural change of PNIPAm upon heating from the micelle to gel state should be easily resolvable. The SANS intensity profiles of $PON_{d7}$(3-25-11) samples under PEP matched conditions at both the micelle (25 ℃) and gel state (55 ℃) are shown in Figure 4.9. The appearance of a single scattering peak of ~0.016 $Å^{-1}$ with a small shoulder on heating is consistent with the conversion of dPNIPAm from Gaussian chains in the corona to micellar cores, and can be fitted using the model equation 4-10 with parameters listed in Table 4.4. It should be noted that the core radii of dPNIPAm micelles are ~8 nm, irrespective of concentration, a reasonable value as expected from the cryo-TEM and SANS analysis of PON triblock samples.

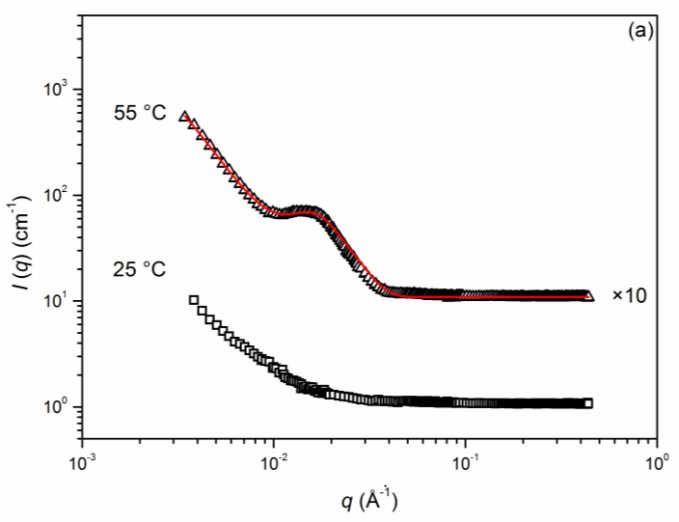
(a)
55 °C
25 °C
×10
I (q) (cm-1)
q (Å-1)

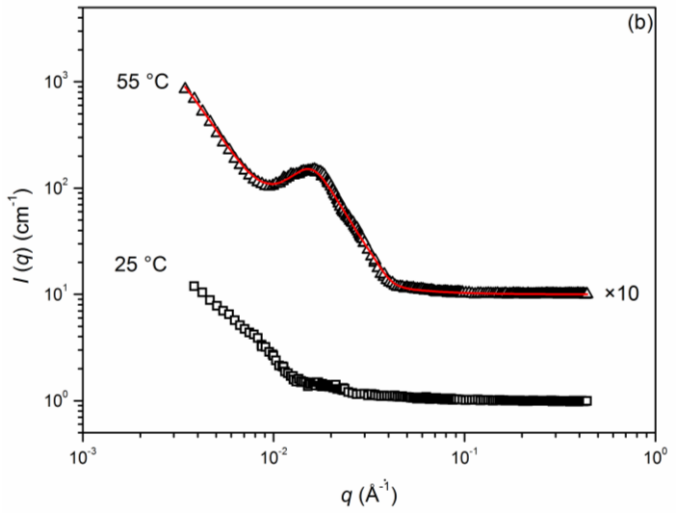
(b)
55 °C
25 °C
×10
I (q) (cm-1)
q (Å-1)

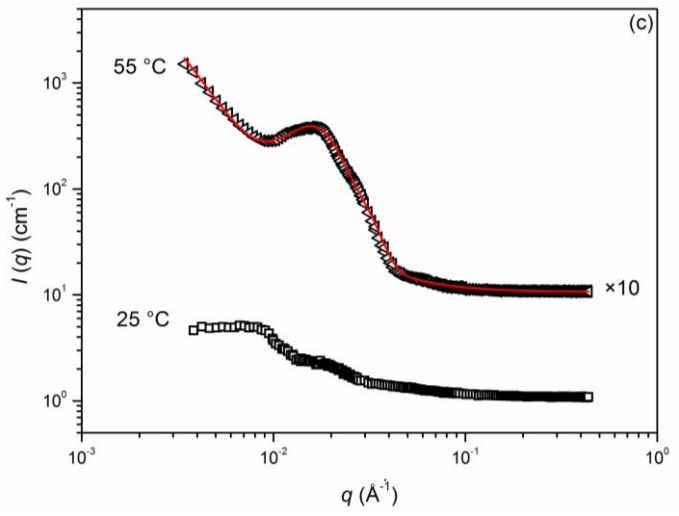
(c)
55 °C
25 °C
×10
I (q) (cm-1)
q (Å-1)

**Figure 4.9** SANS intensity profiles obtained for (a) 1 wt%, (b) 2 wt% and (c) 5 wt% $PON_{d7}$(3-25-11) samples in 96 vol% $H_2O$ (PEP contrast matched) measured at 25 ℃ and 55 ℃. For clarity, the intensity data at 55 ℃ have been shifted vertically: 55 ℃ (×10). The open black circles represent experimental data, while the red curves represent model fits.

**Table 4.4** Fitting parameters for $PON_{d7}$(3-25-11) hydrogels at 55 ℃

| Condition | PEP contrast matched | | | Zero mean contrast | | |
|---|---|---|---|---|---|---|
| Concentration | 1 w% | 2 wt% | 5 wt% | 1 w% | 2 wt% | 5 wt% |
| $R_c$(dPNIPAm) (nm) | 7.5 | 7.6 | 8.0 | 7.6 | 7.7 | 8.0 |
| $\sigma_{int}$(dPNIPAm) (nm) | 3.8 | 3.9 | 3.5 | 4.2 | 3.8 | 3.5 |
| Fraction of $H_2O$ in gel | 21% | 31% | 57% | 30% | 45% | 98% |
| $\eta_{hs}$(PEP) | 2% | 3% | 6% | 5% | 10% | 11% |
| $\eta_{hs}$(dPNIPAm) | 11% | 20% | 21% | 15% | 18% | 26% |
| Micelle attraction ($\tau$) | 18 | 11 | 5 | 12 | 12 | 12 |
| $n$(dPNIPAm)/$n$(PEP)[a] | 3.3 | 3.3 | 2.8 | 3.3 | 3.1 | 2.8 |

[a] Number of dPNIPAm micelles relative to PEP micelles, as determined from $R_c$(dPNIPAm).

The zero mean contrast signal is also informative, since the absence of scattering at low-$q$ would help establish that the PNIPAm really forms 0D, spherical micelles rather than 1D worms, 2D sheets or 3D networks. The SANS intensity profiles of

$PON_{d7}$(3-25-11) samples under zero mean contrast conditions are shown in Figure 4.10. The low-*q* upturn was not observed for $PON_{d7}$(3-25-11) hydrogels at all three concentration, confirming the formation of spherical PNIPAm micelles in the gel state. Again, we obtained reasonable agreement between experimental data and the model fitting results using equation 4-10 with PNIPAm core radii of ~8 nm (Table 4.4).

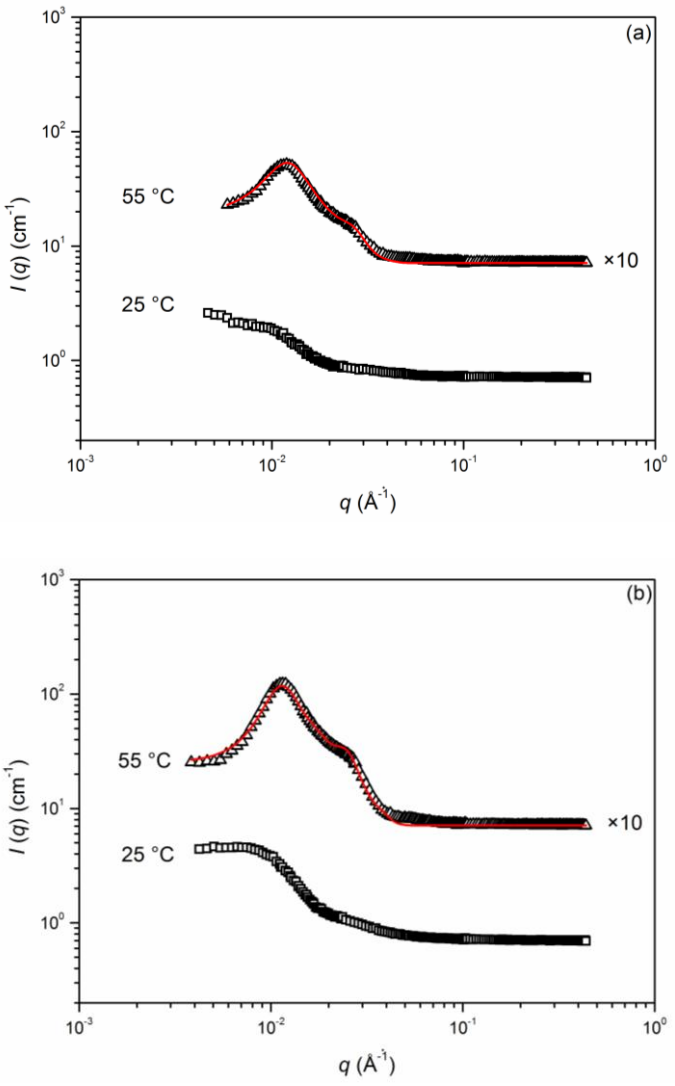

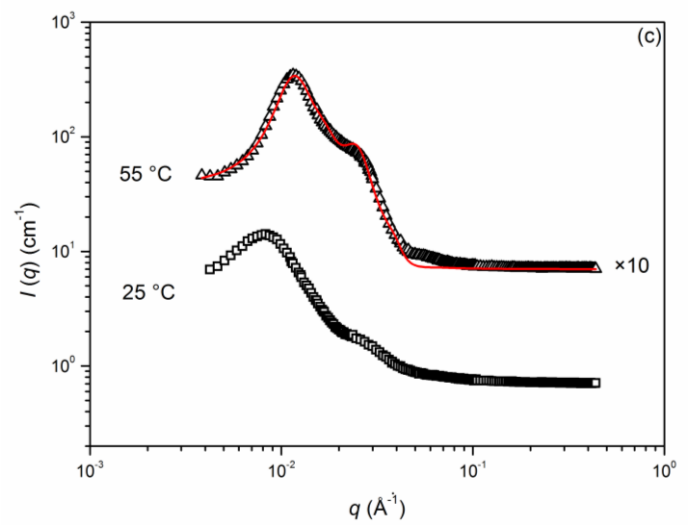


**Figure 4.10** SANS intensity profiles obtained for (a) 1 wt%, (b) 2 wt% and (c) 5 wt% $PON_{d7}$(3-25-11) samples in 67.5 vol% $H_2O$ (zero mean contrast) measured at 25 and 55 ℃. For clarity, the intensity data at 55 ℃ have been shifted vertically: 55 ℃ (×10). The open black circles represent experimental data, while the red curves represent model fits.

### 4.4 Summary

In conclusion, we investigated the morphology of PON micelles and hydrogels using a combination of microscopy and scattering experiments. The cryo-SEM and cryo-TEM analysis suggest that PON triblocks form spherical micelles with PEP core and PEO-PNIPAm corona at room temperature and two-compartment micellar networks, in which both PEP and PNIPAm form spherical micelles, bridged by PEO chains with the presence of water-filled voids, upon heating above the critical gelation temperature. The formation of two discrete spherical PEP and PNIPAm hydrophobic domains in the micellar network is further confirmed by SANS experiments of PON triblocks with a

normal PNIPAm and a deuterated PNIPAm block. This study confirms our assumption that ABC triblocks with two immiscible, hydrophobic endblocks are beneficial for hydrogel formation, resulting from the formation of two-compartment networks with exclusively bridging conformations for the midblocks. Therefore it could help guide the design and development of new physically associated hydrogels with enhanced performance.

### 4.5 References


1. Ringsdorf, H.; Lehmann, P.; Weberskirch, R. *Book of Abstracts*, 217th National Meeting of the American Chemical Society, Anaheim, CA, March 221-225, 1999.
2. Laschewsky, A. *Curr. Opin. Colloid Interface Sci.* **2003**, *8*, 274-281.
3. Lutz, J. F.; Laschewsky, A. *Macromol. Chem. Phys* **2005**, *206*, 813-817.
4. Li, Z.; Kesselman, E.; Talmon, Y.; Hillmyer, M. A.; Lodge, T. P. *Science* **2004**, *306*, 98-101.
5. Li, Z.; Hillmyer, M. A.; Lodge, T. P. *Nano Lett.* **2006**, *6*, 1245-1249.
6. Li, Z.; Hillmyer, M. A.; Lodge, T. P. *Langmuir* **2006**, *22*, 9409-9417.
7. Pochan, D. J.; Chen, Z.; Cui, H.; Hales, K.; Qi, K.; Wooley, K. L. *Science* **2004**, *306*, 94-97.
8. Cui, H.; Chen, Z.; Zhong, S.; Wooley, K. L.; Pochan, D. J. *Science* **2007**, *317*, 647-650.
9. Kubowicz, S.; Baussard, J. F.; Lutz, J. F.; Thunemann, A. F.; von Berlepsch, H.; Laschewsky, A. *Angew. Chem., Int. Ed.* **2005**, *44*, 5262-5265.

10. Von Berlepsch, H.; Bottcher, C.; Skrabania, K.; Laschewsky, A. *Chem. Commun.* **2009**, 2290-2292.
11. Zhu, J.; Jiang, W. *Macromolecules* **2005**, *38*, 9315-9323.
12. Fang, B.; Walther, A.; Wolf, A.; Xu, Y.; Yuan, J.; Muller, A. H. E. *Angew. Chem., Int. Ed.* **2009**, *48*, 2877-2880.
13. Weberskirch, R.; Preuschen, J.; Spiess, H. W.; Nuyken, O. *Macromol. Chem. Phys* **2000**, *201*, 995-1007.
14. Komenda, T.; Luedtke, K.; Jordan, R.; Ivanova, R.; Bonne, T. B.; Papadakis, C. M. *Polym. Prepr. (Am. Chem. Soc., Div. Polym. Chem.)* **2006**, *47*, 763-764.
15. Li, C.; Buurma, N. J.; Haq, I.; Turner, C.; Armes, S. P.; Castelletto, V.; Hamley, I. W.; Lewis, A. L. *Langmuir* **2005**, *21*, 11026-11033.
16. Taribagil, R. R.; Hillmyer, M. A.; Lodge, T. P. *Macromolecules* **2009**, *42*, 1796-1800.
17. Taribagil, R. R.; Hillmyer, M. A.; Lodge, T. P. *Macromolecules* **2010**, *43*, 5396-5404.
18. Zhou, C.; Hillmyer, M. A.; Lodge, T. P. *J. Am. Chem. Soc.* **2012**, *134*, 10365-10368.
19. Zhou, C.; Hillmyer, M. A.; Lodge, T. P. *Macromolecules* **2011**, *44*, 1635-1641.
20. Fetters, L. J.; Lohse, D. J.; Richter, D.; Witten, T. A.; Zirkel, A. *Macromolecules* **1994**, *27*, 4639-4647.
21. Smith, G. D.; Yoon, D. Y.; Jaffe, R. L.; Colby, R. H.; Krishnamoorti, R.; Fetters, L. J. *Macromolecules* **1996**, *29*, 3462-3469.
22. Shields, D. J.; Coover, H. W. *J. Polym. Sci.* **1959**, *39*, 532-533.
23. Jain, S.; Dyrdahl, M. H. E.; Gong, X.; Scriven, L. E.; Bates, F. S. *Macromolecules* **2008**, *41*, 3305-3316.
24. Lee, S.; Arunagirinathan, M. A.; Bates, F. S. *Langmuir* **2010**, *26*, 1707-1715.

25. Glinka, C. J.; Barker, J. G.; Hammouda, B.; Krueger, S.; Moyer, J. J.; Orts, W. J. *J. Appl. Crystallogr.* **1998**, *31*, 430-445.
26. Kline, S. R. *J. Appl. Crystallogr.* **2006**, *39*, 895-900.
27. Castelletto, V.; Hamley, I. W.; Pedersen, J. S. *J. Chem. Phys.* **2002**, *117*, 8124-8129.
28. Castelletto, V.; Hamley, I. W.; Pedersen, J. S. *Langmuir* **2004**, *20*, 2992-2994.
29. Pedersen, J. S.; Svaneborg, C.; Almdal, K.; Hamley, I. W.; Young, R. N. *Macromolecules* **2003**, *36*, 416-433.
30. Pedersen, J. S. *J. Appl. Crystallogr.* **1998**, *31*, 488-489.
31. Pedersen, J. S.; Hamley, I. W.; Ryu, C. Y.; Lodge, T. P. *Macromolecules* **2000**, *33*, 542-550.
32. Castelletto, V.; Hamley, I. W.; Pedersen, J. S. *J. Chem. Phys.* **2002**, *117*, 8124-8129.
33. Ashcroft, N. W.; Langreth, D. C. *Phys. Rev.* **1967**, *156*, 685-692.
34. Robertus, C.; Philipse, W. H.; Joosten, J. G. H.; Levine, Y. K. *J. Chem. Phys.* **1989**, *90*, 4482-4490.
35. Bergenholtz, J.; Romagnoli, A. A.; Wagner, N. J. *Langmuir* **1995**, *11*, 1559-1570.
36. Kline, S. R.; Kaler, E. W. *J. Chem. Phys.* **1996**, *105*, 3813-3822.
37. Convertine, A. J.; Lokitz, B. S.; Vasileva, Y.; Myrick, L. J.; Scales, C. W.; Lowe, A. B.; McCormick, C. L. *Macromolecules* **2006**, *39*, 1724-1730.
38. Magenau, A. J. D.; Martinez-Castro, N.; Savin, D. A.; Storey, R. F. *Macromolecules* **2009**, *42*, 8044-8051.

# Chapter 5

# Micellar Aggregation and Gelation of PO(N/A) Triblock Terpolymers in Water*

## 5.1 Introduction

Stimuli responsive polymers, which can alter their solubility and conformations according to temperature, pH, ionic strength, light, electric or magnetic fields, are of great interest for biomedical and other applications.[1-8] For example, such polymers can form surfaces whose adhesion or wetting properties are modulated by changes in the environment, and therefore can be used in the design of novel chromatographic stationary phases,[9-13] substrates for reversible protein and cell attachment,[14-17] and tissue engineering scaffolds.[18, 19] They are also useful in designing self assembling and stimulus triggered controlled drug release systems.[20, 21]

Temperature is a commonly exploited environmental stimulus, and polymers whose conformations and phase behaviors are significantly altered between room temperature (25 ℃) and human physiological temperature (37 ℃) have received considerable

* This chapter describes the outcome of a collaborative research project carried out by Isha Koonar and Can Zhou and advised by Ronald A. Siegel, Marc A. Hillmyer and Timothy P. Lodge. A report on this research project has been published (Koonar, I.; Zhou, C.; Hillmyer, M. A.; Lodge, T. P.; Siegel, R. A. *Langmuir* **2012**, *28*, 17785-17794).

attention. Of these, poly(*N*-isopropyl acrylamide) (PNIPAm), which exhibits a convenient lower critical solution temperature (LCST) at 32 ℃ in water, is one of the most widely studied.[21-24] When PNIPAm is combined with other monomers or polymers, temperature-driven self assembly into a variety of structures is possible. Thermoresponsive ABA triblocks with PNIPAm end blocks have been shown to associate into micellar colloidal assemblies in aqueous solutions above the LCST.[25-28] In one study, Armes and co-workers observed micellization in dilute aqueous solutions of PNIPAm-*b*-poly(2-methacryloyloxyethyl phosphorylcholine)-*b*-PNIPAm (PNIPAm-*b*-PMPC-*b*-PNIPAm) on increasing temperature above 33 ℃. In more concentrated solutions (>6.5 wt%), intermicellar association of PNIPAm chains led to reversible, physical gelation.[26] Recently, PNIPAm containing ABC triblock polymers have been investigated as stimuli responsive gelators.[29-31] Because of the distinct end domains, the ABC architecture may have an advantage over the ABA architecture due to greater efficiency of inter-micelle interactions, especially at low concentrations.[32] The ABC architecture can suppress elastically ineffective looping conformations of the midblock.[33] For example, we compared the gelation behavior of an ABC triblock terpolymer, poly(ethylene-*alt*-propylene)-*b*-poly(ethylene oxide)-*b*-poly(*N*-isopropylacrylamide) (PON) with the corresponding ABA triblock copolymer PNIPAm-*b*-PEO-*b*-PNIPAm (NON), and found that the ABC triblock polymer undergoes a much sharper sol-gel transition, at significantly lower concentrations.[34]

It is desirable to have other variables besides temperature to control the polymer assembly process. In many biomedical applications, for example, the transition may be required to occur at a prescribed temperature. Interestingly, thermal transitions can be

converted to transitions based on other stimuli if suitable monomers are incorporated into a thermally responsive polymer.[35] Changes in the charge or conformational state of these stimuli-responsive monomers can tune the LCST above or below the temperature set point.[36, 37] In the present work, we are interested in converting the temperature sensitivity of PNIPAm-containing triblocks into pH-sensitivity, due to changes in monomer polarity[36] and the contribution of counterion entropy to the free energy balance when the polymer is charged.[38] Joint temperature and pH-mediated self assembly can be investigated either by fixing temperature and varying pH or by fixing pH and varying temperature.[39]

Acrylic acid (AA) is frequently used to render polymers pH-sensitive.[40] It is well known that pH and temperature effects can be played off one another by copolymerizing NIPAm and AA, with the LCST increasing with increasing ionization of AA.[41-44] These monomers have been combined to form block, graft and statistical copolymers, the last being the most widely investigated. For example, Wu *et al.*[45] reported that P(NIPAm-*co*-AA) random copolymers aggregated to form colloidal nanoparticles when heated to a temperature higher than the LCST of PNIPAm, with the aggregation temperature increasing with increasing AA fraction. Bokias *et al.*[46, 47] studied the solution properties of P(NIPAm-*co*-AA) random copolymers and showed that the cloud point of PNIPAm increased even with low amounts of AA substitution (5 mol%), and with increasing neutralization of AA groups by NaOH. Microgels of P(NIPAm-*co*-AA) were studied by Snowden and coworkers,[48] who observed increased transition temperature and hydrodynamic diameter with increasing pH. This work corroborated results obtained earlier in hydrogels of more macroscopic dimensions.[49, 50] P(NIPAm-*co*-AA) hydrogels,

in which the LCST and gel swelling are affected by the AA fraction in the copolymer, have been studied as controlled release systems for enteric drug delivery[51] and as artificial matrices for tissue engineering.[19]

In this chapter, we report the dual pH- and temperature-sensitive self-assembly of poly(ethylene-*alt*-propylene)-*b*-poly(ethylene oxide)-*b*-poly(*N*-isopropylacrylamide-*co*-acrylic acid) (PEP-*b*-PEO-*b*-P(NIPAm-*co*-AA), PO(N/A)) triblock terpolymers in which the PNIPAm block contains a small fraction of AA monomers in water.[52] These triblocks self assemble into micelles with PEP cores and PEO-P(NIPAm-*co*-AA) coronae at room temperature. Aggregation of these micelles in dilute solutions upon heating is modulated by coronal solubility, which in turn is affected by both temperature and pH. Micellar aggregation at higher polymer concentrations leads to gelation and solid-like rheological properties. This work may be regarded as a natural extension of our previous investigations with PON,[34, 53] since we now augment the latter's thermosensitivity with pH-sensitivity.

## 5.2 Experimental Section

### 5.2.1 Materials

All chemicals were purchased from Sigma Aldrich and used as received unless otherwise noted. 2,2'-Azobisisobutyronitrile (AIBN) was purified by recrystallization from methanol; *N*-isopropylacrylamide (NIPAm) was recrystallized from benzene/n-hexane (65/35 v/v); *tert*-butyl acrylate (*t*BA) was washed with 5% aqueous sodium hydroxide solution and then with water, 3 times each. After drying with anhydrous sodium sulfate for 24 hours, *t*BA was distilled under reduced pressure.[54]

Methyl acrylate was passed through a basic alumina column prior to use. The chain transfer agent (CTA), *S*-1-dodecyl-*S'*-($\alpha,\alpha'$-dimethyl-$\alpha''$-acetic acid) trithiocarbonate (DMAT) was synthesized according to procedure reported by Lai *et al.*[55] Toluene was passed through two columns of activated alumina and a supported copper catalyst. Tetrahydrofuran (THF) was purified by passage through two columns packed with activated alumina and molecular sieves. Dichloromethane ($CH_2Cl_2$) was purified on an MBraun solvent purification system.

### 5.2.2 Synthesis of PO(N/A) Triblock Terpolymers

Two PO(N/A) triblock terpolymers were synthesized by a combination of anionic and RAFT polymerizations, followed by acid hydrolysis (Scheme 5.1).

First, a PEP-PEO (PO) diblock copolymer was prepared by anionic polymerization following a previously reported procedure. Molar masses of the PEP and PEO block were 3,000 and 25,000, respectively, with very narrow molecular weight distribution ($Đ$ = 1.02). The hydroxyl end-groups of PO diblock were coupled to the chain transfer agent to give PEP-PEO-CTA (PO-CTA) macroinitiator *via* an acid chloride intermediate.[53]

The PO-CTA macroinitiator was then used to grow a P(NIPAm-*co*-*t*BA) random copolymer to obtain PEP-PEO-P(NIPAm-*co*-*t*BA)-CTA (PO(N/B)-CTA) triblock terpolymers. In a representative synthesis, PO-CTA macroinitiator (3.0 g, 0.11 mmol), NIPAm (2.1 g, 19 mmol), *t*BA (0.255 g, 2.0 mol) and AIBN (1.8 mg, 0.011 mmol) were dissolved in toluene (30 mL), degassed by three freeze-pump-thaw cycles and reacted at 70 ℃ for 3.2 h. The reaction mixture was then cooled to 0 ℃, diluted with $CH_2Cl_2$, precipitated in pentane three times, and dried at 40 ℃ in a vacuum oven overnight.

Conversion of NIPAm was around 50% as determined by $^{1}$H NMR. The content of *t*BA in the P(NIPAm-*co*-*t*BA) block was varied by controlling the feed ratio of NIPAm to *t*BA.

The trithiocarbonate end group of the resulting PO(N/B)-CTAs was removed by aminolysis and Michael addition to afford PEP-PEO-P(NIPAm-*co*-*t*BA) (PO(N/B)) triblocks according to the procedure reported by Qiu and Winnik.[56] In a typical example towards the synthesis of PO(N/B), PO(N/B)-CTA (2.7 g, 0.069 mmol), *n*-propylamine (0.2 g, 3 mmol) and tris(2-carboxyethyl) phosphine hydrochloride (20 mg, 0.069 mmol) were dissolved in THF (40 mL). The reaction mixture was stirred for 24 h at room temperature under a nitrogen atmosphere after the addition of methyl acrylate (1.5 mL, 17 mmol) at 2.5 h. The reaction mixture was precipitated in pentane. The product was then dissolved in 100 mL $CH_2Cl_2$, filtered through a 0.45 μm HVHP Durapore membrane and passed through a basic alumina column. It was then precipitated two more times in pentane and dried at 40 ℃ in the vacuum oven overnight.

The *t*BA of PO(N/B) triblocks was hydrolyzed to AA *via* acid hydrolysis, resulting in PEP-PEO-P(NIPAm-*co*-AA) (PO(N/A)) triblocks, the final polymer. For example, PO(N/B) (1.0 g, 0.0028 mmol), trifluoroacetic acid (3.0 mL, 39 mmol) and triethylsilane (4.0 mL, 25 mmol) were dissolved in 10 mL $CH_2Cl_2$ and stirred at room temperature for 24 h. After hydrolysis, most of the trifluoroacetic acid and triethylsilane were removed under vacuum. The reaction mixture was then redissolved in $CH_2Cl_2$, precipitated in diethyl ether twice and pentane once and dried at 40 ℃ in a vacuum oven overnight.

**Scheme 5.1** Synthesis of PO(N/A) triblock terpolymers

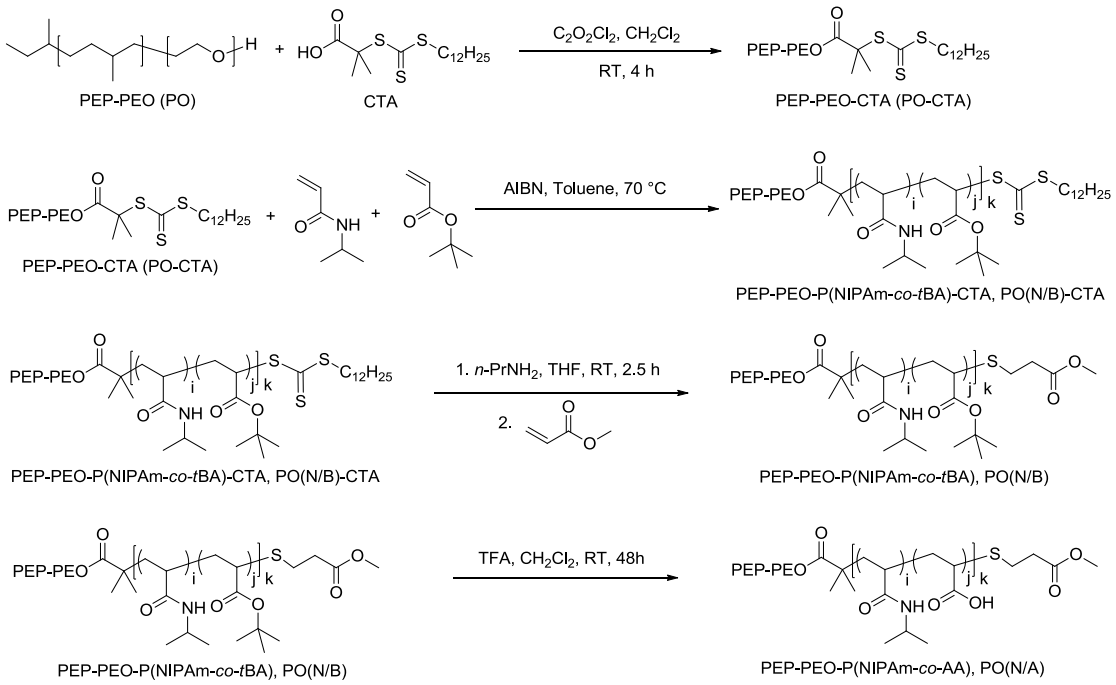


### 5.2.3 Characterization

$^1$H nuclear magnetic resonance ($^1$H NMR) spectra were conducted using a Varian Inova 500 MHz instrument spectrometer with $CDCl_3$ as the solvent. Size exclusion chromatography (SEC) was performed on a Waters 150C ALC/GPC equipped with three Phenogel (Phenomenex) columns with pore sizes of $10^3$, $10^4$, and $10^5$ Å, a Wyatt DAWN multiangle light-scattering detector and a Wyatt OPTILAB rEX refractive index detector. THF containing 1 % tetramethylethylenediamine by volume was used as the eluent at a flow rate of 1.0 mL/min.

AA content in the P(NIPAm-*co*-AA) block of PO(N/A) triblocks was determined by potentiometric titration. 0.1 wt% aqueous solutions of PO(N/A) polymer were titrated against 0.05 M sodium hydroxide aqueous solution using a Metrohm 719S Titrino

equipped with a Metrohm LL Micro glass electrode. AA content was calculated from the titration curve endpoint, as estimated by the titration freeware CurTiPot.

### 5.2.4 Reactivity Ratios

Reactivity ratios of NIPAm and *t*BA were estimated by traditional free radical copolymerization of NIPAm and *t*BA with six NIPAm:*t*BA feed ratios (80:20, 65:35, 50:50, 35:65, 20:80 and 10:90). NIPAm, *t*BA and AIBN were dissolved in deuterated toluene in NMR tubes and sparged with argon. The sample was analyzed by $^1$H NMR in a Varian Innova 300 spectrometer at 70 ℃. NIPAm:*t*BA ratios in the feed and polymer were estimated by comparing the NIPAm and *t*BA peak integrals before the reaction and at approximately 10% monomer conversion, respectively. The data were analyzed by non-linear least squares fitting to the Mayo-Lewis equation.

$$F_2 = \frac{f_1 f_2 + r_2 f_2^{\,2}}{r_1 f_1^{\,2} + 2 f_1 f_2 + r_2 f_2^{\,2}} \tag{5-1}$$

where $f_1$ and $f_2$ are monomer compositions in the feed, $F_1$ and $F_2$ are monomer compositions in the polymer, and $r_1$ and $r_2$ are reactivity ratios, where 1 represents NIPAm and 2 represents *t*BA.

### 5.2.5 Sample Preparation

Aqueous solutions of PO(N/B) with a concentration of 0.5 wt% and PO(N/A) with 0.5 wt% and 5 wt% concentrations were prepared by thin film hydration. Appropriate amounts of bulk polymer were dissolved in $CH_2Cl_2$, followed by evaporation of solvent to yield a thin film on the walls of the vial. The thin film was hydrated, and the resulting

mixture was stirred at room temperature for at least 2 weeks. The aqueous PO(N/A) solutions were then diluted by buffered aqueous solutions prepared at pH 2 (maleate, 0.075 M), 4 (acetate buffer, 0.25 M), 6 (piperazine, 0.05 M) and 8 (phosphate buffer, 0.015 M), at 85 wt% polymer solution/15 wt% buffer, followed by at least one day of stirring at room temperature. All buffers had initial ionic strength of ~0.04 M, hence the buffered polymer solutions had ionic strength of ~0.006 M.

### 5.2.6 Dynamic Light Scattering

Micellization and micellar aggregation of the triblock terpolymers were investigated by dynamic light scattering (DLS). The solutions were passed through 0.45 μm filters into glass tubes (ID=0.25 in). Light scattering was carried out in a Brookhaven BI-200SM DLS system equipped with a Mini L-30 HeNe laser operating at 637 nm, a BI-NDO detector, and a TurboCorr correlator. The sample tubes were immersed in decalin. Intensity correlation functions $g_2(t)$ were recorded at varying temperatures from 25 to 55 ℃ scattering angles of 60 °, 90 °, and 120 °. The squared electric field correlation functions $g_1^2(t)$ were calculated from $g_2(t)$ according to Siegert relation $g_2(t) = 1 + \beta g_1^2(t)$. The cumulant method was used to fit $g_1^2(t)$ to extract the average decay rate Γ.

$$g_1^2(t) = A\exp(-2\Gamma \cdot t)(1+\frac{\mu_2}{2!}t^2 - \frac{\mu_3}{3!}t^3 + \cdots)^2 \quad (5\text{-}2)$$

The mutual diffusion coefficient $D_m$ was determined by linear regression of Γ vs $q^2$ according to the relation $D_m = \Gamma/q^2$, where $q$ is the scattering vector ($q = 4\pi n/\lambda \sin(\theta/2)$, $n$ is the refractive index of the solution, $\lambda$ is the laser wavelength, and $\theta$ is the scattering angle). Then, the hydrodynamic radius ($R_h$) was determined by using the Stoke-Einstein

equation:

$$R_h = \frac{k_B T}{6\pi\eta_s D_m} \tag{5-3}$$

The estimated uncertainty of $R_h$ is $\pm 5$ %. The size distribution could be estimated by the reduced second cumulant ($\mu_2/\Gamma^2$), which is a measure of the width of the decay rate distribution (assuming it is monomodal). The hydrodynamic radius distribution could also be extracted from the decay rate distribution generated through the inverse Laplace transform program REPES,[57] provided in the GENDIST analysis package.[58]

In cases where the size distribution was bimodal with well separated peaks, $g_1^2(t)$ was fit to a double exponential decay.

$$g_1^2(t) = [A_1 \exp(-\Gamma_1 \cdot t) + A_2 \exp(-\Gamma_2 \cdot t)]^2 \tag{5-4}$$

$D_{m,1}$ and $D_{m,2}$ were calculated by linear regression of $\Gamma_1$ and $\Gamma_2$ vs $q^2$, respectively, The corresponding hydrodynamic radii $R_{h,1}$ and $R_{h,2}$ for the two distinct populations were obtained by the Stokes-Einstein equation.

### 5.2.7 Rheology

Rheological measurements were carried out in an AR-G2 rheometer, with a Couette geometry confining the sample in a 1 mm concentric cylindrical gap between the cup (inner diameter 30 mm) and the bob (diameter 28 mm). About 15 mL of the sample was first loaded into the cup at room temperature (25 ℃). This amount filled the gap as the bob was lowered. Temperature was controlled by a Peltier accessory. To avoid water evaporation, the assembly was shielded by a metal cover with a wet sponge attached to the cover rim. Dynamic frequency sweeps were conducted in the linear viscoelastic

regime. Temperature dependences of *G′* and *G″* were measured at 10 rad/s and 1 ℃/min.

## 5.3 Results and Discussion

### 5.3.1 Synthesis of PO(N/A) Triblock Terpolymers

The PO(N/A) triblock terpolymers were prepared by RAFT polymerizations from a PO-CTA macroinitiator (see Chapter 2),[53] followed by acid hydrolysis. Briefly, the macroinitiator was used to grow P(NIPAm-*co*-*t*BA) blocks by RAFT polymerization. Subsequent removal of the dodecyltrithiocarbonate end group for PO(N/B)-CTA was confirmed by the absence of the methylene protons adjacent to the trithiocarbonate unit (δ=3.3 ppm) and the presence of methylene protons of the added methyl acrylate (δ=2.6, 2.8 ppm) (Figure 5.1). In the final step, hydrolysis of *t*BA of PO(N/B) to acrylic acid (AA), TFA was the catalyst. An excess of triethylsilane was used as a carbocation scavenger, ensuring complete hydrolysis of *t*BA, as confirmed by the disappearance of the methyl protons of *t*BA (δ=1.4 ppm) (Figure 5.1).[59]

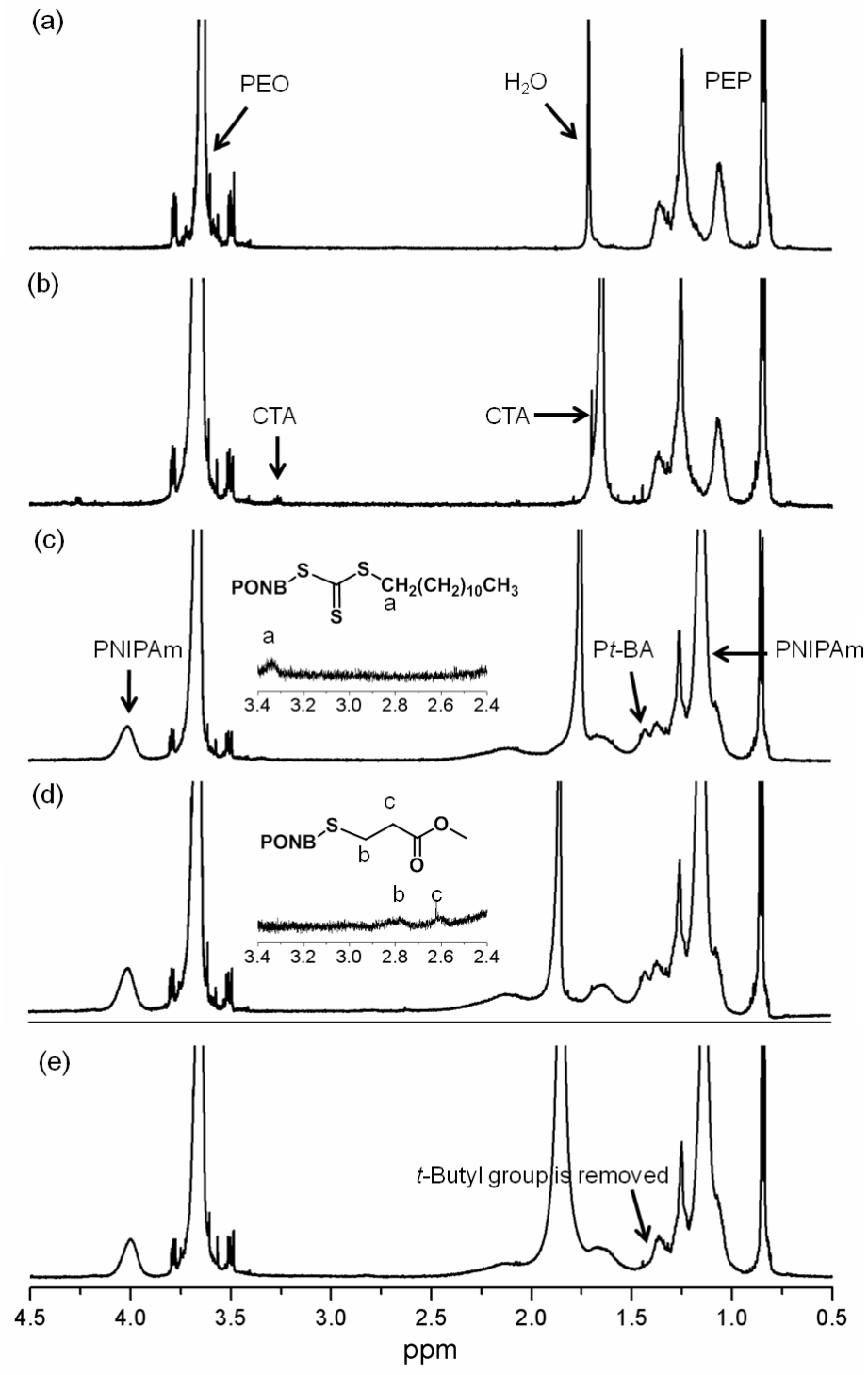


**Figure 5.1** $^{1}$H NMR (500 MHz) spectra of (a) PO and (b) PO-CTA, (c) PO(N/B)-CTA (d) PO(N/B7) and (e) PO(N/A7) polymers in $CDCl_3$. Area from 3.4 to 2.4 ppm of (c) and (d) is enlarged in each spectrum to monitor end group conversion.

The AA content in the P(NIPAm-*co*-AA) block of the PO(N/A) triblock terpolymers was determined by potentiometric titration (Figure 5.2). *t*BA molar content in the P(NIPAm-*co*-*t*BA) block of PO(N/B) is equal to AA molar content due to the complete hydrolysis of *t*BA to AA. We found that it was lower than the *t*BA content in the feed (Table 5.1). This suggested that *t*BA was incorporated to a lesser extent than NIPAm in the P(NIPAm-*co*-*t*BA) block. (The *t*BA content could not be quantified by $^{1}$H NMR spectroscopy due to peak overlap). To confirm this we carried out a reactivity ratio study for the free radical polymerization of NIPAm and *t*BA, without the CTA. Reactivity ratios of NIPAm and *t*BA were estimated to be $r_{t\mathrm{BA}} = 0.88$ and $r_{\mathrm{NIPAm}} = 2.1$ by non-linear least squares fitting to the Mayo-Lewis equation (Figure 5.3), suggesting that the P(NIPAm-*co*-*t*BA) block starts out relatively rich in NIPAm and more *t*BA units are located towards the chain end.

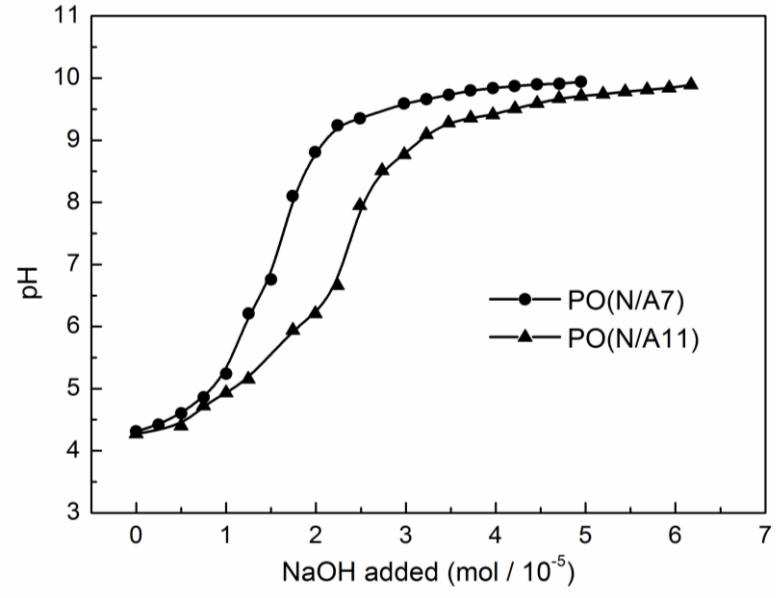


**Figure 5.2** Titration curves for PO(N/A7) (105 mg) and PO(N/A11) (104 mg) against 0.05 M sodium hydroxide solution.

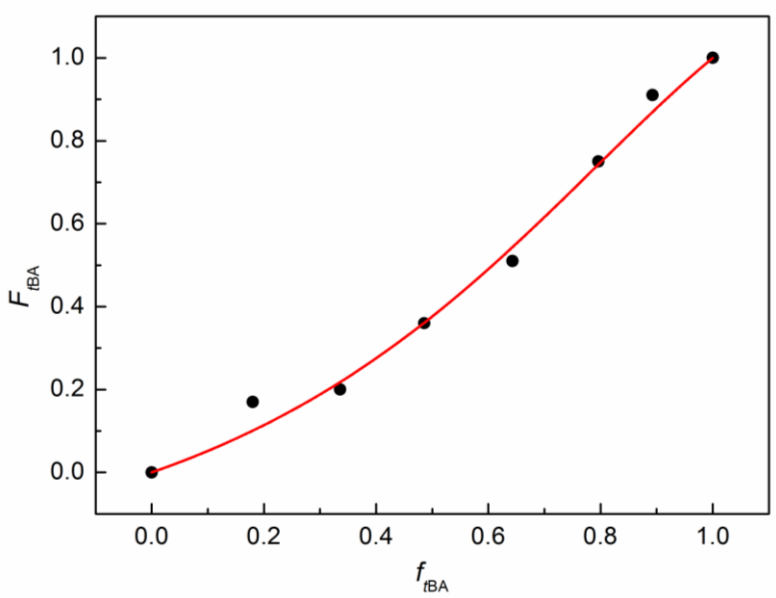


**Figure 5.3** Plot of *t*BA composition in polymer ($F_2$) versus feed ($f_2$). The solid symbol represents experimental data, while the red curve represents model fit.

The product of each reaction step was characterized by size exclusion chromatography (SEC) (Figure 5.4). In the elugrams, some amount of tailing is observed for samples end capped with CTA. Polymer chains with this particular CTA attached may have a tendency to stick to the column, which would lead to an apparent broadening in the SEC trace. Samples investigated in this work and their molecular characteristics are listed in Table 5.1. The percent degree of substitution of *t*BA and ultimately AA in the PNIPAm block is designated following the comonomer identifier in the polymer acronym.

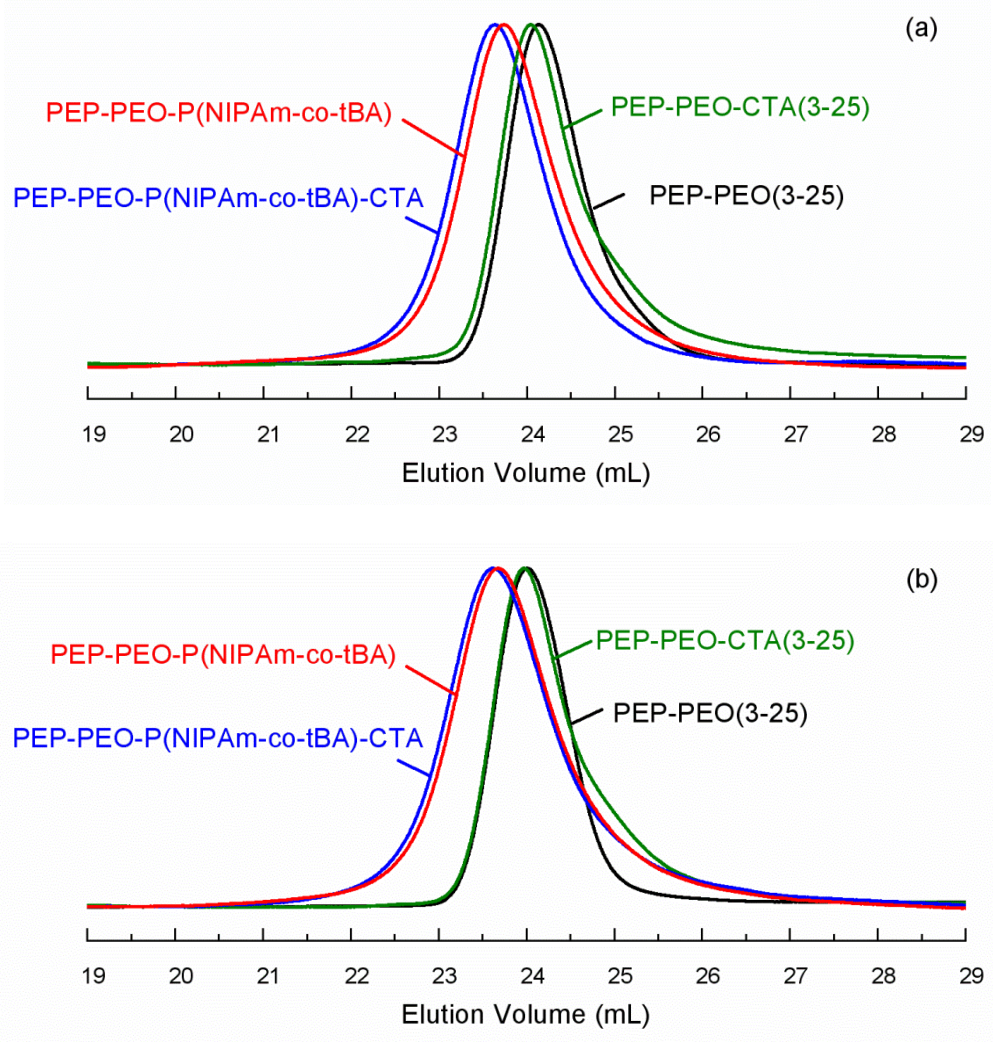


**Figure 5.4** SEC trace of (a) PO(N/B7) and (b) PO(N/B11) and the corresponding precursors. THF/*N*,*N*,*N*',*N*'-tetramethylethylenediamine was used as the eluting solvent at a flow rate of 1.0 mL/min.

**Table 5.1** Molecular characteristics of PO(N/B) and PO(N/A) triblock terpolymers

| Sample | Molecular composition[a] | *t*BA content (feed)[b] | *t*BA or AA content (polymer)[c] | $Đ^d$ |
|---|---|---|---|---|
| PO(N/B7) | $PEP_{45}$-$PEO_{565}$-P(NIPAm$_{80}$-*co*-*t*BA$_5$) (3-25-9-0.7) | 10 | 7 | 1.09 |
| PO(N/A7) | $PEP_{45}$-$PEO_{565}$-P(NIPAm$_{80}$-*co*-AA$_5$) (3-25-9-0.4) | 10 | 7 | - |
| PO(N/B11) | $PEP_{45}$-$PEO_{565}$-P(NIPAm$_{71}$-*co*-*t*BA$_9$) (3-25-8-1.1) | 20 | 11 | 1.08 |
| PO(N/A11) | $PEP_{45}$-$PEO_{565}$-P(NIPAm$_{71}$-*co*-AA$_9$) (3-25-8-0.6) | 20 | 11 | - |

[a]Numbers in parentheses correspond to molecular weights of individual blocks in kg/mol as determined by $^1$H NMR spectroscopy and potentiometric titration. Subscript indicates number average degree of polymerization of each block. [b]Mol % of *t*BA in reaction mixture of NIPAm and *t*BA as determined by $^1$H NMR spectroscopy. [c]Mol % of AA in the P(NIPAm-*co*-AA) block of PO(N/A) as determined by potentiometric titration. Mol % of *t*BA in the P(NIPAm-*co*-*t*BA) block of PO(N/B) is equal to the mol % of AA due to the complete hydrolysis of *t*BA to AA, confirmed by $^1$H NMR. [d]Dispersity was measured by SEC with THF/*N*,*N*,*N*',*N*'-tetramethylethylenediamine as the eluting solvent.

### 5.3.2 Micellar Aggregation of PO(N/B) and PO(N/A) Triblock Terpolymers.

DLS experiments were performed on 0.5 wt% aqueous solutions of four PO(N/B) and PO(N/A) terpolymers for a series of temperatures over the range 25–55 ℃. Figure 5.5 displays mean hydrodynamic radii and scattering intensities as a function of temperature for PO(N/B) and PO(N/A) copolymers in dilute aqueous solutions (0.5 wt%).

At 25 ℃, the micelle radii were around 50 nm for both PO(N/B) and PO(N/A) terpolymers, irrespective of composition. As the solution was heated above a critical temperature, both hydrodynamic radius and scattering intensity increased, indicating formation of micellar aggregates. This transition temperature (the point where hydrodynamic radius and scattering intensity start to increase) will henceforth be called the "critical micellar aggregation temperature" or CMAT. Dispersity in $R_h$ was evident both above and below the CMAT. The reduced second cumulant ($\mu_2/\Gamma^2$) was ~0.20 at lower temperatures, and tended to increase around the CMAT, as expected for an aggregation transition.

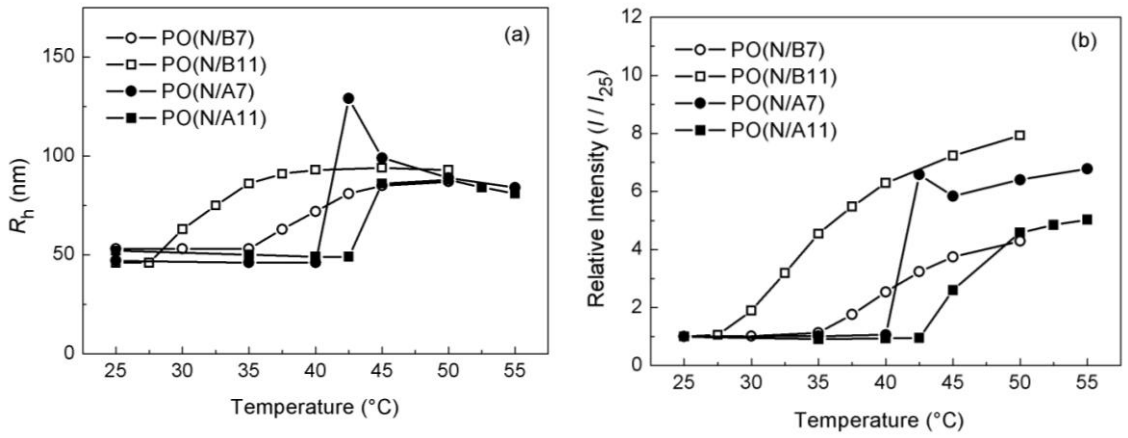


**Figure 5.5** (a) Mean micelle size ($R_h$) and (b) scattering intensity as a function of temperature for aqueous solutions of PO(N/B7) (○), PO(N/B11) (□), PO(N/A7) (●) and PO(N/A11) (■). Polymer concentration: 0.5 wt%. $R_h$ was calculated by the cumulant method. Intensity was measured at 90 °. Ordinate is relative intensity ($I/I_{25}$) where $I_{25}$ is intensity recorded at 25 ℃.

The full size distribution curves are displayed in Figure 5.6. While the PO(N/B) distributions are essentially unimodal, the PO(N/A) distributions are often bimodal at high temperatures, indicating that both micelles and micellar aggregates are present. Thus the CMAT should be taken as the onset of a subpopulation of aggregates, rather than a complete transition from the micellar to the aggregated state.

The PO(N/A7) terpolymer micelles aggregated at 40 ℃ while PO(N/A11) terpolymer micelles began forming micellar aggregates at a slightly higher temperature of 42.5 ℃. Considering that the CMAT for PON is 42 ℃,[53] the transitions for both PON and PO(N/A) triblocks occurred at 40 ℃ or above, in all cases several degrees higher than the LCST of PNIPAm. The covalent linkage of the well solvated PEO to the PNIPAm-based corona and the relatively small molar mass of the PNIPAm block increase the temperature at which the coronal chains aggregate.[60-63] For the PO(N/B7) terpolymers, the CMAT is 35 ℃ while for the PO(N/B11) polymers, it is 27 ℃. Overall, PO(N/B) terpolymer micelles exhibited lower aggregation temperatures than the PO(N/A) triblocks and the CMAT decreased with increasing *t*BA fraction. This observation is consistent with literature observations that the LCST of PNIPAm is lowered upon incorporation of small amounts of *tert*-butyl acrylate, *n*-butyl acrylate or other hydrophobic monomers.[22, 36, 64-66] It should be noted that there was no pH adjustment for these samples. The pH for the PO(N/B) aqueous solutions was around 7.0 while that for the PO(N/A) aqueous solutions was around 4.0, indicating significant release of acidic protons and thus ionization of the AA groups ($pK_a \approx 4.3–4.8$).

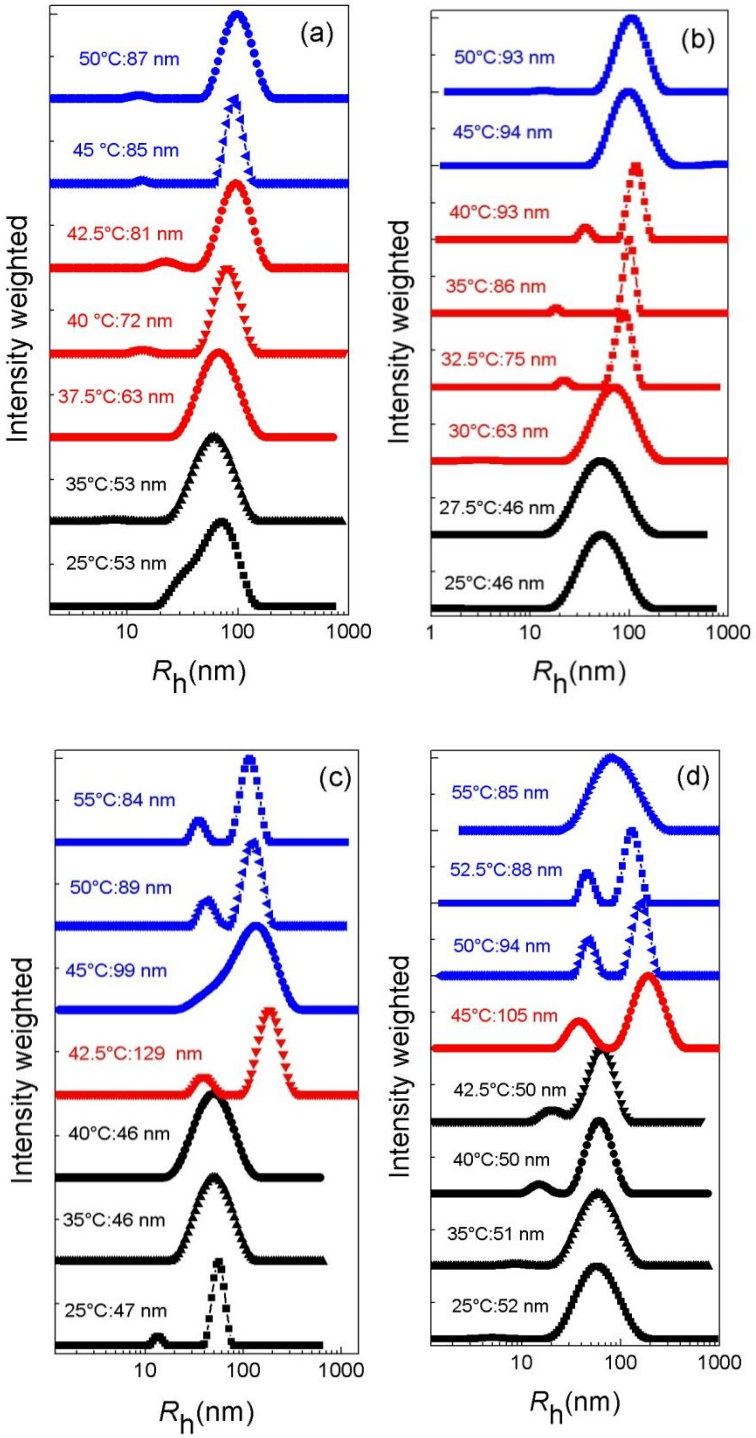


**Figure 5.6** Micelle size ($R_h$) distribution as a function of temperature for (a) PO(N/B7), (b) PO(N/B11), (c) PO(N/A7) and d) PO(N/A11) micelles, as determined by DLS at 90 ° (0.5 wt% polymer concentration).

### 5.3.3 Micellar Aggregation of PO(N/A) Triblock Terpolymers as a Function of pH

DLS experiments were also performed with 0.4 wt% PO(N/A) terpolymer aqueous solutions for pH values ranging from 2 to 8 over the 25–55 ℃ temperature range. Figure 5.7 presents DLS data for 0.4 wt% PO(N/A7) terpolymer solutions. Full size distribution curves are present in Figure 5.8.

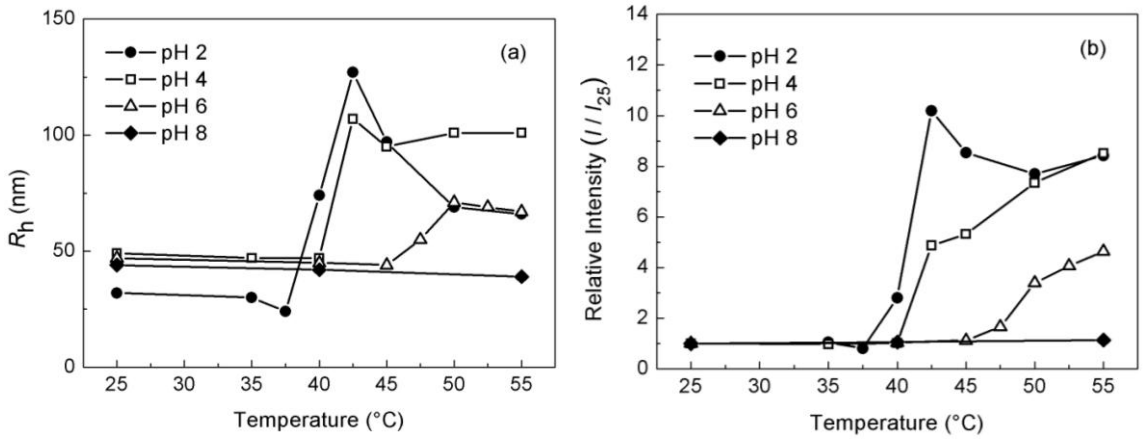


**Figure 5.7** (a) Micelle size and (b) scattering intensity as a function of temperature for PO(N/A7) in aqueous solutions at pH 2 (●), 4 (□), 6 (Δ) and 8 (◆). Polymer concentration: 0.4 wt%. $R_h$ was calculated by the cumulant method. Intensity is measured at a 90 ° scattering angle, and the vertical axis is the relative intensity ($I/I_{25}$) where $I_{25}$ is the intensity recorded at 25 ℃.

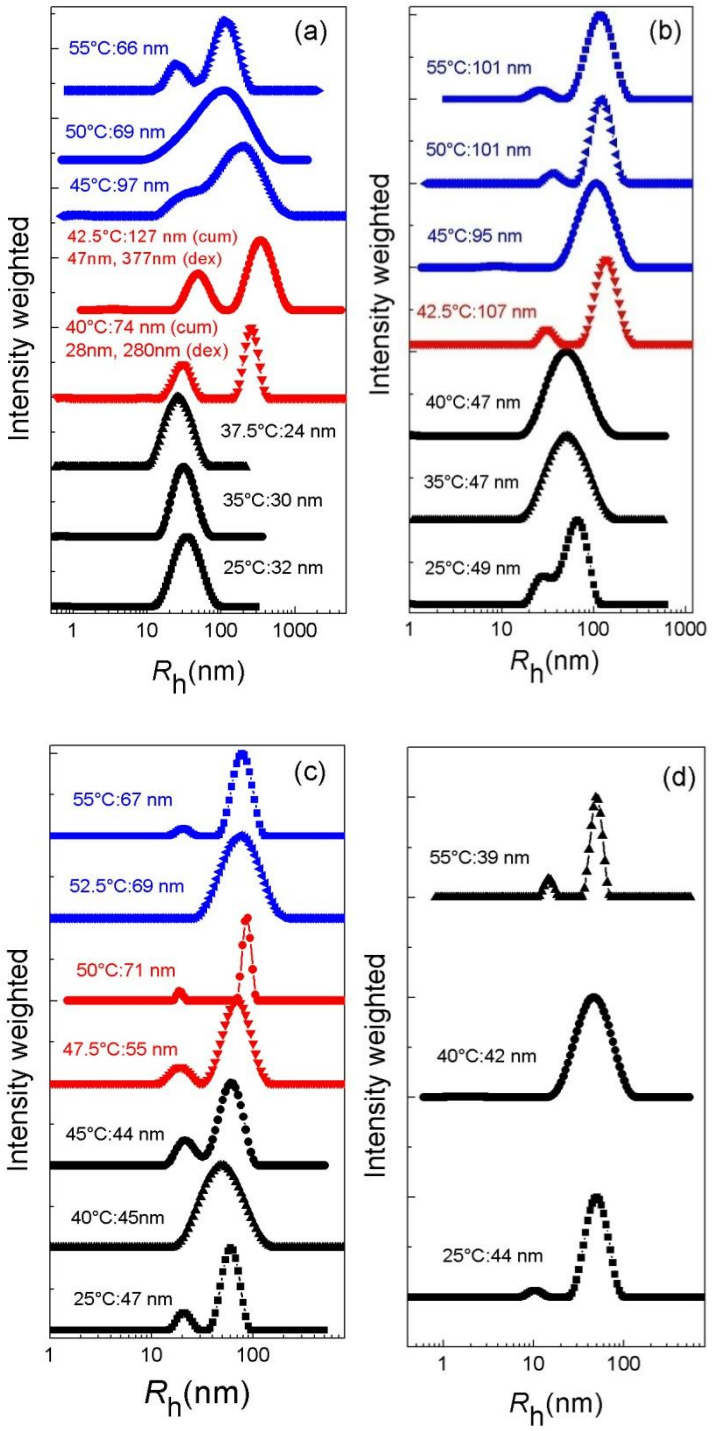


**Figure 5.8** Micelle size distribution as a function of temperature for PO(N/A7) micelles at (a) pH 2, (b) pH 4, (c) pH 6 and (d) pH 8 at 90 ° (0.4 wt% polymer

concentration) [(cum) and (dex) stand for $R_h$ obtained by cumulant and double exponential fitting, respectively].

At room temperature, the typical micelle size was ~50 nm at pH 4, 6 and 8, which is similar to the size of PON[53], PO(N/B) and PO(N/A) micelles in pure water. However, at pH 2, the micelle size was reduced to ~30 nm. This reduction is also observed for PO(N/A11) (see below). At pH 2, virtually all AA units are expected to be protonated and electrically neutral, while increasing fractions of AA will be ionized at the higher pH values, including the case where the PO(N/A) is suspended in pure water, where the pH was observed to be approximately 4. We speculate that the substantially reduced radius of PO(N/A) at pH 2 is due to condensation of the corona into the shell resulting from hydrogen bonding between the protonated AA units and PEO.[67] Although AA can also hydrogen bond with PNIPAm,[44] intra-coronal PNIPAm and PAA hydrogen bonding alone is not likely to be sufficient to bring about a micelle size reduction of this magnitude. Hence, it appears that H-bonding between protonated PAA and PEO causes the P(NIPAM-*co*-AA) corona to collapse onto the PEO shell.

At pH 2, the CMAT was 37.5 ℃, and the aggregation transition shifted to 40 ℃ and 45 ℃ for the pH 4 and 6 solutions, respectively. No aggregation was observed for pH 8 up to 55 ℃. An increase in mean hydrodynamic radius correlated with the rise in scattering intensity upon aggregation, and the ratio of scattering intensity provides a rough estimate of the aggregation number of the average micellar cluster.

Results for the PO(N/A11) samples are shown in Figures 5.9 and 5.10. Trends are similar to the PO(N/A7) sample, but with quantitative differences. CMAT was shown to

be 40 ℃ and 42.5 ℃ at pH 2 and 4, respectively, while no aggregation was observed up to 55 ℃ for the pH 6 and pH 8 solutions. Similar to PO(N/A7), the micelle radius was ~50 nm at 25 ℃ for the pH 4, 6 and 8 solutions and shrank to ~30 nm at pH 2, which can also be attributed to hydrogen bonding between the protonated AA corona and PEO shell as discussed above.

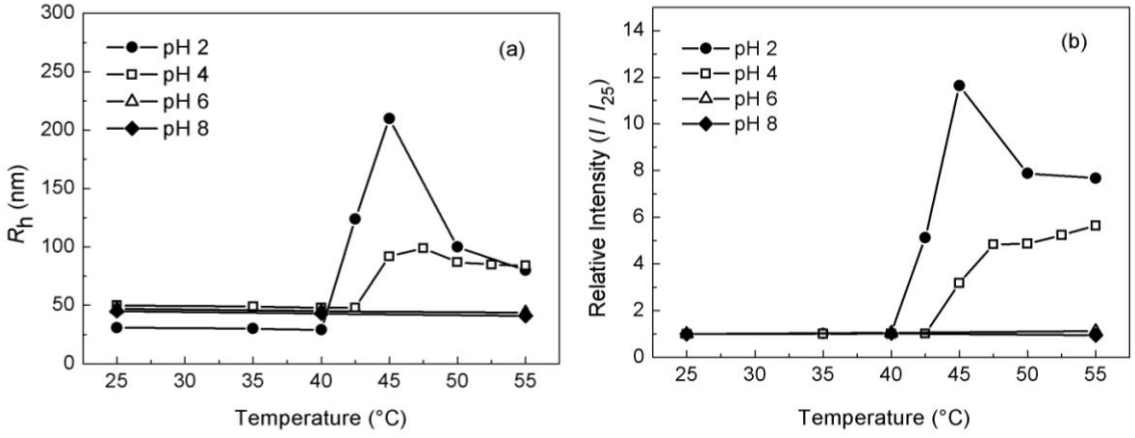


**Figure 5.9** (a) Micelle size and (b) Intensity as a function of temperature for PO(N/A11) in buffered solutions at pH 2 (●), 4 (□), 6 (Δ) and 8 (◆). Polymer concentration: 0.4 wt%. $R_h$ was calculated by the cumulant method. Intensity is measured at a 90 ° scattering angle, and the vertical axis is the relative intensity ($I/I_{25}$) where $I_{25}$ is the intensity recorded at 25 ℃.

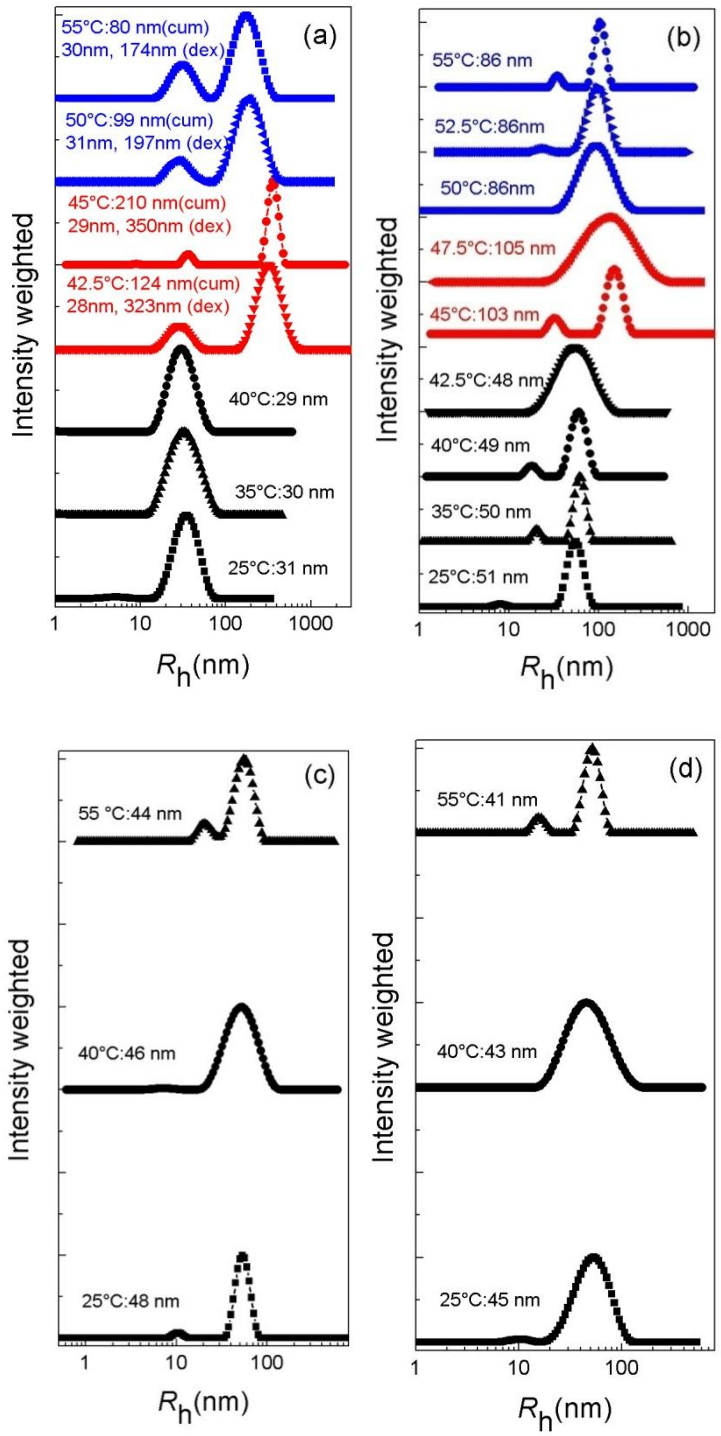


**Figure 5.10** Micelle size distribution as a function of temperature for PO(N/A11) micelles at (a) pH 2, (b) pH 4, (c) pH 6 and (d) pH 8 at 90 ° (0.4 wt% polymer concentration) [(cum) and (dex) stand for $R_h$ obtained by cumulant and double

exponential fitting, respectively].

The CMATs for PO(N/A7) and PO(N/A11) in buffered pH 4 aqueous solutions were the same as those for the corresponding unbuffered solutions, which were of pH ~3.8 and 4.0, respectively. It may therefore be inferred that ionization of the coronal polymer chains was nearly identical in these two cases. At pH 2, the aggregate size peaked near CMAT and then decreased to a smaller $R_h$ value that remained nearly constant with further increase in temperature. This may be explained by examining the micellar size distribution at pH 2. From Figures 5.8a and 5.10a, it is evident that at pH 2, for temperatures ≥ CMAT, the size distribution is bimodal with both micelles and aggregates present. The average hydrodynamic radii plotted in Figures 5.7 and 5.9 are derived from cumulant fitting of DLS data, which is not representative in the case of a bimodal distribution. This may explain the apparently different $R_h$ trend observed for pH 2. $R_h$ values obtained from double exponential fits are also reported in Figures 5.8a and 5.10a. It should be noted that this does not change the CMAT, as it is simply the temperature at which aggregation first appears, irrespective of whether the distribution is unimodal or bimodal.

The DLS results for the PO(N/A) triblock are summarized as a phase diagram in Figure 5.11, which reflects the following trends. First, the CMAT increases with increasing pH, reflecting increased ionization of the corona. Second, the CMAT increases with AA content, for essentially the same reason. The effects of pH and degree of incorporation of AA into the PO(N/A) micelles on the CMAT are consistent with the literature reporting the LCST of NIPAm/AA copolymers, except for the overall shift

toward higher temperatures seen in the micellar systems, as mentioned earlier. The phase diagram is truncated due to lack of data above 55 ℃. For comparison, we also include the CMAT of PON, which is 42 ℃.[53] Under acidic conditions, the CMAT for PO(N/A) is lower than that for PON due to intra-chain H-bonding between the unprotonated AA groups.[68, 69] At higher pH values, PO(N/A) CMAT increases due to acrylic acid ionization.

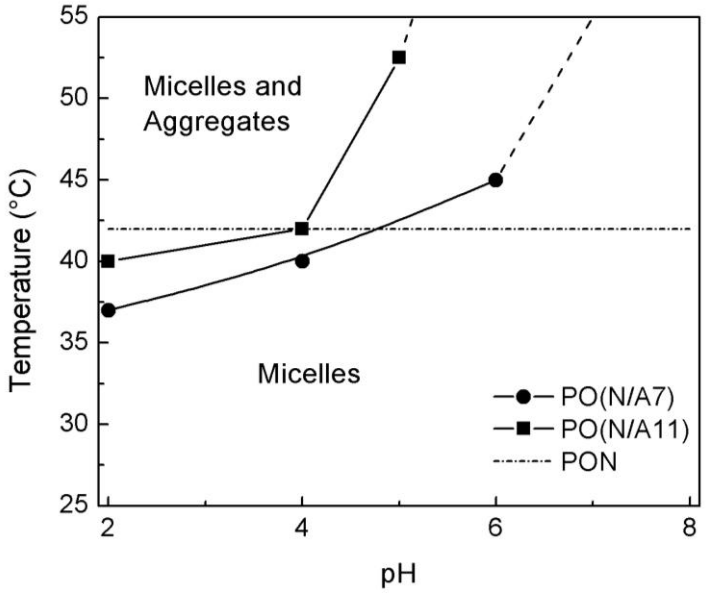


**Figure 5.11** Phase diagram for PO(N/A7) (●), PO(N/A11) (■) as a function of temperature and pH. Dashed lines are extrapolation of trends, which cannot be well specified since data was not taken above 55 ℃. PON CMAT (dash dot) (from the previous study by Zhou *et al.*[53] and assumed to be pH-independent) is presented here for comparison. It should be noted that aggregate phase may include a subpopulation of micelles.

### 5.3.3 Gelation of PO(N/A) Triblock Terpolymers

Results of oscillatory shear measurements conducted with 4 wt% PO(N/A11) and PO(N/A7) in buffered solutions at pH = 2 and 8 over the temperature range 25–60 ℃ are shown in Figure 5.12. As both samples showed similar behavior, only PO(N/A11) samples will be discussed in the following section. As shown in Figure 5.12a, PO(N/A11) show a sharp sol-gel transition near 45 ℃ at pH 2, but no such transition at pH 8. Below 42.5 ℃, *G′* was nearly constant and the same at both pH values while *G″*, again identical at the two pH values, decreased slightly with increasing temperature. While there was no evidence of aggregation at pH 8, up to the highest measured temperature (60 ℃). At pH 2 both *G′* and *G″* increased abruptly near the transition point, with *G′* crossing over *G″*. The sol-gel transition was thermoreversible throughout repeated heating and cooling cycles.

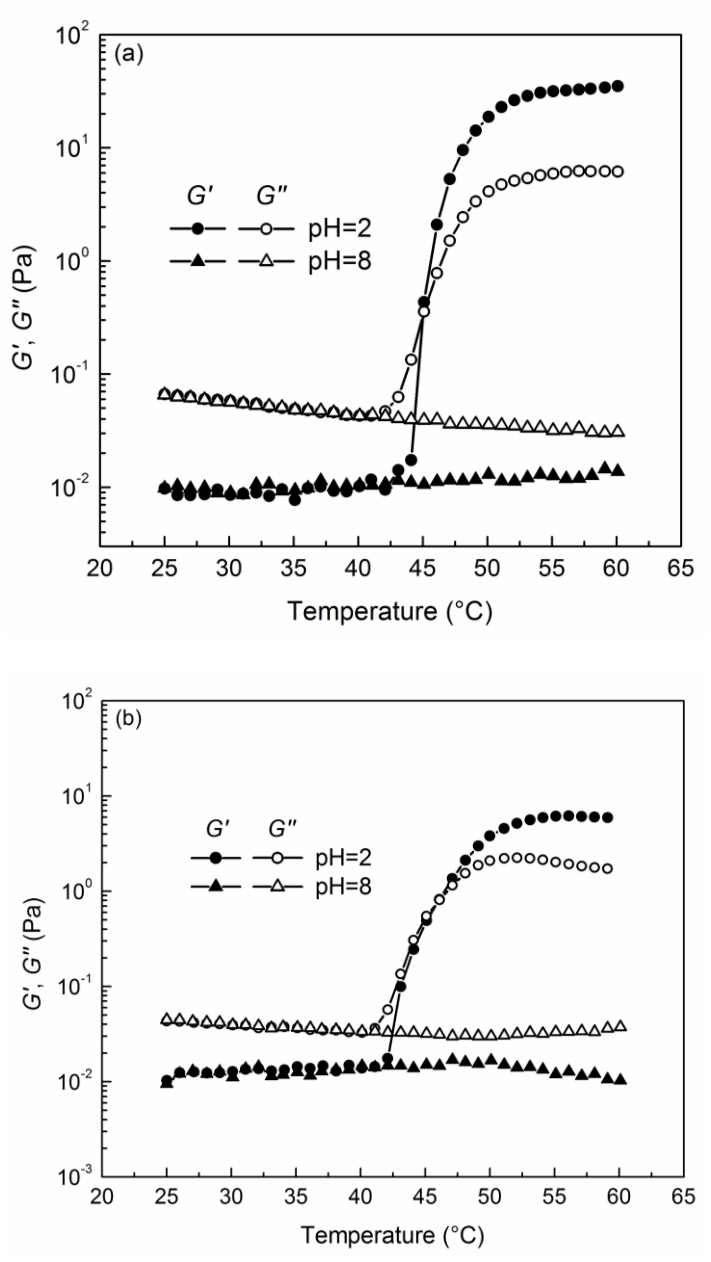


**Figure 5.12** Temperature-dependent dynamic shear moduli ($G'$ and $G''$) for (a) 4 wt% PO(N/A11) and (b) PO(N/A7) in buffered solutions at $\omega$ = 10 rad/s and a heating rate of 1 ℃/min. The pH 2 solution was measured at a strain amplitude $\gamma$ = 50% at low temperatures (below gel point) and $\gamma$ = 2% at high temperatures (above gel point). The pH 8 solution was measured at $\gamma$ = 50%.

The sol-gel transition for the pH 2 solution and sol state for the pH 8 solution were verified using dynamic frequency sweep measurements. Representative data for the pH 2 solution at 25, 43, and 60 ℃ are shown in Figure 5.13a. At 25 ℃, *G′* was smaller than *G″* indicating a free-flowing sol state. At 60 ℃, *G′* was larger than *G″* at all frequencies and was nearly frequency independent, indicating solid-like behavior. At 43 ℃, the sample showed intermediate behavior with nearly identical values for *G′* and *G″*, signifying the transition between liquid-like and solid-like behavior. Dynamic frequency sweeps of the pH 8 solution at 25 and 60 ℃ are presented in Figure 5.13b, and clearly show that *G′* is smaller than *G″* at both temperatures, indicating that the pH 8 solution was in the sol state over the temperature range of 25–60 ℃. These results may be interpreted as follows. At pH 2, the PO(N/A) micelles have a relatively small diameter and do not overlap substantially at low temperatures. Above the CMAT, the coronae become so interconnected as to form a percolating network of adherent micelles. At pH 8, however, such overlap is not permitted at any temperature since it would lead to substantial increase in fixed charge density in the overlapping coronae, leading to osmotic forces that draw water back into the coronae.

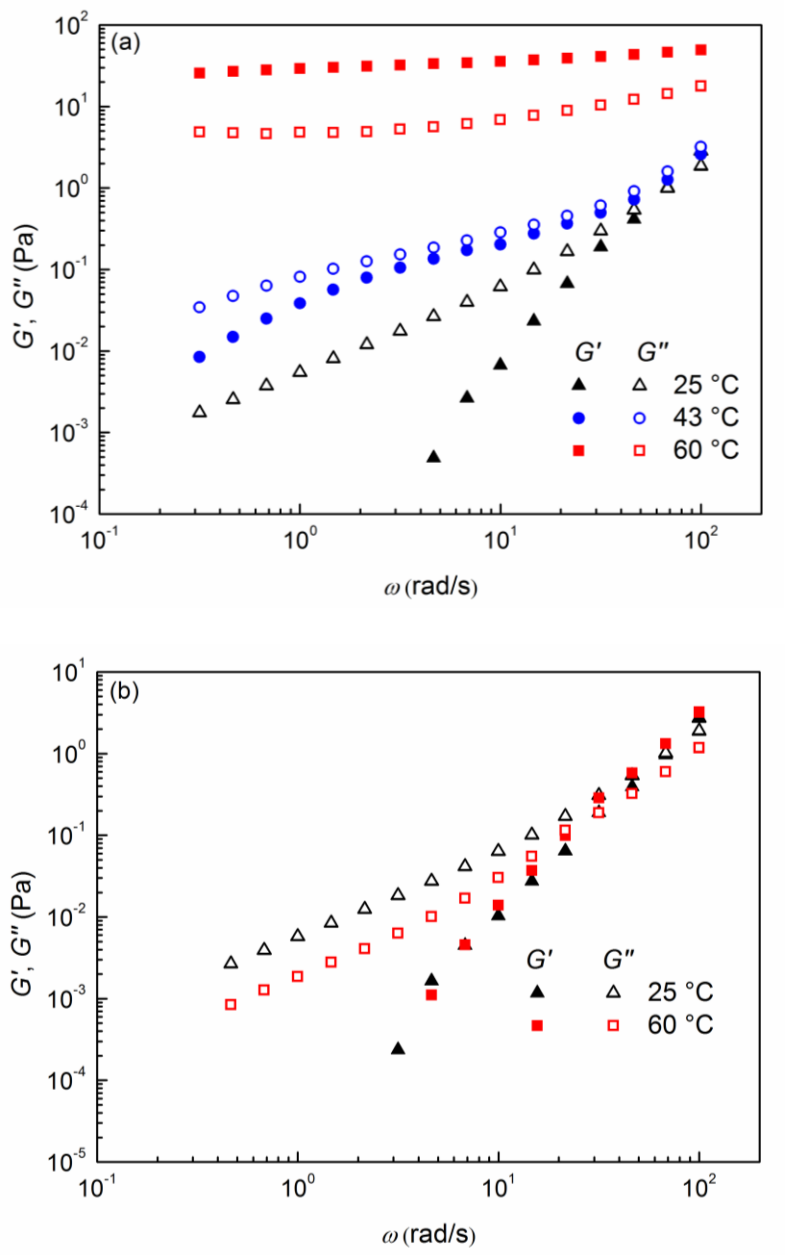


**Figure 5.13** Dynamic shear moduli ($G'$ and $G''$) as a function of frequency for 4 wt% PO(N/A11) in (a) pH 2 and (b) pH 8 buffered solutions measured at indicated temperatures.

The gelation temperature at 45 ℃, observed for PO(N/A11) at pH 2, is a few degrees

higher than the corresponding CMAT (40 ℃). This difference between the CMAT and gelation temperature is not unexpected. While the CMAT, determined by DLS, signals the onset of aggregation, the gelation temperature, as measured by rheology, indicates the point at which micellar aggregates form a percolating three dimensional network strong enough to result in a modulus crossover. Another factor that could account for the difference in transition temperature is the difference in heating rate.

It should be noted that the observed aggregation and gelation transitions were completely reversible, and the reversibility was not influenced by polymer concentration. At 0.5 wt%, upon cooling, the micellar aggregates disaggregated into individual micelles with radius of ~50 nm. Similarly, the gels formed on heating 4wt% PO(N/A) solutions reverted to the sol state on cooling.

### 5.4 Summary

Doubly thermo- and pH-responsive PO(N/A) triblock terpolymers were prepared via hydrolysis of PO(N/B) triblock terpolymers, which were synthesized by a combination of anionic and RAFT polymerization. The PO(N/A) terpolymers spontaneously self assemble into micelles with PEP cores and PEO-P(NIPAm-*co*-AA) coronae in aqueous solution at room temperature. Upon heating, these micelles aggregate in the dilute solutions and form a three dimensional network at higher concentrations. The micelle-micellar aggregate or sol-gel transition is completely reversible and is due to intermicellar association of corona P(NIPAm-*co*-AA) chains above the LCST of the P(NIPAm-*co*-AA) block. The critical micellar aggregation and gelation temperatures are controlled by the mole fraction and degree of acrylic acid (AA) ionization in the

P(NIPAm-*co*-AA) block. Therefore they can be modulated by changing pH of the medium and by varying the polymer composition.

It should be apparent that while measurements were carried out by sweeping temperature at fixed pH, one could fix temperature and vary pH instead. The joint temperature/pH behavior may lead to biomedical applications of these or analogous triblock polymer systems. For example, one might consider an intravaginal drug delivery system incorporating a hydrophilic antiviral, antibacterial, anti-inflammatory or spermicidal agent into a concentrated micellar solution which, at room temperature, remains in the fluid state. Because of the large PEO content relative to PEP and P(NIPAm-*co*-AA), the agent will reside primarily in the PEO shell region. Upon application in the relatively acidic (pH 4-5) vaginal cavity,[70] the increased temperature could instigate gelation. Release of drug could be relatively slow by passive diffusion through the resulting hydrogel, or it could be triggered by introduction of semen, whose pH is ~7.5, which would promote dissociation of the micellar network. However, properties of the terpolymers (CMAT, pH sensitivity, biocompatibility, etc.) should be tuned for such physiological applications.

This work is contributed equally from Isha Koonar and Can Zhou and directed jointly by Ronald A. Siegel, Marc A. Hillmyer and Timothy P. Lodge.

## 5.5 References

1. Jeong, B.; Gutowska, A. *Trends Biotechnol.* **2002**, *20*, 305-311.

2. Nath, N.; Chilkoti, A. *Adv. Mater.* **2002**, *14*, 1243-1247.
3. de las Heras Alarcon, C.; Pennadam, S.; Alexander, C. *Chem. Soc. Rev.* **2005**, *34*, 276-285.
4. Stuart, M. A. C.; Huck, W. T. S.; Genzer, J.; Muller, M.; Ober, C.; Stamm, M.; Sukhorukov, G. B.; Szleifer, I.; Tsukruk, V. V.; Urban, M.; Winnik, F.; Zauscher, S.; Luzinov, I.; Minko, S. *Nat. Mater.* **2010**, *9*, 101-113.
5. Hosoya, K.; Kimata, K.; Araki, T.; Tanaka, N.; Frechet, J. M. J. *Anal. Chem.* **1995**, *67*, 1907-1911.
6. Wischerhoff, E.; Badi, N.; Lutz, J.-F.; Laschewsky, A. *Soft Matter* **2010**, *6*, 705-713.
7. Galperin, A.; Long, T. J.; Ratner, B. D. *Biomacromolecules* **2010**, *11*, 2583-2592.
8. Gil, E. S.; Hudson, S. M. *Prog. Polym. Sci.* **2004**, *29*, 1173-1222.
9. Kanazawa, H.; Yamamoto, K.; Matsushima, Y.; Takai, N.; Kikuchi, A.; Sakurai, Y.; Okano, T. *Anal. Chem.* **1996**, *68*, 100-105.
10. Kanazawa, H.; Sunamoto, T.; Matsushima, Y. *Anal. Chem.* **2000**, *72*, 5961-5966.
11. Kobayashi, J.; Kikuchi, A.; Sakai, K.; Okano, T. *Anal. Chem.* **2001**, *73*, 2027-2033.
12. Kikuchi, A.; Okano, T. *Prog. Polym. Sci.* **2002**, *27*, 1165-1193.
13. Galaev, I. Y.; Mattiasson, B. *Trends Biotechnol.* **1999**, *17*, 335-340.
14. Akiyama, Y.; Kikuchi, A.; Yamato, M.; Okano, T. *Langmuir* **2004**, *20*, 5506-5511.
15. Xu, F. J.; Zhong, S. P.; Yung, L. Y. L.; Kang, E. T.; Neoh, K. G. *Biomacromolecules* **2004**, *5*, 2392-2403.
16. Cole, M. A.; Voelcker, N. H.; Thissen, H.; Griesser, H. J. *Biomaterials* **2009**, *30*, 1827-1850.
17. Mizutani, A.; Kikuchi, A.; Yamato, M.; Kanazawa, H.; Okano, T. *Biomaterials* **2008**,

*29*, 2073-2081.

18. Mano, J. F. *Adv. Eng. Mater.* **2008**, *10*, 515-527.
19. Kim, S.; Healy, K. E. *Biomacromolecules* **2003**, *4*, 1214-1223.
20. Nakamura, K.; Maitani, Y.; Lowman, A. M.; Takayama, K.; Peppas, N. A.; Nagai, T. *J. Controlled Release* **1999**, *61*, 329-335.
21. Schmaljohann, D. *Adv. Drug Deliv. Rev.* **2006**, *58*, 1655-1670.
22. Schild, H. G. *Prog. Polym. Sci.* **1992**, *17*, 163-249.
23. Winnik, F. M. *Macromolecules* **1990**, *23*, 233-242.
24. Heskins, M.; Guillet, J. E. *J. Macromol. Sci. Chem.* **1968**, *A2*, 1441-1455.
25. Lin, H.; Cheng, Y. *Macromolecules* **2001**, *34*, 3710-3715.
26. Li, C.; Tang, Y.; Armes, S. P.; Morris, C. J.; Rose, S. F.; Lloyd, A. W.; Lewis, A. L. *Biomacromolecules* **2005**, *6*, 994-999.
27. Angelopoulos, S. A.; Tsitsilianis, C. *Macromol. Chem. Phys* **2006**, *207*, 2188-2194.
28. Vogt, A. P.; Sumerlin, B. S. *Soft Matter* **2009**, *5*, 2347-2351.
29. Nedelcheva, A. N.; Vladimirov, N. G.; Novakov, C. P.; Berlinova, I. V. *J. Polym. Sci., Part A: Polym. Chem.* **2004**, *42*, 5736-5744.
30. Li, C.; Buurma, N. J.; Haq, I.; Turner, C.; Armes, S. P.; Castelletto, V.; Hamley, I. W.; Lewis, A. L. *Langmuir* **2005**, *21*, 11026-11033.
31. Reinicke, S.; Schmelz, J.; Lapp, A.; Karg, M.; Hellweg, T.; Schmalz, H. *Soft Matter* **2009**, *5*, 2648-2657.
32. Sugihara, S.; Kanaoka, S.; Aoshima, S. *J. Polym. Sci., Part A: Polym. Chem.* **2004**, *42*, 2601-2611.
33. Hillmyer, M. A.; Lodge, T. P. *J. Polym. Sci., Part A: Polym. Chem.* **2002**, *40*, 1-8.

34. Zhou, C.; Hillmyer, M. A.; Lodge, T. P. *J. Am. Chem. Soc.* **2012**, *134*, 10365-10368.

35. O'Lenick, T. G.; Jiang, X.; Zhao, B. *Langmuir* **2010**, *26*, 8787-8796.

36. Feil, H.; Bae, Y. H.; Feijen, J.; Kim, S. W. *Macromolecules* **1993**, *26*, 2496-2500.

37. Yoshida, R.; Sakai, K.; Okano, T.; Sakurai, Y. *J. Biomater. Sci., Polym. Ed.* **1995**, *6*, 585-598.

38. Vasilevskaya, V. V.; Khokhlov, A. R.; Yoshikawa, K. *Macromol. Theory Sim.* **2000**, *9*, 600-607.

39. Kang, S. I.; Bae, Y. H. *Macromol. Chem. Symp.* **2001**, *14*, 145-155.

40. Charbonneau, C.; Chassenieux, C.; Colombani, O.; Nicolai, T. *Macromolecules* **2011**, *44*, 4487-4495.

41. Chen, G.; Hoffman, A. S. *Macromol. Rapid Commun.* **1995**, *16*, 175-182.

42. Mi Kyong, Y.; Yong Kiel, S.; Chong, S. C.; Young, M. L. *Polymer* **1997**, *38*, 2759-2765.

43. Jones, M. S. *Eur. Polym. J.* **1999**, *35*, 795-801.

44. Schilli, C. M.; Zhang, M.; Rizzardo, E.; Thang, S. H.; Chong, Y. K.; Edwards, K.; Karlsson, G.; Müller, A. H. E. *Macromolecules* **2004**, *37*, 7861-7866.

45. Qiu, X.; Kwan, C. M. S.; Wu, C. *Macromolecules* **1997**, *30*, 6090-6094.

46. Bokias, G.; Staikos, G.; Iliopoulos, I. *Polymer* **2000**, *41*, 7399-7405.

47. Bokias, G.; Vasilevskaya, V. V.; Iliopoulos, I.; Hourdet, D.; Khokhlov, A. R. *Macromolecules* **2000**, *33*, 9757-9763.

48. Snowden, M. J.; Chowdhry, B. Z.; Vincent, B.; Morris, G. E. *J. Chem. Soc., Faraday Trans.* **1996**, *92*, 5013-5016.

49. Han, C. K.; Bae, Y. H. *Polymer* **1998**, *39*, 2809-2814.

50. Bae, Y. H.; Vernon, B.; Han, C. K.; Kim, S. W. *J. Controlled Release* **1998**, *53*, 249-258.

51. Dong, L.; Hoffman, A. S. *J. Controlled Release* **1991**, *15*, 141-152.

52. Koonar, I.; Zhou, C.; Hillmyer, M. A.; Lodge, T. P.; Siegel, R. A. *Langmuir* **2012**, *28*, 17785-17794.

53. Zhou, C.; Hillmyer, M. A.; Lodge, T. P. *Macromolecules* **2011**, *44*, 1635-1641.

54. Ibrahim, K.; Lofgren, B.; Seppala, J. *Eur. Polym. J.* **2003**, *39*, 2005-2010.

55. Lai, J. T.; Filla, D.; Shea, R. *Macromolecules* **2002**, *35*, 6754-6756.

56. Qiu, X.; Winnik, F. M. *Macromol. Rapid Commun.* **2006**, *27*, 1648-1653.

57. Jakes, J. *Collect. Czech. Chem. Commun.* **1995**, *60*, 1781-1797.

58. Schillen, K.; Brown, W.; Johnsen, R. M. *Macromolecules* **1994**, *27*, 4825-4832.

59. Mehta, A.; Jaouhari, R.; Benson, T. J.; Douglas, K. T. *Tetrahedron Lett.* **1992**, *33*, 5441-5444.

60. Chung, J. E.; Yokoyama, M.; Aoyagi, T.; Sakurai, Y.; Okano, T. *J. Controlled Release* **1998**, *53*, 119-130.

61. Virtanen, J.; Holappa, S.; Lemmetyinen, H.; Tenhu, H. *Macromolecules* **2002**, *35*, 4763-4769.

62. Qin, S.; Geng, Y.; Discher, D. E.; Yang, S. *Adv. Mater.* **2006**, *18*, 2905-2909.

63. Xia, Y.; Yin, X.; Burke, N. A. D.; Stover, H. D. H. *Macromolecules* **2005**, *38*, 5937-5943.

64. Mueller, K. F. *Polymer* **1992**, *33*, 3470-3476.

65. Zhang, Q.; Zha, L.; Ma, J.; Liang, B. *J. Appl. Polym. Sci.* **2007**, *103*, 2962-2967.

66. Zheng, S.; Shi, S.; Xia, Y.; Wu, Q.; Su, Z.; Chen, X. *J. Appl. Polym. Sci.* **2010**, *118*,

671-677.

67. Osada, Y. *J. Polym. Sci.: Polym. Chem. Ed.* **1979**, *17*, 3485-3498.
68. Maeda, Y.; Yamamoto, H.; Ikeda, I. *Colloid Polym. Sci.* **2004**, *282*, 1268-1273.
69. Yin, X.; Hoffman, A. S.; Stayton, P. S. *Biomacromolecules* **2006**, *7*, 1381-1385.
70. Felber, A. E.; Dufresne, M.-H.; Leroux, J.-C. *Adv. Drug Deliv. Rev.* **2012**, *64*, 979-992.

# Chapter 6

# Gelation of PON Triblock Terpolymers in Ionic Liquids*

## 6.1 Introduction

Ionic liquids are a class of salts with melting points below 100 ℃. They have received significant attention in recent years due to their unique combination of physicochemical properties such as negligible vapor pressure, nonflammability, exceptional thermal, chemical and electrochemical stability, large liquid temperature ranges, optical transparency, high ionic conductivity and wide electrochemical windows. The desirable properties can be readily tuned to meet specific application requirements by changing the chemical structures of the ions.[1] These attributes make ionic liquids a promising class of materials for a number of applications, such as green solvents for chemical synthesis and catalysis,[2] electrolytes for electrochemical devices including dye-sensitized solar cells,[3] lithium ion batteries,[4, 5] organic thin film transistors,[6-10] electromechanical actuators[11, 12] and supercapacitors,[13] and membranes for fuel cells and gas separations.[14, 15]

Ion gels, comprising a polymer network swollen with ionic liquids, are currently of

---

* Research in this chapter was conducted with help from two summer undergraduates, Scott Danielsen and Cecilia Hall.

great interest, as they can overcome the potential challenges of ionic liquids in practical applications, such as ionic liquid leakage and fluidity, by providing ionic liquids with mechanical integrity and persistent structure while retaining many desirable properties of ionic liquids (*e.g.*, ionic conductivity and gas permeability).[16, 17] The common method employed to form network structures in ion gels is crosslinking, which can be realized by either chemically reacting (macro)monomers with functional crosslinkers[16, 18-20] or forming physically associated crosslinks.[17] Physical crosslinking via block copolymer self-assembly is particularly appealing because the structure and properties of ion gels can be easily tuned through variations of the copolymer architecture, block length and sequence and chemical identities. For example, the self-assembly of ABA triblock copolymers with ionic liquid compatible midblocks (B) and insoluble endblock (A) can produce well-defined physical gels through noncovalent association of A endblocks. He and Lodge reported that transparent ion gels from polystyrene-*b*-poly(ethylene oxide)-*b*-polystyrene (SOS) in 1-butyl-3-methylimidazolium hexfluorophosphate ([BMI][$PF_6$]) were achieved with as little as 4 wt% polymer and the ionic conductivity was only slightly decreased from the neat ionic liquid.[21] Physical ion gels could also be prepared from SOS triblock in a different ionic liquid 1-ethyl-3-methylimidazolium bis(trifluoromethylsulfonyl)amide ([EMI][TFSA]),[22] or from a different triblock polystyrene-*b*-poly(methyl methacrylate)-*b*-polystyrene (SMS) in [EMI][TFSA].[23] Thermoreversible ion gels were further developed by gelation of poly(*N*-isopropyl-acrylamide)-*b*-poly(ethylene oxide)-*b*-poly(*N*-isopropylacrylamide) (NON) in [EMI][TFSA] in an attempt to achieve solvent-free processing where the material is processed in its liquid state above room temperature, and used in its solid state at room

temperature.[24] In such physical gels, the crosslinking is reversible upon changing the temperature due to the upper critical solution temperature (UCST) phase behavior of PNIPAm endblocks in [EMI][TFSA]. The critical gelation temperature lies below room temperature in NON/[EMI][TFSA] mixtures and can be raised above room temperature by incorporating insoluble PS blocks into the endblocks of NON to obtain a NSOSN pentablock copolymer.[25]

All the above studies on ion gels are limited to ABA type triblock copolymers. As discussed in Chapter 3, better gelation efficiencies and enhanced mechanical properties can be achieved with ABC triblock terpolymers. It is therefore of interest to explore the gelation behavior of ABC terpolymers in ionic liquids. In this chapter, we report the viscoelastic properties of poly(ethylene-*alt*-propylene)-*b*-poly(ethylene oxide)-*b*-poly(*N*-isopropylacrylamide) (PON) in two ionic liquids [EMI][TFSA] and 1-butyl-3-methylimidazolium tetrafluoroborate ([BMI][$BF_4$]) over the temperature range of – 10–70 ℃ at varying polymer concentrations. [EMI][TFSA] and [BMI][$BF_4$] are used due to the UCST phase behavior of PNIPAm in both ionic liquids, with a distinct difference in UCST value (~ 20 ℃ in [EMI][TFSA][26] and ~67 ℃ in [BMI][$BF_4$][27]). Additionally, we compare the gel formation between the PON terpolymer and corresponding NON copolymer in [EMI][TFSA].

## 6.2 Experimental Section

### 6.2.1 Materials

All chemicals were purchased from Sigma Aldrich and used as received unless otherwise noted. Dichloromethane ($CH_2Cl_2$) was purified on an MBraun solvent

purification system. 1,4-dioxane was purified by refluxing the solvent over Na (1 % w/v) and benzophenone (0.2% w/v) under an inert atmosphere until the blue color of the benzophenone ketyl radical anion persists and distillation. 2,2'-Azobisisobutyronitrile (AIBN) and *N*-isopropylacrylamide (NIPAm) were purchased from Aldrich and purified by recrystallization from methanol and benzene/*n*-hexane (65/35 v/v), respectively.

### 6.2.2 Polymer and Ionic Liquid Synthesis

We prepared one PON triblock terpolymer and one CTA-NON-CTA triblock copolymer (Scheme 6.1). The PON triblock terpolymer was synthesized by RAFT polymerization from the PO(3-25) diblock copolymer[28] and end-group modification following the synthesis protocol described in Chapter 2. The product of each reaction step was confirmed by $^{1}$H NMR spectroscopy and characterized by size exclusion chromatography (SEC) (Figure 6.1). Some amount of tailing is observed for PON-CTA and PON triblocks, which is probably due to interactions between PNIPAm and the column materials in THF without amine additives (see Chapter 4). The CTA-NON-CTA triblock copolymer was synthesized by RAFT polymerization from a *α,ω*-dihydroxy-PEO as described in Chapter 3.[29] Samples investigated in this work are listed in Table 6.1 along with the molecular characteristics.

**Scheme 6.1** Chemical structure of PON and CTA-NON-CTA triblock polymers

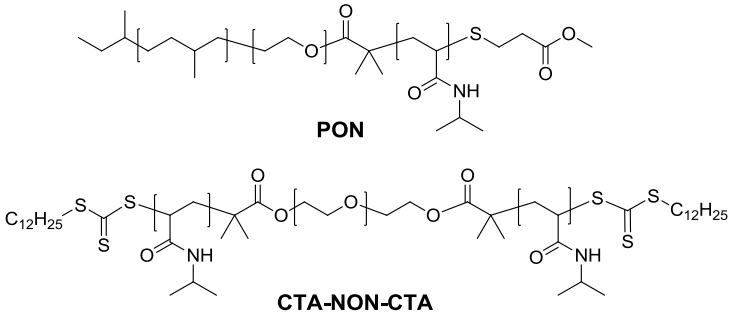

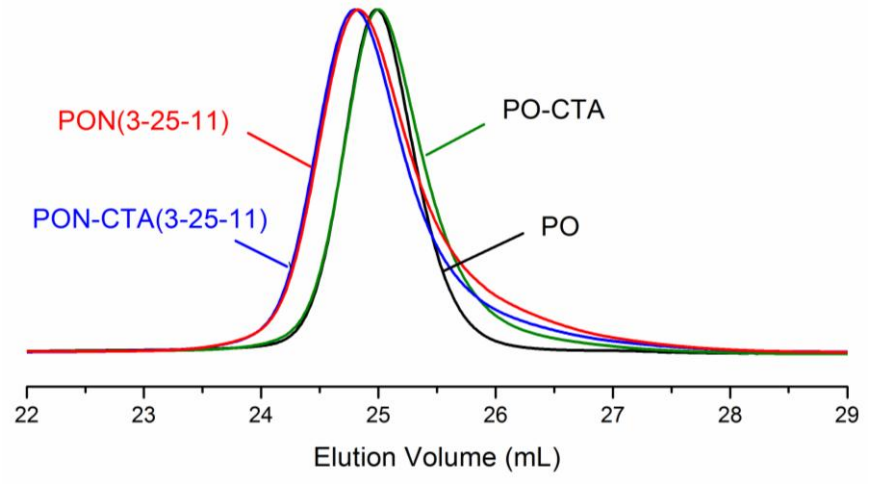


**Figure 6.1** SEC traces of PO, PO-CTA, PON-CTA(3-25-11), PON-CTA(3-25-11). THF was used as the eluting solvent at a flow rate of 1.0 mL/min.

**Table 6.1** Molecular parameters of PON and CTA-NON-CTA polymers

| Sample[a] | $N_{PEP}$[b] | $N_{PEO}$[b] | $N_{PNIPAm}$[b] | $f_{PEP}$[c] | $f_{PEO}$[c] | $f_{PNIPAm}$[c] | $Đ$[d] |
|---|---|---|---|---|---|---|---|
| PON(3-25-11) | 45 | 565 | 97 | 0.10 | 0.62 | 0.28 | 1.10 |
| CTA-NON-CTA (10-20-10) | – | 454 | 91 | – | 0.49 | 0.51 | 1.06 |

[a] The numbers in the parentheses correspond to the molar masses of PEP, PEO, and PNIPAm, respectively, in kg mol$^{-1}$ as determined by $^1$H NMR spectroscopy. [b] Number average degree of polymerization as determined by $^1$H NMR spectroscopy. [c] The volume fraction was calculated using the molecular weight and the RT densities: ρ(PEP) = 0.856 g/cm$^3$,[30] ρ(PEO) = 1.12 g/cm$^3$,[31] and ρ(PNIPAm) = 1.07 g/cm$^3$.[32] [d] The dispersity was measured by SEC with THF (PON) or THF/ *N*,*N*,*N*',*N*'-tetramethylethylenediamine (CTA-NON-CTA) as the eluting solvent.

A PNIPAm homopolymer was synthesized by RAFT polymerization following a

procedure reported previously.[33] NIPAm (2.014 g, 0.0178 mol), AIBN (0.9 mg, 0.0054 mmol), and cumyl benzodithioate (16.45 mg, 0.0604 mmol) were dissolved in 10 mL of 1,4-dioxane, degassed by three freeze-pump-thaw cycles and reacted at 75 ℃ for 8.75 h. After that the reaction was quenched by cooling to 0 ℃. The solution was precipitated in pentane three times. The resulting polymer was dried under vacuum oven at 50 ℃ overnight. PNIPAm has a molar mass of 12 kg $mol^{-1}$ as determined by $^{1}H$ NMR spectroscopy and a low dispersity of $Đ$ = 1.05 as determined by SEC ( Figure 6.2).

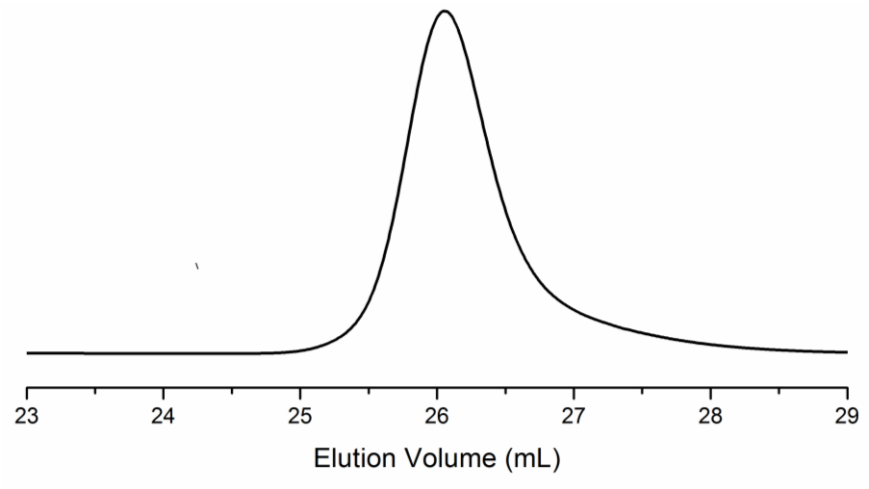


**Figure 6.2** SEC traces of PNIPAm. THF was used as the eluting solvent at a flow rate of 1.0 mL/min.

We prepared two ionic liquids (Scheme 6.2). 1-ethyl-3-methylimidazolium bis(trifluoromethylsulfonyl)amide ([EMI][TFSA]), generously provided by Dr. Yuanyan Gu, was synthesized via an anion exchange reaction following a previously reported procedure.[16] 1-butyl-3-methylimidazolium tetrafluoroborate ([BMI][$BF_4$]) was prepared via the procedure described elsewhere (Scheme 6.3).[34, 35] 1-butyl-3-methylimidazolium

chloride ([BMI][Cl]) was first prepared as follows. 1-methylimidazole (50.5 g, 0.615 mol), 1-chlorobutane (75 g, 0.810 mol), and acetonitrile (26.6 g, 0.648 mol) were added to a round-bottomed flask fitted with a reflux condenser and heated to reflux at 75 ℃ for 48 h. After cooling the solution to room temperature, the acetonitrile and excess 1-chlorobutane was removed by rotary evaporation. The resulting light yellow oil was washed with ethyl acetate three times and then dried under vacuum at 50 ℃ for 48 h. Next, [BMI][$BF_4$] was synthesized by an anion exchange reaction. Briefly, $NaBF_4$ (33.91 g, 0.309 mol) was added to a solution of [BMI][Cl] (45.0 g, 0.258 mol) in $CH_2Cl_2$ (250 mL) and stirred at room temperature for 24 h. The suspension was filtered to remove the precipitated chloride salt and the organic phase was repeatedly washed with water (30 mL) until no precipitation of AgCl was observed in the aqueous phase upon addition of a concentrated $AgNO_3$ solution. The solvent ($CH_2Cl_2$) in the organic pahse was removed by rotary evaporation, and the resulting ionic liquid was dried in a vacuum oven at 50 ℃ for 48 h. The ionic liquid was further purified by passing through a short alumina column (neutral) and dried under vacuum at 50 ℃ for 48 h.

**Scheme 6.2** Chemical Structure of Ionic Liquids [EMI][TFSA] and [BMI][$BF_4$]

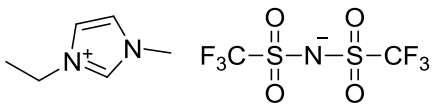

[EMI][TFSA]

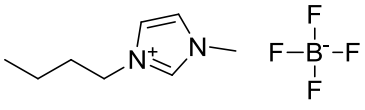

[BMI][$BF_4$]

**Scheme 6.3** Synthesis of Ionic Liquid [BMI][$BF_4$]

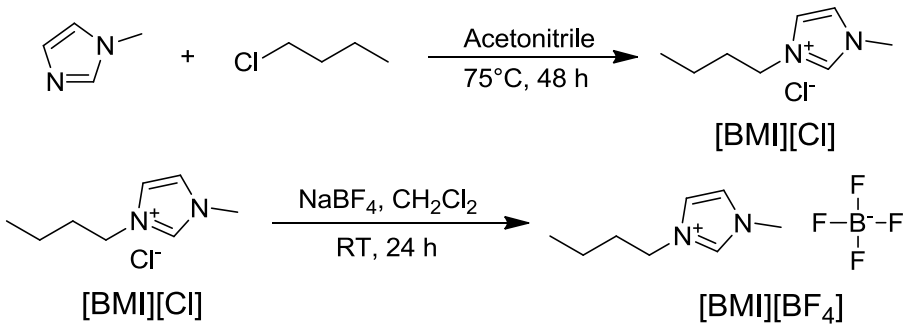


### 6.2.3 Ion Gel Preparation

All the polymer solutions were prepared by the co-solvent method. Appropriate amounts of bulk polymer and ~3 g ionic liquid were dissolved in ~10 mL $CH_2Cl_2$. After 2 hours of stirring at room temperature, the solution was passed through an 0.45 $\mu$m filter and purged under $N_2$ flow overnight to remove most of the solvent ($CH_2Cl_2$). The residual solvent was completely removed by placing the sample in a vacuum oven at ca. 75 ℃ for at least 24 h.

### 6.2.4 Cloud Point Measurements

Cloud points of PNIPAm/IL (upper critical solution temperature, UCST) were determined by optical transmittance measurements. The sample was placed in a temperature-controlled oil bath and heated above the UCST. The temperature dependence of transmittance at 632.8 nm was monitored using a laser power detector at a cooling rate of roughly 1 ℃/min while the solution was stirred. We define the CP values as the temperatures at which the transmittance drops to 80%.

### 6.2.5 Rheology

Rheological measurements were performed using an AR-G2 rheometer with the parallel plate geometry. The 40 mm diameter plates with a gap spacing of approximately 1 mm were used for all measurements. The gap was adjusted at each temperature to compensate for the thermal expansion of the tool set. The temperature was controlled using a Peltier temperature controller. To avoid any avoid any effects of moisture, the whole fixture assembly was covered with a plastic cover. Dynamic strain sweep experiments were first performed at three different angular frequencies (1, 10, 100 rad/s). Dynamic frequency sweeps were then examined in the linear viscoelastic regime, as determined by dynamic strain sweep experiments. The temperature dependences of $G'$ and $G''$ were measured with a frequency of 10 rad/s, and a heating or cooling rate of 1, 0.5 or 0.2 ℃/min.

## 6.3 Results and Discussion

### 6.3.1 UCST of PNIPAm in Ionic Liquids

Watanabe and co-workers reported the upper critical solution temperature (UCST) phase behavior of PNIPAm in an ionic liquid [EMI][TFSA].[26] They found the cloud point (CP) increases as the molecular weight of PNIPAm or polymer concentration increases. As shown in Figure 6.3, the RAFT-synthesized PNIPAm homopolymer ($M_n$ = 12 kg/mol, $Đ$ = 1.05) is phased separated from [EMI][TFSA] at 15 ℃. This is slightly smaller than the reported UCST value of ~ 20 ℃ for PNIPAm ($M_n$ = 15.4 kg/mol, $Đ$ = 1.64), which is reasonable considering the lower molecular weight and narrower MW distribution of the PNIPAm in this study.[26]

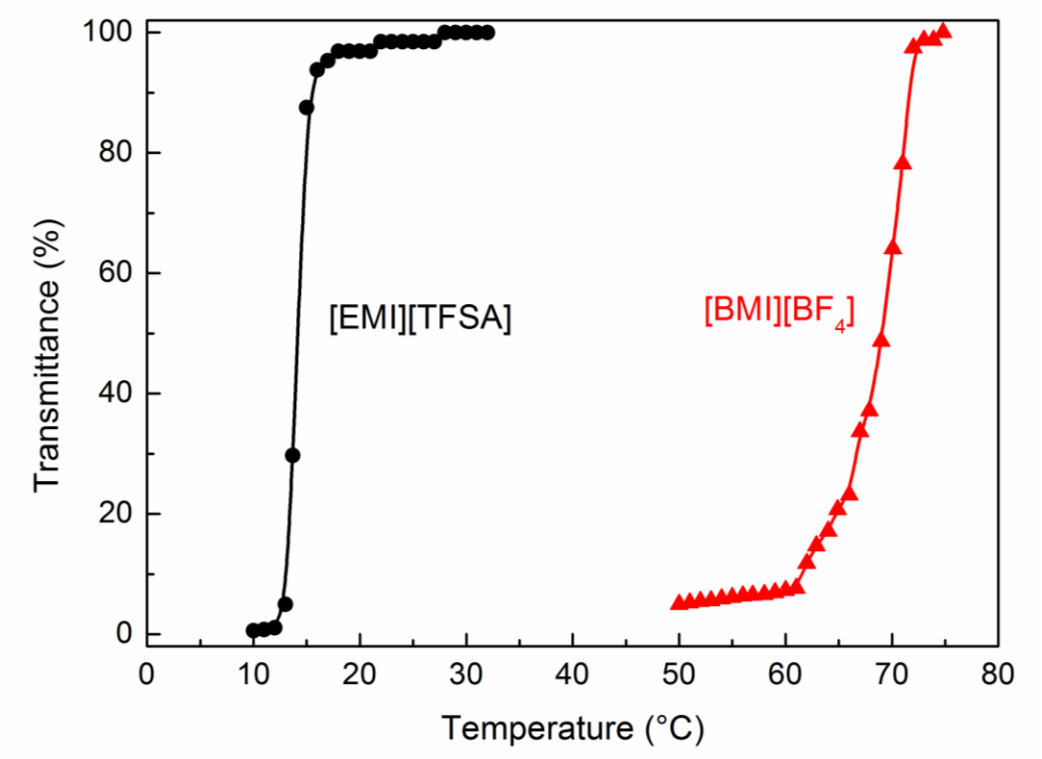


**Figure 6.3** Temperature dependence of transmittance at 632.8 nm for 1 wt% PNIPAm in [EMI][$BF_4$] and [BMI][$BF_4$].

Recently, Lee and Lodge reported the UCST phase behavior of PNIPAm in both [EMI][$BF_4$] and [BMI][$BF_4$].[27] They found that the CP values of PNIPAm ($M_n$ = 40 kg/mol, $Đ$ = 1.7) increase almost linearly from 67 ℃ to 222 ℃ as the weight fraction of [BMI][$BF_4$] in [BMI][$BF_4$]/[EMI][$BF_4$] blends decrease from 100 wt% to 0 wt%. The CP of the RAFT-synthesized PNIPAm in pure [BMI][BF4] was 71 ℃ (Figure 6.3), consistent with the reported UCST value of 67 ℃.

### 6.3.2 Gelation of PON in [EMI][TFSA]

The 5 wt% sample of PON(3-25-11) triblock in [EMI][TFSA] is a viscous transparent liquid at room temperature or higher, and becomes a free-standing ion gel upon cooling to 0 ℃ (Figure 6.4). Repeated heating and cooling experiments indicate that the sol-gel transition is thermoreversible.

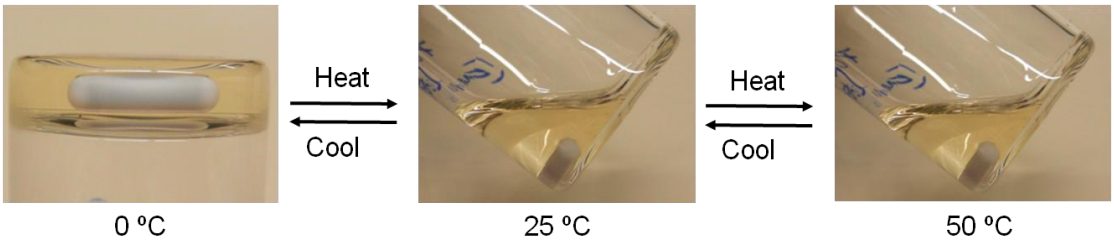


**Figure 6.4** Photographs of 5 wt% PON(3-25-11) in [EMI][TFSA] at different temperatures.

Dynamic shear measurements were performed on the 5 wt% PON(3-25-11) sample over the temperature range of – 10–70 ℃ to study gelation properties. Dynamic strain sweep experiments were first carried out to determine the linear viscoelastic regime. The linear viscoelastic regime is defined as the region below the critical value ($\gamma_c$) where the storage modulus ($G'$) remains invariant with respect to strain. As shown in Figure 6.5, the liquid solution at 70 ℃ has a large $\gamma_c$ value (> 100%) while $\gamma_c$ value of the ion gel at 0 ℃ was smaller (55%). It should be noted that $G'$ of the sample at a frequency $\omega$ = 1 rad/s in Figure 6.5a is not shown due to the measurement uncertainty.

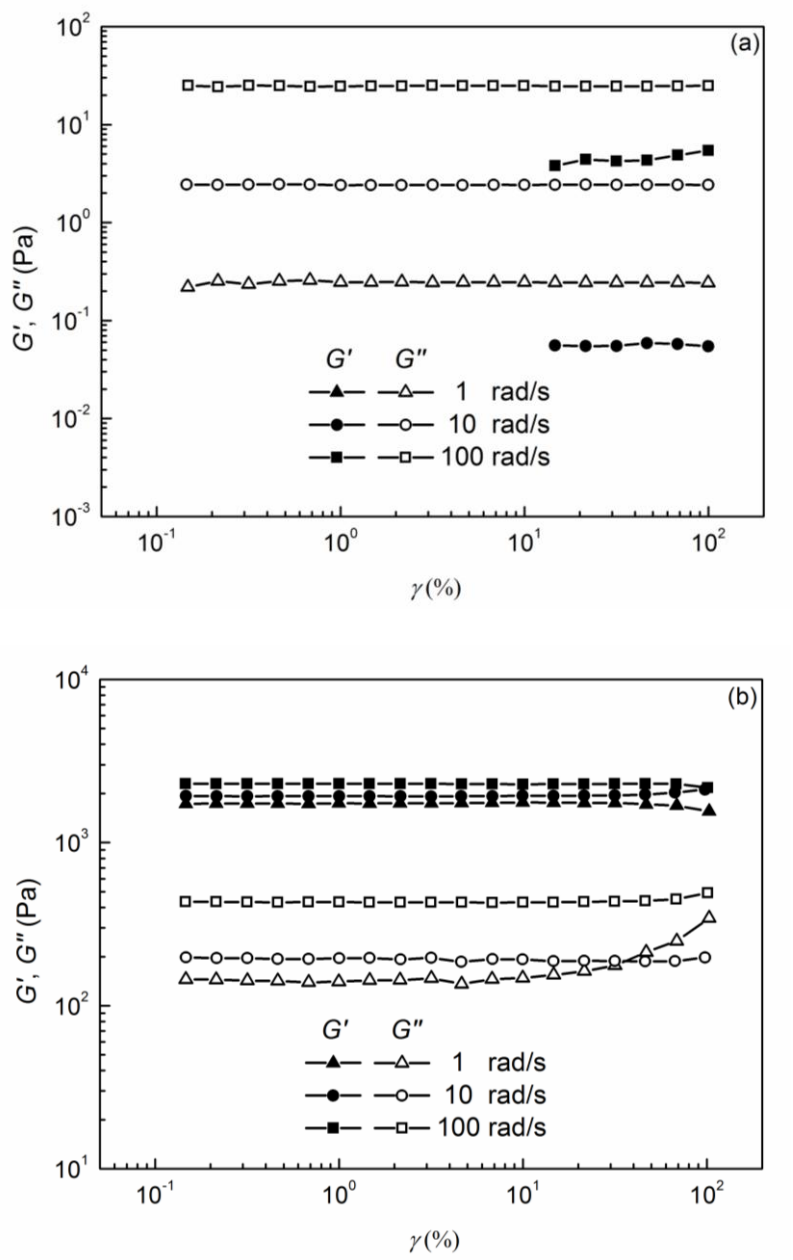


**Figure 6.5** Dynamic shear moduli (*G′* and *G″*) as a function of strain for 5 wt% PON(3-25-11) in [EMI][TFSA] at three frequencies (1, 10, 100 rad/s) and at 70 ℃ (a) and 0 ℃ (b).

A strain amplitude of 10% or lower was then used to ensure that the dynamic

frequency and temperature sweep measurements were taken in the linear viscoelastic regime. Representative data of dynamic frequency sweeps at 50, 20, and 0 ℃ are provided in Figure 6.6. At 50 ℃, $G'$ is significantly smaller than the loss modulus ($G''$) and follows typical terminal rheological behavior for a viscoelastic fluid: $G' \sim \omega^{1.8}$ and $G'' \sim \omega^{1.0}$. The scaling exponent for $G'$ (1.8) is less than 2.0. This is likely due to the measurement uncertainty of relatively small value of $G'$. At an intermediate temperature of 20 ℃, $G'$ is almost equal to $G''$ over the entire frequency range of experiments and both show similar power law dependences on $\omega$: $G' \approx G'' \sim \omega^{0.5}$. This temperature is identified as the critical gelation temperature ($T_{gel}$), which is the signature of the transition between liquid-like and solid-like behavior.[36, 37] At 0 ℃, $G'$ is larger than $G''$ at all frequencies and is nearly frequency independent, indicating solid-like behavior.

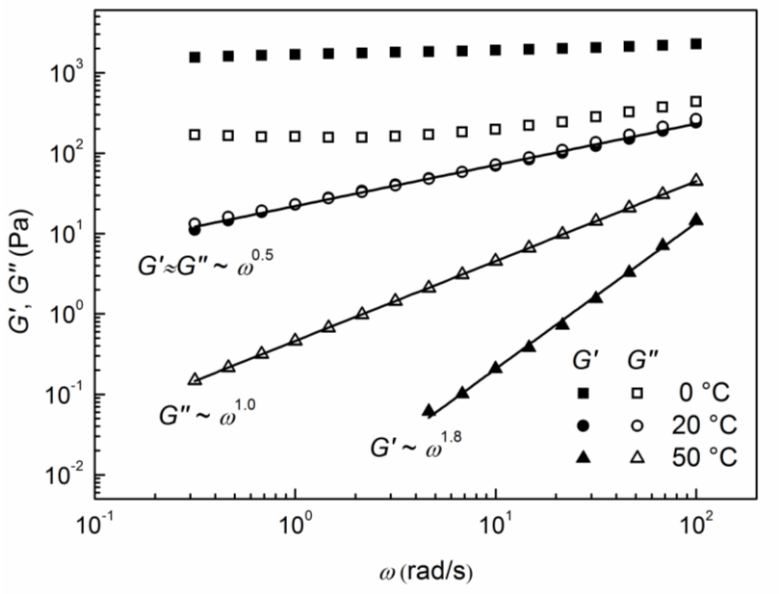


**Figure 6.6** Dynamic shear moduli ($G'$ and $G''$) as a function of frequency for 5 wt% PON(3-25-11) in [EMI][TFSA] at three representative temperatures. The solid lines are

power law fits.

The thermoreversible nature of this sol-gel transition was verified using dynamic temperature sweep measurements, in which $G'$ and $G''$ were measured as a function of temperature at a heating or cooling rate of 1 ℃/min. The temperature-dependent dynamic shear moduli of four PON ion gels with 10, 5, 2 and 1 wt% polymer in a heating–to–cooling thermal cycle are shown in Figure 6.7. In all these cases, there is a sol-gel transition upon cooling and a gel-sol transition upon heating, with the change of $G'$ approaching five orders of magnitude. As shown in Figure 6.7b, for the 5 wt% sample of PON(3-25-11) at high temperatures, the values of both $G'$ and $G''$ are low, and $G' < G''$, indicating a free-flowing sol state. On decreasing temperature, the magnitude of both $G'$ and $G''$ increase abruptly and then $G'$ reaches a plateau. As the increase in $G'$ is more significant than $G''$, $G'$ becomes larger than $G''$ at lower temperatures indicating the solid-like behavior. The crossover of $G'$ and $G''$ in the cooling process, identified as $T_{gel}$, is 18 ℃, consistent with the results (20 ℃) in the dynamic frequency sweep measurements. In addition, a hysteresis loop is observed at all concentrations, and it is nearly independent of heating or cooling rate (Figure 6.8). The hysteresis is consistent with a number of reports concerning PNIPAm-containing block polymer micelles and gels in both water and ionic liquids,[25, 38] suggesting that the gelation arises from the noncovalent association of PNIPAm blocks.

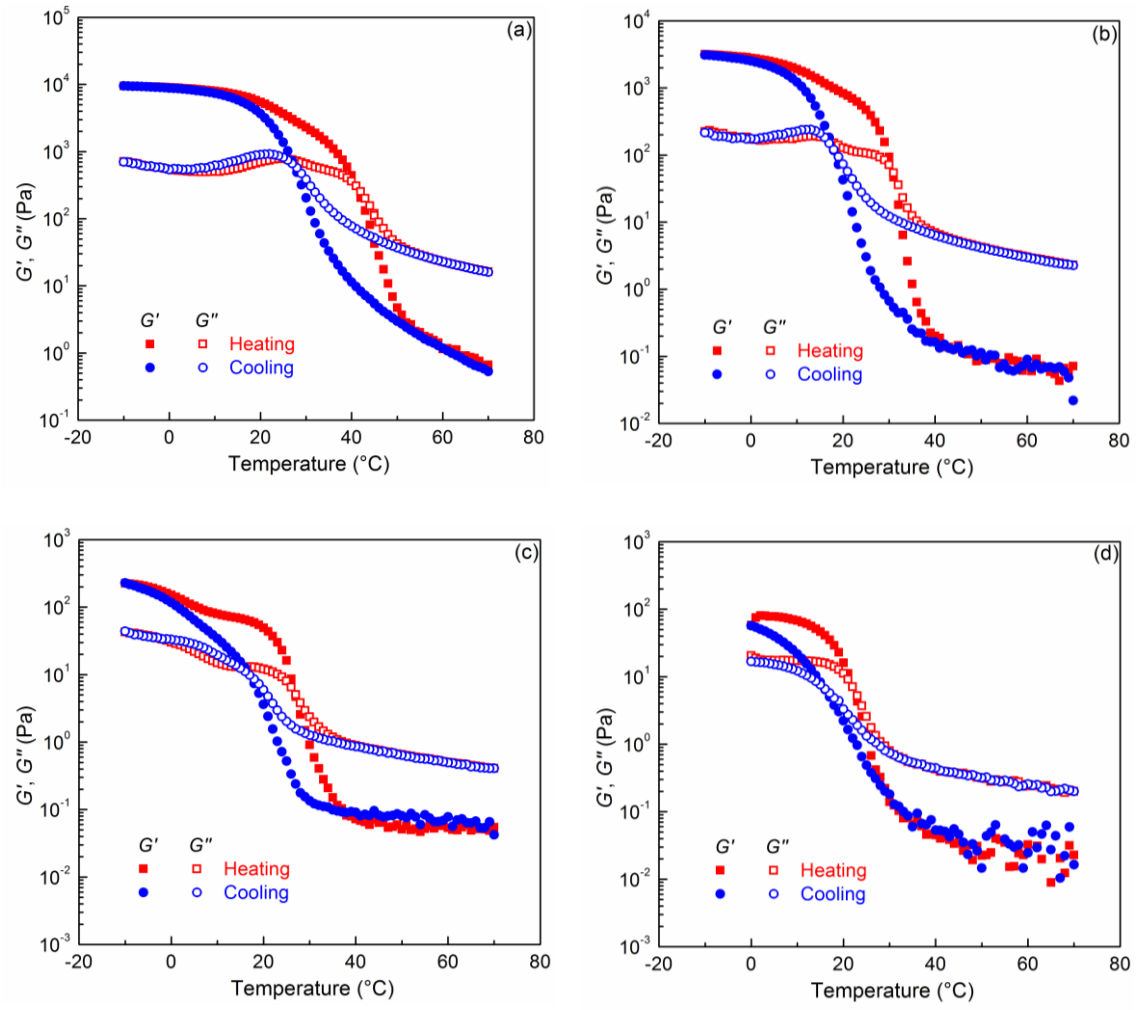


**Figure 6.7** Temperature-dependent dynamic shear moduli (*G′* and *G″*) for PON(3-25-11) in [EMI][TFSA] at a frequency $\omega$ = 10 rad/s and heating or cooling rate of 1 ℃/min with varying concentrations: (a) 10 wt%, (b) 5 wt%, (c) 2 wt% and (d) 1 wt%.

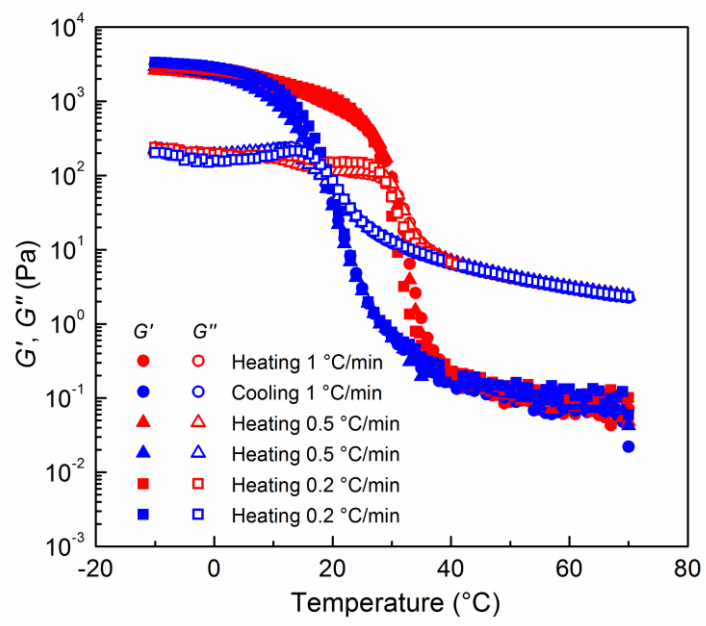


**Figure 6.8** Temperature-dependent dynamic shear moduli (*G′* and *G″*) for 5 wt% PON(3-25-11) sample in [EMI][TFSA] at a frequency $\omega$ = 10 rad/s and heating or cooling rate of 1, 0.5 and 0.2 ℃/min.

The solubility of PEP, PEO and PNIPAm in [EMI][TFSA] are different: PEP is insoluble, PEO has good solubility, and PNIPAm exhibits UCST phase behavior. When PON terpolymers are dissolved in [EMI][TFSA] at a temperature above the UCST of PNIPAm, both PEO and PNIPAm are compatible with [EMI][TFSA], we infer that they self-assemble into PEP micelles with PEO-PNIPAm coronae. As the concentration (10 wt% or lower) is not very high, these micelles are not ordered.[22] Therefore, it is a viscoelastic liquid. As the solution is cooled below the UCST of PNIPAm, the PNIPAm chains on adjacent micelles can associate to form PNIPAm microdomains bridged to the PEP microdomains by the PEO midblocks, leading to the formation of an elastic network.

We compared the gelation properties of PON ion gels with different polymer

concentrations from 10 wt% to 1 wt%. As shown in Figure 6.7, a rubbery plateau of $G'$ is observed upon cooling below $T_{gel}$ at all concentrations. The plateau modulus ($G_N$), determined as the value of $G'$ at the frequency where the loss tangent ($\tan \delta = G'' / G'$) has the minimum or smallest value,[39] drops on decreasing PON concentration. The results are plotted against PON weight fraction in Figure 6.9. A power law fit gives a slope of 2.3 ± 0.2, which is in excellent agreement with the predicted value of 2.3 for entangled solutions of neutral polymers in good solvents[39, 40] and with expectation for gels swollen in a good solvent.[41]

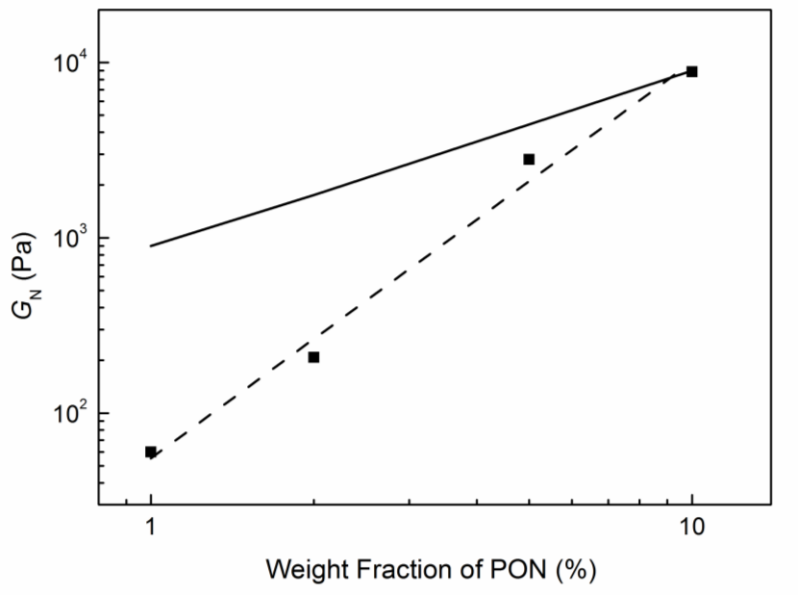


**Figure 6.9** Concentration dependence of plateau modulus ($G_N$) for PON(3-25-11) in [EMI][TFSA] with 1-10 wt % polymer. The dashed line is a power law fit to the measured $G_N$, and the solid line represents the calculated $G_N$ of an ideal network with unentangled midblocks.

According to the classical rubber elasticity theory, $G_N$ for triblock copolymer gels with a midblock in the unentangled regime is given by:

$$G = \nu\ kT = f\ nkT = f\ \frac{cRT}{M} \tag{6-1}$$

where $\nu$ is the number density of elastically effective strands, $k$ is the Boltzmann constant, $T$ is absolute temperature, $f$ is the fraction of elastically effective polymer chains, $n$ is the chain number density of polymer chains, $c$ is the triblock concentration (w/v), $M$ is the triblock molecular weight and $R$ is the ideal gas constant. A prerequisite for equation 6-1 to apply is that system under consideration is in the concentration range where midblock entanglements are not present. An estimate of the number of entanglements per molecule, $n_e$, for a polymer in a good solvent is given by

$$n_e = N_e \varphi_p^{5/4} = \frac{M}{M_e} \varphi_p^{5/4} \tag{6-2}$$

where $N_e$ is the number of entanglements per molecule in the melt, $M$ is the polymer molecular weight, $M$ is the polymer entanglement molecular weight in the melt and $\varphi_p$ is the polymer volume fraction.[42, 43] For the 10 wt% sample of PON(3-25-11) in [EMI][TFSA], $M_{PEO}$ = 25 kg/mol, $M_{e,\,PEO}$ = 1.6 kg/mol, $\varphi_{PEO}$= 8.7%, and an estimation using equation 6-2 yields $n_{e,PEO} \sim 0.7$, which is less than 1. From this analysis we conclude that PEO midblock is not entangled, and therefore equation 6-1 can be applied to estimate the fraction of elastically effective PEO midblocks in PON ion gels. The fraction of elastically effective PEO chains in a network is given by

$$f = \frac{G_N}{nkT} \tag{6-3}$$

where $G_N$ is measured plateau modulus, $nkT$ is the shear modulus of an ideal network in

which 100% chains are elastically effective or f = 1. Table 6.2 displays $G_N$, $f$ and other characteristics of PON ion gels at varying polymer concentrations. We found that the fraction of elastically effective or bridging PEO chains in PON ion gels increased from 7% to 98% when the polymer concentration increased from 1 to 10 wt%. It is likely that a certain fraction of micelles may not be well integrated into the network structure on decreasing the polymer concentration from 10 to 1 wt%, resulting in a decrease of the fraction of bridging chains.

We observed a moderate increase of $T_{gel}$ (from 16 to 27 ℃) with increasing PON weight fraction in ion gels. The concentration dependence of $T_{gel}$ is consistent with the reported UCST phase diagram of PNIPAm/[EMI][TFSA] mixtures.[26] In addition, the values of $T_{gel}$ at low polymer concentrations (5 wt% or lower) agree very well with the measured UCST value of PNIPAm in Figure 6.3. The critical strain ($\gamma_c$) of PON/[EMI][TFSA] mixture is large (> 100%) and invariant with concentration at 70 ℃, that is, in the micelle state. Upon cooling to the gel state at 0 ℃, the $\gamma_c$ becomes smaller and heavily depends on the polymer concentration. A higher PON weight fraction leads to a larger $\gamma_c$ value.

**Table 6.2** Characteristics of PON(3-25-11) ion gels in [EMI][TFSA]

| Conc.[a] (wt%) | $G_N$[b] (Pa) | $f$[c] | $T_{gel}$[d] (℃) | $\gamma_c(70)$[e] | $\gamma_c(0)$[f] |
|---|---|---|---|---|---|
| 10 | 8850 | 98% | 27 | > 100% | 70% |
| 5 | 2800 | 63% | 18 | > 100% | 55% |
| 2 | 210 | 12% | 17 | > 100% | 35% |
| 1 | 60[g] | 7% | 16 | > 100% | 0.4% |

[a] Concentration. [b] Plateau modulus. [c] Fraction of elastically effective PEO chains. [d] Critical gelation temperature as determined from the crossover temperature at which $G' = G''$ in Figure 6.7 in the cooling process. [e] critical strain at 70 ℃, determined from dynamic strain sweep at a frequency $\omega$ = 10 rad/s. [f] critical strain at 0 ℃, determined from dynamic strain sweep at a frequency $\omega$ = 10 rad/s. [g] The plateau modulus was determined as the value of $G'$ at the lowest measured temperature (0 ℃) as no minimum loss tangent was obtained.

### 6.3.3 Comparison between PON and NON Ion Gels in [EMI][TFSA]

We also compared the gelation properties of PON(3-25-11) with CTA-NON-CTA(10-20-10) in [EMI][TFSA] by examining the temperature dependence of $G'$ and $G''$ at 10, 5 and 2 wt% polymer (Figure 6.10). The PON terpolymer shows temperature-induced gelation behavior at all three concentrations, while the CTA-NON-CTA copolymer only displays sol-gel transitions with 10 and 5 wt% polymer and does not form well-defined ion gels at 2 wt% polymer. The sol-gel transition of PON in [EMI][TFSA] can be achieved even we decrease the polymer concentration to 1 wt%

(Figure 6.7). Therefore, we conclude that the critical gelation concentration of PON terpolymer is smaller than that of CTA-NON-CTA copolymer. In addition, $G_N$ of CTA-NON-CTA ion gels at 10 and 5 wt% polymer are 6710 and 1260 Pa, corresponding to a fraction of bridging PEO chain of 79% and 30%, respectively, which is lower than that of PON ion gels. Overall, a lower critical concentration with a higher modulus at a given polymer concentration was achieved with PON ion gels in comparison to CTA-NON-CTA ion gels.

The gelation of CTA-NON-CTA (4.3-20-4.3) in [EMI][TFSA] has been reported previously, and an ion gel can be formed at 10 wt% polymer concentration with good mechanical strength ($G_N$ ~ 5000 Pa).[24] This is consistent with the measured value of $G_N$ for CTA-NON-CTA(10-20-10) ion gels in this study. It is also worth noting that $T_{gel}$s of CTA-NON-CTA(10-20-10) ion gels are ~28 ℃ and show very week concentration dependence.

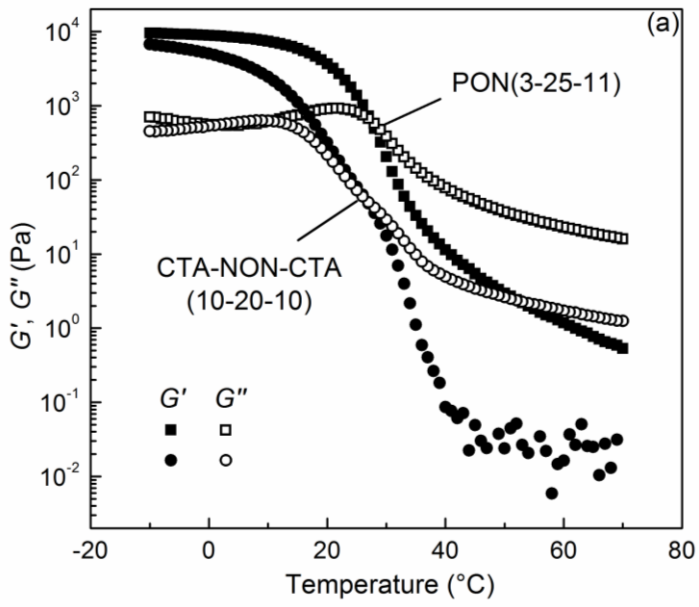

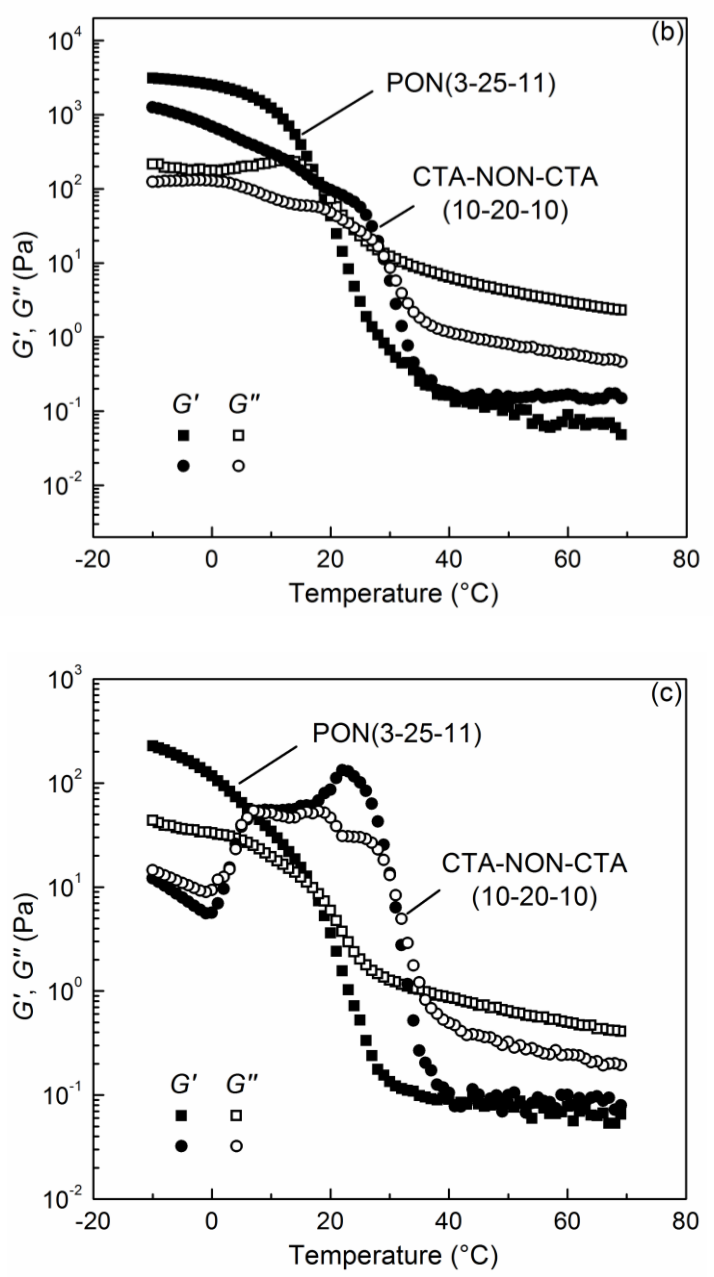


**Figure 6.10** Temperature-dependent dynamic shear moduli (*G′* and *G″*) for (a) 10 wt%, (b) 5 wt% and (c) 2 wt% PON(3-25-11) and CTA-NON-CTA(10-20-10) in [EMI][TFSA] measured at a frequency $\omega$ = 10 rad/s and cooling rate of 1 ℃/min.

Based on these data, we propose that the two-step gelation in the PON ion gels,

which involve the initial formation of micelles with PEP cores at high temperatures[44-46] and gelation due to the noncovalent association of PNIPAm endblocks on cooling, leads to the formation of a two-compartment network with a high fraction of bridged conformations for the PEO midblocks, while both looping and bridging conformations are possible for CTA-NON-CTA ion gels. With more bridging chains in PON ion gels, gelation can be achieved at a lower concentration with larger $G_N$. This study in ionic liquid further confirmed our hypothesis that ABC triblock terpolymers could be beneficial for gel formation in comparison to ABA triblock copolymers.[29]

### 6.3.4 Gelation of PON in [BMI][$BF_4$]

The 5 wt% sample of PON(3-25-11) triblock in [BMI][$BF_4$] is a viscous transparent liquid at 50 ℃. A significant increase in viscosity is clearly visible upon cooling to room temperature and a free-standing ion gel is evident at 0 ℃ (Figure 6.11). Repeated heating and cooling experiments indicate that the sol-gel transition is thermoreversible.

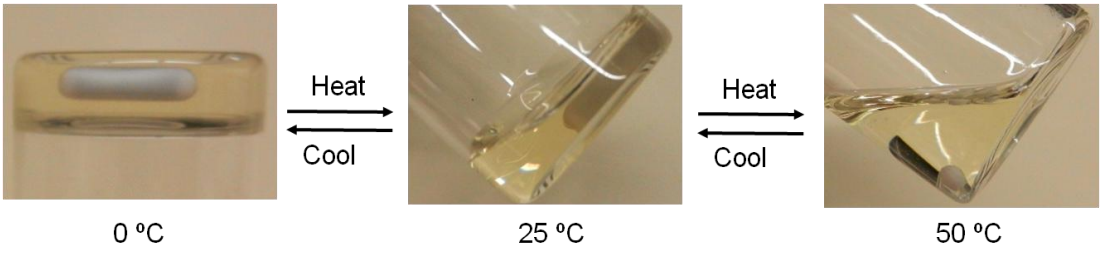


**Figure 6.11** Photographs of 5 wt% PON(3-25-11) in [BMI][$BF_4$] at different temperatures.

We investigated gelation properties of PON(3-25-11) triblock in [BMI][$BF_4$] by

performing dynamic shear measurements over the temperature range of 0–70 ℃ at varying polymer concentrations. The temperature-dependent dynamic shear moduli of four PON ion gels with 10, 5, 2 and 1 wt% polymer in a heating–to–cooling thermal cycle are shown in Figure 6.12. It clearly shows that there is a transition for both $G'$ and $G''$ at all concentrations, with the change of $G'$ approaching five orders of magnitude. At high temperatures, the values of both $G'$ and $G''$ are low, and $G' < G''$, indicating a free-flowing sol state. Upon cooling below a critical temperature, $G'$ becomes larger than $G''$ indicating the solid-like behavior. The critical temperature, which is the crossover of $G'$ and $G''$, is identified as the $T_{gel}$. $T_{gel}$s of PON ion gels in [BMI][$BF_4$] are 40, 20, 35, and 38 ℃, respectively, at 10, 5, 2 and 1 wt% polymer. They are more than 30 ℃ below the value of UCST for PNIPAm in [BMI][$BF_4$] and much lower than those of NON-CTA ion gels (~55 ℃ at 10, 5 and 2 wt%, Figure 6.13). In addition, the sol-gel transition is much broader than that of PON ion gels in [EMI][TFSA]. The reason that PON displays a broad sol-gel transition and low $T_{gel}$ with unusual concentration dependence is not clear at this point. Further investigations are needed. In addition, no hysteresis was observed at all concentrations.

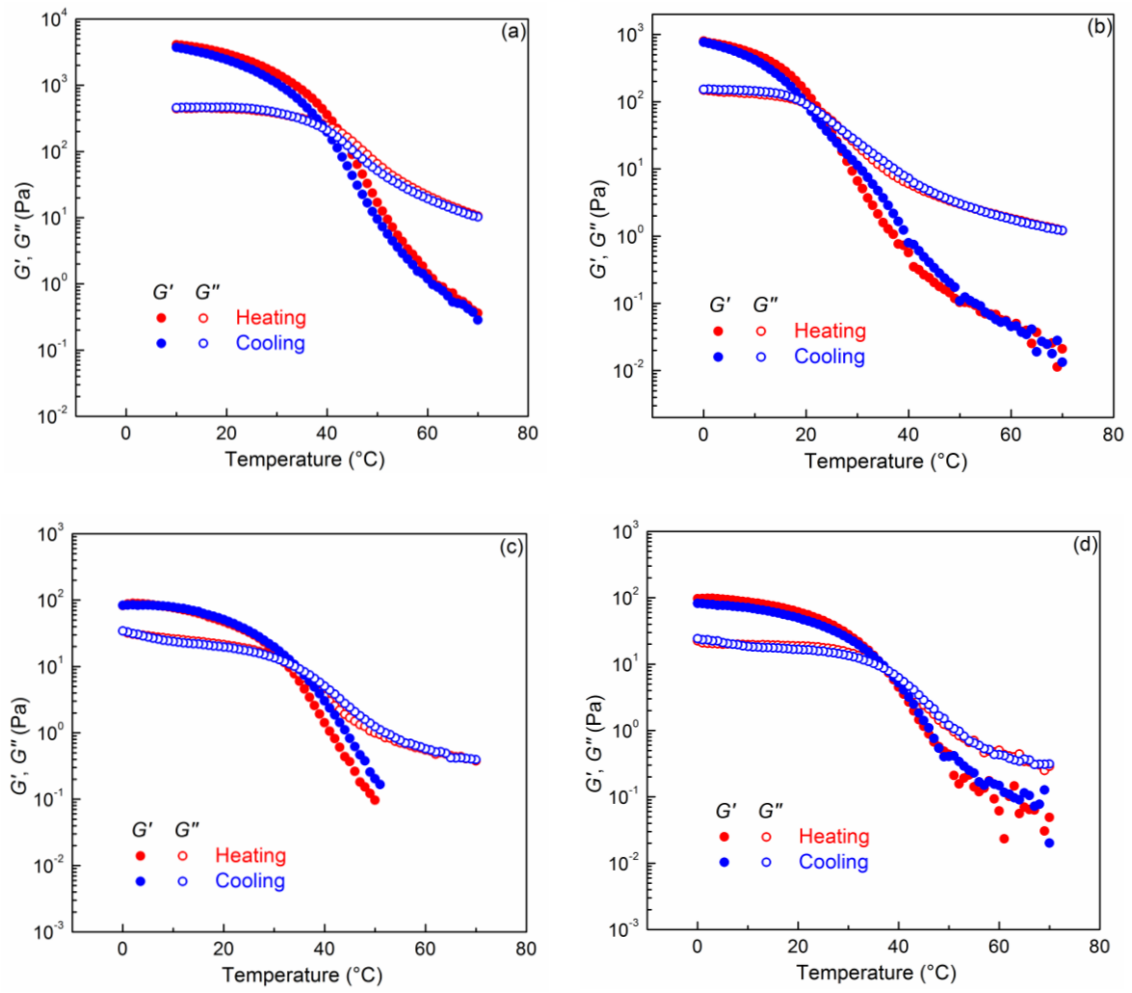


**Figure 6.12** Temperature-dependent dynamic shear moduli (*G′* and *G″*) for PON(3-25-11) in [BMI][$BF_4$] at a frequency $\omega$ = 10 rad/s and heating or cooling rate of 1 ℃/min with varying concentrations: (a) 10 wt%, (b) 5 wt%, (c) 2 wt% and (d) 1 wt%.

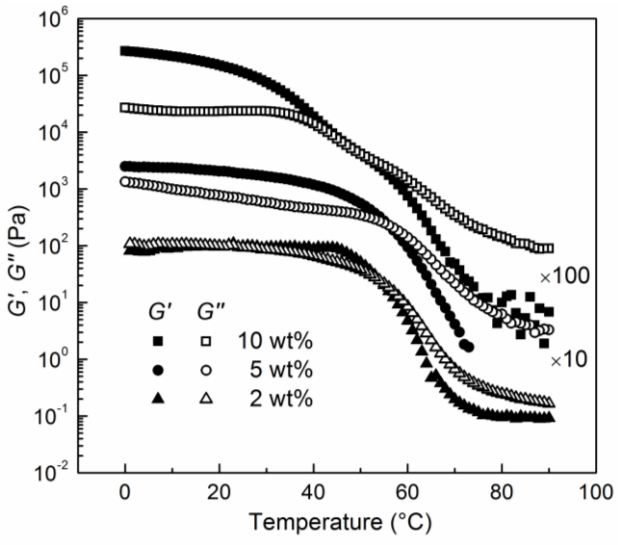


**Figure 6.13** Temperature-dependent dynamic shear moduli (*G′* and *G″*) for CTA-NON-CTA (10-20-10) in [BMI][$BF_4$] at a frequency $\omega$ = 10 rad/s and cooling rate of 1 ℃/min with varying polymer concentrations. For clarity, the modulus data for higher concentrations have been shifted vertically: 5 wt% (×10), 10 wt% (×$10^2$).

## 6.4 Summary

In conclusion, we prepared thermoresponsive ion gels from the self-assembly of PON triblock terpolymers in [EMI][TFSA]. The gelation can be achieved at a lower concentration with a higher plateau modulus as compared to CTA-NON-CTA ion gels, due to the two-step gelation mechanism in PON ion gels. The gelation of PON could also be achieved in [BMI][$BF_4$] although with a broader sol-gel transition.

## 6.5 References

1. Castner, E. W.; Wishart, J. F.; Shirota, H. *Acc. Chem. Res.* **2007**, *40*, 1217-1227.
2. Welton, T. *Chem. Rev.* **1999**, *99*, 2071-2083.

3. Zakeeruddin, S. M.; Gratzel, M. *Adv. Funct. Mater.* **2009**, *19*, 2187-2202.
4. Lewandowski, A.; Swiderska-Mocek, A. *J. Power Sources* **2009**, *194*, 601-609.
5. Kim, G. T.; Jeong, S. S.; Joost, M.; Rocca, E.; Winter, M.; Passerini, S.; Balducci, A. *J. Power Sources* **2011**, *196*, 2187-2194.
6. Yuan, H.; Shimotani, H.; Tsukazaki, A.; Ohtomo, A.; Kawasaki, M.; Iwasa, Y. *Adv. Funct. Mater.* **2009**, *19*, 1046-1053.
7. Lee, J.; Panzer, M. J.; He, Y.; Lodge, T. P.; Frisbie, C. D. *J. Am. Chem. Soc.* **2007**, *129*, 4532-4533.
8. Cho, J. H.; Lee, J.; He, Y.; Kim, B.; Lodge, T. P.; Frisbie, C. D. *Adv. Mater.* **2008**, *20*, 686-690.
9. Cho, J. H.; Lee, J.; Xia, Y.; Kim, B.; He, Y.; Renn, M. J.; Lodge, T. P.; Frisbie, C. D. *Nat. Mater.* **2008**, *7*, 900-906.
10. Kim, S. H.; Hong, K.; Xie, W.; Lee, K. H.; Zhang, S.; Lodge, T. P.; Frisbie, C. D. *Adv. Mater.* **2013**, *25*, 1822-1846.
11. Lu, W.; Fadeev, A. G.; Qi, B.; Smela, E.; Mattes, B. R.; Ding, J.; Spinks, G. M.; Mazurkiewicz, J.; Zhou, D.; Wallace, G. G.; MacFarlane, D. R.; Forsyth, S. A.; Forsyth, M. *Science* **2002**, *297*, 983-987.
12. Imaizumi, S.; Kokubo, H.; Watanabe, M. *Macromolecules* **2012**, *45*, 401-409.
13. Katakabe, T.; Kaneko, T.; Watanabe, W.; Fukushima, T.; Aida, T. *J. Electrochem. Soc.* **2005**, *152*, A1913-A1916.
14. Tang, J.; Tang, H.; Sun, W.; Plancher, H.; Radosz, M.; Shen, Y. *Chem. Commun.* **2005**, 3325-3327.
15. Bara, J. E.; Lessmann, S.; Gabriel, C. J.; Hatakeyama, E. S.; Noble, R. D.; Gin, D. L.

*Ind. Eng. Chem. Res.* **2007**, *46*, 5397-5404.

16. Susan, M. A.; Kaneko, T.; Noda, A.; Watanabe, M. *J. Am. Chem. Soc.* **2005**, *127*, 4976-4983.
17. Lodge, T. P. *Science* **2008**, *321*, 50-51.
18. Klingshirn, M. A.; Spear, S. K.; Subramanian, R.; Holbrey, J. D.; Huddleston, J. G.; Rogers, R. D. *Chem. Mater.* **2004**, *16*, 3091-3097.
19. Matsumoto, K.; Endo, T. *Macromolecules* **2008**, *41*, 6981-6986.
20. Matsumoto, K.; Endo, T. *Macromolecules* **2009**, *42*, 4580-4584.
21. He, Y.; Boswell, P. G.; Buhlmann, P.; Lodge, T. P. *J. Phys. Chem. B* **2007**, *111*, 4645-4652.
22. Zhang, S.; Lee, K. H.; Sun, J.; Frisbie, C. D.; Lodge, T. P. *Macromolecules* **2011**, *44*, 8981-8989.
23. Zhang, S.; Lee, K. H.; Frisbie, C. D.; Lodge, T. P. *Macromolecules* **2011**, *44*, 940-949.
24. He, Y.; Lodge, T. P. *Chem. Commun.* **2007**, 2732-2734.
25. He, Y.; Lodge, T. P. *Macromolecules* **2008**, *41*, 167-174.
26. Ueki, T.; Watanabe, M. *Chem. Lett.* **2006**, *35*, 964-965.
27. Lee, H. N.; Bai, Z.; Newell, N.; Lodge, T. P. *Macromolecules* **2010**, *43*, 9522-9528.
28. Zhou, C.; Hillmyer, M. A.; Lodge, T. P. *Macromolecules* **2011**, *44*, 1635-1641.
29. Zhou, C.; Hillmyer, M. A.; Lodge, T. P. *J. Am. Chem. Soc.* **2012**, *134*, 10365-10368.
30. Fetters, L. J.; Lohse, D. J.; Richter, D.; Witten, T. A.; Zirkel, A. *Macromolecules* **1994**, *27*, 4639-4647.
31. Smith, G. D.; Yoon, D. Y.; Jaffe, R. L.; Colby, R. H.; Krishnamoorti, R.; Fetters, L. J.

*Macromolecules* **1996**, *29*, 3462-3469.

32. Shields, D. J.; Coover, H. W. *J. Polym. Sci.* **1959**, *39*, 532-533.
33. Ganachaud, F.; Monteiro, M. J.; Gilbert, R. G.; Dourges, M. A.; Thang, S. H.; Rizzardo, E. *Macromolecules* **2000**, *33*, 6738-6745.
34. Cammarata, L.; Kazarian, S. G.; Salter, P. A.; Welton, T. *Phys. Chem. Chem. Phys.* **2001**, *3*, 5192-5200.
35. Lee, H. N.; Lodge, T. P. *J. Phys. Chem. Lett.* **2010**, *1*, 1962-1966.
36. Chambon, F.; Petrovic, Z. S.; Macknight, W. J.; Winter, H. H. *Macromolecules* **1986**, *19*, 2146-2149.
37. Winter, H. H.; Chambon, F. *J. Rheol.* **1986**, *30*, 367-382.
38. Li, C.; Tang, Y.; Armes, S. P.; Morris, C. J.; Rose, S. F.; Lloyd, A. W.; Lewis, A. L. *Biomacromolecules* **2005**, *6*, 994-999.
39. Mok, M. M.; Liu, X.; Bai, Z.; Lei, Y.; Lodge, T. P. *Macromolecules* **2011**, *44*, 1016-1025.
40. Colby, R. H. *Rheol. Acta* **2010**, *49*, 425-442.
41. Kobayashi, K.; Huang, C. I.; Lodge, T. P. *Macromolecules* **1999**, *32*, 7070-7077.
42. Milner, S. T. *Macromolecules* **2005**, *38*, 4929-4939.
43. Seitz, M. E.; Burghardt, W. R.; Faber, K. T.; Shull, K. R. *Macromolecules* **2007**, *40*, 1218-1226.
44. He, Y.; Li, Z.; Simone, P.; Lodge, T. P. *J. Am. Chem. Soc.* **2006**, *128*, 2745-2750.
45. Bai, Z.; He, Y.; Lodge, T. P. *Langmuir* **2008**, *24*, 5284-5290.
46. Bai, Z.; Lodge, T. P. *J. Phys. Chem. B* **2009**, *113*, 14151-14157.

# Chapter 7

# Summary and Outlook

## 7.1 Summary

The overall goal of my thesis is to design, develop and characterize two-compartment networks from ABC triblock terpolymers for efficient hydrogel formation. The two-compartment hydrogels were achieved by aqueous self-assembly of poly(ethylene-*alt*-propylene)-*b*-poly(ethylene oxide)-*b*-poly(*N*-isopropylacrylamide) (PEP-*b*-PEO-*b*-PNIPAm, PON) triblock terpolymer with a long hydrophilic midblock PEO, a short hydrophobic endblock PEP and a thermoresponsive endblock PNIPAm. The incorporation of a thermoresponsive PNIPAm polymer into this triblock encourages a stepwise gelation involving micellization at room temperature and gelation at elevated temperatures, which leads to the formation of a two-compartment network with good mechanical properties.

The PON terpolymers were prepared using a combination of anionic and RAFT polymerization. Upon dissolution in water at room temperature, they self-assembled into spherical PEP micelles with hydrophilic PEO shells and PNIPAm coronae. When heated above than the LCST of PNIPAm, they underwent micellar aggregation in dilute solutions (0.05 and 0.5 wt%) and gelation in more concentration solution (1, 2 and 5 wt%) due to intermicellar association of corona PNIPAm chains. The critical micellar aggregation or gelation temperature depended on both the molecular weight of PNIPAm

and PEO and polymer concentration. The longer PNIPAm block length, shorter PEO midblock length and higher polymer concentration resulted in a lower critical micellar aggregation or gelation temperature. However, the plateau storage modulus of PON hydrogels showed reverse trend on PNIPAm and PEO block length and polymer concentration. In addition, gelation of PON terpolymers was achieved at a much lower concentration, with a much higher modulus and sharper sol-gel transition, as compared to NON copolymer hydrogels. This is due to the separation of micellization and gelation, which leads to the formation of a two-compartment network with a very high fraction of bridging conformations for the PEO midblocks. The formation of a micellar network with two discrete PEP and PNIPAm hydrophobic domains in PON hydrogels is supported by cryo-SEM and cryo-TEM experiments and is further verified by SANS measurements.

To extend the control on the self-assembly process of PON terpolymers for future biomedical applications, a small fraction of acrylic acid (AA) was introduced into PNIPAm block to give poly(ethylene-*alt*-propylene)-*b*-poly(ethylene oxide)-*b*-poly(*N*-isopropylacrylamide-*co*-acrylic acid) (PO(N/A)) triblock terpolymers. The polymers form micelles with PEP cores and PEO-P(NIPAm-*co*-AA) coronae in aqueous solution at room temperature. Upon heating above the LCST of the P(NIPAm-*co*-AA) block, the micelles aggregate in the dilute solutions and form a hydrogel at higher concentrations. The critical micellar aggregation and gelation temperatures depended on the mole fraction of AA and degree of AA ionization in the P(NIPAm-*co*-AA) block and can be modulated by changing pH of the medium and by varying the AA content in the P(NIPAm-*co*-AA) block.

To identify the universality of the principle that ABC terpolymer architecture is

beneficial for gel formation in comparison to ABA copolymers, the gelation properties of PON terpolymers in ionic liquid 1-ethyl-3-methylimidazolium bis(trifluoromethyl-sulfonyl)amide ([EMI][TFSA]) was studied and compared with that of NON copolymers. Again, a lower gelation concentration with a higher modulus was achieved in PON ion gels.

## 7.2 Outlook

On the basis of the results presented in this thesis, there are definitely many opportunities for future research in this area.

### 7.2.1 Biodegradable Thermoresponsive ABC Hydrogels

As we have discussed in Chapter 1, stimuli-responsive hydrogels, which exhibit a sol-gel transition in response to external stimuli, such as temperature, pH, light, counterion changes, and biological molecules have attracted considerable attention, since they have wide utility in, e.g., drug delivery and tissue engineering, sensors and valves, surface patterning, and tunable optics. [1-7] Biocompatible and biodegradable thermoresponsive hydrogels are particularly appealing, as they can form a hydrogel in situ upon administration, and therefore have found use as injectable biomaterials for site-specific drug delivery, tissue engineering, and minimally invasive surgery applications.[6-8] To exploit the properties of thermoresponsive hydrogels in such biomedical applications, it is therefore of interest to design and prepare novel biocompatible and biodegradable polymers for this purpose.

We have also demonstrated in the thesis (Chapter 2–4) that better gelation efficiencies and enhanced mechanical properties can be achieved with ABC triblock

terpolymers with two immiscible, hydrophobic endblocks, resulting from the formation of two-compartment networks with a high fraction of bridging conformations for the midblocks. Thermoresponsive PON hydrogels can be prepared in aqueous solutions with as low as 1 wt% polymer, and such low gelation is desirable for biological and pharmaceutical applications.

For future research, it would be interesting to combine the concepts of biodegradability and thermoresponsive ABC triblock terpolymer to develop biodegradable thermoresponsive ABC hydrogels for advanced biomedical applications. PEO can still serve as the hydrophilic midblock, due to its good water solubility, biocompatibility and ability to endow the colloidal assembly with a stealth character for prolonged circulation *in vivo*.[9-11] The hydrophobic PEP block is not degradable, and can be replaced by a biodegradable aliphatic polyester, poly($\gamma$-methyl- $\varepsilon$-caprolactone) (PMCL).[12] PMCL has a low $T_g$ of ca. –60 ℃ and is amorphous. Therefore its block copolymer amphiphiles can form dispersions with simple stirring in water at room temperature, without the need of elevated temperature or organic cosolvents to aid dissolution.[13-16] This is an appealing attribute for drug delivery applications, as it can avoid the use of toxic residual solvents and high temperature that may be detrimental to fragile therapeutics. The thermoresponsive PNIPAm block is also not degradable, and the biocompatibility is not well-established.[17, 18] Biodegradable thermoresponsive polymers have been successfully prepared from polyesters,[19, 20] poly(organophosphazenes)[21, 22] and poly(amino acids)[23, 24] (polypeptides). Some potential candidates, including poly(lactic-*co*-glycolic) acid (PLGA), oligo(ethylene glycol) functionalized poly(trimethylene carbonate) ($PEG_3TMC$), and oligo(ethylene glycol) functionalized

functionalized poly-$_{L}$-glutamates ($PEG_3Glu$) and poly-$_{L}$-cysteine ($PEG_3Cys$), are listed in Scheme 7.1. Among these polymers, the polypeptide materials are especially attractive due to the flexibility in structure modification with different functional groups and additional higher ordering from inherent secondary structures.

**Scheme 7.1** Chemical structure of biodegradable thermoresponsive polymers

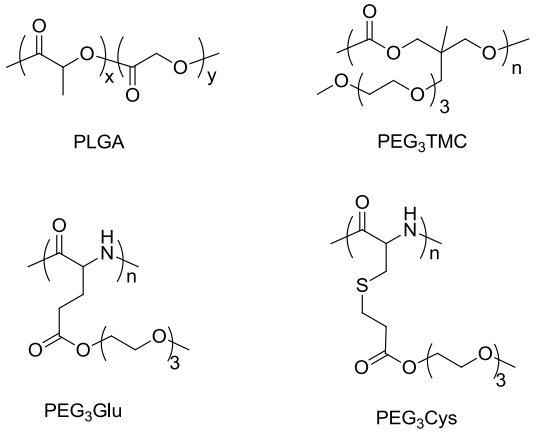


Based on this discussion, poly(*γ*-methyl-*ε*-caprolactone)-*b*-poly(ethylene oxide)-*b*-poly- (oligo(ethylene glycol) functionalized $_{L}$-cysteine) (PMCL-*b*-PEO-*b*-$PEG_3Cys$) triblock terpolymers can serve as the model system to prepare biodegradable thermoresponsive hydrogels with superior gelation properties. The synthetic route to this triblock is provided in Scheme 7.2.

**Scheme 7.2** Synthesis of PMCL-*b*-PEO-*b*-PEG$_3$Cys triblock terpolymers

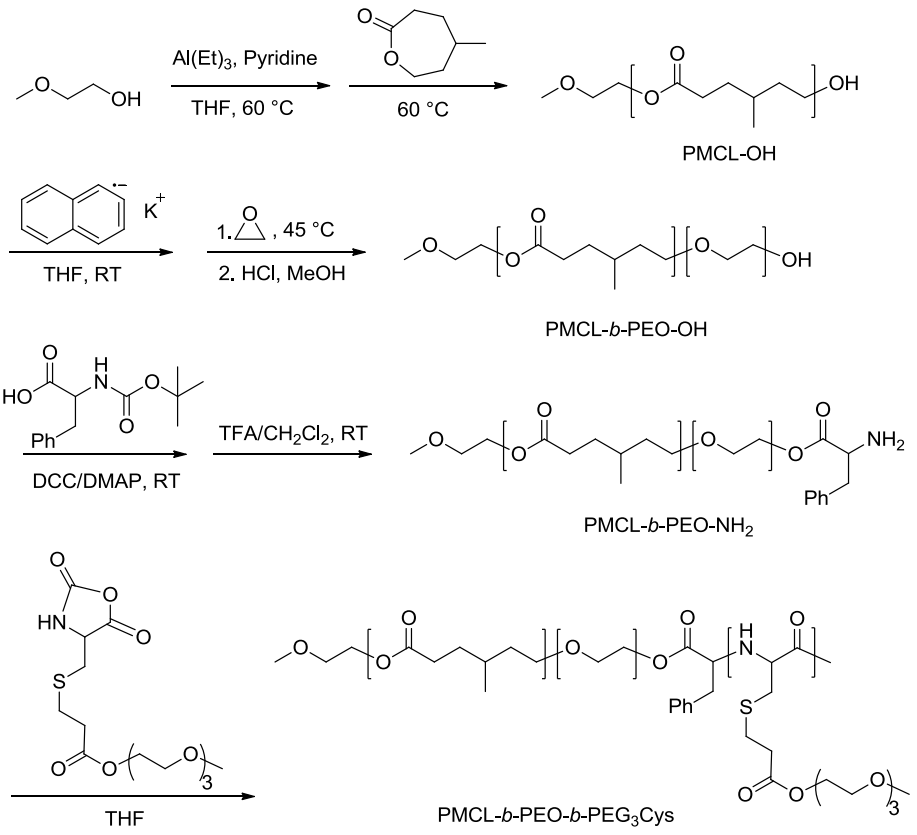


### 7.2.2 Dual Stimuli-responsive Hydrogels

We have demonstrated in Chapter 5 that dual temperature- and pH-responsive hydrogels can be realized by incorporating a pH-responsive monomer (AA) into the thermoresponsive PNIPAm of PON terpolymers. This method could be applied to develop other dual stimuli-responsive hydrogels in which the sol-gel transition is controlled by both temperature and a second stimulus, such as light and biological molecules. The LCST of PNIPAm has been shown to be modulated by light[25] and glucose[26-33] by incorporating appropriate comonomers, and they can be adopted in the present system for the preparation of novel dual stimuli-responsive hydrogels.

### 7.2.3 Thermoresponsive Ion Gels

We have demonstrated in Chapter 6 that gelation of PON terpolymer in [EMI][TFSA] can be achieved at as low as of 1 wt% polymer with good mechanical properties. This material is expected to be advantageous for typical ion gel applications, such as plastic electronics and gas separation membranes. However, the critical gelation temperature $T_{gel}$ lies around room temperature (16–27 ℃), which limits its application. It is therefore of interest to raise $T_{gel}$ well above room temperature to achieve liquid state processing above room temperature, and allow material use in the solid state under ambient conditions.[34] This can be done by incorporating insoluble PS blocks into the PNIPAm endblocks to give PEP-*b*-PEO-*b*-P(NIPAm-*co*-PS) (PO(N/S)) triblock polymer (Scheme 7.3).

**Scheme 7.3** Chemical structure of PO(N/S) triblock polymer

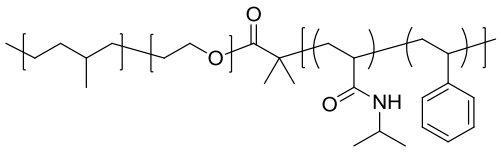


PO(N/S)

Additionally, there are several fundamental questions should be addressed in this area. First, gelation properties of PON terpolymer were compared with that of CTA-NON-CTA instead of NON copolymer. This is because the NON copolymer was found to be degraded from SEC analysis and therefore was not used. The hydrophobic dodecyl end groups from the CTA can impede the micellization of the PON triblock terpolymers in water and its effect in ionic liquid is not explored yet. The effects of the

dodecyl end groups on gelation in ionic liquid can be elucidated by preparing new NON triblock copolymers and studying their viscoelastic properties. In addition, the direct comparison between PON and NON ion gels can be carried out.

Second, there is a relaxation for the storage modulus of PON ion gels before melting (below $T_{gel}$) upon heating. This relaxation becomes more evident as the polymer weight fraction decreases from 10 wt% to 2 wt% (Figure 6.7). We speculate that it corresponds to the relaxation of the PEO midblocks in the ionic liquid. Performing the dynamic frequency in the heating process below $T_{gel}$ would be useful to elucidate this question.

Third, PON displays a relatively broad sol-gel transition with a low $T_{gel}$ and unusual concentration dependence of $T_{gel}$. It is likely that a small amount of impurity is present in [BMI][$BF_4$] and leads to the usual gelation behavior. It also possible that moisture can play a role here. Therefore, it would be important to find a way to make a clean ionic liquid [BMI][$BF_4$] and control the moisture during ion gel preparation and rheological measurements.

### 7.3 References


1. Lin, C.; Metters, A. T. *Adv. Drug Deliv. Rev.* **2006**, *58*, 1379-1408.
2. Tokarev, I.; Minko, S. *Adv. Mater.* **2010**, *22*, 3446-3462.
3. Kopecek, J. *Biomaterials* **2007**, *28*, 5185-5192.
4. Hendrickson, G. R.; Lyon, L. A. *Soft Matter* **2009**, *5*, 29-35.
5. Calvert, P. *Adv. Mater.* **2009**, *21*, 743-756.
6. Jeong, B.; Kim, S. W.; Bae, Y. H. *Adv. Drug Deliv. Rev.* **2002**, *54*, 37-51.
7. Yu, L.; Ding, J. *Chem. Soc. Rev.* **2008**, *37*, 1473-1481.

8. He, C.; Kim, S. W.; Lee, D. S. *J. Controlled Release* **2008**, *127*, 189-207.
9. Kataoka, K.; Kwon, G. S.; Yokoyama, M.; Okano, T.; Sakurai, Y. *J. Controlled Release* **1993**, *24*, 119-132.
10. Otsuka, H.; Nagasaki, Y.; Kataoka, K. *Adv. Drug Deliv. Rev.* **2003**, *55*, 403-419.
11. Photos, P. J.; Bacakova, L.; Discher, B.; Bates, F. S.; Discher, D. E. *J. Controlled Release* **2003**, *90*, 323-334.
12. Trollsas, M.; Kelly, M. A.; Claesson, H.; Siemens, R.; Hedrick, J. L. *Macromolecules* **1999**, *32*, 4917-4924.
13. Zupancich, J. A.; Bates, F. S.; Hillmyer, M. A. *Macromolecules* **2006**, *39*, 4286-4288.
14. Saito, N.; Liu, C.; Lodge, T. P.; Hillmyer, M. A. *Macromolecules* **2008**, *41*, 8815-8822.
15. Petersen, M. A.; Yin, L.; Kokkoli, E.; Hillmyer, M. A. *Polym. Chem.* **2010**, *1*, 1281-1290.
16. Petersen, M. A.; Hillmyer, M. A.; Kokkoli, E. *Bioconjugate Chem.* **2013**, *24*, 533-543.
17. Li, C.; Tang, Y.; Armes, S. P.; Morris, C. J.; Rose, S. F.; Lloyd, A. W.; Lewis, A. L. *Biomacromolecules* **2005**, *6*, 994-999.
18. Allen, L. T.; Fox, E. J. P.; Blute, I.; Kelly, Z. D.; Rochev, Y.; Keenan, A. K.; Dawson, K. A.; Gallagher, W. M. *Proc. Natl. Acad. Sci. U. S. A.* **2003**, *100*, 6331-6336.
19. Yu, L.; Zhang, H.; Ding, J. *Angew. Chem., Int. Ed.* **2006**, *45*, 2232-2235.
20. Ajiro, H.; Takahashi, Y.; Akashi, M. *Macromolecules* **2012**, *45*, 2668-2674.
21. Song, S. C.; Lee, S. B.; Jin, J. I.; Sohn, Y. S. *Macromolecules* **1999**, *32*, 2188-2193.
22. Lee, S. B.; Song, S. C.; Jin, J. I.; Sohn, Y. S. *Macromolecules* **1999**, *32*, 7820-7827.

23. Chen, C.; Wang, Z.; Li, Z. *Biomacromolecules* **2011**, *12*, 2859-2863.

24. Fu, X.; Shen, Y.; Fu, W.; Li, Z. *Macromolecules* **2013**, *46*, 3753-3760.

25. Ivanov, A. E.; Eremeev, N. L.; Wahlund, P. O.; Galaev, I. Y.; Mattiasson, B. *Polymer* **2002**, *43*, 3819-3823.

26. Shiomori, K.; Ivanov, A. E.; Galaev, I. Y.; Kawano, Y.; Mattiasson, B. *Macromol. Chem. Phys* **2004**, *205*, 27-34.

27. Lapeyre, V.; Gosse, I.; Chevreux, S.; Ravaine, V. *Biomacromolecules* **2006**, *7*, 3356-3363.

28. Zhang, Y.; Guan, Y.; Zhou, S. *Biomacromolecules* **2006**, *7*, 3196-3201.

29. Hoare, T.; Pelton, R. *Macromolecules* **2007**, *40*, 670-678.

30. Wang, D.; Liu, T.; Yin, J.; Liu, S. *Macromolecules* **2011**, *44*, 2282-2290.

31. Roy, D.; Cambre, J. N.; Sumerlin, B. S. *Chem. Commun.* **2008**, 2477-2479.

32. Roy, D.; Cambre, J. N.; Sumerlin, B. S. *Chem. Commun.* **2009**, 2106-2108.

33. Roy, D.; Sumerlin, B. S. *Acs Macro Lett.* **2012**, *1*, 529-532.

34. He, Y.; Lodge, T. P. *Macromolecules* **2008**, *41*, 167-174.

# Bibliography


Abbas, S.; Li, Z.; Hassan, H.; Lodge, T. P. *Macromolecules* **2007**, *40*, 4048-4052.

Ajiro, H.; Takahashi, Y.; Akashi, M. *Macromolecules* **2012**, *45*, 2668-2674.

Akiyama, Y.; Kikuchi, A.; Yamato, M.; Okano, T. *Langmuir* **2004**, *20*, 5506-5511.

Allen, L. T.; Fox, E. J. P.; Blute, I.; Kelly, Z. D.; Rochev, Y.; Keenan, A. K.; Dawson, K. A.; Gallagher, W. M. *Proc. Natl. Acad. Sci. U. S. A.* **2003**, *100*, 6331-6336.

Allgaier, J.; Poppe, A.; Willner, L.; Richter, D. *Macromolecules* **1997**, *30*, 1582-1586.

Angelopoulos, S. A.; Tsitsilianis, C. *Macromol. Chem. Phys* **2006**, *207*, 2188-2194.

Annable, T.; Buscall, R.; Ettelaie, R. *Colloids Surf., A* **1996**, *112*, 97-116.

Annable, T.; Buscall, R.; Ettelaie, R.; Whittlestone, D. *J. Rheol.* **1993**, *37*, 695-726.

Ashcroft, N. W.; Langreth, D. C. *Phys. Rev.* **1967**, *156*, 685-692.

Bae, Y. H.; Vernon, B.; Han, C. K.; Kim, S. W. *J. Controlled Release* **1998**, *53*, 249-258.

Bai, Z.; He, Y.; Lodge, T. P. *Langmuir* **2008**, *24*, 5284-5290.

Bai, Z.; Lodge, T. P. *J. Phys. Chem. B* **2009**, *113*, 14151-14157.

Balsara, N. P.; Tirrell, M.; Lodge, T. P. *Macromolecules* **1991**, *24*, 1975-1986.

Bang, J.; Jain, S. M.; Li, Z.; Lodge, T. P.; Pedersen, J. S.; Kesselman, E.; Talmon, Y. *Macromolecules* **2006**, *39*, 1199-1208.

Bara, J. E.; Lessmann, S.; Gabriel, C. J.; Hatakeyama, E. S.; Noble, R. D.; Gin, D. L. *Ind. Eng. Chem. Res.* **2007**, *46*, 5397-5404.

Bellare, J. R.; Davis, H. T.; Scriven, L. E.; Talmon, Y. *J. Electron Microsc.* **1988**, *10*, 87-111.

Bergenholtz, J.; Romagnoli, A. A.; Wagner, N. J. *Langmuir* **1995**, *11*, 1559-1570.

Bokias, G.; Staikos, G.; Iliopoulos, I. *Polymer* **2000**, *41*, 7399-7405.

Bokias, G.; Vasilevskaya, V. V.; Iliopoulos, I.; Hourdet, D.; Khokhlov, A. R. *Macromolecules* **2000**, *33*, 9757-9763.

Calvert, P. *Adv. Mater.* **2009**, *21*, 743-756.

Cammarata, L.; Kazarian, S. G.; Salter, P. A.; Welton, T. *Phys. Chem. Chem. Phys.* **2001**, *3*, 5192-5200.

Cammas, S.; Suzuki, K.; Sone, C.; Sakurai, Y.; Kataoka, K.; Okano, T. *J. Controlled Release* **1997**, *48*, 157-164.

Cao, Y.; Zhu, X.; Luo, J.; Liu, H. *Macromolecules* **2007**, *40*, 6481-6488.

Cao, Z.; Liu, W.; Gao, P.; Yao, K.; Li, H.; Wang, G. *Polymer* **2005**, *46*, 5268-5277.

Castelletto, V.; Hamley, I. W.; Pedersen, J. S. *J. Chem. Phys.* **2002**, *117*, 8124-8129.

Castelletto, V.; Hamley, I. W.; Pedersen, J. S. *Langmuir* **2004**, *20*, 2992-2994.

Castner, E. W.; Wishart, J. F.; Shirota, H. *Acc. Chem. Res.* **2007**, *40*, 1217-1227.

Chambon, F.; Petrovic, Z. S.; Macknight, W. J.; Winter, H. H. *Macromolecules* **1986**, *19*, 2146-2149.

Charbonneau, C.; Chassenieux, C.; Colombani, O.; Nicolai, T. *Macromolecules* **2011**, *44*, 4487-4495.

Chen, C.; Wang, Z.; Li, Z. *Biomacromolecules* **2011**, *12*, 2859-2863.

Chen, G.; Hoffman, A. S. *Macromol. Rapid Commun.* **1995**, *16*, 175-182.

Cheng, C.; Wei, H.; Zhu, J.; Chang, C.; Cheng, H.; Li, C.; Cheng, S.; Zhang, X.; Zhuo, R. *Bioconjugate Chem.* **2008**, *19*, 1194-1201.

Cho, C. S.; Jung, J. H.; Sung, Y. K.; Lee, Y. M. *Macromol. Rapid Commun.* **1994**, *15*, 727-732.

Cho, J. H.; Lee, J.; He, Y.; Kim, B.; Lodge, T. P.; Frisbie, C. D. *Adv. Mater.* **2008**, *20*, 686-690.

Cho, J. H.; Lee, J.; Xia, Y.; Kim, B.; He, Y.; Renn, M. J.; Lodge, T. P.; Frisbie, C. D. *Nat. Mater.* **2008**, *7*, 900-906.

Chung, J. E.; Yokoyama, M.; Aoyagi, T.; Sakurai, Y.; Okano, T. *J. Controlled Release* **1998**, *53*, 119-130.

Chung, J. E.; Yokoyama, M.; Okano, T. *J. Controlled Release* **2000**, *65*, 93-103.

Chung, J. E.; Yokoyama, M.; Suzuki, K.; Aoyagi, T.; Sakurai, Y.; Okano, T. *Colloids Surf., B* **1997**, *9*, 37-48.

Chung, J. E.; Yokoyama, M.; Yamato, M.; Aoyagi, T.; Sakurai, Y.; Okano, T. *J. Controlled Release* **1999**, *62*, 115-127.

Colby, R. H. *Rheol. Acta* **2010**, *49*, 425-442.

Cole, M. A.; Voelcker, N. H.; Thissen, H.; Griesser, H. J. *Biomaterials* **2009**, *30*, 1827-1850.

Convertine, A. J.; Lokitz, B. S.; Vasileva, Y.; Myrick, L. J.; Scales, C. W.; Lowe, A. B.; McCormick, C. L. *Macromolecules* **2006**, *39*, 1724-1730.

Cui, H.; Chen, Z.; Zhong, S.; Wooley, K. L.; Pochan, D. J. *Science* **2007**, *317*, 647-650.

de las Heras Alarcon, C.; Pennadam, S.; Alexander, C. *Chem. Soc. Rev.* **2005**, *34*, 276-285.

Dong, L.; Hoffman, A. S. *J. Controlled Release* **1991**, *15*, 141-152.

Fang, B.; Walther, A.; Wolf, A.; Xu, Y.; Yuan, J.; Muller, A. H. E. *Angew. Chem., Int. Ed.* **2009**, *48*, 2877-2880.

Feil, H.; Bae, Y. H.; Feijen, J.; Kim, S. W. *Macromolecules* **1993**, *26*, 2496-2500.

Felber, A. E.; Dufresne, M.-H.; Leroux, J.-C. *Adv. Drug Deliv. Rev.* **2012**, *64*, 979-992.

Fetters, L. J.; Lohse, D. J.; Richter, D.; Witten, T. A.; Zirkel, A. *Macromolecules* **1994**, *27*, 4639-4647.

Fu, X.; Shen, Y.; Fu, W.; Li, Z. *Macromolecules* **2013**, *46*, 3753-3760.

Fujishige, S.; Kubota, K.; Ando, I. *J. Phys. Chem.* **1989**, *93*, 3311-3313.

Galaev, I. Y.; Mattiasson, B. *Trends Biotechnol.* **1999**, *17*, 335-340.

Galperin, A.; Long, T. J.; Ratner, B. D. *Biomacromolecules* **2010**, *11*, 2583-2592.

Ganachaud, F.; Monteiro, M. J.; Gilbert, R. G.; Dourges, M. A.; Thang, S. H.; Rizzardo, E. *Macromolecules* **2000**, *33*, 6738-6745.

Ge, Z.; Zhou, Y.; Tong, Z.; Liu, S. *Langmuir* **2011**, *27*, 1143-1151.

Gil, E. S.; Hudson, S. M. *Prog. Polym. Sci.* **2004**, *29*, 1173-1222.

Glinka, C. J.; Barker, J. G.; Hammouda, B.; Krueger, S.; Moyer, J. J.; Orts, W. J. *J. Appl. Crystallogr.* **1998**, *31*, 430-445.

Gohy, J. F. *Adv. Polym. Sci.* **2005**, *190*, 65-136.

Green, M. S.; Tobolsky, A. V. *J. Chem. Phys.* **1946**, *14*, 80-92.

Han, C. K.; Bae, Y. H. *Polymer* **1998**, *39*, 2809-2814.

He, C.; Kim, S. W.; Lee, D. S. *J. Controlled Release* **2008**, *127*, 189-207.

He, Y.; Boswell, P. G.; Buhlmann, P.; Lodge, T. P. *J. Phys. Chem. B* **2007**, *111*, 4645-4652.

He, Y.; Li, Z.; Simone, P.; Lodge, T. P. *J. Am. Chem. Soc.* **2006**, *128*, 2745-2750.

He, Y.; Lodge, T. P. *Chem. Commun.* **2007**, 2732-2734.

He, Y.; Lodge, T. P. *Macromolecules* **2008**, *41*, 167-174.

Hendrickson, G. R.; Lyon, L. A. *Soft Matter* **2009**, *5*, 29-35.

Heskins, M.; Guillet, J. E. *J. Macromol. Sci. Chem.* **1968**, *A2*, 1441-1455.

Hillmyer, M. A.; Bates, F. S. *Macromolecules* **1996**, *29*, 6994-7002.

Hillmyer, M. A.; Lodge, T. P. *J. Polym. Sci., Part A: Polym. Chem.* **2002**, *40*, 1-8.

Hoare, T.; Pelton, R. *Macromolecules* **2007**, *40*, 670-678.

Hoffman, A. S. *Adv. Drug Deliv. Rev.* **2002**, *54*, 3-12.

Hong, C.; You, Y.; Pan, C. *J. Polym. Sci., Part A: Polym. Chem.* **2004**, *42*, 4873-4881.

Hosoya, K.; Kimata, K.; Araki, T.; Tanaka, N.; Frechet, J. M. J. *Anal. Chem.* **1995**, *67*, 1907-1911.

Ibrahim, K.; Lofgren, B.; Seppala, J. *Eur. Polym. J.* **2003**, *39*, 2005-2010.

Imaizumi, S.; Kokubo, H.; Watanabe, M. *Macromolecules* **2012**, *45*, 401-409.

Inomata, K.; Nakanishi, D.; Banno, A.; Nakanishi, E.; Abe, Y.; Kurihara, R.; Fujimoto, K.; Nose, T. *Polymer* **2003**, *44*, 5303-5310.

Ivanov, A. E.; Eremeev, N. L.; Wahlund, P. O.; Galaev, I. Y.; Mattiasson, B. *Polymer* **2002**, *43*, 3819-3823.

Jain, S.; Bates, F. S. *Macromolecules* **2004**, *37*, 1511-1523.

Jain, S.; Bates, F. S. *Science* **2003**, *300*, 460-464.

Jain, S.; Dyrdahl, M. H. E.; Gong, X.; Scriven, L. E.; Bates, F. S. *Macromolecules* **2008**, *41*, 3305-3316.

Jakes, J. *Collect. Czech. Chem. Commun.* **1995**, *60*, 1781-1797.

Jeong, B.; Gutowska, A. *Trends Biotechnol.* **2002**, *20*, 305-311.

Jeong, B.; Kim, S. W.; Bae, Y. H. *Adv. Drug Deliv. Rev.* **2002**, *54*, 37-51.

Jiang, X.; Ge, Z.; Xu, J.; Liu, H.; Liu, S. *Biomacromolecules* **2007**, *8*, 3184-3192.

Jones, M. S. *Eur. Polym. J.* **1999**, *35*, 795-801.

Kadam, V.; Nicolai, T.; Nicol, E.; Benyahia, L. *Macromolecules* **2011**, *44*, 8225-8232.

Kanazawa, H.; Sunamoto, T.; Matsushima, Y. *Anal. Chem.* **2000**, *72*, 5961-5966.

Kanazawa, H.; Yamamoto, K.; Matsushima, Y.; Takai, N.; Kikuchi, A.; Sakurai, Y.; Okano, T. *Anal. Chem.* **1996**, *68*, 100-105.

Kang, S. I.; Bae, Y. H. *Macromol. Chem. Symp.* **2001**, *14*, 145-155.

Katakabe, T.; Kaneko, T.; Watanabe, W.; Fukushima, T.; Aida, T. *J. Electrochem. Soc.* **2005**, *152*, A1913-A1916.

Kataoka, K.; Kwon, G. S.; Yokoyama, M.; Okano, T.; Sakurai, Y. *J. Controlled Release* **1993**, *24*, 119-132.

Kelarakis, A.; Havredaki, V.; Yuan, X.; Chaibundit, C.; Booth, C. *Macromol. Chem. Phys* **2006**, *207*, 903-909.

Kelarakis, A.; Yuan, X.; Mai, S.; Yang, Y.; Booth, C. *Phys. Chem. Chem. Phys.* **2003**, *5*, 2628-2634.

Kikuchi, A.; Okano, T. *Prog. Polym. Sci.* **2002**, *27*, 1165-1193.

Kim, G. T.; Jeong, S. S.; Joost, M.; Rocca, E.; Winter, M.; Passerini, S.; Balducci, A. *J. Power Sources* **2011**, *196*, 2187-2194.

Kim, S. H.; Hong, K.; Xie, W.; Lee, K. H.; Zhang, S.; Lodge, T. P.; Frisbie, C. D. *Adv. Mater.* **2013**, *25*, 1822-1846.

Kim, S.; Healy, K. E. *Biomacromolecules* **2003**, *4*, 1214-1223.

Kirkland, S. E.; Hensarling, R. M.; McConaughy, S. D.; Guo, Y.; Jarrett, W. L.; McCormick, C. L. *Biomacromolecules* **2008**, *9*, 481-486.

Kline, S. R. *J. Appl. Crystallogr.* **2006**, *39*, 895-900.

Kline, S. R.; Kaler, E. W. *J. Chem. Phys.* **1996**, *105*, 3813-3822.

Klingshirn, M. A.; Spear, S. K.; Subramanian, R.; Holbrey, J. D.; Huddleston, J. G.; Rogers, R. D. *Chem. Mater.* **2004**, *16*, 3091-3097.

Kobayashi, J.; Kikuchi, A.; Sakai, K.; Okano, T. *Anal. Chem.* **2001**, *73*, 2027-2033.

Kobayashi, K.; Huang, C. I.; Lodge, T. P. *Macromolecules* **1999**, *32*, 7070-7077.

Kobayashi, S.; Song, J.; Silvis, H. C.; Macosko, C. W.; Hillmyer, M. A. *Ind. Eng. Chem. Res.* **2011**, *50*, 3274-3279.

Kogure, H.; Nanami, S.; Masuda, Y.; Toyama, Y.; Kubota, K. *Colloid Polym. Sci.* **2005**, *283*, 1163-1171.

Kohori, F.; Sakai, K.; Aoyagi, T.; Yokoyama, M.; Sakurai, Y.; Okano, T. *J. Controlled Release* **1998**, *55*, 87-98.

Komenda, T.; Luedtke, K.; Jordan, R.; Ivanova, R.; Bonne, T. B.; Papadakis, C. M. *Polym. Prepr. (Am. Chem. Soc., Div. Polym. Chem.)* **2006**, *47*, 763-764.

Koonar, I.; Zhou, C.; Hillmyer, M. A.; Lodge, T. P.; Siegel, R. A. *Langmuir* **2012**, *28*,

17785-17794.

Kopecek, J. *Biomaterials* **2007**, *28*, 5185-5192.

Kubowicz, S.; Baussard, J. F.; Lutz, J. F.; Thunemann, A. F.; von Berlepsch, H.; Laschewsky, A. *Angew. Chem., Int. Ed.* **2005**, *44*, 5262-5265.

Lai, J. T.; Filla, D.; Shea, R. *Macromolecules* **2002**, *35*, 6754-6756.

Lapeyre, V.; Gosse, I.; Chevreux, S.; Ravaine, V. *Biomacromolecules* **2006**, *7*, 3356-3363.

Laschewsky, A. *Curr. Opin. Colloid Interface Sci.* **2003**, *8*, 274-281.

Lee, H. N.; Bai, Z.; Newell, N.; Lodge, T. P. *Macromolecules* **2010**, *43*, 9522-9528.

Lee, H. N.; Lodge, T. P. *J. Phys. Chem. Lett.* **2010**, *1*, 1962-1966.

Lee, J.; Panzer, M. J.; He, Y.; Lodge, T. P.; Frisbie, C. D. *J. Am. Chem. Soc.* **2007**, *129*, 4532-4533.

Lee, S. B.; Song, S. C.; Jin, J. I.; Sohn, Y. S. *Macromolecules* **1999**, *32*, 7820-7827.

Lee, S.; Arunagirinathan, M. A.; Bates, F. S. *Langmuir* **2010**, *26*, 1707-1715.

Lewandowski, A.; Swiderska-Mocek, A. *J. Power Sources* **2009**, *194*, 601-609.

Li, C.; Buurma, N. J.; Haq, I.; Turner, C.; Armes, S. P.; Castelletto, V.; Hamley, I. W.; Lewis, A. L. *Langmuir* **2005**, *21*, 11026-11033.

Li, C.; Tang, Y.; Armes, S. P.; Morris, C. J.; Rose, S. F.; Lloyd, A. W.; Lewis, A. L. *Biomacromolecules* **2005**, *6*, 994-999.

Li, Y.; Lokitz, B. S.; Armes, S. P.; McCormick, C. L. *Macromolecules* **2006**, *39*, 2726-2728.

Li, Y.; Lokitz, B. S.; McCormick, C. L. *Macromolecules* **2006**, *39*, 81-89.

Li, Z.; Hillmyer, M. A.; Lodge, T. P. *Langmuir* **2006**, *22*, 9409-9417.

Li, Z.; Hillmyer, M. A.; Lodge, T. P. *Macromolecules* **2004**, *37*, 8933-8940.

Li, Z.; Hillmyer, M. A.; Lodge, T. P. *Nano Lett.* **2006**, *6*, 1245-1249.

Li, Z.; Kesselman, E.; Talmon, Y.; Hillmyer, M. A.; Lodge, T. P. *Science* **2004**, *306*, 98-101.

Lin, C.; Metters, A. T. *Adv. Drug Deliv. Rev.* **2006**, *58*, 1379-1408.

Lin, H.; Cheng, Y. *Macromolecules* **2001**, *34*, 3710-3715.

Lin, S.; Fuchise, K.; Chen, Y.; Sakai, R.; Satoh, T.; Kakuchi, T.; Chen, W. *Soft Matter* **2009**, *5*, 3761-3770.

Liu, H.; Zhu, X. *Polymer* **1999**, *40*, 6985-6990.

Liu, J.; Chen, G.; Guo, M.; Jiang, M. *Macromolecules* **2010**, *43*, 8086-8093.

Liu, R.; Fraylich, M.; Saunders, B. R. *Colloid Polym. Sci.* **2009**, *287*, 627-643.

Lodge, T. P. *Science* **2008**, *321*, 50-51.

Lodge, T. P.; Bang, J. A.; Li, Z.; Hillmyer, M. A.; Talmon, Y. *Faraday Discuss.* **2005**, *128*, 1-12.

Lodge, T. P.; Hillmyer, M. A.; Zhou, Z.; Talmon, Y. *Macromolecules* **2004**, *37*, 6680-6682.

Lodge, T. P.; Rasdal, A.; Li, Z.; Hillmyer, M. A. *J. Am. Chem. Soc.* **2005**, *127*, 17608-17609.

Lokitz, B. S.; Convertine, A. J.; Ezell, R. G.; Heidenreich, A.; Li, Y.; McCormick, C. L. *Macromolecules* **2006**, *39*, 8594-8602.

Lu, W.; Fadeev, A. G.; Qi, B.; Smela, E.; Mattes, B. R.; Ding, J.; Spinks, G. M.; Mazurkiewicz, J.; Zhou, D.; Wallace, G. G.; MacFarlane, D. R.; Forsyth, S. A.; Forsyth, M. *Science* **2002**, *297*, 983-987.

Lutz, J. F.; Laschewsky, A. *Macromol. Chem. Phys* **2005**, *206*, 813-817.

Madsen, J.; Armes, S. P.; Lewis, A. L. *Macromolecules* **2006**, *39*, 7455-7457.

Maeda, Y.; Higuchi, T.; Ikeda, I. *Langmuir* **2000**, *16*, 7503-7509.

Maeda, Y.; Yamamoto, H.; Ikeda, I. *Colloid Polym. Sci.* **2004**, *282*, 1268-1273.

Magenau, A. J. D.; Martinez-Castro, N.; Savin, D. A.; Storey, R. F. *Macromolecules* **2009**, *42*, 8044-8051.

Mano, J. F. *Adv. Eng. Mater.* **2008**, *10*, 515-527.

Matsumoto, K.; Endo, T. *Macromolecules* **2008**, *41*, 6981-6986.

Matsumoto, K.; Endo, T. *Macromolecules* **2009**, *42*, 4580-4584.

McCormick, C. L.; Sumerlin, B. S.; Lokitz, B. S.; Stempka, J. E. *Soft Matter* **2008**, *4*, 1760-1773.

Mehta, A.; Jaouhari, R.; Benson, T. J.; Douglas, K. T. *Tetrahedron Lett.* **1992**, *33*, 5441-5444.

Mei, A.; Guo, X.; Ding, Y.; Zhang, X.; Xu, J.; Fan, Z.; Du, B. *Macromolecules* **2010**, *43*, 7312-7320.

Meli, L.; Lodge, T. P. *Macromolecules* **2009**, *42*, 580-583.

Meli, L.; Santiago, J. M.; Lodge, T. P. *Macromolecules* **2010**, *43*, 2018-2027.

Meng, X.; Russel, W. B. *J. Rheol.* **2006**, *50*, 189-205.

Mi Kyong, Y.; Yong Kiel, S.; Chong, S. C.; Young, M. L. *Polymer* **1997**, *38*,

2759-2765.

Milner, S. T. *Macromolecules* **2005**, *38*, 4929-4939.

Mizutani, A.; Kikuchi, A.; Yamato, M.; Kanazawa, H.; Okano, T. *Biomaterials* **2008**, *29*, 2073-2081.

Mok, M. M.; Liu, X.; Bai, Z.; Lei, Y.; Lodge, T. P. *Macromolecules* **2011**, *44*, 1016-1025.

Motokawa, R.; Morishita, K.; Koizumi, S.; Nakahira, T.; Annaka, M. *Macromolecules* **2005**, *38*, 5748-5760.

Moughton, A. O.; Hillmyer, M. A.; Lodge, T. P. *Macromolecules* **2012**, *45*, 2-19.

Mueller, K. F. *Polymer* **1992**, *33*, 3470-3476.

Nakamura, K.; Maitani, Y.; Lowman, A. M.; Takayama, K.; Peppas, N. A.; Nagai, T. *J. Controlled Release* **1999**, *61*, 329-335.

Nakayama, M.; Okano, T. *Macromolecules* **2008**, *41*, 504-507.

Nakayama, M.; Okano, T.; Miyazaki, T.; Kohori, F.; Sakai, K.; Yokoyama, M. *J. Controlled Release* **2006**, *115*, 46-56.

Nath, N.; Chilkoti, A. *Adv. Mater.* **2002**, *14*, 1243-1247.

Nedelcheva, A. N.; Vladimirov, N. G.; Novakov, C. P.; Berlinova, I. V. *J. Polym. Sci., Part A: Polym. Chem.* **2004**, *42*, 5736-5744.

Nuopponen, M.; Ojala, J.; Tenhu, H. *Polymer* **2004**, *45*, 3643-3650.

Nyrkova, I. A.; Semenov, A. N. *Macromol. Theory Simul.* **2005**, *14*, 569-585.

O'Lenick, T. G.; Jiang, X.; Zhao, B. *Langmuir* **2010**, *26*, 8787-8796.

O'Lenick, T. G.; Jin, N.; Woodcock, J. W.; Zhao, B. *J. Phys. Chem. B* **2011**, *115*, 2870-2881.

Ono, Y.; Shikata, T. *J. Am. Chem. Soc.* **2006**, *128*, 10030-10031.

Osada, Y. *J. Polym. Sci.: Polym. Chem. Ed.* **1979**, *17*, 3485-3498.

Otsuka, H.; Nagasaki, Y.; Kataoka, K. *Adv. Drug Deliv. Rev.* **2003**, *55*, 403-419.

Patrickios, C. S.; Forder, C.; Armes, S. P.; Billingham, N. C. *J. Polym. Sci., Part A: Polym. Chem.* **1997**, *35*, 1181-1195.

Patrickios, C. S.; Georgiou, T. K. *Curr. Opin. Colloid Interface Sci.* **2003**, *8*, 76-85.

Pedersen, J. S. *J. Appl. Crystallogr.* **1998**, *31*, 488-489.

Pedersen, J. S.; Hamley, I. W.; Ryu, C. Y.; Lodge, T. P. *Macromolecules* **2000**, *33*, 542-550.

Pedersen, J. S.; Svaneborg, C.; Almdal, K.; Hamley, I. W.; Young, R. N. *Macromolecules* **2003**, *36*, 416-433.

Peppas, N. A.; Hilt, J. Z.; Khademhosseini, A.; Langer, R. *Adv. Mater.* **2006**, *18*, 1345-1360.

Petersen, M. A.; Hillmyer, M. A.; Kokkoli, E. *Bioconjugate Chem.* **2013**, *24*, 533-543.

Petersen, M. A.; Yin, L.; Kokkoli, E.; Hillmyer, M. A. *Polym. Chem.* **2010**, *1*, 1281-1290.

Photos, P. J.; Bacakova, L.; Discher, B.; Bates, F. S.; Discher, D. E. *J. Controlled Release* **2003**, *90*, 323-334.

Pochan, D. J.; Chen, Z.; Cui, H.; Hales, K.; Qi, K.; Wooley, K. L. *Science* **2004**, *306*, 94-97.

Qin, S.; Geng, Y.; Discher, D. E.; Yang, S. *Adv. Mater.* **2006**, *18*, 2905-2909.

Qiu, X.; Kwan, C. M. S.; Wu, C. *Macromolecules* **1997**, *30*, 6090-6094.

Qiu, X.; Winnik, F. M. *Macromol. Rapid Commun.* **2006**, *27*, 1648-1653.

Qu, T.; Wang, A.; Yuan, J.; Gao, Q. *J. Colloid Interface Sci.* **2009**, *336*, 865-871.

Quirk, R. P.; Ma, J. *J. Polym. Sci., Part A: Polym. Chem.* **1988**, *26*, 2031-2037.

Reinicke, S.; Karg, M.; Lapp, A.; Heymann, L.; Hellweg, T.; Schmalz, H. *Macromolecules* **2010**, *43*, 10045-10054.

Reinicke, S.; Schmalz, H. *Colloid Polym. Sci.* **2011**, *289*, 497-512.

Reinicke, S.; Schmelz, J.; Lapp, A.; Karg, M.; Hellweg, T.; Schmalz, H. *Soft Matter* **2009**, *5*, 2648-2657.

Ricardo, N. M. P. S.; Honorato, S. B.; Yang, Z.; Castelletto, V.; Hamley, I. W.; Yuan, X. F.; Attwood, D.; Booth, C. *Langmuir* **2004**, *20*, 4272-4278.

Ringsdorf, H.; Lehmann, P.; Weberskirch, R. *Book of Abstracts*, 217th National Meeting of the American Chemical Society, Anaheim, CA, March 221-225, 1999.

Robertus, C.; Philipse, W. H.; Joosten, J. G. H.; Levine, Y. K. *J. Chem. Phys.* **1989**, *90*, 4482-4490.

Rodriguez-Hernandez, J.; Checot, F.; Gnanou, Y.; Lecommandoux, S. *Prog. Polym. Sci.* **2005**, *30*, 691-724.

Roy, D.; Cambre, J. N.; Sumerlin, B. S. *Chem. Commun.* **2008**, 2477-2479.

Roy, D.; Cambre, J. N.; Sumerlin, B. S. *Chem. Commun.* **2009**, 2106-2108.

Roy, D.; Sumerlin, B. S. *Acs Macro Lett.* **2012**, *1*, 529-532.

Rzayev, J.; Hillmyer, M. A. *J. Am. Chem. Soc.* **2005**, *127*, 13373-13379.

Saito, N.; Liu, C.; Lodge, T. P.; Hillmyer, M. A. *Macromolecules* **2008**, *41*, 8815-8822.

Schild, H. G. *Prog. Polym. Sci.* **1992**, *17*, 163-249.

Schild, H. G.; Tirrell, D. A. *J. Phys. Chem.* **1990**, *94*, 4352-4356.

Schillen, K.; Brown, W.; Johnsen, R. M. *Macromolecules* **1994**, *27*, 4825-4832.

Schilli, C. M.; Zhang, M.; Rizzardo, E.; Thang, S. H.; Chong, Y. K.; Edwards, K.; Karlsson, G.; Müller, A. H. E. *Macromolecules* **2004**, *37*, 7861-7866.

Schmaljohann, D. *Adv. Drug Deliv. Rev.* **2006**, *58*, 1655-1670.

Seitz, M. E.; Burghardt, W. R.; Faber, K. T.; Shull, K. R. *Macromolecules* **2007**, *40*, 1218-1226.

Semenov, A. N.; Joanny, J. F.; Khokhlov, A. R. *Macromolecules* **1995**, *28*, 1066-1075.

Shen, H.; Zhang, L.; Eisenberg, A. *J. Am. Chem. Soc.* **1999**, *121*, 2728-2740.

Shen, W.; Kornfield, J. A.; Tirrell, D. A. *Soft Matter* **2007**, *3*, 99-107.

Shen, W.; Zhang, K.; Kornfield, J. A.; Tirrell, D. A. *Nat. Mater.* **2006**, *5*, 153-158.

Shibayama, M.; Morimoto, M.; Nomura, S. *Macromolecules* **1994**, *27*, 5060-5066.

Shields, D. J.; Coover, H. W. *J. Polym. Sci.* **1959**, *39*, 532-533.

Shiomori, K.; Ivanov, A. E.; Galaev, I. Y.; Kawano, Y.; Mattiasson, B. *Macromol. Chem. Phys* **2004**, *205*, 27-34.

Shunmugam, R.; Smith, C. E.; Tew, G. N. *J. Polym. Sci., Part A: Polym. Chem.* **2007**, *45*, 2601-2608.

Smith, G. D.; Yoon, D. Y.; Jaffe, R. L.; Colby, R. H.; Krishnamoorti, R.; Fetters, L. J. *Macromolecules* **1996**, *29*, 3462-3469.

Snowden, M. J.; Chowdhry, B. Z.; Vincent, B.; Morris, G. E. *J. Chem. Soc., Faraday Trans.* **1996**, *92*, 5013-5016.

Song, J.; Baker, A. M.; Macosko, C. W.; Ewoldt, R. H. *AlChE J.* **2013**, *59*, 3391-3402.

Song, J.; Bringuier, A.; Kobayashi, S.; Baker, A. M.; Macosko, C. W. *Polym. J.* **2012**, *44*, 939-945.

Song, J.; Ewoldt, R. H.; Hu, W.; Silvis, H. C.; Macosko, C. W. *AlChE J.* **2011**, *57*, 3496-3506.

Song, J.; Thurber, C. M.; Kobayashi, S.; Baker, A. M.; Macosko, C. W.; Silvis, H. C. *Polymer* **2012**, *53*, 3636-3641.

Song, S. C.; Lee, S. B.; Jin, J. I.; Sohn, Y. S. *Macromolecules* **1999**, *32*, 2188-2193.

Stuart, M. A. C.; Huck, W. T. S.; Genzer, J.; Muller, M.; Ober, C.; Stamm, M.; Sukhorukov, G. B.; Szleifer, I.; Tsukruk, V. V.; Urban, M.; Winnik, F.; Zauscher, S.; Luzinov, I.; Minko, S. *Nat. Mater.* **2010**, *9*, 101-113.

Sugihara, S.; Kanaoka, S.; Aoshima, S. *J. Polym. Sci., Part A: Polym. Chem.* **2004**, *42*, 2601-2611.

Sun, P.; Zhang, Y.; Shi, L.; Gan, Z. *Macromol. Biosci.* **2010**, *10*, 621-631.

Sundararaman, A.; Stephan, T.; Grubbs, R. B. *J. Am. Chem. Soc.* **2008**, *130*, 12264-+.

Susan, M. A.; Kaneko, T.; Noda, A.; Watanabe, M. *J. Am. Chem. Soc.* **2005**, *127*, 4976-4983.

Tae, G.; Kornfield, J. A.; Hubbell, J. A.; Johannsmann, D.; Hogen-Esch, T. E. *Macromolecules* **2001**, *34*, 6409-6419.

Tam, K. C.; Jenkins, R. D.; Winnik, M. A.; Bassett, D. R. *Macromolecules* **1998**, *31*, 4149-4159.

Tanaka, F.; Edwards, S. F. *Macromolecules* **1992**, *25*, 1516-1523.

Tang, J.; Tang, H.; Sun, W.; Plancher, H.; Radosz, M.; Shen, Y. *Chem. Commun.* **2005**, 3325-3327.

Taribagil, R. R.; Hillmyer, M. A.; Lodge, T. P. *Macromolecules* **2009**, *42*, 1796-1800.

Taribagil, R. R.; Hillmyer, M. A.; Lodge, T. P. *Macromolecules* **2010**, *43*, 5396-5404.

Tokarev, I.; Minko, S. *Adv. Mater.* **2010**, *22*, 3446-3462.

Topp, M. D. C.; Dijkstra, P. J.; Talsma, H.; Feijen, J. *Macromolecules* **1997**, *30*, 8518-8520.

Trollsas, M.; Kelly, M. A.; Claesson, H.; Siemens, R.; Hedrick, J. L. *Macromolecules* **1999**, *32*, 4917-4924.

Tsitsilianis, C.; Katsampas, I.; Sfika, V. *Macromolecules* **2000**, *33*, 9054-9059.

Ueki, T.; Watanabe, M. *Chem. Lett.* **2006**, *35*, 964-965.

Vasilevskaya, V. V.; Khokhlov, A. R.; Yoshikawa, K. *Macromol. Theory Sim.* **2000**, *9*, 600-607.

Vermonden, T.; Besseling, N. A. M.; van Steenbergen, M. J.; Hennink, W. E. *Langmuir* **2006**, *22*, 10180-10184.

Virtanen, J.; Holappa, S.; Lemmetyinen, H.; Tenhu, H. *Macromolecules* **2002**, *35*, 4763-4769.

Vogt, A. P.; Sumerlin, B. S. *Soft Matter* **2009**, *5*, 2347-2351.

Von Berlepsch, H.; Bottcher, C.; Skrabania, K.; Laschewsky, A. *Chem. Commun.*

**2009**, 2290-2292.

Wang, D.; Liu, T.; Yin, J.; Liu, S. *Macromolecules* **2011**, *44*, 2282-2290.

Weberskirch, R.; Preuschen, J.; Spiess, H. W.; Nuyken, O. *Macromol. Chem. Phys* **2000**, *201*, 995-1007.

Wei, H.; Zhang, X.; Zhou, Y.; Cheng, S.; Zhuo, R. *Biomaterials* **2006**, *27*, 2028-2034.

Welton, T. *Chem. Rev.* **1999**, *99*, 2071-2083.

Winnik, F. M. *Macromolecules* **1990**, *23*, 233-242.

Winter, H. H.; Chambon, F. *J. Rheol.* **1986**, *30*, 367-382.

Winter, H. H.; Chambon, F. *J. Rheol.* **1986**, *30*, 367-382.

Wischerhoff, E.; Badi, N.; Lutz, J.-F.; Laschewsky, A. *Soft Matter* **2010**, *6*, 705-713.

Won, Y. Y.; Brannan, A. K.; Davis, H. T.; Bates, F. S. *J. Phys. Chem. B* **2002**, *106*, 3354-3364.

Won, Y. Y.; Davis, H. T.; Bates, F. S. *Macromolecules* **2003**, *36*, 953-955.

Wu, C.; Wang, X. *Phys. Rev. Lett.* **1998**, *80*, 4092-4094.

Xia, Y.; Burke, N. A. D.; Stover, H. D. H. *Macromolecules* **2006**, *39*, 2275-2283.

Xia, Y.; Yin, X.; Burke, N. A. D.; Stover, H. D. H. *Macromolecules* **2005**, *38*, 5937-5943.

Xu, B.; Li, L.; Yekta, A.; Masoumi, Z.; Kanagalingam, S.; Winnik, M. A.; Zhang, K.; Macdonald, P. M. *Langmuir* **1997**, *13*, 2447-2456.

Xu, F. J.; Zhong, S. P.; Yung, L. Y. L.; Kang, E. T.; Neoh, K. G. *Biomacromolecules* **2004**, *5*, 2392-2403.

Xu, H.; Meng, F.; Zhong, Z. *J. Mater. Chem.* **2009**, *19*, 4183-4190.

Xu, J.; Liu, S. *Soft Matter* **2008**, *4*, 1745-1749.

Xu, X.; Liu, C.; Huang, J. *J. Appl. Polym. Sci.* **2008**, *108*, 2180-2188.

Yamaguchi, D.; Cloitre, M.; Panine, P.; Leibler, L. *Macromolecules* **2005**, *38*, 7798-7806.

Yan, J.; Ji, W.; Chen, E.; Li, Z.; Liang, D. *Macromolecules* **2008**, *41*, 4908-4913.

Yin, X.; Hoffman, A. S.; Stayton, P. S. *Biomacromolecules* **2006**, *7*, 1381-1385.

York, A. W.; Kirkland, S. E.; McCormick, C. L. *Adv. Drug Deliv. Rev.* **2008**, *60*, 1018-1036.

Yoshida, R.; Sakai, K.; Okano, T.; Sakurai, Y. *J. Biomater. Sci., Polym. Ed.* **1995**, *6*, 585-598.

Yu, L.; Ding, J. *Chem. Soc. Rev.* **2008**, *37*, 1473-1481.

Yu, L.; Zhang, H.; Ding, J. *Angew. Chem., Int. Ed.* **2006**, *45*, 2232-2235.

Yuan, H.; Shimotani, H.; Tsukazaki, A.; Ohtomo, A.; Kawasaki, M.; Iwasa, Y. *Adv. Funct. Mater.* **2009**, *19*, 1046-1053.

Zakeeruddin, S. M.; Gratzel, M. *Adv. Funct. Mater.* **2009**, *19*, 2187-2202.

Zana, R.; Marques, C.; Johner, A. *adv. Colloid Interface Sci.* **2006**, *123*, 345-351.

Zhang, H.; Yu, L.; Ding, J. *Macromolecules* **2008**, *41*, 6493-6499.

Zhang, J.; Pelton, R. *J. Polym. Sci., Part A: Polym. Chem.* **1999**, *37*, 2137-2143.

Zhang, Q.; Zha, L.; Ma, J.; Liang, B. *J. Appl. Polym. Sci.* **2007**, *103*, 2962-2967.

Zhang, S.; Lee, K. H.; Frisbie, C. D.; Lodge, T. P. *Macromolecules* **2011**, *44*, 940-949.

Zhang, S.; Lee, K. H.; Sun, J.; Frisbie, C. D.; Lodge, T. P. *Macromolecules* **2011**, *44*, 8981-8989.

Zhang, W. Q.; Shi, L. Q.; Ma, R. J.; An, Y. L.; Xu, Y. L.; Wu, K. *Macromolecules* **2005**, *38*, 8850-8852.

Zhang, W.; Jiang, X.; He, Z.; Xiong, D.; Zheng, P.; An, Y.; Shi, L. *Polymer* **2006**, *47*, 8203-8209.

Zhang, W.; Shi, L.; Wu, K.; An, Y. *Macromolecules* **2005**, *38*, 5743-5747.

Zhang, Y.; Guan, Y.; Zhou, S. *Biomacromolecules* **2006**, *7*, 3196-3201.

Zheng, S.; Shi, S.; Xia, Y.; Wu, Q.; Su, Z.; Chen, X. *J. Appl. Polym. Sci.* **2010**, *118*, 671-677.

Zhou, C.; Hillmyer, M. A.; Lodge, T. P. *J. Am. Chem. Soc.* **2012**, *134*, 10365-10368.

Zhou, C.; Hillmyer, M. A.; Lodge, T. P. *Macromolecules* **2011**, *44*, 1635-1641.

Zhou, Z.; Li, Z.; Ren, Y.; Hillmyer, M. A.; Lodge, T. P. *J. Am. Chem. Soc.* **2003**, *125*, 10182-10183.

Zhu, J.; Jiang, W. *Macromolecules* **2005**, *38*, 9315-9323.

Zhu, P.; Napper, D. H. *Langmuir* **2000**, *16*, 8543-8545.

Zhu, P.; Napper, D. H. *Macromolecules* **1999**, *32*, 2068-2070.

Zupancich, J. A.; Bates, F. S.; Hillmyer, M. A. *Macromolecules* **2006**, *39*, 4286-4288.